Effects of Magmatic Intrusions on the Mechanical and Physical Properties of Volcanic Host Rock: Pinnacle Ridge, Mt. Ruapehu, New Zealand

Stanley Paul Mordensky

A Thesis Submitted in Partial Fulfilment of the Requirements

for the Degree of

Doctor of Philosophy

College of Science

Department of Geological Sciences

University of Canterbury

March 2019

The Crossing

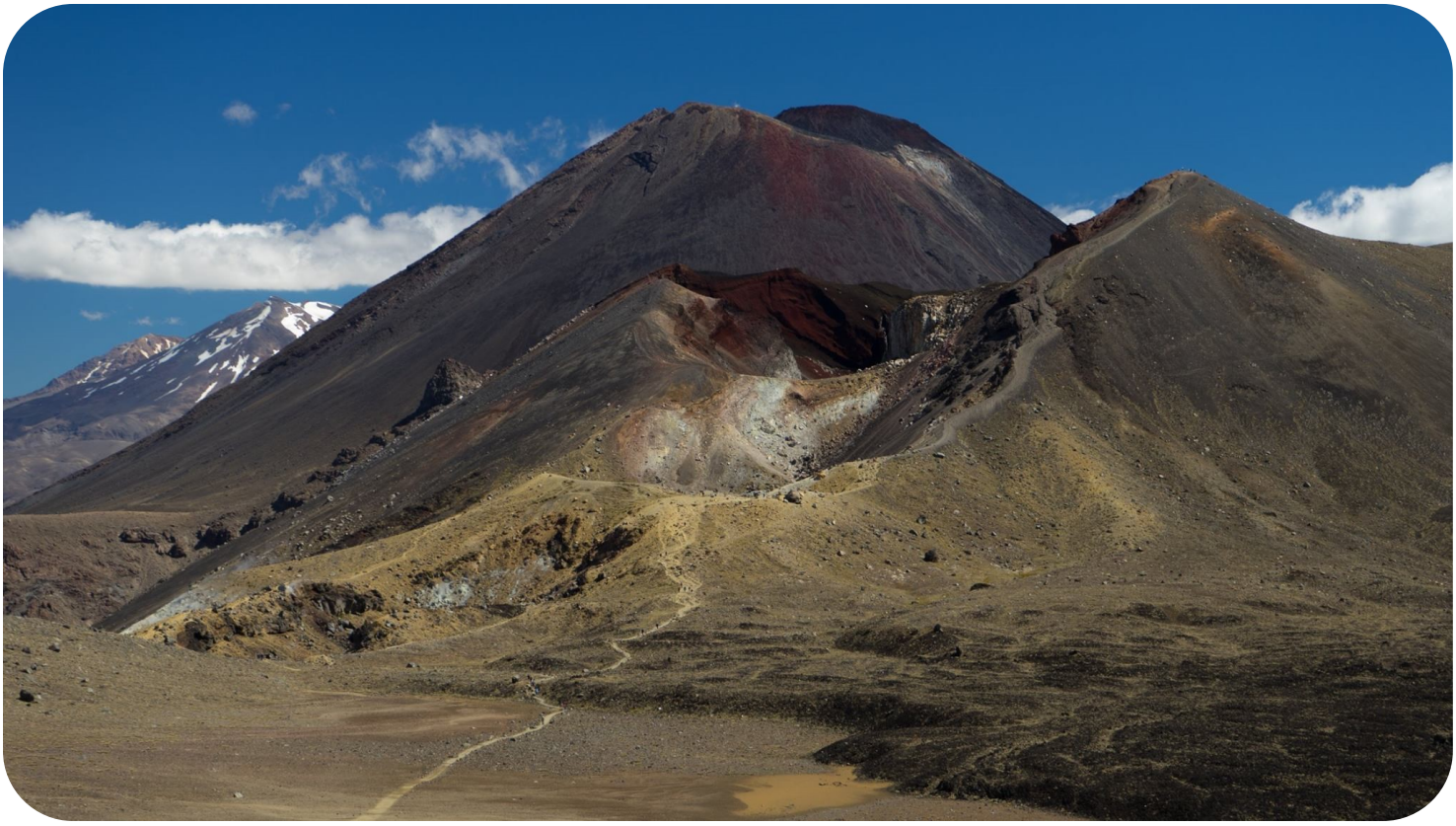

View from Blue Lake toward the Tongariro Crossing. In order from front to back: Red Crater; Ngauruhoe; and Mt. Ruapehu. Although the samples in this study were not collected from Mt. Ngauruhoe or Red Crater, this image provides another example of hydrothermal features and their resulting alteration (see near side of Red Crater). Photo from Blue Lake toward southwest.

Contents

List of Figures

List of Figures (continued)

List of Tables

*Supplemental tables are found as electronic appendices (see Chapter 7)

Dedication

For my family,

Thank you

“I can smell the sea”

Acknowledgements

My time at the University of Canterbury was funded by the University of Canterbury Doctoral Scholarship. I am grateful for this support without which my studies would not have been possible.

I thank my supervisors, Marlène Villeneuve, Ben Kennedy, and Darren Gravley for their guidance, patience, and support throughout this academic process. I am grateful to have worked with a team who equally promoted mutual respect, learning, and fun. Marlène Villeneuve, thanks for being patient enough to work with someone who had had no prior experience in material sciences. Ben, thanks for seeing the best in everybody. Darren, thanks for always being someone I could count on to have a smile.

I also thank Jim Cole, who served as an unofficial supervisor for all of my doctoral work. Jim, your wisdom, kindness, and laugh stayed with me long after our discussions had ended.

I thank the staff with whom I collaborated in Strasbourg, France. Mike Heap, Jamie Farquharson, and Thierry Reuschlé, thank you for introducing me to your many pieces of analytical equipment and making sure I collected the best data possible from my samples. Patrick Baud, thank you for your frank discussions and valuable insight from another perspective. Mike Heap, Jamie Farquharson and Luke Griffiths, thanks for the informative discussions and letting me crash at your respective abodes. I also extend thanks to my other co-authors, Hans Albert Gilg, Yan Lavallée, Marc Reichow, Paul Siratovich, and Paul Wallace. I am grateful for the knowledge and fortitude you have shared with me.

I would like to acknowledge the support I received from GNS. Graham Leonard, thank you for organizing the permitting and for providing my earliest instruction on how to handle alpine environments in New Zealand. Dougal Townsend, thank you for always being there to keep Graham in check and offer a highly valued opinion. Isabelle Chambefort, thank you for encouraging me to look deeper into the alteration assemblages at Pinnacle Ridge. Mark Simpson, thank you for taking the time to instruct me on the use of the TerraSpec.

I thank the Tongariro National Park staff, Harry Keys, Blake McDavitt, Hollei Gabrielsen, and Julian Tovey, who worked with me to sort out permitting, air traffic restrictions, and accommodation when doing fieldwork throughout the park. I also thank the people of Ngāti Tūwharetoa and Ngāti Rangi for their permission and support of my work at Mt. Ruapehu.

I thank Ludmila Adam and James Kelly Russell for their review and critique of this dissertation.

I send endearment to those with whom I shared the field seasons: Leo Purê, Rosie Cole, Marlene Villeneuve, Jamie Farquharson, Stephanie Ferreira dos Santos, Rebecca Fitzgerald, and "Corpse Grinder". Thank you for putting up with me.

"Cathy, I broke the lab." To the UC geology technicians and administrative staff, Rob Spiers, Cathy Higgins, Sarah Pope, Sacha Baldwin, Matt Cockcroft, Chris Grimshaw, Anekant Wandres, John Southward, Rebekah Hunt, and Janet Warburton, you are my guardian angels.

To my fellow post-graduate students and staff at the University of Canterbury, my friends, it would have been nothing without you. Too many to name here, but my time at the university would have been incomplete without each of you.

I must also acknowledge my undergraduate mentors. Without their support, I never would have had the chance at starting this work. To the late Professor George C. Stephens, thank you for helping me to keep perspective. To Professor Richard Tollo, thank you for allowing me to change my major in my senior year. I also thank you for your guidance and wisdom.

To my family, particularly my mother and father, thank you for immersing me in the sciences and outdoors at an early age, for giving me every opportunity I could ask for, and not being afraid to let me fall. You have taught me how to get up again.

Finally, Elizabeth, rather, Etch, I do not think I would have completed this PhD without you. Thank you.

Abstract

Magmatic intrusions are common to volcanoes worldwide. The emplacement of these intrusions disturbs the temperature and pressure conditions within the volcano and presents a potential heat source to develop and drive a hydrothermal system. Consequently, magmatic intrusions change the volume, topography, and properties of the volcano. In this thesis, I investigate the physical and mechanical effects a small shallow intrusion produces in its andesitic host rock.

The thesis opens with a preliminary study (Chapter 2) in which I thermally stress andesitic samples to demonstrate the geomechanical effects a rapidly emplaced and cooled magma body would have in hydrothermally altered andesitic lavas. Then, the thesis focuses the investigation (Chapters 3, 4, 5, and 6) to the primary field area, Pinnacle Ridge, Mt. Ruapehu, New Zealand, where a glacially dissected fossil hydrothermal system serves as a natural laboratory for studying the effects of an intrusion on the physical and mechanical rock properties of an andesitic host rock.

The opening study (Chapter 2) of this thesis considers the effects thermal stresses have on hydrothermally altered andesite from the Rotokawa Geothermal Field. The experiments demonstrate that short-duration thermal exposure (350 – 739 °C) in 20 MPa of $H_2O_{fluid/vapour}$ can increase permeability by over an order of magnitude (10^{-18} m^2 to > 10^{-17} m^2) as a result of an increase in porosity (< 1 % – > 7 %) driven by both chemical reaction and microfracturing. These results imply that intrusions may increase the porosity and permeability in the host rocks proximal to their emplacement, serving as targets for geothermal exploration.

Pinnacle Ridge is composed of several distinct geotechnical units surrounding small, irregularly shaped intrusions. I collected samples from the differing geotechnical units at varying distances to the largest intrusion (Chapter 3). Intact rock testing reveals the physical and mechanical (i.e. petrophysical and geomechanical) rock properties of one geotechnical unit, the brecciated lava margins, correlate with distance to the largest intrusion. Porosity and permeability of the brecciated lava margins decrease while strength increases approaching the intrusion. The study also finds a previously unclassified geotechnical unit (i.e. hydrothermal vein) for which I argue its own geotechnical classification on the grounds of its unique combination of low permeability and low uniaxial compressive strength.

The intact rock characterization from Pinnacle Ridge revealed a unique sample block with two distinct types of alteration (intermediate and advanced argillic). In Chapter 4, triaxial deformation testing of cores from this sample reveal that the alteration type changes the deformation mode (brittle to ductile) of andesite at low effective confining pressures (~10 MPa). The change in deformation behaviour is the result of

advanced argillic alteration increasing the porosity through dissolution and partially replacing the primary mineral assemblage with weaker more ductile clay (i.e. kaolinite and smectite). I argue that this transition could explain the absence of volcano tectonic earthquakes at certain depths prior to volcanic eruptions.

When investigating the physical and mechanical effects of magmatic intrusion emplacement, scale requires consideration. In Chapter 5, I present my field observations from Pinnacle Ridge and consider them in conjunction with the lab data presented in Chapter 3. In general, discontinuities in altered rock masses are more abundant and have smoother surfaces than in unaltered rock masses. Numerical modeling demonstrates that the dichotomy between the discontinuity properties of the unaltered and altered rock masses creates the potential for altered brecciated lava margins to be weaker than unaltered brecciated lava margins despite the higher intact rock porosity and lower intact rock strength of the latter.

The numerical modeling in Chapter 5 demonstrates that outcrop scale properties must be measured in tandem with intact rock properties when considering rock mass strength. However, the modeling presented in Chapter 5 relied upon rock parameter assumptions for generic andesite, because the specialized data for altered andesite did not exist. In Chapter 6, I conduct triaxial deformation testing for all the geotechnical units of Pinnacle Ridge to complete the first full set of Generalised Hoek-Brown failure criterion parameters for an intrusion and its altered host rock. Using these data, I numerically model volcano stability with varying pore pressures within the geotechnical units. In doing so, I demonstrate that hydrothermal vein material is the weakest rock mass in the fossil hydrothermal system at Pinnacle Ridge. These results have implications for the importance of modelling even thin geotechnical units such as the hydrothermal vein when considering volcano stability.

In summary, I use a combination of lab- and field-based rock property testing, and finite element numerical modelling to examine the full physical and mechanical effects intrusions produce in volcanic host rock. I show that the effects of intrusions in volcanic (andesitic) rock varies with time (Chapter 2 versus Chapter 3), distance (Chapter 3), and scale (Chapter 3 versus Chapter 5; Chapter 6) as well as the environmental conditions (e.g. effective confining pressure) of the host rock (Chapters 3 and 6) and alteration type of the host rock (Chapter 4). Given the global and ubiquitous distribution of magmatic intrusions, these results have profound worldwide implications for the geothermal power industry (Chapters 2, 3, and 5), volcano monitoring (Chapters 4, 5, and 6), and volcano slope stability (Chapters 2, 3, 4, 5, and 6).

Glossary of Abbreviations

ABLM – altered brecciated lava margin

ADCL – altered dense coherent lava

AI – altered Intrusion

DEM – digital elevation model

EDS – energy-dispersive X-ray spectroscopy

HV – hydrothermal vein

TG – thermo-gravimetric analysis

TVZ – Taupō Volcano Zone

SEM – scanning electron microscopy

STA – simultaneous thermal analysis

UBLM – unaltered brecciated lava margin

UCS – uniaxial compressive strength

UDCL – unaltered dense coherent lava

UI – unaltered intrusion

XRD – X-ray diffraction

UNIVERSITY OF CANTERBURY
Te Whare Wānanga o Waitaha
CHRISTCHURCH NEW ZEALAND

Deputy Vice-Chancellor's Office
Postgraduate Research Office

Co-Authorship Form

This form is to accompany the submission of any thesis that contains research reported in co-authored work that has been published, accepted for publication, or submitted for publication. A copy of this form should be included for each co-authored work that is included in the thesis. Completed forms should be included at the front (after the thesis abstract) of each copy of the thesis submitted for examination and library deposit.

Please indicate the chapter/section/pages of this thesis that are extracted from co-authored work and provide details of the publication or submission from the extract comes:

Chapter 2, written with the intent to submit to the Journal of Volcanology and Geothermal Research

Please detail the nature and extent (%) of contribution by the candidate:

95% of the research is the candidates original work. The temperature treatment, characterisation, and deformation experiments, and writing of the manuscript was completed by the candidate. Co-authors provided the STA analyses, XRD analyses, dialogue, suggestions for revision, and editorial comments.

Certification by Co-authors:

If there is more than one co-author then a single co-author can sign on behalf of all

The undersigned certifies that:

- The above statement correctly reflects the nature and extent of the PhD candidate's contribution to this co-authored work
- In cases where the candidate was the lead author of the co-authored work he or she wrote the text

Name: *Ben Kennedy* Signature:  Date: *9/11/2018*

Deputy Vice-Chancellor's Office
Postgraduate Research Office

UNIVERSITY OF CANTERBURY
Te Whare Wānanga o Waitaha
CHRISTCHURCH NEW ZEALAND

Co-Authorship Form

This form is to accompany the submission of any thesis that contains research reported in co-authored work that has been published, accepted for publication, or submitted for publication. A copy of this form should be included for each co-authored work that is included in the thesis. Completed forms should be included at the front (after the thesis abstract) of each copy of the thesis submitted for examination and library deposit.

Please indicate the chapter/section/pages of this thesis that are extracted from co-authored work and provide details of the publication or submission from the extract comes:

Chapter 3, published in the Journal of Volcanology and Geothermal Research

Please detail the nature and extent (%) of contribution by the candidate:

100% of the research is the candidates original work. Co-authors provided dialogue, suggestions for revision, and editorial comments.

Certification by Co-authors:

If there is more than one co-author then a single co-author can sign on behalf of all

The undersigned certifies that:

- The above statement correctly reflects the nature and extent of the PhD candidate's contribution to this co-authored work
- In cases where the candidate was the lead author of the co-authored work he or she wrote the text

Name: *Ben Kennedy* Signature:  Date: *9/11/18*

Deputy Vice-Chancellor's Office
Postgraduate Research Office

UNIVERSITY OF CANTERBURY
Te Whare Wānanga o Waitaha
CHRISTCHURCH NEW ZEALAND

Co-Authorship Form

This form is to accompany the submission of any thesis that contains research reported in co-authored work that has been published, accepted for publication, or submitted for publication. A copy of this form should be included for each co-authored work that is included in the thesis. Completed forms should be included at the front (after the thesis abstract) of each copy of the thesis submitted for examination and library deposit.

Please indicate the chapter/section/pages of this thesis that are extracted from co-authored work and provide details of the publication or submission from the extract comes:

Chapter 4, submitted to Geophysical Research Letters

Please detail the nature and extent (%) of contribution by the candidate:

95% of the research is the candidates original work. Co-authors provided XRD analyses, dialogue, suggestions for revision, and editorial comments.

Certification by Co-authors:

If there is more than one co-author then a single co-author can sign on behalf of all

The undersigned certifies that:

- The above statement correctly reflects the nature and extent of the PhD candidate's contribution to this co-authored work
- In cases where the candidate was the lead author of the co-authored work he or she wrote the text

Name: *Ben Kennedy* Signature:  Date: *9/11/2018*

Deputy Vice-Chancellor's Office
Postgraduate Research Office

UNIVERSITY OF CANTERBURY
Te Whare Wānanga o Waitaha
CHRISTCHURCH NEW ZEALAND

Co-Authorship Form

This form is to accompany the submission of any thesis that contains research reported in co-authored work that has been published, accepted for publication, or submitted for publication. A copy of this form should be included for each co-authored work that is included in the thesis. Completed forms should be included at the front (after the thesis abstract) of each copy of the thesis submitted for examination and library deposit.

Please indicate the chapter/section/pages of this thesis that are extracted from co-authored work and provide details of the publication or submission from the extract comes:

Chapter 5, published in the Journal of Volcanology and Geothermal Research

Please detail the nature and extent (%) of contribution by the candidate:

100% of the research is the candidates original work. Co-authors provided dialogue, suggestions for revision, and editorial comments.

Certification by Co-authors:

If there is more than one co-author then a single co-author can sign on behalf of all

The undersigned certifies that:

- The above statement correctly reflects the nature and extent of the PhD candidate's contribution to this co-authored work
- In cases where the candidate was the lead author of the co-authored work he or she wrote the text

Name: *Ben Kennedy* Signature:  Date: *9/11/18*

Deputy Vice-Chancellor's Office
Postgraduate Research Office

UNIVERSITY OF CANTERBURY
Te Whare Wānanga o Waitaha
CHRISTCHURCH NEW ZEALAND

Co-Authorship Form

This form is to accompany the submission of any thesis that contains research reported in co-authored work that has been published, accepted for publication, or submitted for publication. A copy of this form should be included for each co-authored work that is included in the thesis. Completed forms should be included at the front (after the thesis abstract) of each copy of the thesis submitted for examination and library deposit.

Please indicate the chapter/section/pages of this thesis that are extracted from co-authored work and provide details of the publication or submission from the extract comes:

Chapter 6, written to be submitted to Engineering Geology

Please detail the nature and extent (%) of contribution by the candidate:

100% of the research is the candidates original work. Co-authors provided dialogue, suggestions for revision, and editorial comments.

Certification by Co-authors:

If there is more than one co-author then a single co-author can sign on behalf of all

The undersigned certifies that:

- The above statement correctly reflects the nature and extent of the PhD candidate's contribution to this co-authored work
- In cases where the candidate was the lead author of the co-authored work he or she wrote the text

Name: *Ben Kennedy* Signature:  Date: *9/11/18*

Chapter 1
Introduction

1.1 Research background, intentions, and context

Volcanic edifices host a wide array of materials with varied and heterogenous material properties (e.g. Apuani et al., 2005; Moon et al., 2005; del Potro & Hürlimann, 2008; Adam & Otheim, 2013; Kanakiya et al., 2017; Ryan et al., 2018). Most of these materials are deposited on the flanks of the edifice (e.g. dense lavas, breccias, ash deposits). Magmatic intrusions emplaced into the subsurface also increase the complexity of the material properties of a volcanic edifice (Sigurdsson et al., 2000; and references therein).

Magmatic intrusions have varied morphologies and material properties. They can be planar (e.g. sills and dikes), or equant (i.e. stocky), but can also be more amorphous (Vigneresse et al., 1999; Valentine & Krogh, 2006; Keating et al., 2007). Intrusive events occur in compressional and extensional environments, and the pressures intrusive magma exerts on its surrounding environment produces compressional and tensile stresses under near-surface conditions (Lipman, 2000; Galland et al., 2003; Casey et al., 2006; Galland et al., 2009).

Depending on several parameters (e.g. volume, magma flux, initial emplacement temperature, initial host-rock temperature, magma composition, local hydrology) an intrusion may remain sufficiently hot long enough to host a hydrothermal system (e.g. Cathles et al., 1997). Consequently, hydrothermal alteration, the interaction of hot, ion-rich fluids and rock, can lead to dissolution, deposition, and secondary mineralization, around the intruding magma. (e.g. Frank, 1995; Finizola et al., 2002; Hurwitz et al., 2002; Hase et al., 2005; Pola et al., 2012; Pola et al., 2014). Therefore, intrusions present the potential to increase the material complexity of its volcanic host not simply by introducing itself as a new material but also through alteration of the existing material(s).

Magmatic intrusions and/or their accompanying hydrothermal systems can be located by several indirect methods (e.g. seismicity (e.g. Planke, 1999), electrical resistivity (e.g. Ogawa et al., 1998), ground penetrating radar (e.g. Davis and Annan, 1989) and ground magnetics (e.g. Davis and Annan, 1989)). Existing research describes environmental conditions (e.g. lithostatic pressure, pore pressure, and temperature; e.g. Browne, 1978; Giggenbach & Sheppard, 1989; Day, 1996) and provides some details of the physical and mechanical properties (e.g. porosity, permeability, P- and S-wave velocity, strength; e.g.

Browne, 1978; Pola et al., 2014; Siratovich et al., 2014) of rocks from hydrothermal systems. However, direct observation of active geothermal system and geospatial distribution of the structure and geomechanical properties is limited to drill core samples (e.g. Wyering et al., 2014), or surface temperature and geochemistry (e.g. Rissmann et al., 2011) which do not provide sufficient resolution to firmly understand the local geological complexities with respect to the intrusive body.

1.2 Thesis intent and format

This thesis describes the effects, consequences, and implications a magmatic heat source and its corresponding hydrothermal alteration produce in the physical and mechanical properties of volcanic host rock. The initial study of this thesis (Chapter 2) begins by investigating the effect high-temperature, low-gradient thermal stress produces in hydrothermally altered rock from the Rotokawa Geothermal Field. The results of this study then allow an informed approach to a sub-aerially exposed fossil geothermal system in Pinnacle Ridge, Mt. Ruapehu (New Zealand) in Chapters 3 – 6. Then, the key topics are summarized in Chapter 7 followed by their general implications and related research ideas stemming from the work done in this thesis.

The thesis is predominantly composed of published papers (Chapter 3 and 5) or manuscripts prepared for publication (Chapters 2, 4, 6) in international peer-reviewed journals. Some sections of these chapters contain repetition of core concepts and previous research. This repetition is intended to allow each chapter to serve as an independent manuscript that provides the readers with sufficient context to understand the material presented. Similarly, the references specific to each chapter are provided at the end of each chapter rather than a single, comprehensive reference list following the main body of the thesis. Doing so provides the reader with easy reference to the cited materials. Although each chapter is self-contained, all chapters share the common theme of understanding how a shallow magmatic heat source can change the physical and mechanical properties of its volcanic host rock. Consequently, each subsequent chapter directly and indirectly builds from the last and contributes to our knowledge of geomechanical properties in a volcanic domain.

1.3 Scientific context

This section provides a background review for the topics presented and discussed in this thesis. Specifically, the principal components of a hydrothermal system are introduced and the key geomechanical properties are discussed. A complete literature review is not provided here because each chapter serves as

a stand-alone publishable article complete with its own specific literature review. Instead, this section serves as a foundation to understand the knowledge gaps addressed in this thesis.

Hydrothermal systems are diversely varied structures, but can be divided into their commonly shared constituent components (i.e. fluid, heat source, permeable pathways, and caprock; Corrado et al., 2014). Fluid comes from meteoric groundwater (e.g. Nemčok et al., 2007) and magmatic volatiles (e.g. Rye, 1993). Magma often provides the necessary heat, which leads to the fluid convection through a combination of the intact rock matrix and discontinuities (e.g. fractures, joints, faults; Rowland & Sibson, 2004; Kissling & Weir, 2005; Rissmann et al., 2011). However, several processes can change the permeability and other geomechanical properties of the rock within a hydrothermal system (e.g. dissolution, precipitation, fracturing; e.g. Ferry, 1979; Giggenbach, 1984; Henneberger & Browne, 1988; Esmaeily et al., 2012). The manner and degree to which geomechanical properties are affected appears to be a product of alteration conditions to which a rock is exposed. For example, Rejeki et al. (2005) found illite-rich samples from the Darajat Geothermal Field, West Java, Indonesia to have lower porosity and higher density than samples abundant with smectitic clays. Wyering et al. (2014) observed that samples from the shallow and low-temperature (< 150 °C) regions had higher porosity (15 – 56 %) and lower density (1222 – 2114 kg/m^3) than the samples from a deeper and high-temperature (> 200 °C) regions (1.5 – 20 % and 2072 – 2837 kg/m^3, respectively). These studies demonstrate that the processes that affect geomechanical properties are governed in part by the alteration zone in which the rock resides but modified by the local fluid and rock chemistry.

Conventional hydrothermal systems are divided into three zones of alteration (smectitic, argillic, and propylitic) that are primarily dependent on mineralogical assemblage and, thereby, temperature (Carranza, 2005; Stimac et al., 2008; Cumming, 2009; Esmaeily et al., 2012; Wyering et al., 2014). Smectitic alteration forms under low temperatures and is predominated by smectite clay. Argillic alteration forms under low to moderate temperatures and contains abundant illite and other low- to moderate-temperature minerals (Carranza, 2005; Lutz et al., 2010; Pola et al., 2012). Argillic alteration can then be further divided into low-sulfidation states (argillic alteration) and high-sulfidation states (advanced argillic alteration; Henley & Ellis, 1983). Propylitic alteration forms under the highest temperatures and produces chlorite, epidote, and quartz with some calcite and albite (Browne, 1978; Carranza, 2005). This thesis includes hydrothermally altered rocks from two hydrothermal systems, and details observations of hydrothermally altered rock from propylitic (Chapter 2) and advanced argillic (Chapters 3 – 6) alteration zones.

1.4 Study area and previous work

The two hydrothermal systems on which this thesis focuses are located within the Taupo Volcanic Zone (TVZ), North Island, New Zealand (Fig. 1.1). The 300-km-by-60-km TVZ, delineated by geothermal fields, hydrothermal vents, and active calderas (Wilson et al., 1995; Rowland & Sibson, 2001), is a rifted arc basin produced by the oblique subduction of the Pacific plate beneath the Indian-Australian plate below New Zealand's North Island (Cole, 1990). The geothermal systems of the TVZ convect groundwater through fractures, faults, and pores, with convection driven by the heat of magmatic systems at depth (Henneberger & Browne, 1988; Hochstein, 1995; Rowland & Sibson, 2004; Rowland & Simmons, 2012), creating hydrothermal systems in the shallow subsurface of the TVZ (e.g. Christenson et al., 2002).

This study focuses on two centers of hydrothermal alteration in the TVZ, the Rotokawa Geothermal Field and Pinnacle Ridge, Mt. Ruapehu. The Rotokawa Geothermal field is a large industrial complex located 14 km NE of Lake Taupo. At 1.5 – 2.5 km depth in the TVZ (Fig. 1.1), the Rotokawa andesite serves as the primary reservoir rock of the Rotokawa Geothermal Field. The lavas have undergone extensive hydrothermal alteration to argillic – propylitic assemblages (Crowley & Zimbelman, 1997; Rae, 2007) in a high-enthalpy hydrothermal system starting around ~0.34 *Ma* (Chambefort et al., 2014; McNamara et al., 2016). A shallow intrusion was intersected in the neighboring Ngatamariki geothermal field at 2.2 km depth (see Chambefort et al., 2014), indicating that these rocks can be affected by shallow intrusions. The experiments in Chapter 2 thermally stress samples from the Rotokawa Geothermal Field to examine the effects of the increased temperature during intrusion on porosity, permeability, P-wave velocity, and strength.

After observing the effects of different maximum temperatures on hydrothermally altered volcanic rock, the thesis turns its focus toward Pinnacle Ridge, Mt. Ruapehu. Mt. Ruapehu is a predominantly andesitic stratovolcano located at the southern end of the TVZ. Pinnacle Ridge extends northwest from the summit plateau of Mt. Ruapehu. Pinnacle Ridge, where a fossil hydrothermal system is sub-aerially exposed, provides a unique opportunity to observe how magmatic intrusions affect the physical and mechanical properties of their host rock.

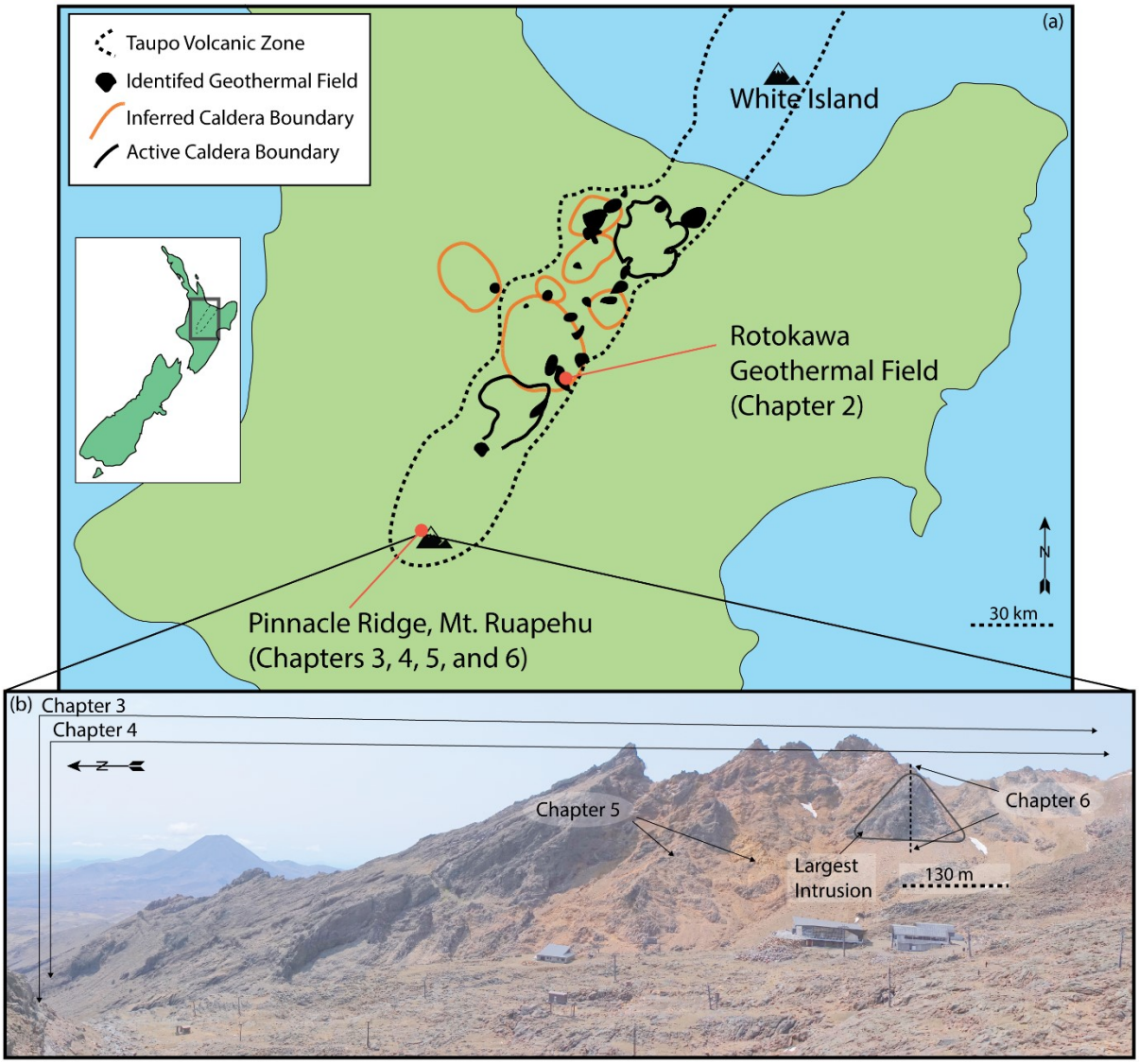

Figure 1.1 Primary site locations specific to the research presented in this thesis. (a) Sites of the two hydrothermal systems in New Zealand discussed in this thesis. (b) Sites specific to Chapters 3 – 6 at Pinnacle Ridge. Solid black polygon marks boundary of the largest young intrusion. Scale is approximate.

Pinnacle Ridge rocks are of the Te Herenga Formation (~170 *ka*), the oldest formation of Mt. Ruapehu. The central portion of the ridge is a nearly vertical sequence of lava flows composed of plagioclase- and pyroxene-phyric andesite and basaltic andesite lavas and subsequent intrusions of similar composition exposed by 10 *ka* glaciation (Hackett, 1985; Price et al., 2012). An orange, 400 m-wide alteration halo surrounds the largest intrusion (130 m-wide; Hackett, 1985). Using field observations (e.g. hypabyssal textures of the intrusives, brittle deformation of the tuff breccias, and deposition of silica and kaolinite around the aureole edge), Hackett (1985) interpreted that the hydrothermal alteration occurred under near-surface, epithermal conditions (approximately 50 – 500 m below the surface). Chapters 3-6 undertake a

detailed engineering geology appraisal of the rock mass, and rock mechanical analysis of the material properties of the rocks that comprise the ridge.

1.4.1 Rock properties critical to this research

All the studies presented in this thesis address the mechanical and physical properties common to rock mechanics. In this section, we present the rock properties (e.g. porosity, uniaxial compressive strength, triaxial deformation, permeability, and elastic wave velocity [e.g. p-wave velocity, and s-wave velocity]) discussed at length throughout this thesis. For more complete description of these properties and the related methods, refer to the corresponding Methods section for each of the studies within this thesis.

1.4.1.1 Porosity

Porosity is the void space within a rock (see Deuchar, 1823). Porosity and the microstructure governing porosity act as first-order controls on other rock properties (e.g. deformation behaviour (e.g. Bal'shin, 1949; Walsh, 1965b; Dunn et al., 1973), permeability (e.g. Fraser, 1935; Lacabanne, 1960), elastic wave velocity (e.g. Rubey, 1927; Wyllie et al., 1956; Balakshrina, 1957; Wyllie et al., 1958; Walsh, 1965a)). In hydrothermally altered volcanics, porosity is composed of vesicles and fractures. Understanding how porosity responds to external forces (e.g. stress and alteration) aids in understanding how the other rock properties respond to external forces.

1.4.1.2 Compressive strength and deformation

Rock strength is dependent on several mechanical properties (e.g. Griffith, 1921; Bal'shin, 1949; Heard, 1960); however, porosity exerts the greatest control. It is well documented that as porosity increases, uniaxial compressive strength decreases (e.g. Rozos & Koukis, 1986; Ulusay et al., 1994; Palchik, 1999); however, alteration can have variable effects on uniaxial compressive rock strength (see Wyering et al., 2015). There has yet to be a study detailing the changes in rock strength geospatially with an intrusive magma body.

While rock strength correlates with confining pressures (Hoek, 1968; Hoek & Brown, 1980), porosity also controls triaxial deformation behaviour. As porosity increases, compressibility increases (Knudsen et al., 1960; Lama & Vutukuri, 1978). Depending on the porosity of a rock and the confining pressure to which that rock is exposed, dilatant or compactant deformation behaviour will be exhibited (e.g. Böker, 1915; Brace, 1964; Brace et al., 1966). Dilation deformation is the increase in porosity under strain and compactant deformation is the decrease of porosity under strain. Under low-effective pressure

conditions, rocks dilatantly fail (e.g. axial splitting and shear failure) regardless of rock porosity (e.g. Faulkner, 2006). Under high-effective pressures, low-porosity rocks still fail dilatantly, but high-porosity rocks experience compaction through cataclastic pore collapse and grain crushing (e.g. Kennedy et al., 2009; Zhu et al., 2011; Loaiza et al., 2012; Wong & Baud, 2012; Adelinet et al., 2013; Heap et al., 2014a; Heap et al., 2015b). For example, an aphanitic basalt (8 % porosity) from Reykjanes (Iceland) and a Mt. St. Helens dacite (8 % porosity) both began expressing compactant behaviour at 75 MPa (Kennedy et al., 2009; Adelinet et al., 2013). Similarly, an aphanitic trach andesite (18 % porosity) from the Açores (Portugal) began to experience compactant failure as effective pressure exceeded 90 MPa (Loaiza et al., 2012). Siratovich et al. (2016) found Rotokawa andesites of 7 – 18 % expressed compactant deformation at high effective pressures (70 – 90MPa); however, the effects of mineralogical alteration on dilatant and compactant behaviour in a geothermal setting has yet to be studied thoroughly.

1.4.1.3 Permeability

Permeability is the measure of a material to transmit fluid. Microstructure, specifically pore connectivity, governs permeability in volcanic rock (e.g. Heap et al., 2014b; Siratovich et al., 2014). Although the volume percent porosity in a rock is not the sole control of permeability, increased porosity is often associated with increased permeability. For example, Heap et al. (2014a) observed an 8 % to 29 % change in porosity increases permeability by four orders of magnitude in fractured andesites, and through-cutting microfractures in unaltered andesite can increase permeability to ~10^{-11} m^2 regardless of the initial permeability of the rock (Heap & Kennedy, 2016).

Under compressive conditions, deformation style controls change in permeability. Compactant deformation decreases permeability (e.g. David et al., 1994; Fortin et al., 2005; Baud et al., 2012; Heap et al., 2015a), whereas dilatant deformation behaves variably. Dilatant deformation in low-porosity rock is linked with an increase in permeability (e.g. Nara et al., 2011), but high-porosity rock deformation decreases permeability (e.g. Zhu & Wong, 1997).

The influence of hydrothermal alteration on permeability in volcanic material is poorly constrained. Furthermore, the effect of hydrothermal alteration on the factors that influence permeability (e.g. porosity change and pore connectivity) remain unstudied geospatially with respect to a heat source. I address these subjects in my thesis.

1.4.1.4 Elastic wave velocity

In this thesis, one type of elastic wave is specifically examined – the P-wave (i.e. the compression wave). Like strength and permeability, P-wave velocity correlates with porosity. As porosity increases, P-wave velocity decreases (e.g. Ayling et al., 1995; Tugrul & Gurpinar, 1997; Al-Harthi et al., 1999; Fortin et al., 2005; Vinciguerra et al., 2005; Chaki et al., 2008; Nara et al., 2011; Rajabzadeh et al., 2011; Adam et al., 2013; Heap et al., 2014b; Siratovich et al., 2014; Kanakiya et al., 2017). Similarly, fractures decrease P-wave velocity (see Rutherford & Lucas, 1962). Microstructure and stress conditions are critical considerations when discussing the mechanical properties of rocks. I also collect S-wave velocity data in order to produce dynamic deformation moduli. Although I do not address questions specific and exclusive to elastic wave velocity, I use these data to inform of microstructural consideration in unaltered and altered samples.

1.5 Thesis organization

This thesis was written and formatted so that the chapters with novel research (i.e. Chapters 2 – 6) are presented as independent manuscripts intended or already accepted for publication in international, peer-reviewed journals. This introductory chapter serves to introduce the main topics and describe the structure of this thesis.

Chapter 2 describes the effect of thermal stressing on hydrothermally altered andesitic lavas from the Rotokawa Geothermal Field (Fig. 1.1). *This chapter serves as a preliminary study examining the petrophysical effects that varying peak temperatures (350 – 739 °C) in a 20 MPa water-saturated environment produce in (propylitic) hydrothermally altered Rotokawa andesite with subtly differing mineral assemblages* (Table 1.1). A strong contrast in pre- and post-treatment properties suggests that some physical rock properties are noticeably affected at these temperatures (e.g. porosity and permeability increase; Fig. 1.2).

Chapter 3 expands from the single-borehole samples of Chapter 2 by investigating the intact-rock properties of samples collected from four seasons of fieldwork at Pinnacle Ridge, Mt. Ruapehu (Fig. 1.1). There, a shallow magmatic intrusion and its corresponding advanced argillic hydrothermal system were exposed by glaciation ~10 *ka*. *This research investigates the geospatial relationship between the rock properties and distance to the heat source and finds that the intact-rock porosity, permeability, and strength of brecciated lava margins display a moderate correlation with distance to the host rock-intrusion contact* (Table 1.1). The relevance of this data is discussed and compared to data from previous rock-property studies. Implications for volcanic processes (e.g. seismic, eruptive, slope stability) are debated. A new geotechnical unit (i.e. hydrothermal vein material) is presented and a conceptual model of the geotechnical units surrounding a

small, shallow intrusion depicts the decreasing permeability in the altered volcanics and impermeable rock formed by the unaltered intrusion and hydrothermal vein material (Fig. 1.2).

Chapter 4 uses an auspicious sample block from Pinnacle Ridge to expand from Chapter 3 detailing how (intermediate and advanced argillic) alteration affects the deformation mode (i.e. the mechanical properties) of andesitic lava at varying effective confining pressures (Table 1.1). In this study, we conduct water-saturated triaxial testing on altered andesite cored from the same sample block of andesitic lava from Pinnacle Ridge. Some samples have only intermediate argillic alteration. Other samples have late-stage advanced argillic alteration superimposed on the early intermediate argillic alteration. By directly comparing these two stages of alteration from the same primary volcanics, we precisely depict the extent of weakening that advanced argillic alteration produces in its host rock. Moreover, the deformation mode of the andesite with only intermediate argillic alteration (i.e. dilatant) differs from that of the samples with advanced argillic alteration (i.e. compactant; Fig. 1.2). We then discuss the implications this has for permeability, pore pressure augmentation, and, thereby, volcanic processes (i.e. seismicity).

Chapter 5 adds discontinuity data of the geotechnical units from Pinnacle Ridge to the laboratory data presented in Chapter 3. *Chapter 5 attempts to answer the question concerning the effects a small, shallow intrusion on the discontinuities in a volcanic host rock mass* (Table 1.1). The discontinuities at Pinnacle Ridge are, in general, more closely spaced and have smoother surfaces inside the altered zone than outside the altered zone (Fig. 1.2). After considering the discontinuity characteristics, the altered rock masses have the potential to be the weakest rock masses in the ridge.

Chapter 6 combines the laboratory data of Chapter 3 and field data of Chapter 5 with newly presented triaxial deformation data for the geotechnical units at Pinnacle Ridge in order to model principal stress envelopes using the Generalised Hoek-Brown failure criterion. *Chapter 6 attempts to answer which rock masses have the highest potential for failure in the shallow hydrothermal system at Pinnacle Ridge and what the effects of varying pore pressure on the strength of rock masses are in a hydrothermal system.* Finite element models with varying pore pressure conclusively show that hydrothermal veining constitutes the weakest rock mass within the alteration halo (Fig. 1.2). Although unaltered brecciated lava margins are weaker rock masses, the higher permeability of the unaltered brecciated lava margins reduce the probability of pore pressure augmentation and, consequently, decrease the probability of slope instability. However, the weak nature and low permeability of hydrothermal vein material coupled with its cross-cutting orientation give the hydrothermal vein a substantial potential to destabilize an edifice-hosting hydrothermally alteration.

Chapter 7 summarizes the key points made by the other chapters (see Fig. 1.2) and presents ideas for future research (Table 1.1). Chapter 7 finishes with a description of the electronic appendices containing the data presented and discussed in Chapters 2 – 6. The appendices can be found in the electronic files accompanying this thesis.

Chapter	Questions	Specific Aim(s)
Chapter 2	*How does temperature affect petrophysical properties in (propylitic) hydrothermally altered andesite?*	Detail the petrophysical effects that varying peak temperatures (350 – 739 °C) at 20 MPa produces in hydrothermally altered Rotokawa andesite
Chapter 3	*How do rock properties change with distance to the intrusion in a shallow hydrothermal system?* *Measure the effect of confining pressure on the permeability of hydrothermally altered (advanced argillic) rocks?*	Characterise the mechanical and physical rock properties of the geotechnical units related to the emplacement of a small, shallow intrusion in a volcanic domain.
Chapter 4	*How does (intermediate argillic and advanced argillic) hydrothermal alteration affect the deformation mode of andesite?*	Identify the relevant pressure conditions for a change in brittle to ductile failure mode in argillic and advanced argillic altered andesites with a range of porosity.
Chapter 5	*Are the rock mechanical properties measured in the lab on cm scale cores applicable on outcrop scale?*	Characterise the discontinuity properties of the shallow hydrothermal system at Pinnacle Ridge Assign the rock mass properties of the intrusions at Pinnacle Ridge and the host rocks of the shallow hydrothermal system
Chapter 6	*What are the triaxial deformation characteristics of the geotechnical units associated with a shallow hydrothermal system?* *How likely is Pinnacle ridge to fail under present and past active conditions?*	Define the Generalised Hoek-Brown failure criterion parameters for the geotechnical units of Pinnacle Ridge associated with the shallow hydrothermal system. Asses the pore pressure influence on the rock mass strength of the geotechnical units associated with a hydrothermal system.
Chapter 7	*How do the previously presented works (Chapters 2 - 6) relate and what are the next topics of research?*	Discuss the relevance of the research presented in this thesis at a broader scale. Present topics of potential future research.

Table 1.1 Key research topics and specific aims of this thesis.

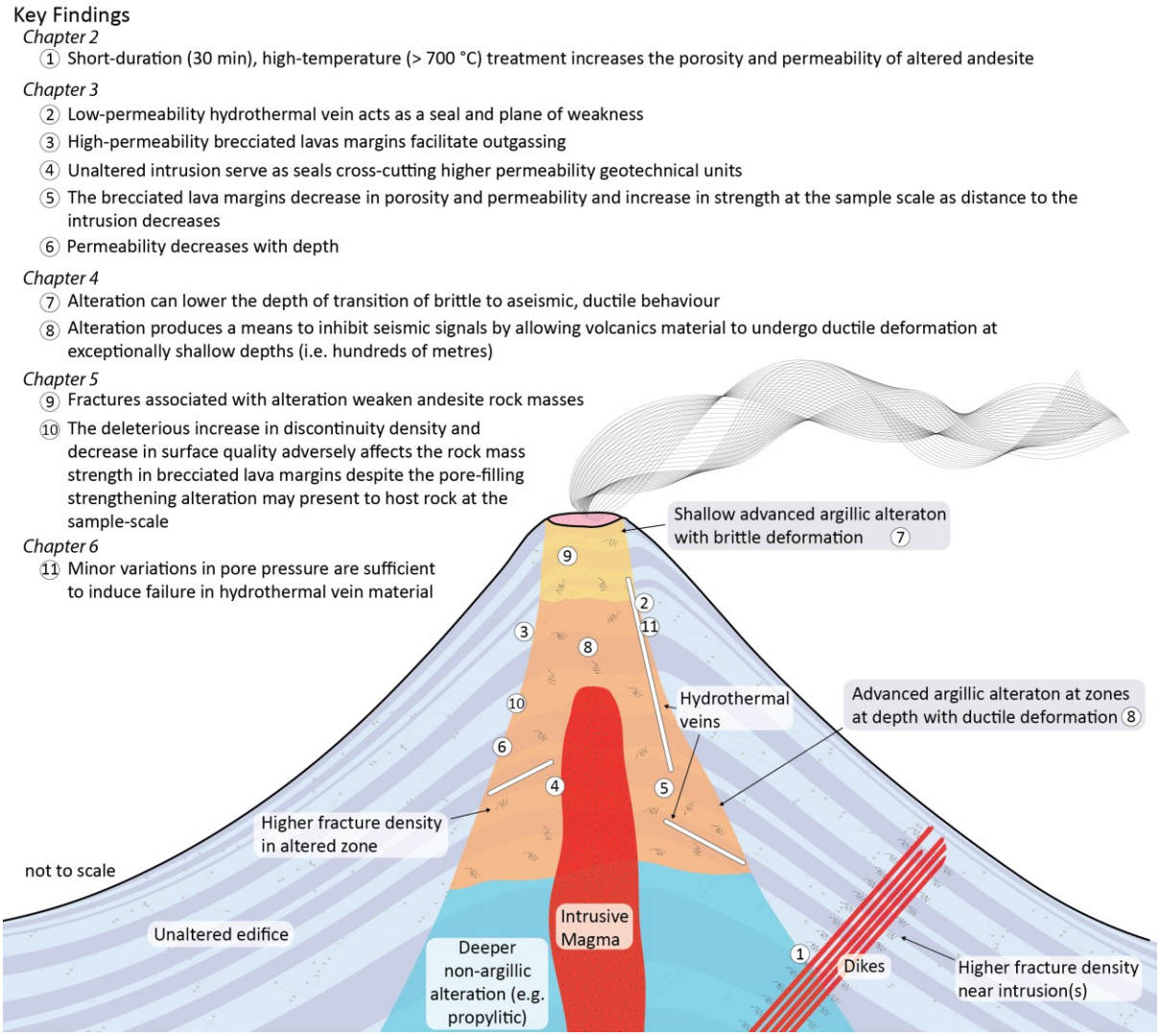

Figure 1.2 Key findings in dissertation. Major conclusions are provided by their respective chapters of the dissertation. For additional detail, see each respective chapter.

1.6 Scientific contributions arising from this work

Chapters 2 – 6 are written with the intention of publishing their material in peer-reviewed research journals. At the time of this submission of this thesis, Chapters 3 and 4 have been accepted for publication in the Journal of Volcanology and Geothermal Research, and Chapter 4 is in review for consideration in Geophysical Research Letters. The contents of Chapters 2 – 6 were presented at conferences (see list of journal articles and conference abstracts below).

1.6.1 Peer-reviewed journal articles

Mordensky, S. P., Villeneuve, M. C., Kennedy, B. M., Heap, M. J., Gravley, D. M., Farquharson, J. I., Reuschlé, T. (2018) Physical and mechanical property relationships of a shallow intrusion and volcanic host rock, Pinnacle Ridge, Mt. Ruapehu, New Zealand. *Journal of Volcanology and Geothermal Research* 359, 1-20. https://doi.org/10.1016/j.jvolgeores.2018.05.020

Mordensky, S. P., Villeneuve, M. C., Farquharson, J. I., Kennedy, B. M., Heap, M. J., Gravley, D. (2018) Rock mass properties and edifice strength data from Pinnacle Ridge, Mt. Ruapehu, New Zealand. *Journal of Volcanology and Geothermal Research* 367, 42-62. https://doi.org/10.1016/j.jvolgeores.2018.09.012

Mordensky, S. P., Heap, M. J., Kennedy, B. M., Villeneuve, M. C., Farquharson, J. I., Gravley, D. M. (In Review) Influence of alteration on the mechanical behavior and failure mode of andesitic lavas: implications for shallow seismicity and volcano monitoring. *Bulletin of Volcanology*.

1.6.2 Conference presentations

Mordensky, S. P., Kennedy, B. M., Villeneuve, M. C., Farquharson, J. I., Heap, M. J., Gravley, D. M. (2018) Considering scale (spatial and temporal) – the effect of intrusions on geomechanical properties of a volcanic host. Presentation at the Energy Straight from Magma Workshop on Krafla (Iceland) Magma Drilling, Wairakei, New Zealand.

Mordensky, S. P., Villeneuve, M. C., Kennedy, B. M., Gravley, D. M., Heap, M. J., Leonard, G., Farquharson, J. I., Reuschlé, T. (2017) Shallow Intrusions and Their Effects on Physical Properties in Volcanic Strata, Mt. Ruapehu, New Zealand. Presentation at the International Association of Volcanology and Chemistry of the Earth's Interior Annual Meeting, Portland, Oregon.

Mordensky, S.P., Kennedy, B. M., Heap, M. J., Villeneuve, M. C., Gravley, D. M., Farquharson, J. I., Leonard, G. (2017) Rock Properties and Jointing Around Shallow Intrusions, Mt. Ruapehu. Presentation at American Association of Petroleum Geologists Workshop. Oamaru, New Zealand.

Mordensky, S. P., Kennedy, B. M., Villeneuve, M. C., Gravley, D. M., Heap, M. J., Farquharson, J. I., Leonard, G. (2016) Rock Strength, Permeability, and Jointing Around Shallow Intrusions, Mt. Ruapehu. Presentation at the Geological Society of New Zealand Annual National Meeting. Wanaka, New Zealand.

Mordensky, S. P., Kennedy, B. M., Villeneuve, M. C., Gravley, D. M., Heap, M. J., Farquharson, J. I., Leonard, G. (2016) Mechanical Properties of a Fossil Geothermal System. Presentation at the Society of Exploration Geophysicists Workshop. Hilo, Hawaii.

1.7 Thesis originality

For completeness, the co-authors of their associated manuscript are listed at the start of each chapter. Having collected (except for the simultaneous thermal and X-ray diffraction analyses for Chapter 2 and X-ray diffraction analysis, Raman spectroscopy, and scanning electron spectroscopy analyses for Chapter 4), processed, and interpreted the data, drafted the manuscripts, and served as the nexus for all related communication, I am the first author of these publications. I cannot thank my co-authors enough for their

collaboration and discussions; however, I emphasize that the material presented herein in the product of my work and research.

The central ideas for this research came from conversations between Ben Kennedy, Marlène Villeneuve, Mike Heap, and Paul Siratovich. More specifically, Paul Siratovich presented the idea and opportunity to study the effects of thermal stress on cored altered Rotokawa Andesite from the Rotokawa Geothermal Field (Chapter 2) with the co-operation of Mercury Ltd. Paul Ashwell provided an introduction to the use of the high-pressure, high-temperature bomb (dubbed the *Magma Brewery*) at the University of Canterbury. Yan Lavallée completed simultaneous thermal analysis at the University of Liverpool (England) and provided instruction on how to interpret the data. Marc Reichow completed X-ray diffraction analysis and mineral identification from this data at the University of Leicester (England). Hans Albert Gilg completed quantitative X-ray diffraction analysis, Raman spectroscopy, scanning electron spectroscopy, and mineral identification from these techniques at the Technische Universität München (Germany).

The core concepts approached at Pinnacle Ridge (Chapters 3, 4, 5, and 6) were developed by Ben Kennedy, Marlène Villeneuve, Darren Gravley, Mike Heap, and Paul Siratovich from years of leading groups on and around Mt. Ruapehu. Ben Kennedy oversaw and guided my coordination with varying government (GNS, DOC, USGS) and academic institutions (University of Canterbury, Université de Strasbourg, University of Liverpool, University of Leicester, Technische Universität München). Marlène Villeneuve, Ben Kennedy, Jamie Farquharson, Rosie Cole, Stephanie Ferreira dos Santos, and *"Corpse Grinder"* assisted with the field collection of samples, scanline data, and rock mass classification. Isabelle Chambefort and Mark Simpson assisted with the collection and understanding of Terraspec data. Marlène Villeneuve, Mike Heap, Jamie Farquharson, and Thierry Reuschlé provided valuable insight and understanding of not just the principles of the rock-property testing equipment but also the necessary practicality to complete the analyses on schedule. Heidy Mader and at least two anonymous reviewers provided valuable feedback during the peer-review of Chapters 3 and 5 in the Journal of Volcanology and Geothermal Research. Rebecca Carey and at least two anonymous reviewers provided valuable feedback during the peer-review of Chapter 4 for Geophysical Research Letters. Discussions between me, my supervisors (Marlène Villeneuve, Ben Kennedy, Darren Gravley), and the other co-authors of these manuscripts (Mike Heap, Jamie Farquharson, Thierry Reuschlé, Marc Reichow, Yan Lavallée, Paul Siratovich, Hans Albert Gilg, and Joe Struthers) helped refine the form of the ideas presented in these works. Although Jim Cole did not serve as an official supervisor for this work in an official capacity, his

eagerness and willingness to provide guidance at many stages throughout these works improved the quality of this thesis and my perspective as a geoscientist. The University of Canterbury technicians, Rob Spiers, Cathy Higgins, Sarah Pope, Matt Cockcroft, Sacha Baldwin, and Anekant Wandres provided assistance (and untold patience) in the technical use of field and lab equipment. This thesis also benefited from conservations with Lauren Schaefer, Cécile Massiot, Stefan Cook, Romy Ridl, Sophie Hill, Alan Bishoff, Elodie Saubin, Andrea Barrier, Gilles Seropian, Janina Gillies, Dale Cusack, Stephanie Gates, and Carlos Kazianis.

1.8 References

Adam, L., & Otheim, T. (2013). Elastic laboratory measurements and modeling of saturated basalts. *Journal of Geophysical Research: Solid Earth, 118*(3), 840-851. doi:10.1002/jgrb.50090.

Adam, L., van Wijk, K., Otheim, T., & Batzle, M. (2013). Changes in elastic wave velocity and rock microstructure due to basalt-CO2-water reactions. *Journal of Geophysical Research: Solid Earth, 118*(8), 4039-4047. doi:10.1002/jgrb.50302.

Adelinet, M., Fortin, J., Schubnel, A., & Guéguen, Y. (2013). Deformation modes in an Icelandic basalt: From brittle failure to localized deformation bands. *Journal of Volcanology and Geothermal Research, 255*, 15-25. doi:10.1016/j.jvolgeores.2013.01.011.

Al-Harthi, A. A., Al-Amri, R. M., & Shehata, W. M. (1999). The porosity and engineering properties of vesicular basalt in Saudi Arabia. *Engineering Geology, 54*(3-4), 313-320. doi:10.1016/s0013-7952(99)00050-2.

Apuani, T., Corazzato, C., Cancelli, A., & Tibaldi, A. (2005). Physical and mechanical properties of rock masses at Stromboli: a dataset for volcano instability evaluation. *Bulletin of Engineering Geology and the Environment, 64*, 419-431.

Ayling, M. R., Meredith, P. G., & Murrell, S. A. F. (1995). Microcracking during triaxial deformation of porous rocks monitored by changes in rock physical properties, I. Elastic-wave propagation measurements on dry rocks. *Tectonophysics, 245*(3-4), 205-221. doi:10.1016/0040-1951(94)00235-2.

Bal'shin, M. Y. (1949). Relation of mechanical properties of powder metals and their porosity and the ultimate properties of porous metal-ceramic materials. *Akad. Nauk SSSR Doklady, 67*, 831-834.

Balakshrina, S. (1957). Elastic behaviour of rocks. *Current Science, 26*(12), 377-379.

Baud, P., Meredith, P., & Townend, E. (2012). Permeability evolution during triaxial compaction of an anisotropic porous sandstone. *J. Geophys. Res., 117*(B5), n/a-n/a. doi:10.1029/2012jb009176.

Böker, H. (1915). Die mechanik der bleibenden formänderung in kristallinisch aufgebauten Körpern. *Ver. Deut. Ing. Mitt. Forsch., 175*(1-51).

Brace, W. F. (1964). State of Stress in Earth's Crust. 111.

Brace, W. F., Paulding, B., & Scholz, C. (1966). Dilatancy in the fracture of crystalline rocks. *Journal of Geophysical Research, 71*, 3939-3953.

Browne, P. R. L. (1978). Hydrothermal Alteration in Active Geothermal Fields. *Annu. Rev. Earth Planet. Sci., 6*(1), 229-248. doi:10.1146/annurev.ea.06.050178.001305.

Carranza, J. (2005). Introduction to Ore-forming Processes by Laurence Robb, Blackwell Publishing, Oxford, 2004. 373 pp. 32.50 (paperback). ISBN 0-632-06378. *Geochemistry: Exploration, Environment, Analysis, 5*(2), 190-190. doi:10.1144/1467-7873/05-073.

Casey, M., Ebinger, C., Keir, D., Gloaguen, R., & Mohamed, F. (2006). Strain accomodation in transitional rifts: extension by magma intrusion and faulting in Ethiopian rift magmatic segments. *Geological Society, London, Special Publications, 259*, 143-163. doi:10.1144/GSL.SP.2006.259.01.13.

Cathles, L. M., Erendi, H. J., & Barrie, T. (1997). How long can a hydrothermal system be sustained by a single intrusive event. *Economic Geology, 92*, 766-771. doi:0361-0128/97/1946/766-65.

Chaki, S., Takarli, M., & Agbodjan, W. P. (2008). Influence of thermal damage on physical properties of a granite rock: Porosity, permeability and ultrasonic wave evolutions. *Construction and Building Materials, 22*(7), 1456-1461. doi:10.1016/j.conbuildmat.2007.04.002.

Chambefort, I., Lewis, B., Wilson, C. J. N., Rae, A. J., Coutts, C., Bignall, G., & Ireland, T. R. (2014). Stratigraphy and structure of the Ngatamariki geothermal system from new zircon U–Pb geochronology: implications for Taupo Volcanic Zone evolution. *Journal of Volcanology and Geothermal Research, 274*, 51-70. doi:10.1016/j.jvolgeores.2014.01.015.

Christenson, B. W., Mroczek, E. K., Kennedy, B. M., Van Soest, M. C., Stewart, M. K., & Lyon, G. (2002). Ohaaki reservoir chemistry: Characteristics of an arc-type hydrothermal system in the Taupo Volcanic Zone, New Zealand. *Journal of Volcanology and Geothermal Research, 115*(1-2), 53-82. doi:10.1016/S0377-0273(01)00309-2.

Cole, J. (1990). Structural control and origin of volcanism in the Taupo Volcanic Zone, New Zealand. *Bulletin of Volcanology*, 445-459. doi:10.1007/BF00268925.

Corrado, S., Aldega, L., Celano, A. S., De Benedetti, A. A., & Giordano, G. (2014). Cap rock efficiency and fluid circulation of natural hydrothermal systems by means of XRD on clay minerals (Sutri, Northern Latium, Italy). *Geothermics, 50*, 180-188. doi:10.1016/j.geothermics.2013.09.011.

Crowley, J. K., & Zimbelman, D. R. (1997). Mapping hydrothermally altered rocks on Mount Rainer, Washington, with airborne visible/infrared imaging spectrometer (AVIRS) data. *Geology, 25*(6), 559-562.

Cumming, W. (2009, February). *Geothermal resource conceptual models using surface exploration data.* Paper presented at the Thirty-Fourth Workshop on Geothermal Reservoir Engineering, Standford Univesity, Californa.

David, C., Wong, T.-F., Zhu, W., & Zhang, J. (1994). Laboratory measurement of compaction-induced permeability change in porous rocks: Implications for the generation and maintenance of pore pressure excess in the crust. *PAGEOPH, 143*(1-3), 425-456. doi:10.1007/bf00874337.

Davis, J. L., & Annan, A. P. (1989). Ground-penetrating radar for high-resolution mapping of soil and rock stratigraphy. *Geophysical Prospecting, 37*(5), 531-551.

Day, S. J. (1996). Hydrothermal pore fluid pressure and the stability of porous, permeable volcanoes. *Geological Society, London, Special Publications, 110*(1), 77-93. doi:10.1144/gsl.sp.1996.110.01.06.

del Potro, R., & Hürlimann, M. (2008). Geotechnical classification and characterisation of materials for stability analyses of large volcanic slopes. *Engineering Geology, 98*(1-2), 1-17. doi:10.1016/j.enggeo.2007.11.007.

Deuchar, J. (1823). On the porosity of glass and siliceous bodies. *American Journal of Science and Arts, 7*(1), 192.

Dunn, D. E., La Fountain, L. J., & jackson, R. E. (1973). Porosity dependence and mechanism of brittle fracture in sandstones. *Journal of Geophysical Research, 78*, 2403-2417.

Esmaeily, D., Afshooni, S. Z., Mirnejad, H., & Rashidnejad-e-Omran, N. (2012). Mass changes during hydrothermal alteration associated with gold mineralization in the Astaneh granitoid rocks, western Iran. *Geochemistry: Exploration, Environment, Analysis, 12*(2), 161-175. doi:10.1144/1467-7873/10-mindep-052.

Faulkner, D. R. (2006). PATERSON, M. S. & WONG T.-F. 2005. Experimental Rock Deformation – The Brittle Field, 2nd ed. x + 348 pp. Berlin, Heidelberg, New York: Springer-Verlag. Price Euros 89.95

(+ VAT at local rate), SFr 152.50, £69, US $119 (hard covers). ISBN 3 540 24023 3. *Geological Magazine, 143*(06), 934. doi:10.1017/s0016756806242973.

Ferry, J. M. (1979). Reaction mechanisms, physical conditions, and mass transfer during hydrothermal alteration of mica and feldspar in granitic rocks from south-central Maine, USA. *Contr. Mineral. and Petrol., 68*(2), 125-139. doi:10.1007/bf00371895.

Finizola, A., Sortino, F., Lénat, J.-F., & Valenza, M. (2002). Fluid circulation at Stromboli volcano (Aeolian Islands, Italy) from self-potential and CO2 surveys. *Journal of Volcanology and Geothermal Research, 116*(1-2), 1-18. doi:10.1016/s0377-0273(01)00327-4.

Fortin, J., Schubnel, A., & Guéguen, Y. (2005). Elastic wave velocities and permeability evolution during compaction of Bleurswiller sandstone. *International Journal of Rock Mechanics and Mining Sciences, 42*(7-8), 873-889. doi:10.1016/j.ijrmms.2005.05.002.

Frank, D. (1995). Surficial extent and conceptual model of a hydrothermal system at Mount Rainier, Washington. *Journal of Volcanology and Geothermal Research, 65*(1-2), 51-80. doi:10.1016/0377-0273(94)00081-q.

Fraser, H. J. (1935). Experimental Study of the Porosity and Permeability of Clastic Sediments. *The Journal of Geology, 43*(8), 910-1010.

Galland, O., de Bremond d'Ars, J., Cobbold, P. R., & Hallot, E. (2003). Physical models of magmatic intrusion during thrusting. *Terra Nova, 15*(6), 405-409. doi:10.1046/j.1365-3121.2003.00512.x.

Galland, O., Planke, S., Neumann, E., & Malthe-Sørenssen, A. (2009). Experimental modelling of shallow magma emplacement: application to saucer-shaped intrusions. *Earth and Planetary Science Letters, 277*, 373-383.

Giggenbach, W. F. (1984). Mass transfer in hydrothermal alteration systems—A conceptual approach. *Geochimica et Cosmochimica Acta, 48*(12), 2693-2711. doi:10.1016/0016-7037(84)90317-x.

Giggenbach, W. F., & Sheppard, D. S. (1989). Variations in the temperature and chemistry of White Island fumarole discharges. *N.Z. Geological Survey Bulletin, 103*(1972-1985), 119-126.

Griffith, A. A. (1921). The phenomena of rupture and flow in solids. *Phil. Trans. Roy. Soc. London, 221*, 163.

Hackett, W. R. (1985). *Geology and Petrology of Ruapehu Volcano and Related Vents.* (PhD Thesis), Victoria University of Wellington, Wellington, New Zealand.

Hase, H., Hashimoto, T., Sakanaka, S., Kanda, W., & Tanaka, Y. (2005). Hydrothermal system beneath Aso volcano as inferred from self-potential mapping and resistivity structure. *Journal of Volcanology and Geothermal Research, 143*(4), 259-277. doi:10.1016/j.jvolgeores.2004.12.005.

Heap, M. J., Baud, P., Meredith, P. G., Vinciguerra, S., & Reuschlé, T. (2014a). The permeability and elastic moduli of tuff from Campi Flegrei, Italy: implications for ground deformation modelling. *Solid Earth, 5*(1), 25-44. doi:10.5194/se-5-25-2014.

Heap, M. J., Farquharson, J., Baud, P., Lavallée, Y., & Reuschlé, T. (2015a). Fracture and compaction of andesite in a volcanic edifice. *Bulletin of Volcanology, 77*(55). doi:10.1007/s00445-015-0938-7.

Heap, M. J., & Kennedy, B. (2016). Exploring the scale-dependent permeability of fractured andesite. *Earth and Planetary Science Letters, 447*, 139-150.

Heap, M. J., Kennedy, B. M., Pernin, N., Jacquemard, L., Baud, P., Farquharson, J. I., et al. (2015b). Mechanical behaviour and failure modes in the Whakaari (White Island volcano) hydrothermal system, New Zealand. *Journal of Volcanology and Geothermal Research, 295*, 26-42. doi:10.1016/j.jvolgeores.2015.02.012.

Heap, M. J., Lavallée, Y., Petrakova, L., Baud, P., Reuschlé, T., Varley, N. R., & Dingwell, D. B. (2014b). Microstructural controls on the physical and mechanical properties of edifice-forming andesites at Volcán de Colima, Mexico. *Journal of Geophysical Research: Solid Earth, 119*(4), 2925-2963. doi:10.1002/2013JB010521.

Heard, H. C. (1960). Transition from brittle failure to ductile flow in Solenhofen Limestone as a function of temperature, confining pressure, and interstitial fluid pressure. *Geological Society of America Memoirs, 79*, 193-216.

Henley, R. W., & Ellis, A. J. (1983). Geothermal systems ancient and modern: a geochemical review. *Earth-Science Reviews, 19*, 1-50.

Henneberger, R. C., & Browne, P. R. L. (1988). Hydrothermal alteration and evolution of the Ohakuri hydrothermal system, Taupo volcanic zone, New Zealand. *Journal of Volcanology and Geothermal Research, 34*(3-4), 211-231. doi:10.1016/0377-0273(88)90034-0.

Hochstein, M. P. (1995). Crustal heat transfer in the Taupo Volcanic Zone (New Zealand): comparison with other volcanic arcs and explanatory heat source models. *Journal of Volcanology and Geothermal Research, 68*, 117-151. doi:10.1016/0377-0273(95)00010-R.

Hoek, E. (1968). *Brittle Failure of Rock*. London: Wiley and Sons.

Hoek, E., & Brown, E. T. (1980). Empirical strength criterion for rock masses. *Journal of Geotechnical and Geoenvironmental Engineering, 106*, 1013-1035.

Hurwitz, S., Ingebritsen, S. E., & Sorey, M. L. (2002). Episodic thermal perturbations associated with groundwater flow: an example from Kilauea Volcano, Hawaii. *Journal of Geophysical Research, 107*(B11), ECV 13-11-ECV 13-10. doi:10.1029/2001jb001654.

Kanakiya, S., Adam, L., Esteban, L., Rowe, M., & Shane, P. (2017). Dissolution and secondary mineral precipitation in basalts due to reactions with carbonic acid. *Journal of Geophysical Research, 122*(6), 4312-4327.

Keating, G. N., Valentine, G. A., Krier, D. J., & Perry, F. V. (2007). Shallow plumbing systems for small-volume basaltic volcanoes. *Bulletin of Volcanology, 70*(5), 563-582. doi:10.1007/s00445-007-0154-1.

Kennedy, L. A., Russell, J. K., & Nelles, E. (2009). Origins of Mount St. Helens cataclasites: Experimental insights. *American Mineralogist, 94*(7), 995-1004. doi:10.2138/am.2009.3129.

Kissling, W. M., & Weir, G. J. (2005). The spatial distribution of the geothermal fields in the Taupo Volcanic Zone, New Zealand. *Journal of Volcanology and Geothermal Research, 145*(1-2), 136-150. doi:10.1016/j.jvolgeores.2005.01.006.

Knudsen, F. P., Parker, H. S., & Burdick, M. D. (1960). Flexural strength of specimens prepared from several uranium dioxide powders; its dependenceo n porosity and grain size and the influence of additions of titania. *Am. Ceramic Soc. Jour., 43*, 641-647.

Lacabanne, W. D. (1960). Porosity-permeability characteristics of sedimentary rocks. *Proceedings of the Minnesota Academy of Science, 25-26*, 270-280.

Lama, R. D., & Vutukuri, V. S. (1978). *Handbook on Mechanical Properties of Rocks* (Vol. 2). Clausthal, Germany: Editor Trans Tech Publications.

Lipman. (2000). Calderas. In H. Sigurdsson (Ed.), *Encyclopedia of Volcanoes* (pp. 651-652). San Diego, California: Academic Press.

Loaiza, S., Fortin, J., Schubnel, A., Gueguen, Y., Vinciguerra, S., & Moreira, M. (2012). Mechanical behavior and localized failure modes in a porous basalt from the Azores. *Geophys. Res. Lett., 39*(19), n/a-n/a. doi:10.1029/2012gl053218.

Lutz, S. J., Hickman, S., Davatzes, N., Zemach, E., Drakos, P., & Robertson-Tait, A. (2010, February). *Rock mechanical testing and petrological analysis in support of well stimulation activities at the desert peak geothermal field, Nevada.* Paper presented at the 37th Workshop on Geo- thermal Reservoir Engineering, Stanford, California, USA.

McNamara, D., Sewell, S., Buscarlet, E., & Wallis, I. C. (2016). Micromechanics of brittle faulting and cataclastic flow in Berea sandstone. *Journal of Structural Geology, 18*, 1-16.

Moon, V., Bradshaw, J., Smith, R., & de Lange, W. (2005). Geotechnical characterization of stratocone crater wall sequences, White Island volcano, New Zealand. *Engineering Geology, 81*, 146-178.

Nara, Y., Meredith, P. G., Yoneda, T., & Kaneko, K. (2011). Influence of macrofractures and microfractures on permeability and elastic wave velocities in basalt at elevated pressure. *Tectonophysics, 503*(1-2), 52-59. doi:10.1016/j.tecto.2010.09.027.

Nemčok, M., Moore, J. N., Christensen, C., Allis, R., Powell, T., Murray, B., & Nash, G. (2007). Controls on the Karaha–Telaga Bodas geothermal reservoir, Indonesia. *Geothermics, 36*(1), 9-46. doi:10.1016/j.geothermics.2006.09.005.

Ogawa, Y., Matsushima, N., Oshima, H., Takakura, S., Utsugi, M., Hirano, K., et al. (1998). A resistivity cross-section of Usu volcano, Hokkaido, Japan, by audiomagnetotelluric soundings. *Earth Planets Space, 50*, 339-346.

Palchik, V. (1999). Influence of porosity and elastic modulus on uniaxial compressive strength in soft brittle porous sandstones. *Rock Mech Rock Eng, 32*(4), 303-309.

Planke, S. (1999). Seismic characteristics of basalt extrusive and intrusive rocks. *The Leading Edge, 18*(3), 342-348. doi:10.1190/1.1438289.

Pola, A., Crosta, G., Fusi, N., Barberini, V., & Norini, G. (2012). Influence of alteration on physical properties of volcanic rocks. *Tectonophysics, 566-567*, 67-86. doi:10.1016/j.tecto.2012.07.017.

Pola, A., Crosta, G. B., Fusi, N., & Castellanza, R. (2014). General characterization of the mechanical behaviour of different volcanic rocks with respect to alteration. *Engineering Geology, 169*, 1-13. doi:10.1016/j.enggeo.2013.11.011.

Price, R. C., Gamble, J. A., Smith, I. E. M., Maas, R., Waight, T., Stewart, R. B., & Woodhead, J. D. (2012). The anatomy of an andesite volcano: a time-stratigraphic study of andesite petrogenesis and crustal evolution at Ruapehu volcano, New Zealand. *Journal of Petrology, 42*(10), 2139-2189.

Rae, A. (2007). *Rotokawa Geology and Geophysics*. Retrieved from

Rajabzadeh, M. A., Moosavinasab, Z., & Rakhshandehroo, G. (2011). Effects of Rock Classes and Porosity on the Relation between Uniaxial Compressive Strength and Some Rock Properties for Carbonate Rocks. *Rock Mech Rock Eng, 45*(1), 113-122. doi:10.1007/s00603-011-0169-y.

Rejeki, S., Hadi, J., & Suhayati, I. (2005, April). *Porosity study for detail reservoir characterization in Darajat Geothermal Field, West Java, Indonesia.* Paper presented at the World Geothermal Congress, Antalya, Turkey.

Rissmann, C., Nicol, A., Cole, J., Kennedy, B., Fairley, J., Christenson, B., et al. (2011). Fluid flow associated with silicic lava domes and faults, Ohaaki hydrothermal field, New Zealand. *Journal of Volcanology and Geothermal Research, 204*(1-4), 12-26. doi:10.1016/j.jvolgeores.2011.05.002.

Rowland, J. V., & Sibson, R. H. (2001). Extensional fault kinematics within the Taupo Volcanic Zone, New Zealand: soft-linked segmentation of a continental rift system. *New Zealand Journal of Geology and Geophysics, 44*(2), 271-283. doi:10.1080/00288306.2001.9514938.

Rowland, J. V., & Sibson, R. H. (2004). Structural controls on hydrothermal flow in a segmented rift system, Taupo Volcanic Zone, New Zealand. *Geofluids, 4*(4), 259-283. doi:10.1111/j.1468-8123.2004.00091.x.

Rowland, J. V., & Simmons, S. F. (2012). Hydrologic, magmatic, and tectonic controls on hydrothermal flow, Taupo Volcanic Zone, New Zealand: Implications for the formation of epithermal vein deposits. *Economic Geology, 107*(3), 427-457. doi:10.2113/econgeo.107.3.427.

Rozos, D., & Koukis, G. (1986). An investigation of the mineralogical, physical and mechanical properties of greek laterites. *Bulletin of the International Association of Engineering Geology, 33*, 91-96.

Rubey, W. W. (1927). The effect of gravitational compaction on the structure of sedimentary rocks. *Bulletin of AAPG, 11*, 624.

Rutherford, H. E., & Lucas, J. R. (1962). Evaluation of specific rock properties by ultrasonic principles. *Transactions of the Society of Mining Engineers of American Institute of Mining, Metallurgical and Petroleum Engineers Incorporated, 223*(3), 319-324.

Ryan, A. G., Friedlander, E. A., Russell, J. K., Heap, M. J., & Kennedy, L. A. (2018). Hot pressing in conduit faults during lava dome extrusion: Insights from Mount St. Helens 2004-2008. *Earth and Planetary Science Letters, 482*, 171-180.

Rye, R. O. (1993). The evolution of magmatic fluids in the epithermal environment: the stable isotope perspective. *Economic Geology, 88*(3), 733-753.

Sigurdsson, H., Houghton, B. F., McNutt, S. R., Rymer, H., Stix, J., & McBirney, A. R. (2000). Encyclopedia of Volcanoes. *Physics Today, 53*(10), 84-85. doi:10.1063/1.1325206.

Siratovich, P. A., Heap, M. J., Villeneuve, M. C., Cole, J., Kennedy, B., Davidson, J. P., & Reuschlé, T. (2016). Mechanical behaviour of the Rotokawa Andesites (New Zealand): insight into permeability evolution and stress-induced behaviour in an actively utilised geothermal reservoir. *Geothermics, 64*, 163-179. doi:10.1016/j.geothermics.2016.05.005.

Siratovich, P. A., Heap, M. J., Villeneuve, M. C., Cole, J. W., & Reuschlé, T. (2014). Physical property relationships of the Rotokawa Andesite, a significant geothermal reservoir rock in the Taupo Volcanic Zone, New Zealand. *Geothermal Energy, 2*(1), 10-10. doi:10.1186/s40517-014-0010-4.

Stimac, J., Nordquist, G., Suminar, A., & Sirad-Azwar, L. (2008). An overview of the Awibengkok geothermal system, Indonesia. *Geothermics, 37*(3), 300-331. doi:10.1016/j.geothermics.2008.04.004.

Tugrul, A., & Gurpinar, O. (1997). The Effect of Chemical Weathering on the Engineering Properties of Eocene Basalts in Northeastern Turkey. *Environmental & Engineering Geoscience, III*(2), 225-234. doi:10.2113/gseegeosci.iii.2.225.

Ulusay, R., Tureli, K., & Ider, M. H. (1994). Prediction of engineering properties of a selected litharenite sandstone from its petrographic characteristics using correlation and multivariate statistical techniques. *Engineering Geology, 38*(1-2), 135-157.

Valentine, G., & Krogh, K. (2006). Emplacement of shallow dikes and sills beneath a small basaltic volcanic center – the role of pre-existing structure (Paiute Ridge, southern Nevada, USA). *Earth and Planetary Science Letters, 246*(3-4), 217-230. doi:10.1016/j.epsl.2006.04.031.

Vigneresse, J.-L., Tikoff, B., & Améglio, L. (1999). Modification of the regional stress field by magma intrusion and formation of tabular granitic plutons. *Tectonophysics, 302*(3-4), 203-224. doi:10.1016/S0040-1951(98)00285-6.

Vinciguerra, S., Trovato, C., Meredith, P. G., & Benson, P. M. (2005). Relating seismic velocities, thermal cracking and permeability in Mt. Etna and Iceland basalts. *International Journal of Rock Mechanics and Mining Sciences, 42*(7-8), 900-910. doi:10.1016/j.ijrmms.2005.05.022.

Walsh, J. B. (1965a). The effect of cracks in rocks on Poisson's ratio. *J. Geophys. Res., 70*(20), 5249-5257. doi:10.1029/jz070i020p05249.

Walsh, J. B. (1965b). The effect of cracks on the compressibility of rock. *J. Geophys. Res., 70*(2), 381-389. doi:10.1029/jz070i002p00381.

Wilson, C. J. N., Houghton, B. F., McWilliams, M. O., Lanphere, M. A., Weaver, S. D., & Briggs, R. M. (1995). Volcanic and structural evolution of Taupo Volcanic Zone, New Zealand: a review. *Journal of Volcanology and Geothermal Research, 68*(1-3), 1-28. doi:10.1016/0377-0273(95)00006-g.

Wong, T.-f., & Baud, P. (2012). The brittle-ductile transition in porous rock: A review. *Journal of Structural Geology, 44*, 25-53. doi:10.1016/j.jsg.2012.07.010.

Wyering, L. D., Villeneuve, M. C., Wallis, I. C., Siratovich, P. A., Kennedy, B. M., & Gravley, D. M. (2015). The development and application of the alteration strength index equation. *Engineering Geology, 199*, 48-61. doi:10.1016/j.enggeo.2015.10.003.

Wyering, L. D., Villeneuve, M. C., Wallis, I. C., Siratovich, P. A., Kennedy, B. M., Gravley, D. M., & Cant, J. L. (2014). Mechanical and physical properties of hydrothermally altered rocks, Taupo Volcanic Zone, New Zealand. *Journal of Volcanology and Geothermal Research, 288*, 76-93. doi:10.1016/j.jvolgeores.2014.10.008.

Wyllie, M. R. J., Gregory, A. R., & Gardner, G. H. F. (1958). An Experimental Investigation of factors affecting elastic wave velocities in porous media. *Geophysics, 23*(3), 459-493. doi:10.1190/1.1438493.

Wyllie, M. R. J., Gregory, A. R., & Gardner, L. W. (1956). Elastic wave velocities in heterogeneous and porous media. *Geophysics, 21*(1), 41-70.

Zhu, W., Baud, P., Vinciguerra, S., & Wong, T.-f. (2011). Micromechanics of brittle faulting and cataclastic flow in Alban Hills tuff. *J. Geophys. Res., 116*(B6). doi:10.1029/2010jb008046.

Zhu, W., & Wong, T.-f. (1997). The transition from brittle faulting to cataclastic flow: Permeability evolution. *J. Geophys. Res., 102*(B2), 3027-3041. doi:10.1029/96jb03282.

Chapter 2 Preamble

In Chapter 1, I introduce the overarching theme of this thesis (i.e. the investigation of the influence magmatic intrusions have on the physical and mechanical properties of volcanic host rock) by providing a brief context of intrusions in a volcanic setting and providing some questions that remain unanswered regarding the intrusions and their host rock. In Chapter 2, I describe a laboratory study in which I thermally stress hydrothermally altered andesite from the Rotokawa Geothermal Field (Fig. 1) to simulate the short-term, high-temperature (350 – 739 °C) influence of magmatic intrusions on altered host rock (Fig. 1). This investigation serves as a preliminary study to observe the effects a nearby high-temperature source may have on altered materials.

Chapter 2 has been written for submission to the *Journal of Volcanology and Geothermal Research*.

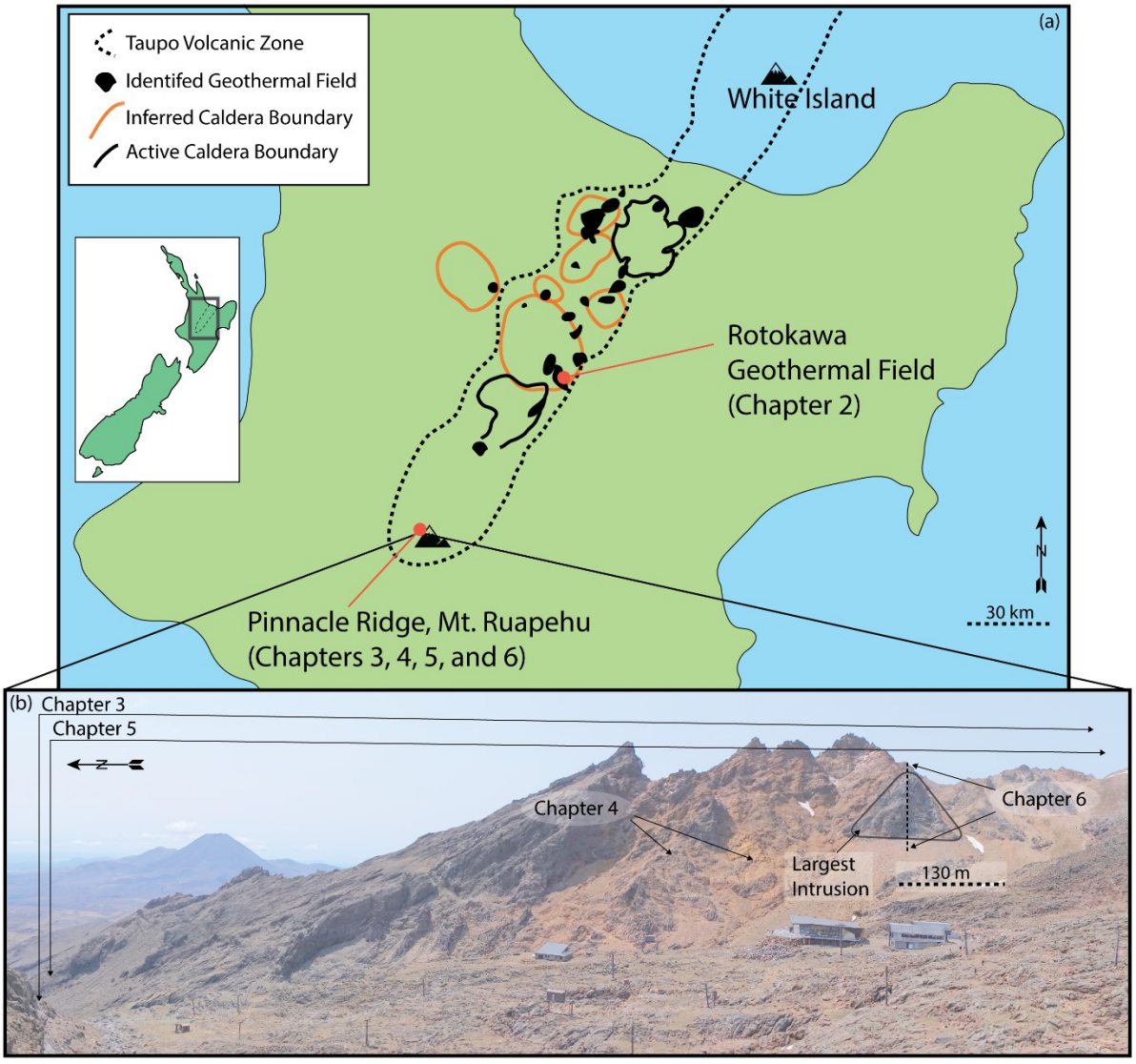

Figure 1. Primary site locations specific to the research presented in this study. (a) Sites of the two hydrothermal systems in New Zealand. (b) Sites specific to Chapters 3 – 6 at Pinnacle Ridge. Solid black polygon marks boundary of the largest young intrusion. Scale is approximate.

Chapter 2

Increasing the permeability of hydrothermally altered andesite by transitory thermal stressing

S. P. Mordensky[1]; B. M. Kennedy[1]; M. C. Villeneuve[1]; Y. Lavallée[2]; M. K. Reichow[3]; P. A. Wallace[2]; P. A. Siratovich[4]; D. M. Gravley[1]

[1]Department of Geological Sciences, University of Canterbury, Private Bag 4800, Christchurch 8140, New Zealand

[2]Earth, Ocean and Ecological Sciences, University of Liverpool, Liverpool L69 3GP, UK

[3]School of Geography, Geology and the Environment, University of Leicester, University Road, Leicester, LE1 7RH, UK

[4]Upflow Ltd., 3 Winston St., Acacia Bay, Taupo 3330, New Zealand

Abstract

Changes in the permeability of hydrothermal systems can affect fluid flow and impact geological processes, geohazards, and geothermal energy production. Many factors influence the permeability of materials, including porosity, pore connectivity, tortuosity, lithostatic stress, and pore pressure. In hydrothermal systems, high-temperature heat sources drive fluid convection through the porous network of reservoir rocks; yet, thermal fluctuations may induce microfracturing and jeopardise the mineralogical stability of the reservoir rock, thus modifying the fluid pathways. This study describes the results of short-duration (30-minu) thermal stressing events on two suites of hydrothermally altered andesite hosting two distinct propylitic alteration assemblages (i.e. plagioclase-clinochlore-calcite-quartz and plagioclase-clinozoisite-quartz-clinochlore) from the Rotokawa Geothermal Field. We use a low thermal gradient (< 2 °C/min) in an H_2O-saturated, 20-MPa environment to constrain changes in reservoir petrophysical properties associated with transitory thermal phenomena between 350 °C to 739 °C before chemical equilibrium is achieved. We find that as the treatment temperature increases, the mass of the samples is reduced through mineral breakdown from circulating fluids, thereby increasing porosity and permeability. These effects were greater in the altered plagioclase-clinochlore-calcite-quartz andesite than in the altered plagioclase-

clinozoisite-quartz-clinochlore andesite. Energy-dispersive X-ray spectroscopy finds microfracturing is responsible for these changes at lower temperatures (e.g. 400 °C). At higher temperatures (e.g. 739 °C), microfracturing remains partially responsible for these rock property changes (e.g. higher permeability); however, X-ray diffraction and simultaneous thermal analysis also reveal these changes are partially a product of clinochlore, quartz, and (when present) calcite reacting out of the altered andesite. Our data suggest that short-duration, high-temperature conditions commonly associated with the margins of even small volume intrusions can substantially increase permeability and decrease the strength of some hydrothermally altered volcanic materials.

2.1 Introduction

Hydrothermal fluids have long been sought out for their utilisation as a heat source and conversion to electrical energy (Cataldi, 1993). Geothermal systems, especially those hosting an active hydrothermal system, provide a substantial resource to supply large populations with reliable, environmentally-friendly, sustainable energy. The driving geological components of a hydrothermal system (i.e. heat source, convecting fluid, and permeable conductive zone; Grant & Bixley, 2011; Corrado et al., 2014) are complexly interrelated. Therefore, the interplay between these three variables is of utmost interest. Active magmatic provinces commonly host important hydrothermal systems (e.g. Grunder et al., 1987; Ingebritsen et al., 1989; Rowland & Sibson, 2004). The thermal conditions directly adjacent to magmatic intrusions may reach *circa* 1200 °C (Sigurdsson et al., 2000; and references therein), promoting vigorous fluid circulation (Scott et al., 2015). The profitable development of a geothermal power plant that uses high-enthalpy fluids targets reservoir rock with a narrow range of permeability (Scott et al., 2015): in hydrothermal systems for which the reservoir rock permeability is lower than 10^{-16} m^2, it is expected that heat transport is primarily controlled by conduction, which is substantially less efficient for heat transport than convection (Ingebritsen et al., 2006). In contrast if permeability of the reservoir rock exceeds 10^{-14} m^2, fluid convection is too rapid to promote optimal fluid enthalpy (Cathles, 1977; Norton & Knight, 1977; Hayba & Ingebritsen, 1997). Therefore, understanding the impacts of heat sources on adjacent host-rock permeability will serve to increase the efficiency of ongoing and future geothermal energy production efforts.

Hydrothermal systems are dynamic environments, in which heat, fluid composition, and reservoir rock permeability fluctuate. Thermal stressing may cause relative expansion of solid (e.g. mineral) phases in the host rock (e.g. Barlett, 1832; Rosenholtz & Smith, 1941; Siratovich et al., 2015b). When the rock temperature surpasses those previously experienced, permanent damage may occur (i.e. the Kaiser effect; e.g. Wyering et al., 2014, and references therein). Thermal cracking during heating has been attributed to

several processes: the mismatched thermal expansion of minerals, temperature gradients induced as a function of heating rate, anisotropic thermal diffusivity of minerals, the bursting of fluid inclusions, mineral decomposition and devolatilization (e.g. Simmons & Cooper, 1978; Wong & Brace, 1979; Lo & Wai, 1982; Keshavarz et al., 2010; Heap et al., 2012). The generation of these thermal fractures augments the permeability of the rock (Kendrick et al., 2013; Heap et al., 2014b; Browning et al., 2016; Eggertsson et al., 2018). Hydrothermal fluids and heat input may also dissolve or breakdown rock-forming minerals, thus creating additional permeable porous pathways for fluid flow (e.g. Nemčok et al., 2007; Kanakiya et al., 2017; Cant et al., 2018). Alternatively, hydrothermal fluids may force the precipitation of minerals (e.g. clays, salts, carbonates, silica polymorphs) within the pores and cracks (e.g. Rowland & Sibson, 2004; Kanakiya et al., 2017) and thereby decreasing permeability (e.g. Heap et al., 2017). The permeability evolution of the reservoir rock are ultimately governed by the temperature, pressure, and chemistry of the system (fluids and solids), which control fluid convection (Fournier, 1985; and references therein). Magma provides the heat in many hydrothermal systems. The intrusion and subsequent cooling of magma in host rock can (re)activate and/or modify hydrothermal systems (Cathles et al., 1997; Grant & Bixley, 2011; Liotta et al., In Press). An extreme example of this was documented at Krafla (Mortensen et al., 2014; Scott et al., 2015), where large changes in rock mass properties were encountered during drilling close to an active shallow rhyolite intrusion providing evidence of the thermal and chemical impact of the intrusion on the surrounding host rock.

The effects of temperature on the physical, chemical, and mineralogical properties of volcanic rocks has been the subject of a range of studies (e.g. Kitao et al., 1990; Björnsson, 2004; Siratovich et al., 2015a; Siratovich et al., 2015b; Browning et al., 2016), but the range of scenarios (e.g. heating versus cooling), conditions (e.g. magnitude of temperature fluctuations), and reservoir rock types (e.g. unaltered versus altered) has prevented the generalisation of the impact on the resultant reservoir rock permeability. For instance, cooling results in contraction which may generate thermal cracks to promote fluid flow (Lamur et al., 2018); yet it may also precipitate secondary mineralisation that can block otherwise permeable pathways (Heap et al., 2017). In contrast, the impact of temperature increase (e.g. from magma intrusion) on the resultant rock permeability remains poorly constrained as it has received noticeably less attention than that of pressure-induced stresses (e.g. Gudmundsson, 2006; Gudmundsson, 2011). Understanding how the permeability of reservoir rock changes in response to thermal fluctuation is critical to elaborate solutions to maintain the economic potential of hydrothermal resources.

In this study, we expose water-saturated reservoir rock (i.e. two suites of andesite with propylitic alteration assemblages) from the Rotokawa Geothermal Field, New Zealand to high temperatures (up to 739 °C) over a relatively brief (30-min) duration to investigate the impact on porosity, permeability, and mineralogy.

2.1.1 Geological context of the Rotokawa hydrothermal system

New Zealand, a world leader in geothermal power, hosts the majority of its geothermal power production within the Taupo Volcanic Zone (TVZ; Fig. 2.1). The Rotokawa andesite, encountered at 1.5 – 2.5 km depth in the TVZ serves as the primary reservoir rock for the Rotokawa Geothermal Field. The Rotokawa geothermal system sits 14 km NE of Taupo and hosts > 13 production wells as part of a large industrial complex, producing 24 MWe at the Rotokawa I power station and 140 MWe at the Nga Awa Purua power station. The Nga Awa Purua station houses the single largest geothermal turbine in the world, providing almost 3% of New Zealand's electrical consumption (Legmann & Sullivan, 2003; Horie & Muto, 2010).

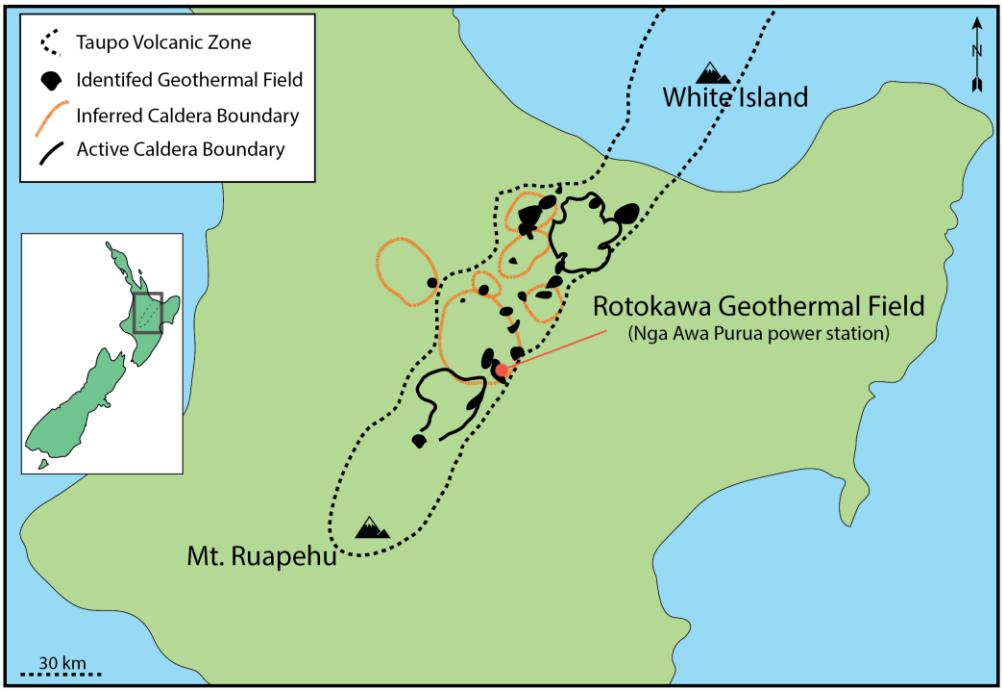

Figure 2.1 North Island, New Zealand and the active TVZ boundaries (dashed black) with the locations of geothermal fields (black), active caldera boundaries (black outline), and inferred caldera boundaries (orange outline). Rotokawa Geothermal Field indicated by red circle. Adapted from Wilson et al. (1995).

The 1.9 Ma Rotokawa andesite has a primary composition of medium- to low-K, calc-alkaline andesitic lavas; however, these lavas have undergone extensive propylitic hydrothermal alteration in a high-enthalpy hydrothermal system following their burial 0.34-0.30 Ma ago (Chambefort et al., 2014; McNamara et al., 2016). Pre-alteration mineralogy was predominantly composed of plagioclase and

pyroxene phenocrysts in a microlitic groundmass consisting plagioclase and titanomagnetite. Rock-fluid interaction variably altered the primary plagioclase to albite, adularia, calcite, pyrite, and epidote. Pyroxene crystals were partially to completely altered to chlorite, quartz, calcite, and epidote. The groundmass was replaced with chlorite, leucoxene, haematite, and silica minerals (see Figs. 5, 6; Siratovich et al., 2016).

The aqueous ion chemistry in the Rotokawa hydrothermal fluids varies spatially and temporally and remains the product of interaction with rock and meteoric, magmatic and/or connate fluids (Rowland & Simmons, 2012; Siratovich et al., 2016). Consequently, the chemistry is partially dependent on the permeability of the crystallizing magma body and surrounding host rocks (Norton, 1984), leading to the high degree of alteration and rock property variability found in the hydrothermal system. The variation of *in situ* temperatures (currently reaching 340 °C) and reservoir pressures (e.g. pore pressure varying around 15 – 20 MPa; lithostatic pressures from 0 – 60 MPa with effective mean pressures of 0 – 10 MPa; Davidson et al., 2012) throughout the andesites' history has promoted the spatial development of rocks with a range of mechanical and physical rock properties (Siratovich et al., 2012; Siratovich et al., 2014; Wyering et al., 2014; Siratovich et al., 2016).

The mechanical and physical rock properties of the Rotokawa andesite are highly variable because the petrological signature of the rock varies with alteration facies over short distances (< 0.5 m; Siratovich et al., 2016). Vesicles (commonly irregularly shaped), fractures, and inter-granular pore space are variably filled with secondary minerals (e.g. chlorite, quartz, epidote, and/or calcite; Figs. 5, 6; Siratovich et al., 2016). The intensity of alteration may evolve from moderate to high over short distances across transitions between the inner, coherent parts of lavas to their brecciated margins (Siratovich et al., 2016). Consequently, the samples collected from coring exhibit a spectrum of mechanical properties; for instance, highly altered samples are weaker and dilate less than moderately altered rocks during deformation in the brittle field, and microscopic damage is more diffuse in high-porosity than in low-porosity samples (Siratovich et al., 2016).

2.2 Methods

Here, we investigate the impact of thermal stressing on the porosity and permeability of hydrothermally altered andesite using two different mineral assemblages from the Rotokawa hydrothermal system: an altered plagioclase-clinochlore-calcite-quartz andesite, which we label as the moderately altered andesite herein, and an altered plagioclase-clinozoisite-quartz-clinochlore andesite, which we label as the highly altered andesite herein. Spot cores of the moderately and highly altered Rotokawa andesite were obtained during the drilling of Rotokawa production wells RK28 and RK29, respectively (Fig. 2.S1; Siratovich et al.,

2016). The spot cores were further cored with a 20 mm-diameter diamond bit. The samples were cut and ground to a length of 40 mm. Before the temperature treatment, we characterised the physical rock properties of the samples to compare to those of post-treatment. Porosity and density were measured by means of the Archimedes Triple Weight method. P- and S-wave velocities were collected using a GCTS CATS interfaced with transducer-mounted piezoelectric quartz crystals operating at a 900 kHz resonance frequency under unconfined atmospheric conditions. Permeability was collected using a PDP-200 permeameter at an effective confining pressure of 1 MPa. We ensured that the physical properties of the cores produced from each respective rock types (moderately and highly altered) were similar (i.e. porosity, permeability, p-wave velocity) so as to minimize the potential impact of sample variability in such heterogeneous materials. See Mordensky et al. (2018) for additional details on physical characterization methods performed at the University of Canterbury.

2.2.1 Thermal treatment

Altogether, we thermally stressed 18 samples (9 moderately altered and 9 highly altered) in the temperature-pressure *Magma Brewery* autoclave at the University of Canterbury, New Zealand (Fig. 2.2). A pump applied 20 MPa pressure using distilled H_2O. The temperature was then raised to 350, 400, 450, 500, 550, 600, 650, 700, or 739 °C. As temperature increased, excess H_2O was bled from the system to maintain 20 MPa pressure. To minimise the generation of thermal cracks from thermal gradients caused by rapid heating (e.g. Todd, 1973; Richter & Simmons, 1974; David et al., 1999; Siratovich et al., 2011; Browning et al., 2016) and thus concentrate our investigation to the impact of mineral instability of the resultant physical properties of the rock, we heated the cores at a rate of < 2 °C/min (Fig. 2.3). To assess the impact from short exposure to high temperatures in an H_2O-saturated environment, we heated the samples (for 6 to 13 hrs) and left them to dwell for 30 min; this timescale is insufficient to cause complete mineral reactions at the dwell temperatures, however, we were satisfied with such a timescale to reflect rapid thermal fluctuations imparted by brief incursion from hot magmatic fluids in reservoir rock. The samples were then cooled at < 2 °C/min to ambient temperatures. In order to avoid barometrically stressing the samples due to phase changes associated with the liquid-vapour phase transition during cooling, pressure was eased to ambient atmospheric conditions (~50 kPa/min) once the sample reached 390 °C. After thermal treatment, the physical properties were characterised again.

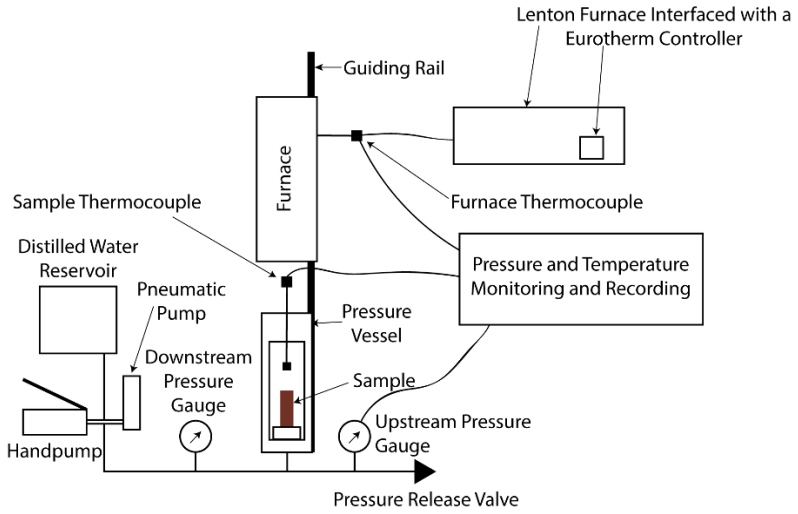

Figure 2.2 Schematic outline of the *'Magma Brewery'* autoclave (diagram not to scale). Furnace followed guiding rail down to envelope pressure vessel. This autoclave system has an operational limit of 739 °C.

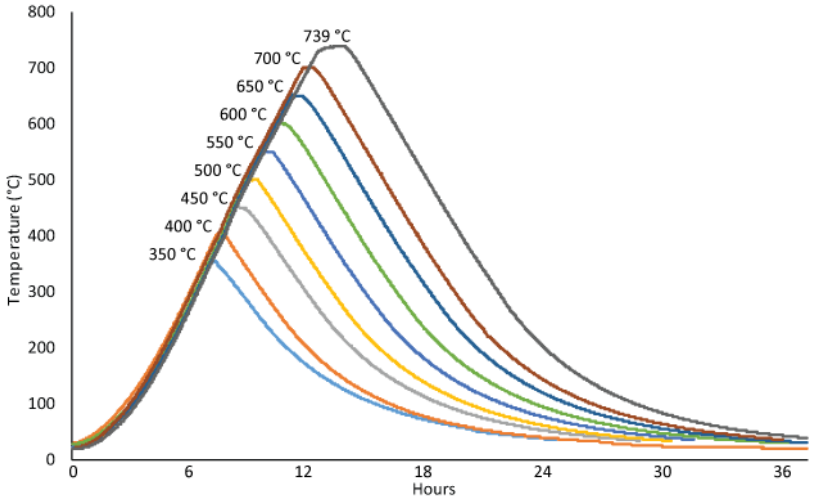

Figure 2.3 Heating and cooling profiles of thermal treatment of the Rotokawa andesite.

2.2.2 Scanning electron microscopy

Energy-dispersive X-ray spectroscopy (EDS) analysis was completed by a JEOL IT-300 scanning electron microscope (SEM) interfaced with an Oxford X-MAX^N 50 using an accelerating voltage of 15 kV, a working distance of 10 mm, a spot size equivalent to a 40 JEOL probe current as defined by Japan Electron Optics Laboratory Company Ltd. Samples were cut, ground, and polished using diamond-tipped instruments and then carbon coated. Backscattered electron images were collected for both sample suites on untreated, 400 °C-treated, and 739 °C-treated samples.

2.2.3 X-ray diffraction analysis

Sample compositions were determined by X-ray powder diffraction (XRD) analysis using a Bruker D8 Advance Bragg-Brentano theta-theta powder diffractometer at the University of Leicester, UK. The machine uses Cu Kα radiation and is equipped with a LynxEye position-sensitive detector and a 90-position auto-sampler. The scan range was 4 to 90 degrees 2-theta, with a step size of 0.01 degrees and a scan rate of 0.5 s per step. Phase identification was carried out using DIFFRAC.EVA software, interfaced with the PDF-4 database from the International Centre for Diffraction Data (ICDD), Philadelphia, USA. This analysis was conducted on the original (untreated) moderately and highly altered samples as well as on these samples subjected to temperatures of 600 °C and 739 °C.

2.2.4 Thermo-gravimetric analysis

Simultaneous thermal analysis (STA) was conducted using a Netzsch STA 449 F1 Jupiter at the University of Liverpool, UK (see also Siratovich et al. [2015b] for details on the measurements of the Rotokawa andesites). Sample chips (*circa* 50-60 mg) were oven dried at 70 °C for several hours and held in an air-tight desiccator for thermal equilibration to atmospheric temperature and to minimise the presence of residual water molecules (that could affect weight determination) prior to testing. The sample chips were then loaded in a platinum sample crucible in an atmosphere flushed by argon gas using a flow rate of 20 ml/min. The sample assembly was heated at a rate of 5 °C/min to 900 °C, whilst measuring thermo-gravimetric (TG) changes in sample weight (at an accuracy of ± 25 ng), which may fluctuate due to reactions (e.g. dehydration, calcination or oxidation/reduction). These measurements were conducted on 6 samples (i.e. untreated, 600 °C-treated, and 739 °C-treated samples from the moderately and highly altered andesites).

2.3 Results

2.3.1 Sample composition and microstructural analysis

Thermal treatment induced microfracturing in moderately and highly altered andesite. The few microfractures in the untreated samples are short (< 200 μm (Fig. 2.4a,d) and do not intersect. Following relatively low treatment temperature (e.g. 400 °C), the microfractures, although longer than in the untreated samples, remain relatively short (< 300 μm) and predominantly independent of each other (Fig. 2.4b,e). After treatment to the highest temperature (i.e. 739 °C), long (> 500 μm), microfractures cross-cut phenocrysts (Fig. 2.4c,f). In the moderately altered andesite, the long, through-cutting microfractures intersect other microfractures. In the highly altered andesite, microfracture density and intersection does not appear as prevalent following high-temperature treatment.

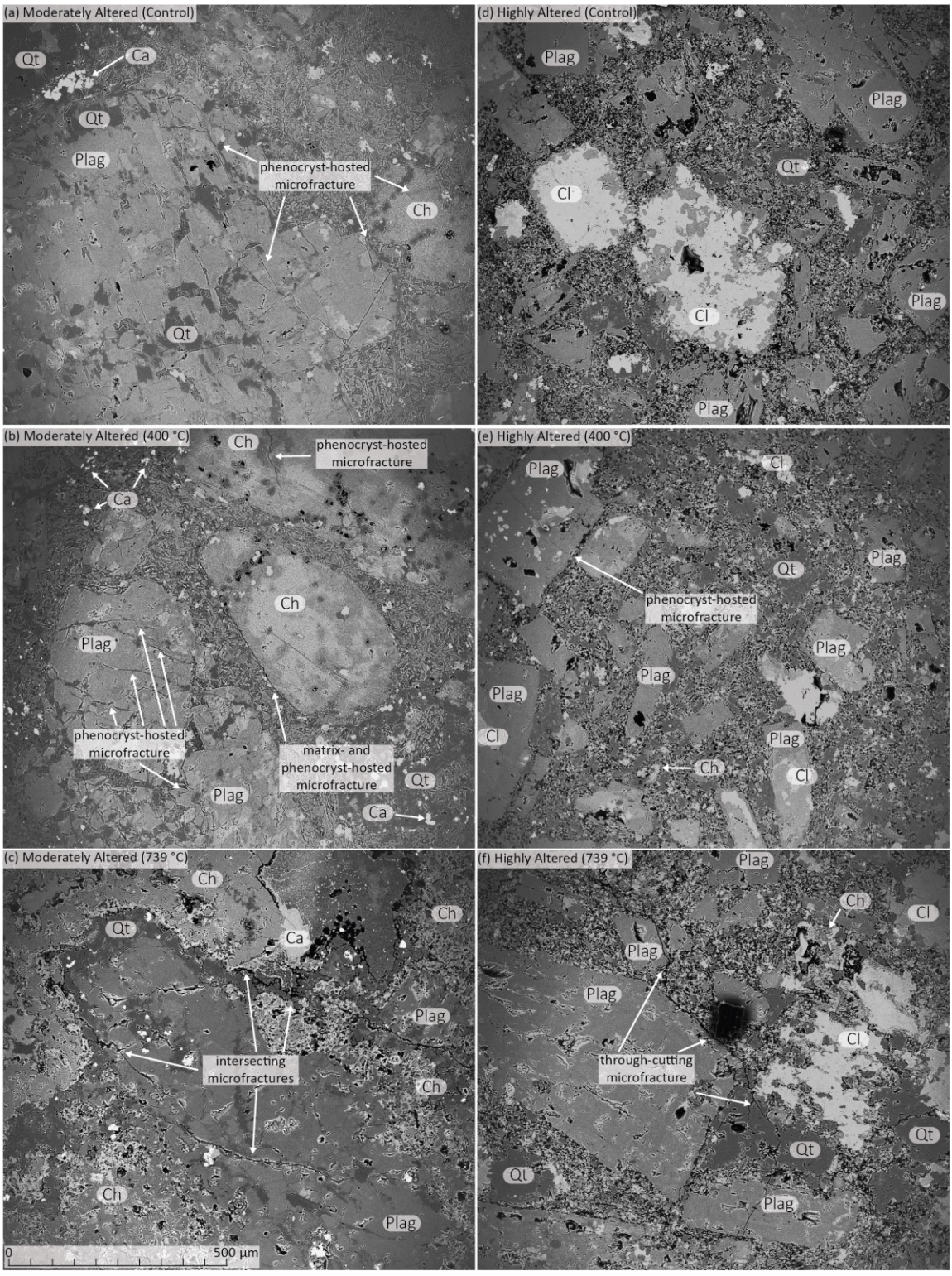

Figure 2.4 Backscattered electron images of sample microstructure. (a) Untreated moderately altered andesite. (b) Moderately altered andesite treated at 400 °C. (c) Moderately altered andesite treated at 739 °C. (d) Untreated highly altered andesite. (e) Highly altered andesite treated at 400 °C. (f) Highly altered andesite treated at 739 °C. Porosity is black. Plag – Plagioclase; Qt – Quartz; Ch – Clinochlore; Ca – Calcite; Cl – Clinozoisite. All images were collected at 100x magnification.

The EDS and XRD composition analyses produced generally consistent results. Electron-dispersive X-ray spectroscopy finds that the moderately altered andesite is composed of plagioclase (45 – 55%), clinochlore (OH-bearing, magnesium-rich chlorite; 30 – 35%), and quartz (5 – 10%), and calcite (5 – 10%) phenocrysts with a ground mass predominated by 10 – 20 μm interlocking crystals with the same composition as the phenocrysts (Fig. 2.5a,c). The highly altered andesite has plagioclase (80 – 95%) and quartz (5 – 20%) phenocrysts with interstitial clinochore. The plagioclase grains display varying states of partial alteration into clinozoisite (10 – 30%). The 10 – 20 μm crystalline groundmass is predominantly plagioclase and clinochlore with traces of clinozoisite and quartz (Fig. 2.5b,d). These results are confirmed by XRD analysis (Fig. 2.S2).

X-ray diffraction analysis of the samples treated at 600 °C also found the same phases as in the untreated samples, whereas clinochlore was not detected in samples treated at 739 °C by XRD analysis. That is, XRD analysis only detected plagioclase, quartz, and calcite in the moderately altered samples treated at 739 °C and plagioclase, quartz, and clinozoisite in the highly altered samples treated at 739 °C. However, EDS finds all phases that are present in the control samples are also present in samples treated at 739 °C (Fig. 2.5a,c), but EDS also provides evidence of reaction in these samples. In the samples treated to 739 °C, the clinochlore, quartz, and calcite have reaction textures not present in the control samples (Fig. 2.5b,d). This is particularly observable in Fig. 2.5b, in which substantial volumes of clinochlore and quartz have reacted out of the rock with a breakdown texture also visible in the clinochlore-quartz-plagioclase groundmass.

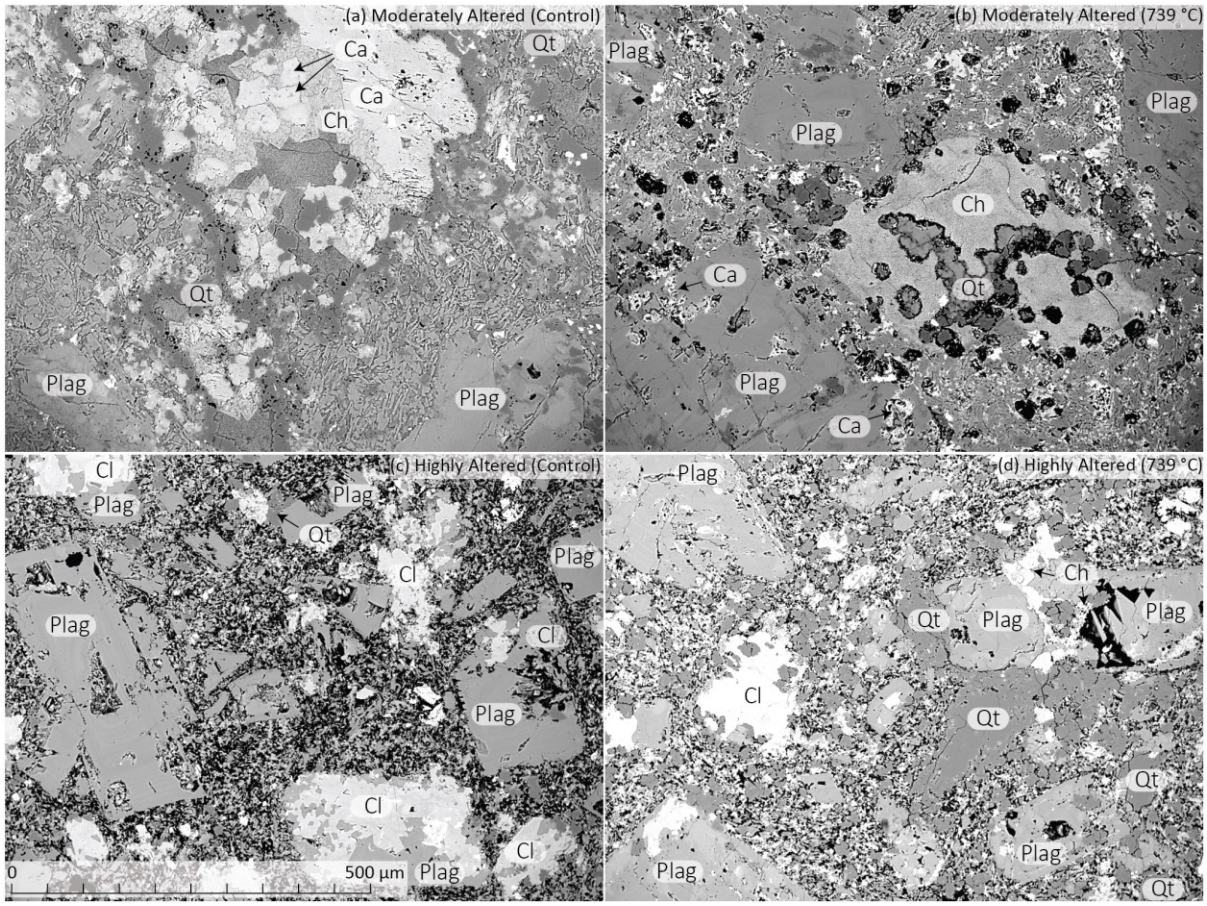

Figure 2.5 Backscattered electron images of sample mineralogy identified by EDS. (a) Untreated moderately altered andesite. (b) Moderately altered andesite treated at 739 °C with reaction textures in clinochlore, quartz, and calcite. (c) Untreated highly altered andesite. (d) Highly altered andesite treated at 739 °C with reaction textures in quartz and clinochlore. Plag – Plagioclase; Qt – Quartz; Ch – Clinochlore; Ca – Calcite; Cl – Clinozoisite. All images were collected at 150x magnification.

2.3.2 Thermo-gravimetric analysis

The TG analyses of the control samples of moderately altered and highly altered andesites exhibit two reactions initiating around 500 °C and then 650 °C (Fig. 2.6). For the moderately altered sample stressed to 739 °C, the minerals involved in the reaction initiating at ~500 °C are not present, but those of the second reaction (initiating at *circa* 650 °C) remain.

The highly altered control samples have noticeably smaller total mass loss than the moderately altered samples during both reactions. The highly altered sample subjected to 600 °C exhibits greater weight loss compared to its respective control sample. We note some weight loss at low temperatures (< 100 °C) during STA in the highly altered sample previously treated to 739 °C. Siratovich et al. (2015b) observed comparable mass loss at similarly low temperatures in untreated samples from the Rotokawa

andesite. When considered with the XRD analysis, this anomalous TG behaviour is most likely adsorbed atmospheric molecular water loss.

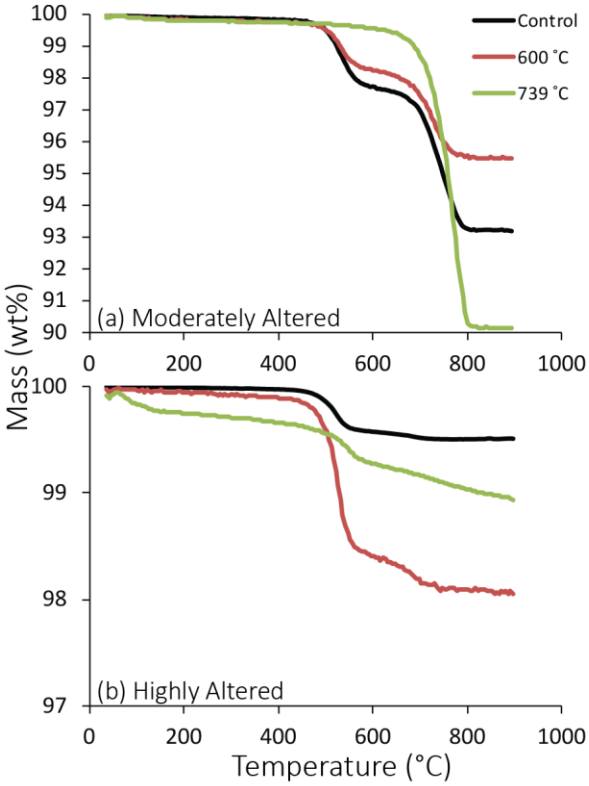

Figure 2.6 Results of thermo-gravimetric analysis for a) the moderately altered andesite (originally collected as well as previously stressed to 600 °C and 739 °C) and b) the highly altered andesite samples. All samples display evidence of reactions initiating during heating beyond *circa* 500 °C and 650 °C. Note the discrepancy in scale between (a) and (b).

2.3.3 Comparison of the pre- and post-treatment physical properties of the Rotokawa andesite

The initial bulk rock density of the moderately altered andesite was higher than that of the highly altered andesite (Table 2.1). This distinction is the product of the difference in porosity between the two sample series and remains true irrespective of the temperature reached for the short duration of thermal stresses imposed in this study (Table 2.1). It is also important to note that sample volume increased as a result of higher treatment temperatures (> 650 °C). Neither sample suite displays a clear density evolution with the hydrothermal conditions experienced (Table 2.1); however, the density of both, the moderately and highly altered andesites generally decreases with thermal stressing. In general, the changes in bulk sample density are < 1% for thermal stressing to moderate temperatures (350 – 500 °C) and decrease more (by > 2%) at higher temperatures (≥ 550 °C in the moderately altered andesite and ≥ 739 °C in the highly altered andesite; Table 2.1). The temperature at which we note the greatest changes in density correspond

with those indicated by the initial reaction suggested by the TG analyses in the moderately altered andesite and the increase in sample volume in the highly altered andesite (Fig. 2.6; Table 2.1).

Thermal stressing resulted in the creation of porosity for both andesites (Fig. 2.7a). The relative increase in porosity of both andesites non-linearly increases with the temperature experienced (Fig. 2.7a). The relative increase in porosity of the highly altered samples is less than that for the moderately altered samples.

The moderately altered andesite suites exhibit consistently lower original (pre-treatment) permeability than the highly altered andesite (Table 2.1). The treatment increased the permeability of the moderately altered andesite by up to one order of magnitude (Fig. 2.7b; Table 2.1). Thermal treatment also increased the permeability in the highly altered andesite, but not to the same magnitude as in the moderately altered andesite. Higher permeability generally coincides with higher porosity (Fig. 2.8). Thus, the experimental results indicate that even brief (30-min) excursions to higher temperatures may modify the mineralogical and physical (e.g. porosity and permeability) properties of altered volcanic rocks in active hydrothermal systems.

Sample	Temperature (°C)	Sample Volume (cm^3)		Mass (g)		Density (kg/m^3)		Porosity (%)		Permeability (m^2)		P-wave Velocity (m/s)		S-Wave Velocity (m/s)		Poisson Ratio		Young Modulus (GPa)	
		Pre	Post	Pre	Post	Pre	Post	Pre	Post	Pre	Post	Pre	Post	Pre	Post	Pre	Post	Pre	Post
M10	Control	12.58		31.23		2439		9.98		1.63×10^{-18}		4069		2335		0.25		3.49	
M2	350	12.65	12.64	31.94	31.90	2508	2498	7.59	7.74	4.91×10^{-18}	5.42×10^{-18}	3862	3890	2066	1984	0.30	0.32	2.87	2.69
M1	400	12.65	12.65	31.63	31.55	2504	2484	8.11	8.49	3.13×10^{-18}	1.13×10^{-17}	3958	3986	2177	1328	0.28	0.43	3.15	0.32
M3	450	12.57	12.57	31.57	31.38	2488	2460	8.53	9.62	3.04×10^{-18}	1.46×10^{-17}	4044	3888	1748	1899	0.39	0.34	2.18	2.47
M5	500	12.66	12.64	31.26	30.91	2451	2412	9.92	11.59	2.72×10^{-18}	1.24×10^{-17}	3913	4158	1944	1349	0.34	0.44	2.58	1.33
M8	550	12.51	12.51	31.13	30.59	2452	2382	9.55	11.99	2.51×10^{-18}	1.63×10^{-17}	3990	3880	2168	1042	0.29	0.46	3.10	0.80
M9	600	12.74	12.75	31.52	30.91	2486	2406	8.71	11.70	2.19×10^{-18}	1.55×10^{-17}	3980	4031	1666	1362	0.39	0.44	1.99	0.32
M7	650	12.71	12.78	31.57	30.94	2476	2402	8.71	12.24	2.08×10^{-18}	3.20×10^{-17}	3991	3809	2043	1802	0.32	0.36	2.85	2.22
M4	700	12.74	12.85	31.56	29.32	2476	2283	8.97	16.10	1.06×10^{-18}	8.88×10^{-17}	3887	3301	2498	1557	0.15	0.36	3.68	1.50
M6	739	12.73	12.83	31.90	30.55	2505	2367	7.75	15.12	1.09×10^{-18}	7.33×10^{-17}	4253	3368	2416	2227	0.26	0.11	3.82	2.61
H4	Control	12.75		29.16		2460		7.79		1.12×10^{-16}		3777		1933		0.32		2.36	0.00
H6	350	12.71	12.73	28.86	28.83	2285	2286	16.38	18.09	4.90×10^{-16}	5.11×10^{-16}	3450	3578	1967	1133	0.26	0.44	2.38	0.85
H3	400	12.62	12.67	28.43	28.32	2246	2245	18.53	20.26	8.05×10^{-16}	8.75×10^{-16}	3268	3300	1713	1525	0.31	0.36	1.87	1.42
H2	450	12.69	12.77	28.39	28.24	2264	2262	17.42	19.26	7.62×10^{-16}	8.48×10^{-16}	3369	3514	1838	1346	0.29	0.41	2.12	1.15
H9	500	12.75	12.75	29.03	28.94	2297	2295	15.21	17.24	3.26×10^{-16}	3.51×10^{-16}	3630	3564	1907	1658	0.31	0.36	2.33	1.71
H5	550	12.67	12.73	28.52	28.41	2278	2270	16.26	17.69	3.40×10^{-16}	3.84×10^{-16}	3596	3574	1827	1594	0.33	0.38	2.16	1.59
H10	600	12.71	12.72	29.20	29.08	2301	2267	14.66	16.48	1.46×10^{-16}	2.28×10^{-16}	3727	3550	2066	1755	0.28	0.34	2.66	2.02
H8	650	12.68	12.91	29.07	28.93	2279	2260	15.52	18.03	2.87×10^{-16}	4.67×10^{-16}	3602	3156	1700	1556	0.36	0.34	0.48	1.47
H1	700	12.74	12.89	29.55	30.25	2335	2355	12.04	14.50	4.34×10^{-17}	6.01×10^{-17}	3869	3552	2020	1757	0.31	0.34	2.61	1.94
H7	739	12.68	12.92	29.13	28.69	2291	2233	14.92	20.23	2.04×10^{-16}	2.56×10^{-16}	3747	3178	2018	1416	0.30	0.38	2.57	0.42

Table 2.1 Physical and mechanical property data. White-background columns depict pre-treatment data. Grey-background columns depict post-treatment data. Standard Error ≤ 1% of the reported values.

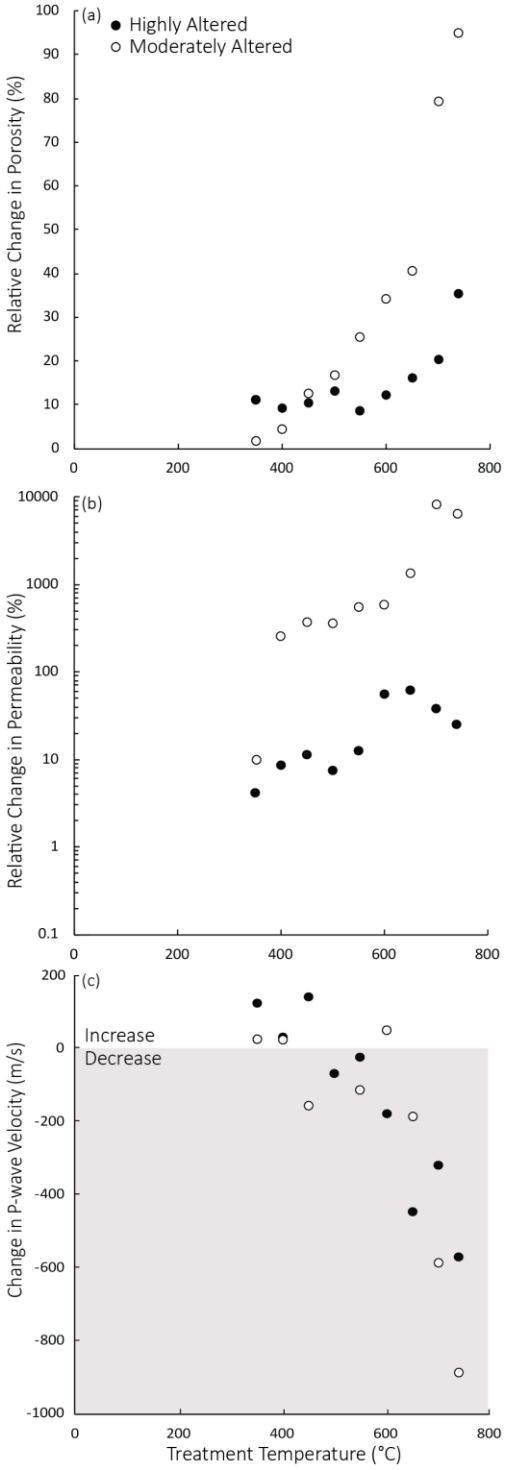

Figure 2.7 Changes in rock properties by treatment temperature. (a) Relative change in porosity versus treatment temperature. Higher treatment temperature is associated with greater changes in porosity. (b) Relative change in permeability following temperature treatment. Treatment temperatures increases permeability more in the moderately altered samples than in the highly altered samples. (c) Change in P-wave velocity versus temperature. Treatment temperature decreases ultrasonic P-wave velocity in the moderately and highly altered Rotokawa andesite at > 600 °C. Standard Error ≤ 1% of the reported values.

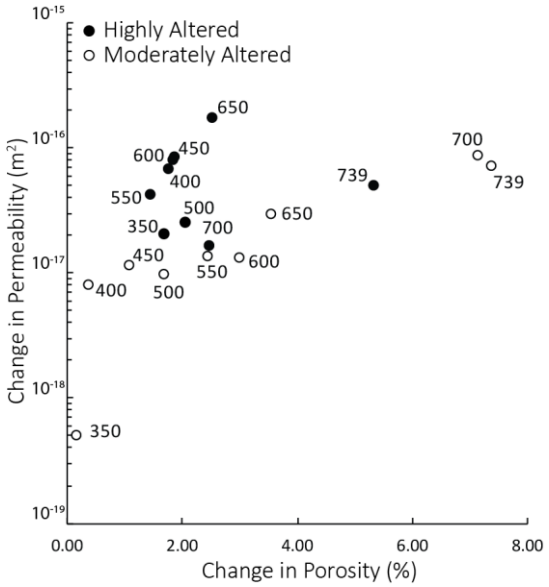

Figure 2.8 Change in porosity versus change in permeability. Treatment temperatures provided adjacent to respective data points in °C. Standard Error ≤ 1% of the reported values.

The initial P- and S-wave velocities of the moderately altered samples are generally higher than those of the highly altered samples (Table 2.1). When comparing post-treatment P-wave velocities from moderately and highly altered andesite to treatment temperature, only samples from the moderately altered andesite exposed to temperatures > 700 °C have noticeably lower values (< 3400 m/s) than the other samples of the same suite (> 3800 m/s; Table 2.1). However, the change in P-wave velocity from the original analysis to post-treatment analysis corresponds with the treatment temperatures when exceeding 600 °C in the moderately and highly altered samples (Fig. 2.7c). While post-treatment S-wave velocity values are generally lower than the initial values, there is no clear distinction between treatment temperature and post-treatment S-wave velocity or change in S-wave velocity in the highly altered andesite (Table 2.1).

2.4 Interpretation and discussion

2.4.1 Porosity and permeability

It is critical to acknowledge that the original samples used in this study contained varying fractions of mineral phases (Figs. 2.4, 2.5, 2.S1, 2.S2a,d) and spatially variable microstructure as the samples were sourced from a naturally occuring hydrothermal system. The compositional heterogeneity also explains the discrepency between the XRD and TG analyses (i.e. phase(s) absent after 739 °C treatment) and the EDS results. Therefore, the relative changes in physical properties between samples subjected to different temperature increments may not be entirely attributable to the different thermal conditions, as abundances of certain phases or structures may affect thermal susceptibility. Nonetheless, we observe that the physical

properties of moderately and highly altered Rotokawa andesite change after brief exposure to thermal stresses as low as 350 °C, and that temperature increase consistently resulted in an increase in porosity (Table 2.1). We interpret the observed porosity increase to a combination of mineralogical breakdown and microcracking.

2.4.2 Porosity and permeability: mineralogical breakdown

Thermo-gravimetric analyses indicate mass loss events at temperatures consistent with previous studies on the Rotokawa andesitic lavas. For example, Siratovich et al. (2015b) observed no significant change in sample mass after thermal stressing in altered andesites exposed to < 450 °C, but observed mass loss exceeding 2% (in the case of the moderately altered andesite) and ~1% (in the case of the highly altered andesite) following temperature excursion above 500 °C (Fig. 2.6) due to the breakdown of chlorite, quartz, and calcite. It is important to note that the treatment of the samples in our study occurred at high pressure (20 MPa) in water-saturated conditions (as opposed to the dry, ambient pressure conditions in the STA and XRD analyses); therefore, the reactions (and resultant physical changes) following the thermal treatment may not exactly occur at the same temperatures as in the XRD and STA analyses. For example, the second reaction in the moderately altered andesite begins at ~650 °C (see Fig. 2.6) a substantial change in permeability is not observed around this temperature until > 700 °C. The increased mass loss of the 600 °C experimental samples compared to the controls could indicate that hydration reactions may have occurred during the extended heat up time, or cooling period; however, the SEM (Fig. 2.5, 2.4), physical property (Fig. 2.7), and XRD (Figs. 2.S1, 2.S2b,e), data do not support this scenario.

The XRD data (Fig. 2.S2) suggest that the short-duration (30-min) dwell period imposed in our tests may have been sufficient to allow complete reaction of some phases; however, EDS mapping finds no changes in the phases present between the control and high-temperature samples. Clinochlore, quartz, and, to a lesser extent, calcite have reaction textures after having been exposed to high treatment temperature (e.g. 739 °C; Fig. 2.5). The prevalence of reaction textures in clinoclore and quartz (Fig. 2.5b,d) suggests the lower temperature reactions from the TG analyses (Fig. 2.6) can be attributed to these phases and is consistent with the breakdown of chlorite-quartz into talc, cordierite, and water at 500 - 600 °C observed in other studies (e.g. Fleming & Fawcett, 1976; Massonne & Massonne, 1989; Vidal et al., 2001). The relative large second reaction observed in the TG analyses of the moderately altered andesite (Fig. 2.6a) is consistent with devolatilization reactions of calcite in this temperature range (e.g. Mollo et al., 2012; Heap et al., 2013b). The reaction texture in calcite exposed to high-temperatures (Fig. 2.5b) supports intrepretation. The

changes observe in the clinochlore, quartz, and calcite demonstrates the susceptiblity hydrothermal systems with these minerals to changes in physical properties.

2.4.3 Porosity and permeability: microcracking

The microstructure of rocks serves as a first-order control on their mechanical and physical properties (e.g. Heap et al., 2014b). This is especially important in a geological context where rocks may be subjected to microcracking imparted by strong temperature fluctuations and/or gradients (e.g. magmatic dike emplacement, contact metamorphism, cooling of magma bodies; Siratovich et al., 2015a, and references therein). Thermal stressing of rock cores conducted in an oven (heating all sides of a sample) has been described to generate microcracks without preferred orientation that promote isotropic elastic wave velocities (e.g. Vinciguerra et al., 2005; Fortin et al., 2011; Heap et al., 2013a; Heap et al., 2014a; Browning et al., 2016). Elastic wave velocity analysis of the thermally stressed samples in our study suggests that the microfracturing and/or mineralogical reaction(s) associated with the short-lived thermal input events began to inhibit P-wave velocity in samples subjected to temperatures > 600 °C in the moderately and highly altered Rotokawa andesite (Fig. 2.7c). Post-treatment S-wave velocities, while slower than pre-treatment S-wave velocities (Table 2.1), do not display a relationship with temperature. This lack of correlation suggests the heterogenous distribution crystal size and composition within the altered andesites led to the anisotropic generation of microfractures (e.g. Simmons & Cooper, 1978; Wong & Brace, 1979; Lo & Wai, 1982; Keshavarz et al., 2010), which then produced a complex interaction of splitting S-waves (see Ryall & Savage, 1974). These data are consistent with our backscattered electron SEM images, which show that microfractures are predominantly absent and, when present, short, in untreated samples (Fig. 2.4a,d) but become more abundant and longer in phenocrysts as treatment temperature increases (Fig. 2.4c,f).

Porosity and permeability changes increase with higher treatment temperatures in both sample suites. At lower temperatures microfracturing (e.g. Fig. 2.4c,f) imparts higher porosity and permeability, especially in the moderately altered andesite (Figs. 2.7a,b, 2.8; Table 2.1). As temperature surpasses > 550 °C, the temperature at which the TG data (Fig. 2.6) depict the initial (likely clinochlore-quartz) reaction, we observe an increase in the rate at which permeability changes relative to temperature suggesting mass loss contributes substantially to the increase in permeability at this temperature. The next increase in the rate of permeability change relative to temperature is above the temperature of the second reaction (Figs. 2.6, 2.7b). In the highly altered andesite, change in permeability does not appear to change as drastically as in the moderately altered andesite (Figs. 2.7b, 2.8); however, permeability is noticeably higher in samples treated

to > 550 °C, the temperature of the initial (likely clinochlore-quartz) reaction. Thus, under the imposed conditions at temperatures below the mineralogical reactions (< 500 °C), microfracturing substantially augments permeability, but above the clinochlore-quartz reaction temperature, permeability change is driven by microfracturing and mineralogical reaction(s).

2.5 Implications

The consequences of these observations may have implications for a range of phenomena and applications (e.g. slope stability, seismic interpretation, and geothermal power production), which we evaluate here. However, before discussing the potential consequences of the data in this study, we highlight several of the characterisation techniques (e.g. porosity, P-wave velocity, S-wave velocity) were performed under atmospheric or near-surface conditions (e.g. permeability). The data reported would likely differ slightly if characterisation had been completed under the pressure (~20 MPa) and temperature (> 275 °C) conditions commonly associated with the Rotokawa andesite reservoir rock. The microfractures created during thermal exposure would close as confining pressure increases; therefore, porosity and permeability would decrease, while P-wave and S-wave velocities would increase.

2.5.1 Slope stability

The data presented in this study suggest porosity increases as treatment temperature increases (Fig. 2.7; Table 2.1). Generally, an increase in porosity is associated with a decrease in the strength of hydrothermally altered rock (e.g. Wyering et al., 2014; Wyering et al., 2015; Mordensky et al., 2018). Weakening intact rock (i.e. rock at the sample scale) contributes to weakened rock masses (Hoek et al., 2013) and may compromise the structural stability of a volcanic edifice (e.g. Voight & Elsworth, 1997; Apuani et al., 2005; Moon et al., 2009).

Volcanic rocks are frequently exposed to extreme temperatures and alteration; the data we present in this study suggests that altered volcanic rock masses can be weakened by temperatures as low as 350 °C (Cook et al., 2018; Schaefer et al., 2018). While it is worth noting that Heap et al. (2014b) concluded that exposing unaltered andesite to high temperatures (450 °C) over short timescales (60-min) would not greatly affect edifice strength and that Rocchi et al. (2004) found temperatures < 600 °C (60-min timescale) would not affect the strength of unaltered basalt, these volcanic materials did not contain hydrothermally altered materials. This distinction is important because primary volcanics are ubiquitously microcracked (e.g. Heap et al., 2014b) as a result of their cooling histories (e.g. David et al., 1999; Vinciguerra et al., 2005). Hydrothermal alteration infills and/or seals these microfractures (e.g. Pola et al., 2012; Pola et al., 2014;

Wyering et al., 2014, and references therein). Our data suggest that reheating to temperatures as low as 350 °C over short-time scales (30-min) can permanently damage hydrothermal material through additional microcracking (Figs. 2.4, 2.7c; e.g. David et al., 1999) and mineralogical reaction (Figs. 2.5, 2.6; e.g. Siratovich et al., 2015b). Therefore, the presence of alteration, especially when infilling original pore space, may increase the susceptibility of volcanic rock to thermal weakening. The variation in pre-treatment porosity between individual samples precluded the possibility of conducting meaningful strength tests in this study. We suggest future research with hydrothermally altered volcanics of similar porosity be conducted in order to observe the effect of high-temperature treatment on strength. Nonetheless, mass wasting event deposits are already linked with hydrothermally altered volcanics (e.g. Mt. Ruapehu, New Zealand (Hackett & Houghton, 1989), Mt. Shasta, USA (Crandell, 1989), Citlaltépetl, Mexico (Carrasco-Núñez & Gomez-Tuena, 1993) Mt. Rainer, USA (Reid et al., 2001)). Our data suggest that the hydrothermally altered rocks found in these mass collapse deposits contributed to the initial failure processes that initiated the mass wasting events.

2.5.2 Geothermal power

Permeability plays a critical role in geothermal power production (e.g. Cathles, 1977; Norton & Knight, 1977; Hayba & Ingebritsen, 1997). Our data suggest that the alteration assemblage and the degree of alteration of a rock determine the susceptibility of its physical properties (e.g. permeability) to change as a result of exposure to high temperature (Figs. 2.4, 2.5, 2.6, 2.7). Both sample suites experience the greatest change in permeability at temperatures > 550 °C, but the permeability of the highly altered andesite does not appear to be as comparatively affected or correlate as strongly with increasing temperatures (Fig. 2.7). Given that alteration zones are several times the dimensions of their heat source, affected by local geology, and difficult to map due to poor exposure (e.g. Shanks, 2012), we emphasize the importance of constraining the lithologies thermally stressed by geological or industrial development. Our data also suggest that lower elastic wave velocities within a lithological unit could indicate zones of potentially higher permeability as a consequence of short-lived, high-temperature thermal stressing (Fig. 2.7c; Table 2.1). Therefore, we conclude that it is imperative to understand the lithology when attempting to understand how a short-lived heat source will affect the mechanical and physical characteristics of a rock mass.

2.6 Conclusion

In this study, we subject andesite lavas with plagioclase-clinochlore-calcite-quartz and plagioclase-clinozoisite-quartz-clinochlore alteration assemblages from the Rotokawa Geothermal Field to short-lived

thermal input (350–739 °C) at a low thermal gradient (< 2 °C/min) and constant pressure (20 MPa). Increasing the thermal stress increased porosity (e.g. 7.8% to 15.1%) and permeability (e.g. 10^{-18} m^2 to 10^{-17} m^2) while decreasing P-wave velocity (e.g. 4253 to 3368 m/s) in the altered andesites. The effects of the thermal stressing appear greater in the altered plagioclase-clinochlore-calcite-quartz andesite than in the altered plagioclase-clinozoisite-quartz-clinochlore andesite. Previous studies have suggested that short-duration excursion to high temperatures of similar duration would not have significant impact on volcanics and, thereby, edifice strength, structural stability, and geothermal reservoir operation. Our data suggest that hydrothermally altered andesite is more susceptible to mineralogical and microstructural change than unaltered andesite to temperature fluctuations. These results demonstrate that the presence of altered material in a volcanic edifice may make the edifice more prone to failure upon temperature fluctuations. Our data also show that lithology partially controls the degree to which the thermal stresses change the permeability in the geothermal reservoir.

2.7 Acknowledgements

We greatly appreciate the help from Cheryl Haiden with the analytical XRD analysis at the University of Leicester. The authors of this study acknowledge the support of the UC Doctoral Scholarship, UC Mason Trust Fund, Hubert Curien Partnership (PHC) Dumont D'Urville travel grant (number 31950RK), MBIE catalyst grant "Energy straight from magma", and Mercury NZ Limited (formerly Mighty River Power) "Source to Surface" grant. Yan Lavallée acknowledges financial support from the European Research Council Starting Grant on Strain Localisation in Magma (SLiM, No. 306488) and research funds from Landsvirkjun National Power Company of Iceland (NÝR-20 – 2017).

2.8 Supplemental figures

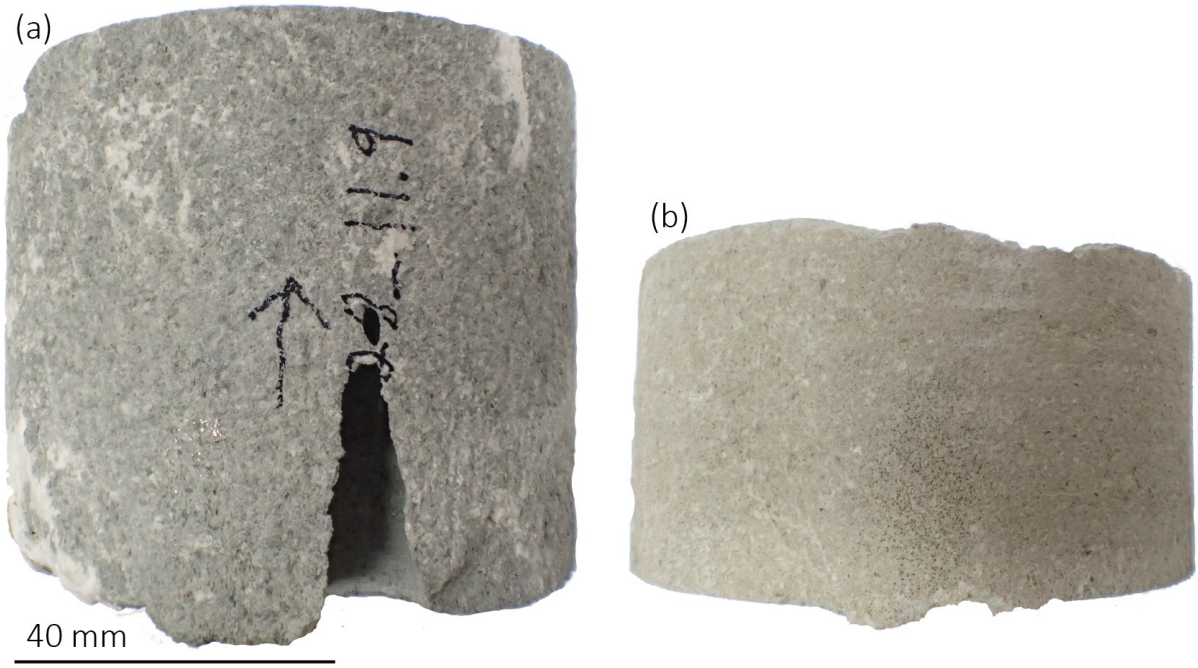

Figure 2.S1. Spot core photos of RK28 (moderately altered andesite [a]) and RK29 (highly altered andesite [b]). Note the variability of relative mineral abundance across both spot cores.

Figure 2.S2. X-ray diffraction analyses of altered Rotokawa andesite. (a) Moderately altered Rotokawa andesite control (M10). (b) Moderately altered Rotokawa andesite treated at 600 °C. (c) Moderately altered Rotokawa andesite treated at 739 °C. (d) Highly altered Rotokawa andesite control (H4). (e) Highly altered Rotokawa andesite treated at 600 °C. (f) Highly altered Rotokawa andesite treated at 739 °C.

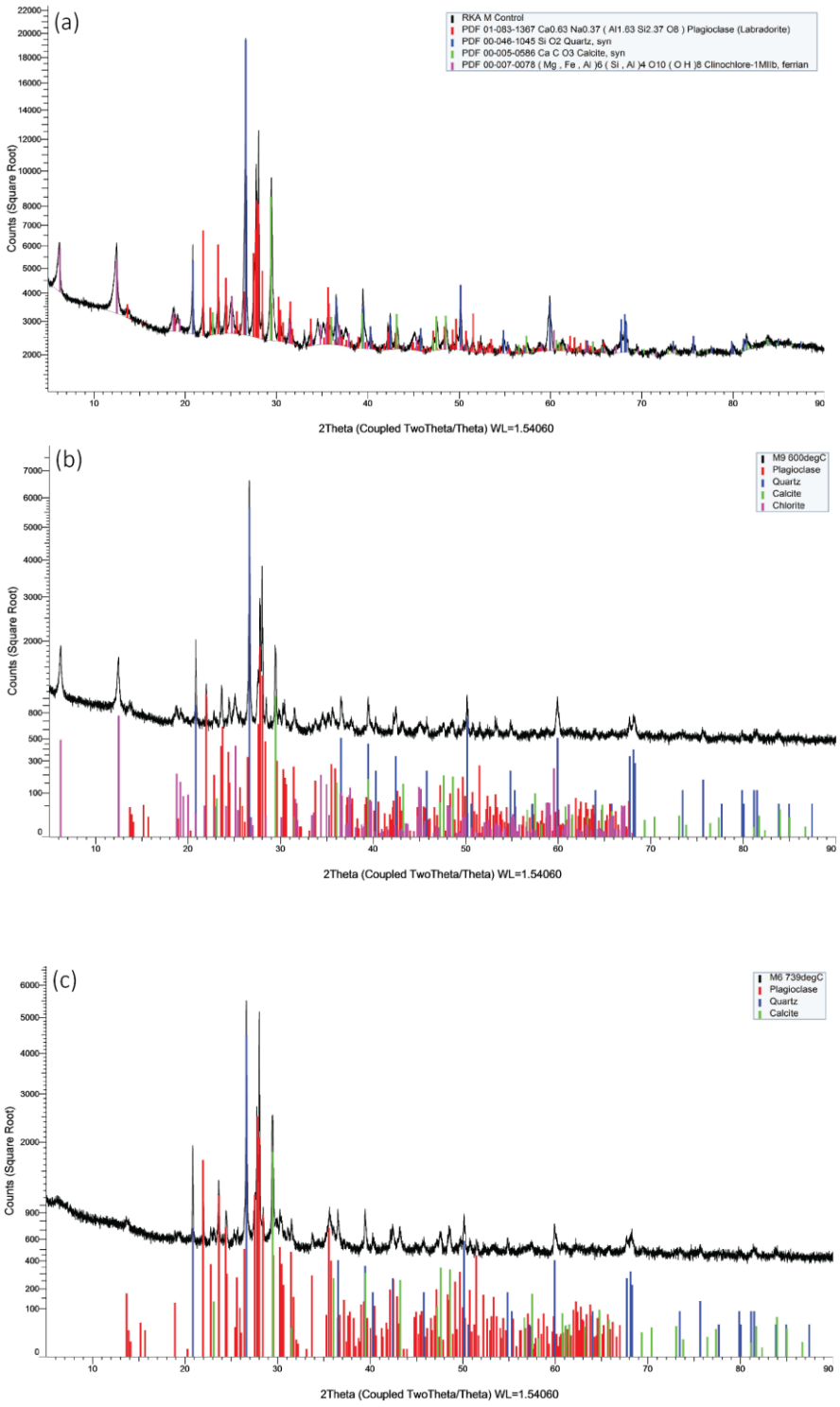

(Figure 2.S2 continued)

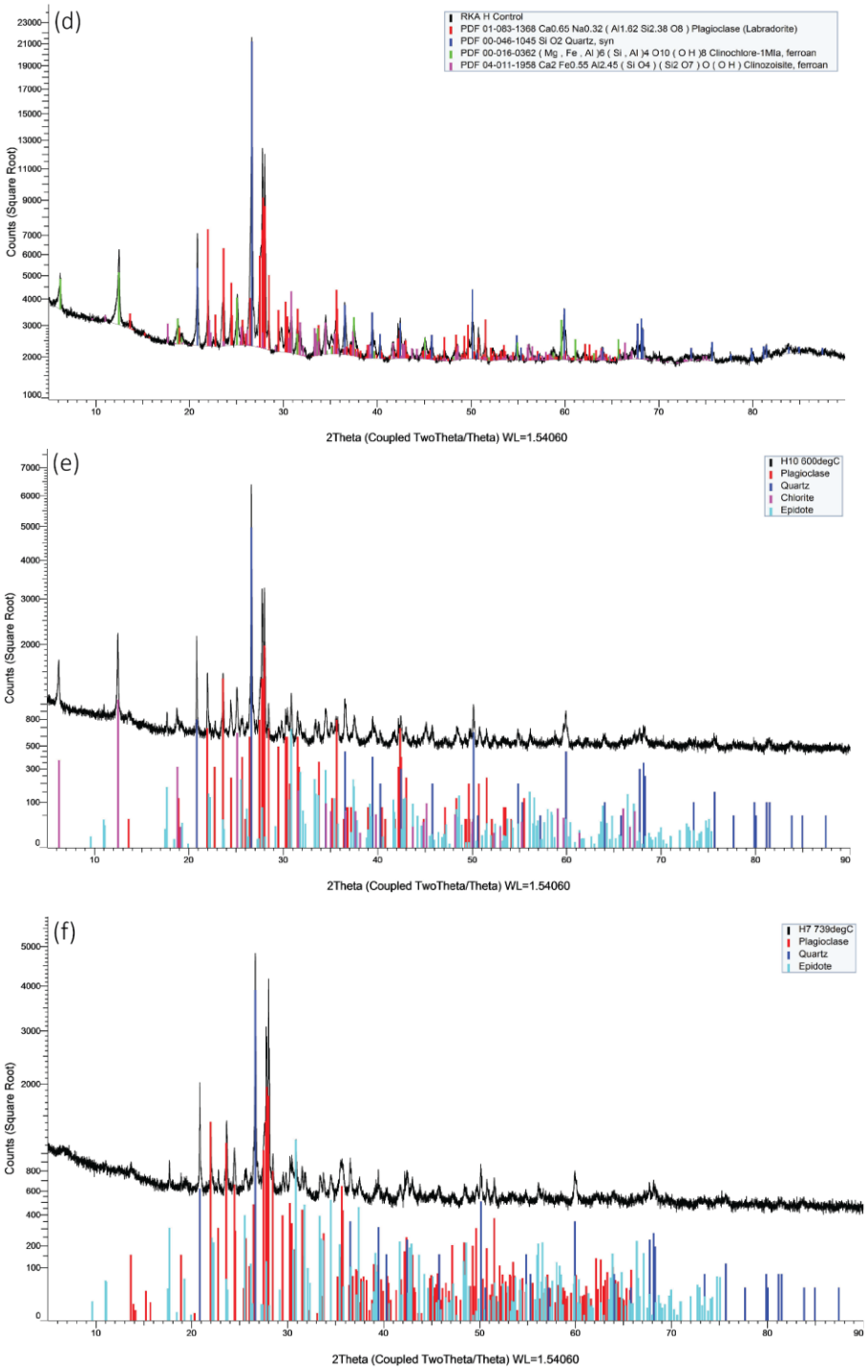

2.9 References

Apuani, T., Corazzato, C., Cancelli, A., & Tibaldi, A. (2005). Stability of a collapsing volcano (Stromboli, Italy): limit equilibrium analysis and numerical modelling. *Journal of Volcanology and Geothermal Research, 144*(1-4), 191-210.

Barlett, W. H. C. (1832). Experiments on the expansion and contraction of building stones by variation of temperature. *American Journal of Science and Arts, 22*(1), 136-140.

Björnsson, G. (2004, January 26-28). *Reservoir conditions at 3-6 km depth in the Hellisheidi Geothermal Field, SW-Iceland, estimated by deep drilling, cold water injection and seismic monitoring.* Paper presented at the Twenty-Ninth Workshop on Geothermal Reservoir Engineering, Stanford University, Stanford, California, USA.

Browning, J., Meredith, P. G., & Gudmundsson, A. (2016). Cooling-dominated cracking in thermally stressed volcanic rocks. *Geophys. Res. Lett., 42*. doi:10.1002/2016GL070532.

Cant, J. L., Siratovich, P. A., Cole, J. W., Villeneuve, M. C., & Kennedy, B. M. (2018). Matrix permeability of reservoir rocks, Ngatamariki geothermal field, Taupo Volcanic Zone, New Zealand. *Geothermal Energy, 6*(2).

Carrasco-Núñez, G., & Gomez-Tuena, A. (1993). A voluminous avalanche-induced lahar from Citlaltepetl Volcano, Mexico: implications for hazard assessment. *Journal of Volcanology and Geothermal Research, 59*, 35-46.

Cataldi, R. (1993). Review of historiographic aspects of geothermal energy in the Mediterranean and Mesoamerican areas prior to the Modern Age. *Geo-Heat Center Quarterly Bulletin, 15*(1).

Cathles, L. M. (1977). An analysis of the cooling of the intrusions by ground-water convection that includes boiling. *Economic Geology, 72*, 804-826.

Cathles, L. M., Erendi, H. J., & Barrie, T. (1997). How long can a hydrothermal system be sustained by a single intrusive event. *Economic Geology, 92*, 766-771. doi:0361-0128/97/1946/766-65.

Chambefort, I., Lewis, B., Wilson, C. J. N., Rae, A. J., Coutts, C., Bignall, G., & Ireland, T. R. (2014). Stratigraphy and structure of the Ngatamariki geothermal system from new zircon U–Pb geochronology: implications for Taupo Volcanic Zone evolution. *Journal of Volcanology and Geothermal Research, 274*, 51-70. doi:10.1016/j.jvolgeores.2014.01.015.

Cook, S., Kennedy, B., & Villeneuve, M. C. (2018). Engineering geology model of the Crater Lake outlet, Mt. Ruapehu, New Zealand, to inform rim breakout hazard. *Journal of Volcanology and Geothermal Research, 350*(15), 69-83.

Corrado, S., Aldega, L., Celano, A. S., De Benedetti, A. A., & Giordano, G. (2014). Cap rock efficiency and fluid circulation of natural hydrothermal systems by means of XRD on clay minerals (Sutri, Northern Latium, Italy). *Geothermics, 50*, 180-188. doi:10.1016/j.geothermics.2013.09.011.

Crandell, D. R. (1989). Gigantic debris avalanche of Pleistocene age from ancestral Mount Shasta volcano, California, and debris-avalanche hazard zonation. *US Geological Survey Bulletin, 1861*.

David, C., Menéndez, B., & Darot, M. (1999). Influence of stress-induced and thermal cracking on physical properties and microstructure of La Peyratte granite. *International Journal of Rock Mechanics and Mining Sciences, 36*(4), 433-448. doi:10.1016/s0148-9062(99)00010-8.

Davidson, J. P., Siratovich, P. A., Wallis, I. C., Gravley, D., & McNamara, D. (2012). *Quantifying the stress distribution at the Rotokawa Geothermal Field.* Paper presented at the New Zealand Geothermal Workshop (November), Auckland, New Zealand.

Eggertsson, G. H., Lavallée, Y., Kendrick, J. E., & Markússon, S. H. (2018). Improving fluid flow in geothermal reservoirs by thermal and mechanical stimulation: The case of Krafla volcano, Iceland. *Journal of Volcanology and Geothermal Research*.

Fleming, P. D., & Fawcett, J. J. (1976). Upper stability of chlorite+quartz in the system MgO– FeO–AlrOs–SiO2–H2O at 2 kbar water pressure. *Amerincan Minerologist, 61*, 1175-1193.

Fortin, J., Stanchits, S., Vinciguerra, S., & Gueguen, Y. (2011). Influence of thermal and mechanical cracks on permeability and elastic wave velocities in a basalt from Mt. Etna volcano subjected to elevated pressure. *Tectonophysics, 503*, 60-74.

Fournier, R. O. (1985). The behavior of silica in hydrothermal solutions. *Reviews in Economic Geology*(2), 45-59.

Grant, M. A., & Bixley, P. F. (2011). *Geothermal Reservoir Engineering* (Vol. 2nd Edition). San Diego, CA: Elsevier.

Grunder, A. L., Thompson, J. M., & Hildreth, W. (1987). The hydrothermal system of the Calabozos caldera, Central Chilean Andes. *Journal of Volcanology and Geothermal Research, 32*, 287-298.

Gudmundsson, A. (2006). How local stresses control magma-chamber ruptures, dyke injections, and eruptions in composite volcanoes. *Earth-Science Reviews, 79*, 1-31.

Gudmundsson, A. (2011). *Rock Fractures in Geological Processes*. United Kingdom: Cambridge University Press (CUP).

Hackett, W. R., & Houghton, B. F. (1989). A facies model for a Quaternary andesitic composite volcano: Ruapehu, New Zealand. *Bulletin of Volcanology, 51*(1), 51-68.

Hayba, D. O., & Ingebritsen, S. E. (1997). Multiphase groundwater flow near cooling plutons. *J. Geophys. Res., 102*, 12235-12252.

Heap, M. J., Baud, P., Meredith, P. G., Vinciguerra, S., & Reuschlé, T. (2014a). The permeability and elastic moduli of tuff from Campi Flegrei, Italy: implications for ground deformation modelling. *Solid Earth, 5*(1), 25-44. doi:10.5194/se-5-25-2014.

Heap, M. J., Kennedy, B., Farquharson, J., Ashworth, J., Gilg, H. A., Scheu, B., et al. (2017). A multidisciplinary approach to quantify the permeability of a volcanic hydrothermal system (Whakaari/White Island, Taupo Volcanic Zone, New Zealand). *Journal of Volcanology and Geothermal Research, 332*, 88-108.

Heap, M. J., Lavallée, Y., Laumann, A., Hess, K., & Dingwell, D. B. (2012). How tough is tuff in the event of fire? *Geology, 40*, 311-314.

Heap, M. J., Lavallée, Y., Laumann, A., Hess, K., Meredith, P. G., Dingwell, D. B., et al. (2013a). The influence of thermal-stressing (up to 1000 °C) on the physical, mechanical, and chemical properties of siliceous-aggregate, high-strength concrete. *Construction and Building Materials, 42*(248-265).

Heap, M. J., Lavallée, Y., Petrakova, L., Baud, P., Reuschlé, T., Varley, N. R., & Dingwell, D. B. (2014b). Microstructural controls on the physical and mechanical properties of edifice-forming andesites at Volcán de Colima, Mexico. *Journal of Geophysical Research: Solid Earth, 119*(4), 2925-2963. doi:10.1002/2013JB010521.

Heap, M. J., Mollo, S., Vinciguerra, S., Lavallée, Y., Hess, K. U., Dingwell, D. B., et al. (2013b). Thermal weakening of the carbonate basement under Mt. Etna volcano (Italy): implications for volcano instability. *Journal of Volcanology and Geothermal Research, 250*, 42-60.

Hoek, E., Carter, T. G., & Diederichs, M. (2013). *Quantification of the Geological Strength Index*. Paper presented at the 47th US Rock Mechanics / Geomechanics Symposium, San Francisco, CA.

Horie, T., & Muto, T. (2010). The world's largest single cylinder geothermal power generation unit - Nga Awa Purua Geothermal Power Station, New Zealand. *Geothermal Resources Council Transactions, 34*, 1039-1044.

Ingebritsen, S. E., Sanford, W., & Neuzil, C. (2006). *Groundwater in Geologic Processes* (2nd ed.). New York, USA: Cambridge University Press.

Ingebritsen, S. E., Sherrod, D. R., & Mariner, R. H. (1989). Heat flow and hydrothermal circulation in the Cascade Range, North-Central Oregon. *Science, 243*(4897), 1458-1462.

Kanakiya, S., Adam, L., Esteban, L., Rowe, M., & Shane, P. (2017). Dissolution and secondary mineral precipitation in basalts due to reactions with carbonic acid. *Journal of Geophysical Research, 122*(6), 4312-4327.

Kendrick, J. E., Smith, R., Sammonds, P., Meredith, P. G., Dainty, M., & Pallister, J. S. (2013). The influence of thermal and cyclic stressing on the strength of rocks from Mount St. Helens, Washington. *Bulletin of Volcanology, 75(7)*(728). doi:10.1007/s00445-013-0728-z.

Keshavarz, M., Pellet, F. L., & Loret, B. (2010). Damage and Changes in Mechanical Properties of a Gabbro Thermally Loaded up to 1,000°C. *Pure and Applied Geophysics, 167*(12), 1511-1523. doi:10.1007/s00024-010-0130-0.

Kitao, K., Ariki, K., Hatakeyama, K., & Wakita, K. (1990). Well Stimulation Using Cold-Water Injection Experiments in The Sumikawa Geothermal Field, Akita Perfecture, Japan. *Geothermal Resources Council Transactions, 14*, 1219-1224.

Lamur, A., Lavallée, Y., Iddon, F., Hornby, A. J., Kendrick, J. E., von Aulock, F. W., & Wadsworth, F. B. (2018). Disclosing the temperature of columnar jointing and fluid flow in lavas. *Nature communications, 9*, 1432. doi:10.1038/s41467-018-03842-4.

Legmann, H., & Sullivan, P. (2003, September). *The 30 MW Rotokawa I geothermal project five years of operation.* Paper presented at the International Geothermal Conference, Reykjavik, Iceland.

Liotta, D., Brogi, A., Ruggieri, G., Rimondi, V., Zucchi, M., Helgadóttir, H. M., et al. (In Press). Fracture analysis, hydrothermal mineralization and fluid pathways in the Neogene Geitafell central volcano: insights for the Krafla active geothermal system, Iceland. *Journal of Volcanology and Geothermal Research*.

Lo, K. Y., & Wai, R. S. C. (1982). Thermal expansion, diffusivity, and cracking of rock cores from Darlington, Ontario. *Canadian Geotechnical Journal, 19*, 154-166.

Massonne, H.-J., & Massonne, H.-J. (1989). The upper thermal stability of chlorite + quartz: an experimental study in the system MgO-Al2O3-SiO2-H2O. *Journal of Metamorphic Geology, 7*(6).

McNamara, D., Sewell, S., Buscarlet, E., & Wallis, I. C. (2016). Micromechanics of brittle faulting and cataclastic flow in Berea sandstone. *Journal of Structural Geology, 18*, 1-16.

Mollo, S., Heap, M. J., Jezzi, G., Hess, K., Scarlato, P., & Dingwell, D. B. (2012). Volcanic edifice weakening via decarbonation: a self-limiting process? *Geophys. Res. Lett., 39*(15).

Moon, V., Bradshaw, J., & de Lange, W. (2009). Geomorphic development of White Island volcano based on slope stability modelling. *Engineering Geology, 104*, 16-30.

Mordensky, S. P., Villeneuve, M. C., Kennedy, B. M., Heap, M. J., Gravley, D., Farquharson, J. I., & Reuschlé, T. (2018). Physical and mechanical property relationships of a shallow intrusion and volcanic host rock, Pinnacle Ridge, Mt. Ruapehu, New Zealand. *Journal of Volcanology and Geothermal Research, 359*(15), 1-20. doi:10.1016/j.jvolgeores.2018.05.020.

Mortensen, A. K., Egilson, Þ., Gautason, B., Árnadóttir, S., & Gudmundsson, A. (2014). Stratigraphy, alterationmineralogy,permeabilityandtemperature conditions ofwellIDDP-1,Krafla,NE-Iceland. *Geothermics, 49*, 31-41. doi:10.1016/j.geothermics.2013.09.013.

Nemčok, M., Moore, J. N., Christensen, C., Allis, R., Powell, T., Murray, B., & Nash, G. (2007). Controls on the Karaha–Telaga Bodas geothermal reservoir, Indonesia. *Geothermics, 36*(1), 9-46. doi:10.1016/j.geothermics.2006.09.005.

Norton, D. (1984). Theory of Hydrothermal Systems. *Annual Review of Earth and Planetary Sciences, 12*, 155-177.

Norton, D., & Knight, J. (1977). Transport phenomena in hydrothermal systems: cooling plutons. *American Journal of Science, 277*, 937-981.

Pola, A., Crosta, G., Fusi, N., Barberini, V., & Norini, G. (2012). Influence of alteration on physical properties of volcanic rocks. *Tectonophysics, 566-567*, 67-86. doi:10.1016/j.tecto.2012.07.017.

Pola, A., Crosta, G. B., Fusi, N., & Castellanza, R. (2014). General characterization of the mechanical behaviour of different volcanic rocks with respect to alteration. *Engineering Geology, 169*, 1-13. doi:10.1016/j.enggeo.2013.11.011.

Reid, M. E., Sisson, T. W., & Brien, D. L. (2001). Volcano collapse promoted by hydrothermal alteration and edifice shape, Mount Rainier, Washington. *Geology, 29*(9), 779. doi:10.1130/0091-7613(2001)029<0779:vcpbha>2.0.co;2.

Richter, D., & Simmons, G. (1974). Thermal Expansion Behavior of Igneous Rocks. *International Journal of Rock Mechanics and Mining Sciences, 11*, 403-411.

Rocchi, V., Sammonds, P. R., & Kilburn, C. R. J. (2004). Fracturing of Etnean and Vesuvian rocks at high temperatures and low pressures. *Journal of Volcanology and Geothermal Research, 132*(2-3), 137-157.

Rosenholtz, J. L., & Smith, D. T. (1941). Linear thermal expansions and inversions of quartz, var. rock crystal. *American Mineralogist, 26*(2), 103-109.

Rowland, J. V., & Sibson, R. H. (2004). Structural controls on hydrothermal flow in a segmented rift system, Taupo Volcanic Zone, New Zealand. *Geofluids, 4*(4), 259-283. doi:10.1111/j.1468-8123.2004.00091.x.

Rowland, J. V., & Simmons, S. F. (2012). Hydrologic, magmatic, and tectonic controls on hydrothermal flow, Taupo Volcanic Zone, New Zealand: Implications for the formation of epithermal vein deposits. *Economic Geology, 107*(3), 427-457. doi:10.2113/econgeo.107.3.427.

Ryall, A., & Savage, W. (1974). S-wave splitting; key to earthquake prediction? *Bulletin of the Seismological Society of America, 64*(6), 1943-1951.

Schaefer, L. N., Kennedy, B., Villeneuve, M. C., Cook, S. C. W., Jolly, A., Keys, H., & Leonard, G. J. (2018). Stability assessment of the Crater Lake overflow/Te Wai-ā-moe channel at Mt. Ruapehu (New Zealand), and implications for volcanic lake break-out triggers. *Journal of Volcanology and Geothermal Research, 358*, 31-44. doi:10.1016/j.jvolgeores.2018.06.011.

Scott, S. W., Driesner, T., & Weis, P. (2015). Geologic controls on supercritical geothermal resources above magmatic intrusions. *Nature communications, 6*, 7837-7837. doi:10.1038/ncomms8837.

Shanks, W. C. (2012). *Volcanogenic Massive Sulfide Occurrence Model*. Retrieved from Reston, Virginia:

Sigurdsson, H., Houghton, B. F., McNutt, S. R., Rymer, H., Stix, J., & McBirney, A. R. (2000). Encyclopedia of Volcanoes. *Physics Today, 53*(10), 84-85. doi:10.1063/1.1325206.

Simmons, G., & Cooper, H. W. (1978). Thermal cycling cracks in three igneous rocks. *International Journal of Rock Mechanics and Mining Sciences, 15*(145-148).

Siratovich, P., Cole, J., Heap, M., Villeneuve, M., Reuschlé, T., Swanson, K., et al. (2015a). Experimental thermal stimulation of the Rotokawa Andesite. *Proceedings World Geothermal Congress 2015*(April), 1-6.

Siratovich, P. A., Heap, M. J., Villeneuve, M. C., Cole, J., Kennedy, B., Davidson, J. P., & Reuschlé, T. (2016). Mechanical behaviour of the Rotokawa Andesites (New Zealand): insight into permeability evolution and stress-induced behaviour in an actively utilised geothermal reservoir. *Geothermics, 64*, 163-179. doi:10.1016/j.geothermics.2016.05.005.

Siratovich, P. A., Heap, M. J., Villeneuve, M. C., Cole, J. W., & Reuschlé, T. (2014). Physical property relationships of the Rotokawa Andesite, a significant geothermal reservoir rock in the Taupo Volcanic Zone, New Zealand. *Geothermal Energy, 2*(1), 10-10. doi:10.1186/s40517-014-0010-4.

Siratovich, P. A., Sass, I., Homuth, S., & Bjornsson, A. (2011). Thermal stimulation of geothermal reservoirs and laboratory investigation of thermally induced fractures. *Transactions - Geothermal Resources Council, 35 2*, 1529-1535.

Siratovich, P. A., von Aulock, F. W., Lavallée, Y., Cole, J. W., Kennedy, B. M., & Villeneuve, M. C. (2015b). Thermoelastic properties of the Rotokawa Andesite: A geothermal reservoir constraint. *Journal of Volcanology and Geothermal Research, 301*, 1-13. doi:10.1016/j.jvolgeores.2015.05.003.

Siratovich, P. D. J., Villeneuve, M. G. D. K. B. C. J. W. L., & Price, L. (2012). Physical and Mechanical Properties of the Rotokawa Andesite From Production Wells Rk 27 _ L2 , Rk 28 and Rk 30. *New Zealand Geothermal Workshop 19-21 November*(November), 7-7.

Todd, T. (1973). *Effect of cracks on elastic properties of low porosity rocks.* (PhD), Massachusetts Institute of Tech, Cambridge, MA.

Vidal, O., Parra, T., & Trotet, F. (2001). Thermodynamicmodel for Fe–Mg aluminous chlorite using data from phase equilibrium experiments and natural perlitic assemblages in the 100° to 600 °C, 1 to 25 kb range. *American Journal of Science, 301*, 557-592.

Vinciguerra, S., Trovato, C., Meredith, P. G., & Benson, P. M. (2005). Relating seismic velocities, thermal cracking and permeability in Mt. Etna and Iceland basalts. *International Journal of Rock Mechanics and Mining Sciences, 42*(7-8), 900-910. doi:10.1016/j.ijrmms.2005.05.022.

Voight, B., & Elsworth, D. (1997). Failure of volcano slopes. *Geotechnique, 47*(1), 1-31.

Wilson, C. J. N., Houghton, B. F., McWilliams, M. O., Lanphere, M. A., Weaver, S. D., & Briggs, R. M. (1995). Volcanic and structural evolution of Taupo Volcanic Zone, New Zealand: a review. *Journal of Volcanology and Geothermal Research, 68*(1-3), 1-28. doi:10.1016/0377-0273(95)00006-g.

Wong, T. F., & Brace, W. F. (1979). Thermal expansion of rocks: some measurements at high pressure. *Tectonophysics, 57*, 95-117.

Wyering, L. D., Villeneuve, M. C., Wallis, I. C., Siratovich, P. A., Kennedy, B. M., & Gravley, D. M. (2015). The development and application of the alteration strength index equation. *Engineering Geology, 199*, 48-61. doi:10.1016/j.enggeo.2015.10.003.

Wyering, L. D., Villeneuve, M. C., Wallis, I. C., Siratovich, P. A., Kennedy, B. M., Gravley, D. M., & Cant, J. L. (2014). Mechanical and physical properties of hydrothermally altered rocks, Taupo Volcanic Zone, New Zealand. *Journal of Volcanology and Geothermal Research, 288*, 76-93. doi:10.1016/j.jvolgeores.2014.10.008.

Chapter 3 Preamble

In Chapter 2, I describe a laboratory study in which I thermally stress hydrothermally altered andesite and find that temperatures exceeding 700 °C have the strongest influence on the altered rock (lower porosity, higher permeability). In the next chapter, I use this data to approach a sub-aerial, fossil hydrothermal system and, in doing so, shift our focus from the Rotokawa Geothermal Field to Pinnacle Ridge, Mt. Ruapehu, New Zealand, the primary field area of this thesis. In Chapter 3, I present laboratory-derived data from a hydrothermal system exposed by glacial dissection (Fig. 1). I use the auspicious display of the hydrothermal system to identify the related geotechnical units (Fig. 2 [Fig. 3.15]) and compare the mechanical and physical property data of altered host rock with distance to the intrusion.

Chapter 3 has been published in the *Journal of Volcanology and Geothermal Research*. This chapter is presented in its published format:

> Mordensky, S. P., Villeneuve, M. C., Kennedy, B. M., Heap, M. J., Gravley, D. M., Farquharson, J. I., Reuschlé, T. (2018) Physical and mechanical property relationships of a shallow intrusion and volcanic host rock, Pinnacle Ridge, Mt. Ruapehu, New Zealand. *Journal of Volcanology and Geothermal Research* 359, 1-20. https://doi.org/10.1016/j.jvolgeores.2018.05.020

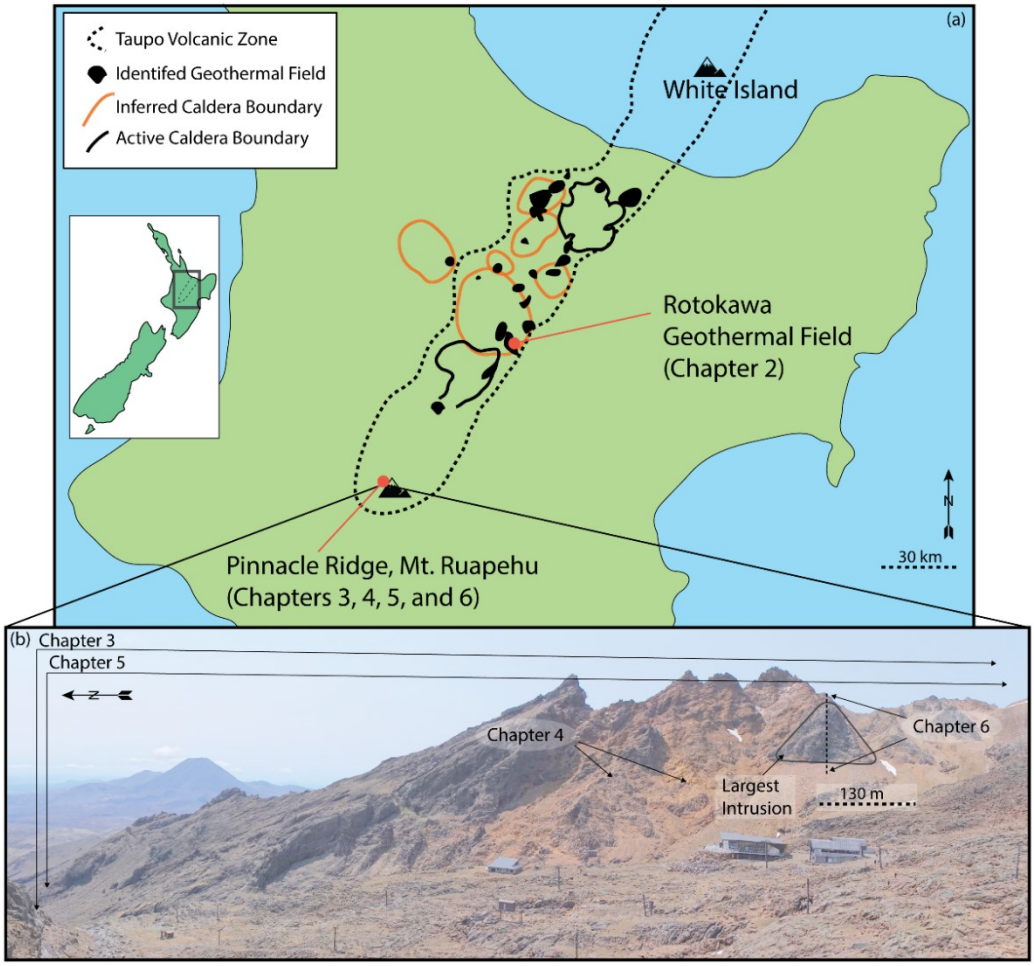

Figure 1. Primary site locations specific to the research presented in this study. (a) Sites of the two hydrothermal systems in New Zealand. (b) Sites specific to Chapters 3 – 6 at Pinnacle Ridge. Solid black polygon marks boundary of the largest young intrusion. Scale is approximate.

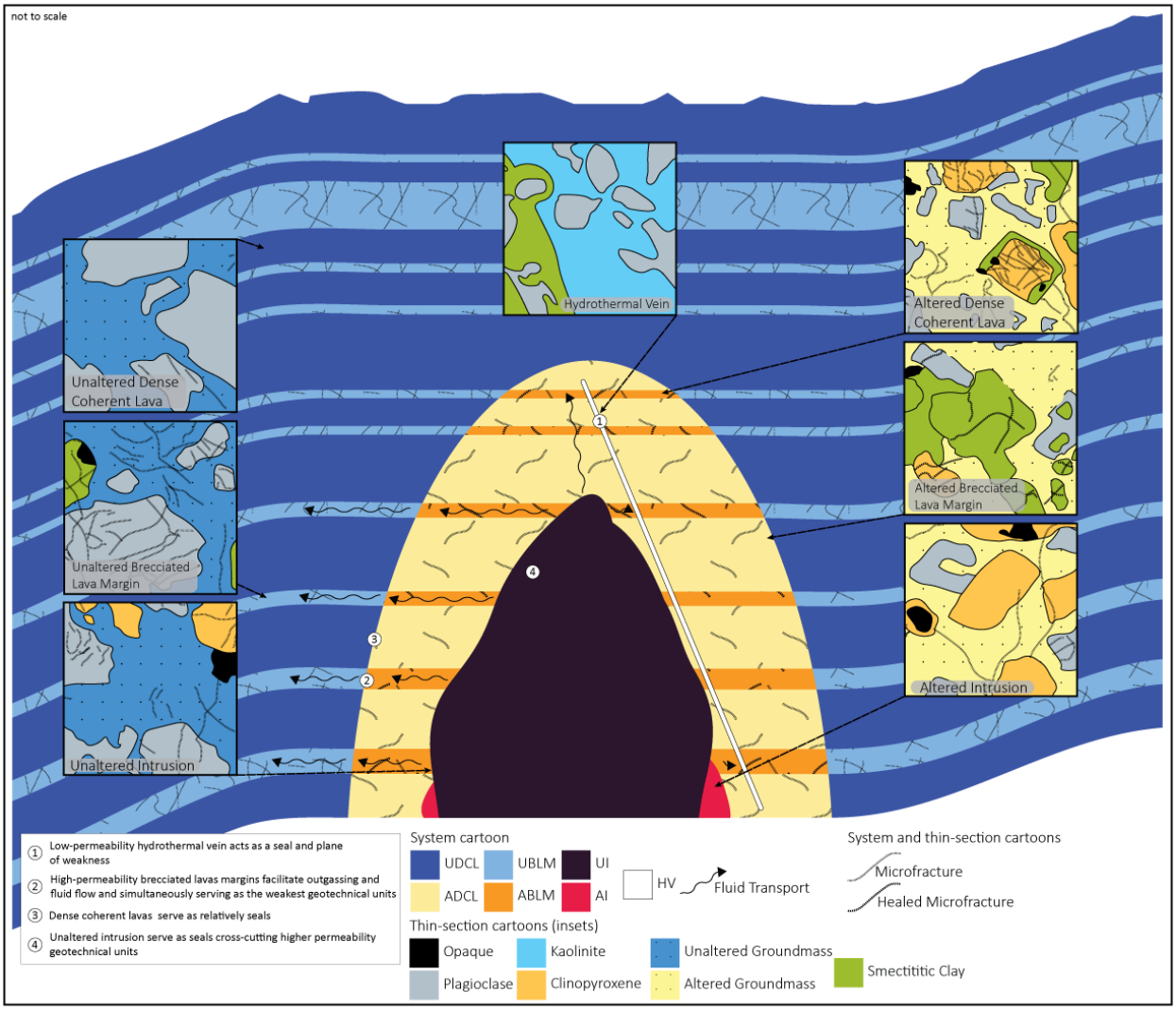

Figure 2 (Fig. 3.15). Conceptual model of the shallow hydrothermal system from a small intrusion at Pinnacle Ridge. This figure serves to introduce the framework and relevance for the geotechnical units introduced in Chapter 3. See Chapters 3 and 5 for detailed descriptions of each geotechnical unit. Sketches of each geotechnical unit by thin section according to major mineral assemblage and properly scaled microfractures are linked to their respective geotechnical units (straight arrows). The general structural relationships between geotechnical units are depicted in the larger cartoon model. Fluid transport arrows depict preferential flow within brecciated lava margins inside and outside of the alteration halo. Geotechnical units and fractures are not to scale.

Chapter 3

Physical and Mechanical Property Relationships of a Shallow Intrusion and Volcanic Host Rock, Pinnacle Ridge, Mt. Ruapehu, New Zealand

S. P. Mordensky[1], M. C. Villeneuve[1], B. M. Kennedy[1], M. J. Heap[2], D. M. Gravley[1], J. I. Farquharson[2], T. Reuschlé[2]

[1]Department of Geological Sciences, University of Canterbury, Private Bag 4800, Christchurch 8140, New Zealand

[2]Institut de Physique de Globe de Strasbourg (UMR 7516 CNRS, Université de Strasbourg/EOST), 5 rue René Descartes, 67084 Strasbourg cedex, France

Abstract

Shallow magmatic intrusions are prevalent in volcanic settings worldwide. Understanding how these intrusions interact and influence their volcanic host rocks is therefore relevant to many engineering geology, geothermal, and volcanological applications. In this study, we present the most comprehensive dataset for a shallow intrusion and its host rock in a volcanic setting to date, detailing the mechanical and physical properties of volcanic rocks from Pinnacle Ridge, Mt. Ruapehu, New Zealand. Based on the geomechanical properties of 194 measured samples, we identify seven geotechnical units: (1) unaltered dense coherent lava, (2) altered dense coherent lava, (3) unaltered brecciated lava margin, (4) altered brecciated lava margin, (5) unaltered intrusion, (6) altered intrusion, and (7) hydrothermal veining. We detail the mineralogy (andesite compositions ranging from primary to an advanced argillic alteration assemblage), porosity (0.7–31%), permeability (10^{-21}–10^{-12} m^2), elastic wave velocities (1994–5615 m/s), uniaxial compressive strength (1–332 MPa) of these geotechnical units. Our laboratory analyses indicate that primary lithology is the predominant control on the physical and mechanical properties of the geotechnical units. Additionally, the data suggest that there is a correlation between distance to the largest intrusion; this is particularly evident for the measurements on the brecciated lava margin samples. Towards the largest intrusion, this breccia shows decreasing porosity (30.92 to 5.49%) and permeability (10^{-12} to 10^{-17} m^2) and increasing elastic wave velocities (1994 to 4157 m/s) and uniaxial compressive strength (3 to 61

MPa). Thin-section analysis suggests that these correlations are due to mineral precipitation within fractures and pores in the brecciated lava margins. These correlations with distance to the largest intrusion are not shared by the altered intrusions or dense coherent lavas. We suggest that the high primary permeability of the unaltered breccia facilitated efficient hydrothermal fluid circulation and mineral precipitation adjacent to the intrusion. The other geotechnical units are less affected because hydrothermal fluid flow, alteration, and mineral precipitation were limited due to low initial permeability (10^{-21}–10^{-16} m^2). Our study shows that the initial properties of the host rock (i.e. porosity and permeability) control the extent of hydrothermal alteration and the susceptibility to modifications of rock geomechanical properties. Modifications to porosity and permeability can influence edifice-scale behaviour; for example, a reduction in permeability can result in pore pressure augmentation, which exerts a primary control on volcanic slope stability, seismicity, and eruptive behaviour. This study provides the most comprehensive and complete geomechanical properties data suite on a shallow intrusion in volcanic host rock to date and will support monitoring and modelling of volcanic hazards associated with shallow igneous intrusions.

3.1 Introduction

The links between intrusions and volcanic rock properties are poorly understood, despite the prevalence of shallow intrusions within volcanoes. The influence of intrusions on host strata is critical to volcanic hazards (e.g. Voight, 2000; del Potro and Hürlimann, 2008, 2009) and operation of nearby industrial infrastructure (e.g. geothermal power facilities: Rosenberg et al., 2009; Scott et al.,2015). Although the physical and mechanical properties of rocks in non-volcanic (e.g. Brace et al., 1966; Byerlee, 1967; Lundborg, 1968; Vutukuri et al., 1974; Tapponnier and Brace, 1976; Tullis and Yund, 1977) and volcanic (e.g. Saar and Manga, 1999; Rocchi et al., 2004; Apuani et al., 2005; Farquharson et al., 2015; Heap et al., 2015a; Schaefer et al., 2015) settings has been studied for many decades, we build on recent academic momentum (e.g. Stimac et al., 2004; Moon et al., 2005; Pola et al., 2012; Siratovich et al., 2014; Wyering et al., 2014; Heap et al., 2015c, 2017a; Siratovich et al., 2015; Mayer et al., 2016) and systematically focus on spatially constrained altered volcanic rocks. A prerequisite to understanding the rock mass behaviour (i.e. the macro-scale) of the geotechnical units that comprise a volcanic edifice is to first understand the intact rock properties at the micro- and meso-scale (e.g. Martin and Chandler, 1994; Hoek and Diederichs, 2006). Therefore, the aim of this study is to identify the geotechnical units that comprise the shallow fossil geothermal system surrounding intrusions at Pinnacle Ridge (Mt. Ruapehu, New Zealand). Samples of these units are then characterised in terms of their physical and mechanical rock properties, providing useful constraints for geomechanical modelling, both at Pinnacle Ridge specifically, but also in intrusion-hosting volcanic or

geothermal environments elsewhere. Our objective is to identify the controls on the physical and mechanical properties of the rocks hosting the intrusions to inform future modelling of outgassing of magmatic volatiles from the magma-filled conduit (e.g. Collombet, 2009; Collinson and Neuberg, 2012), subsurface hydrothermal activity (e.g. Hurwitz et al., 2007; Peltier et al., 2009; Christenson et al., 2010; Todesco et al., 2010; Fournier and Chardot, 2012; Scott and Driesner, in press), gas monitoring (e.g. Bloomberg et al., 2014; Peiffer et al., 2014), geothermal resources (Scott et al., 2016), and volcano seismicity (e.g. Leet, 1988; Nishi et al., 1996; Sherburn et al., 1998; Bean et al., 2014; Chardot et al., 2015). In particular, we aim to quantify the changes to the host rock as a function of the distance from the intrusion. To accomplish this, we categorize the intrusives and host rock according to their properties and field relations to assign geomechanical descriptions and define geotechnical units. We then compare the rock properties of these units with distance from the intrusion.

Magmatic intrusion into volcanic edifices is ubiquitous across an array of edifice sizes and shapes (e.g. Mount Kilauea (United States), South Sister (United States), Mt. Ruapehu (New Zealand), Red Crater (New Zealand), Mount Vesuvius (Italy), Colima Volcano (Mexico); Sigurdsson et al., 2000; and references therein). Intrusions affect volcanic host rock as a result not only of the intrusive process itself, but also by the subsequent establishment and persistence of hydrothermal systems. Intrusive events are commonly accepted to be driven by buoyancy disequilibria (Thomson and Schofield, 2008), and Vigneresse et al. (1999) suggest that local stress patterns—resulting from the interaction of the magma and host rock—exert the predominant control on the ultimate depth and geometry of a large intrusion. The local stresses associated with intrusive events are complex as they occur in both compressional and extensional environments, and the pressures that intrusive magma exerts on its surrounding environment can produce compressional and tensile stresses under near-surface conditions (Lipman, 2000; Galland et al., 2003, 2009; Casey et al., 2006). Hence, magmatic intrusions are highly variable subsurface structures that exist in several forms. They can be planar (e.g. sills and dikes), stocky (i.e. equant) or as amorphous bodies of magma (Vigneresse et al., 1999; Valentine and Krogh, 2006; Keating et al., 2007; Grant and Bixley, 2011).

Depending on the size, temperature, magma flux, and longevity of an intrusion—as well as the availability of water in and permeability of the host rock—an intrusion may produce a hydrothermal system (Hedenquist and Lowenstern, 1994; Hedenquist et al., 1998). Larger intrusions, kilometres in size (e.g. 10 km by 15 km), can take ~106 years to cool (e.g. large ultramafic sills; Cathles et al., 1997). Large intrusions can therefore foster long-lived, complex hydrothermal systems that can comprehensively change the mineralogical and chemical composition of their host rock (Henley and Ellis, 1983; Cathles et al., 1997).

Alternatively, small magmatic bodies (e.g. dikes 10 s of metres or less in width) cool relatively quickly (b5 years; Petcovic and Dufek, 2005). Recent heat conduction modelling has shown that an un-replenished (i.e. stagnant) 30 and 100 m-diameter dike containing magma at 940 °C would take almost two years and almost 20 years, respectively, to completely cool within a host rock at 50 °C (Heap et al., 2017b). Consequently, the effect of small dykes and sills on host-rock temperature and, in turn, alteration, is considered relatively minor when compared to those of larger systems (Barrington and Kerr, 1962; Quaderer et al., 2016).

Given the frequent occurrence of intrusions and the attendant generation of stresses within volcanic edifices (e.g. Gudmundsson, 2006 and references therein), magmatic intrusions may exert a crucial influence on the physical and mechanical properties of the edifice host rock. For example, the porosity of volcanic materials (and in turn, their permeability) may increase or decrease as a result of alteration imparted by an intrusion (Henneberger and Browne, 1988). Understanding intrusion-induced changes in physical and mechanical properties of the host rock is of relevance to numerous volcanic and hydrothermal processes (e.g. rock strength, fluid transport, slope stability; e.g. Apuani et al., 2005; Moon et al., 2009; Schaefer et al., 2015).

Pinnacle Ridge (Mt. Ruapehu, New Zealand) presents an ideal site at which to study the effects of intrusions on host volcanic strata as the intrusions are uniquely dissected and accessible with a well-constrained geological history. The results garnered from studying the physical rock properties of Pinnacle Ridge can be used to infer relationships between intrusions and the physical and mechanical properties produced by intrusions in other regions of the world for a range of geotechnical applications (e.g. Wyering et al., 2015). Furthermore, Mt. Ruapehu is a volcano frequently visited by the public and consequently presents a risk of landslide, rockfall, and volcanic eruption hazards to its visitors (e.g. Kilgour et al., 2010; Cook et al., 2018; Schaefer et al., 2018), and understanding how these small intrusions change the physical host-rock properties at Pinnacle Ridge may in turn play a greater role in hazard assessment for the continued safe use of Mt. Ruapehu as a recreational area.

3.1.1 Geological Setting

Mt. Ruapehu sits at the south end of the Taupō Volcanic Zone (TVZ) on New Zealand's North Island and serves as the most southernmost manifestation of the 1375-km Tonga-Kermadec volcanic arc (Fig. 3.1). The 300 × 60-kmTVZ, delineated by volcanic cones, domes, geothermal fields, hydrothermal vents, and active calderas (Wilson et al., 1995; Rowland and Sibson, 2001; Wilson and Rowland, 2016), is a rifted arc basin produced by the oblique subduction of the Pacific plate beneath the Indian-Australian plate (Cole, 1990; Bibby et al., 1995; Wilson et al., 2009; Rowland et al., 2010; Seebeck et al., 2014; Wilson and Rowland, 2016).

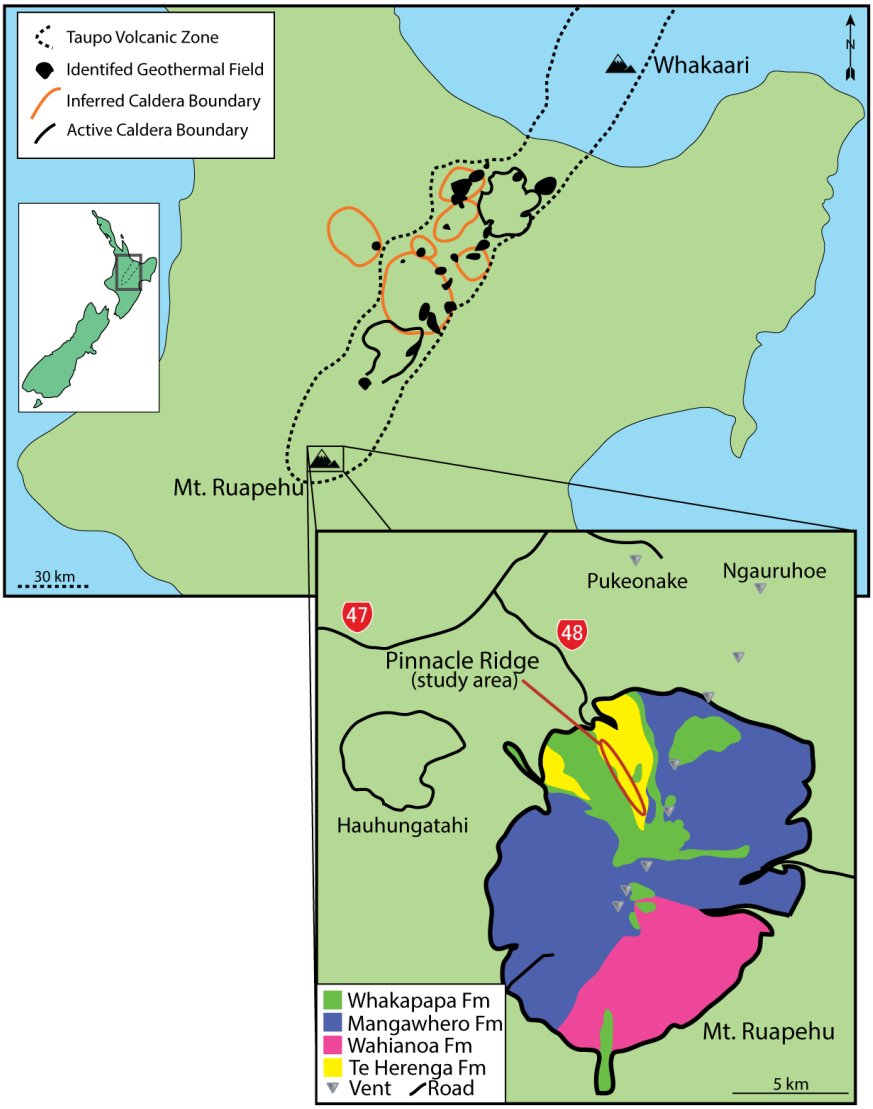

Figure 3.1 Location of Pinnacle Ridge on Mt. Ruapehu (green, blue, pink, and yellow), North Island, New Zealand and the active TVZ boundaries (dashed black) with the locations of geothermal fields (black), active caldera boundaries (black outline), and inferred caldera boundaries (red outline). Major roads for reference. Adapted from Hackett (1985), Wilson et al. (1995), Bibby et al. (1995), Rowland and Sibson (2004), Kissling and Weir (2005), Rowland et al. (2012), and Wyering et al. (2014).

Pinnacle Ridge has been subjected only to limited mapping and description in the past (i.e. Hackett, 1985; Hackett and Houghton, 1985). Hackett (1985) found Pinnacle Ridge to be composed of the Te Herenga Formation (~170 ka), the oldest formation of Mt. Ruapehu, exposed in a nearly vertical sequence by glaciation (~10 ka; Fig. 3.1). Hackett (1985) described the Te Herenga Fm as a stack of thin lava flows and autoclastic breccias radially dipping away from a now-eroded central cone. Te Herenga Fm flows are commonly plagioclase- and pyroxene-phyric andesites and basaltic andesites (54.9–58.0 wt% SiO2, 4.4–5.4 wt% MgO) and are typical of lava flows found on Mt. Ruapehu (Hackett, 1985; Price et al., 2012). Jointed

intrusions cut vertically through the dipping volcanic strata. An alteration halo approximately 400 m across is made apparent by an orange discolouration and surrounds the largest intrusion (~130 m across; Fig. 3.2). From field observations, Hackett (1985) suggested illite, montmorillonite, and minor pyrophyllite replaced most of the plagioclase in the altered host rock and intrusives. Pyroxene is replaced by clay and subhedral sulphides. Hackett (1985) proposed that the hydrothermal alteration occurred under near-surface conditions (approximately 50–500mbelowthe surface) from the hypabyssal textures of the intrusives, brittle deformation of the tuff breccias, and deposition of silica and kaolinite around the aureole edge, as is common for near-surface, oxidizing hydrothermal systems.

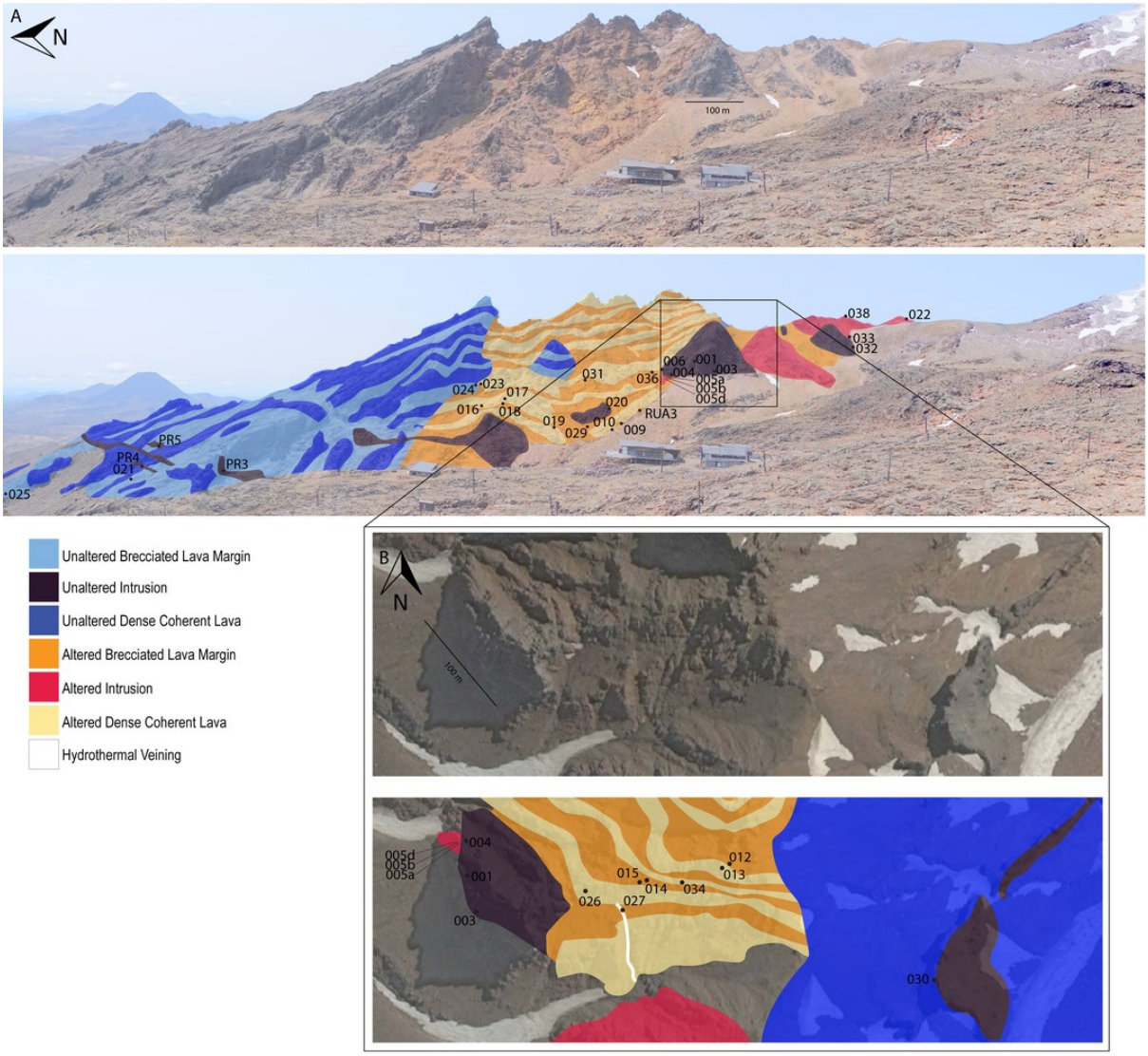

Figure 3.2 Geotechnical units of Pinnacle Ridge. Where possible, units were ground-truthed; however, some areas of the ridge were inferred from photography due to limited accessibility arising from terrain hazards. Sample locations (numbers) are provided in the main [A] and inset [B] frames. The geotechnical units labelled in the key (Unaltered dense coherent lava, Altered dense coherent lava, Unaltered brecciated

lava margin, Altered brecciated lava margin, Unaltered intrusions, Altered intrusions, and Hydrothermal veining) are defined and described in the Results section of this manuscript. Main Frame [A]: Photo taken from 600 m east (bearing 270°) of the largest intrusion of Pinnacle Ridge. North is frame-left. Foreground is composed of Whakapapa lavas on which sits the resort café (bottom, left of centre). Inset [B]: The inset is an aerial perspective to display data for features behind the largest intrusion which are not visible from the profile perspective. North is frame-up.

3.2 Methods

3.2.1 Sampling geotechnical units

Four field expeditions between 2015 and 2018 at Mt. Ruapehu identified the volcanic geotechnical unit classifications in line with those established by del Potro and Hürlimann (2008); however, where del Potro and Hürlimann (2008) define geotechnical units by rock mass, this study focusses on the intact (i.e. sample-scale) rock properties. We have subdivided these rocks according to their physical and mechanical properties and slightly modify their classification to keep our classifications more character descriptive and less process driven (i.e. "lava flow core" of del Potro and Hürlimann (2008) is equivalent to "coherent dense lava", and "autoclastic breccia margin" is equivalent to "brecciated lava margin"). Each geotechnical unit was further sub-classified as altered or unaltered based on field and thin-section mineral and textural observations. We collected samples from 35 locations over a range of distances (<100 m to >500 m) to the large intrusion of Pinnacle Ridge in the Te Herenga Formation (Fig. 3.2) for laboratory analyses. In order to reduce the probability of damaging the internal structure of the samples, blocks were collected without striking blows from a hammer. Instead, chisels and wedges were used to pry in situ rock away from the surface. The collected blocks were drilled in the laboratory with a 20-mm diamond bit and ground to a nominal length of 40 mm to produce between one to seven sample cores per block (depending on the size of the initial blocks). Attention was given to ensure that the bored cores did not include weathering rinds. Excess material was returned to Mt. Ruapehu to comply with the permitting agreement and to respect local cultural sensitivity.

3.2.2 Alteration and mineral identification

We describe the extent of alteration as fresh, light, moderate, heavy, and complete, as described in British Standard 5930 and used in other studies of hydrothermal altered volcanic materials (e.g. Watters and Delhaut, 1995; Shanks, 2012). A TerraSpec Spectrometer was used to identify the alteration products. The TerraSpec is designed for non-destructive mineral identification in mining and geology applications and has proved to be a reliable and tested method to this end (e.g. Simpson et al., 2006, Simpson et al., 2009; Kerr et al., 2011; Simpson, 2015). We manually discerned and identified the minerals by spectra form,

clarity, and intensity produced by each of the tested samples. When samples were too dark, the results are termed aspectral. Aspectral results do not suggest a lack of alteration materials, only that the particular sample was too dark for TerraSpec analysis to be a reliable mineral identification technique.

3.2.3 Porosity & density

The dry mass of each sample was measured after drying cores in an oven at 60 °C for a minimum of 48 h. Thereafter, all samples were saturated with distilled water, again for a minimum of 48 h. Measuring their saturated and saturated-immersed weights then allowed the determination of the bulk (water-saturated) density and connected water porosity based on the Archimedes principle (e.g. Gueguen and Palciauskas, 1994; Ulusay and Hudson, 2007).

3.2.4 Permeability

Given the wide range of sample permeability and the limitations of individual permeameters, three permeameters were used to evaluate the sample suite. The consistency of data between the three permeameters suggests there was no inherent bias in any one permeameter.

All samples were oven-dried at 60 °C for at least 48 h prior to permeability analysis and were left to equilibrate under confining conditions for at least 1 h before measurements commenced to allow time for the samples' microstructure to equilibrate with the applied confining pressure.

3.2.5 Steady-state permeametry

For the relatively high-permeability samples (>10^{-17} m^2), permeability was collected using a steady-state Vinci Technologies benchtop permeameter interfaced with a Bronkhorst El-Flow volumetric flowmeter at the Université de Strasbourg (see Farquharson et al., 2016; Heap and Kennedy, 2016). The steady-state permeameter records the volumetric flow rate through the sample core, driven by the imposed pressure differential of an inert pore fluid (argon) upstream and ambient atmospheric pressure downstream. Samples were radially confined at 1 MPa in order to prevent fluid flow around the sample's edge. Flow rate measurements were collected at several pressure gradients, allowing permeability to be calculated using Darcy's Law (Eq. (1)):

$$-\frac{dp}{L} = \frac{(\mu Q)}{Ak_D} \quad (1)$$

where p is the pressure, L is the length of the sample, A is the cross-sectional area, k_D is the gas permeability, μ is the dynamic viscosity coefficient of the pore fluid, and Q is the discharge volume per time (i.e. flow

rate). Forchheimer and Klinkenberg corrections were applied when appropriate (see Appendix 3.A.1). All measurements were collected at room temperature.

3.2.6 Pulse decay permeametry

For samples with a permeability of $<10^{-17}$ m^2, measurements were collected using either of two pulse decay permeameters: a Core Laboratories PDP-200 at the University of Canterbury and a custom-built prototype at the Université de Strasbourg. Both permeameters are similar in principle and in practice.

Samples were placed in Viton® fluoroelastomer sleeves between two steel end-caps. All samples were subject to an effective pressure (herein we assume that the effective pressure is simply the confining pressure minus the pore pressure) of ~2 MPa. Additionally, we ran representative samples of each major geotechnical unit under 2, 4, 7, 9, and 14 MPa effective pressure to observe how permeability changes with effective pressure. In the case of the Canterbury Pulse Decay Permeameter (PDP), the confining pressure was applied by oil. In case of the Strasbourg permeameter, the confining pressure was applied by distilled water. Although the pulse-decay analyses at Canterbury and Strasbourg operated at temperatures (30 °C and ~17 °C, respectively) the permeability measurements between the two apparatuses were consistent.

Both permeameters used the transient, pulse-decay method, in which the change in differential pressure was monitored over time. Both apparatuses used the ambient atmospheric pressure as the downstream pressure. The maximum pressure differential between the upstream and downstream pressures was 0.07 MPa. Permeability was calculated through a function (Eq. (2)) provided in Brace et al. (1968):

$$k_{\text{gas}} = \left(\frac{2\eta L}{A}\right)\left(\frac{V_{\text{up}}}{p_{\text{up}}^2 - p_{\text{down}}^2}\right)\left(\frac{\Delta p_{\text{up}}}{\Delta t}\right) \qquad (2)$$

in which k_{gas} is gas permeability, η is the viscosity of the pore fluid, Δt is change in time, L is the length of the sample, A is the cross-sectional area of the sample, V_{up} is the volume of gas in the upstream reservoir and piping, p_{up} is the pressure of the gas in the upstream reservoir and piping, and p_{down} is the pressure of gas in the downstream reservoir and piping. Δp_{up} is the change in p_{up} during elapsed time. While p_{down} remained constant, p_{up} decreased, which decreased Δp_{up} and produced a decrease in mean pore pressure. As with the steady-state permeameter, Klinkenberg corrections were applied when appropriate.

3.2.7 Acoustic wave velocities and dynamic elastic moduli

Compressional wave velocities (Vp) and shear wave velocities (Vs) were collected using a GCTS CATS interfaced with transducer-mounted piezoelectric quartz crystals operating at a 900 kHz resonance frequency and a 20 MHz-pulse acquisition rate with a minimum of 100 waveforms per compression wave type per sample. To collect dry and water-saturated velocities, the acoustic wave analyses were completed in two stages: 1) after drying at >40 °C for longer than 48 h; and 2) after being submerged in water under vacuum for longer than 72 h. Dynamic deformation moduli (see Appendix 3.A.2) were determined according to ISRM standard (Ulusay and Hudson, 2007). All measurements were collected at room temperature (17–30 °C).

3.2.8 Uniaxial compressive strength

We collected uniaxial compressive strength (UCS) measurements with a Technotest 3000 kN servo-controlled loading frame. Three types of experiment were performed: 1) we assigned each geotechnical unit a representative plug to which we attached 20 mm Tokyo Sokki Kenkyuujo Co. Ltd. gauges with a 2.12-gauge factor, two vertically for axial strain and two laterally for radial strain. These samples were subject to a constant load rate specific to each sample to ensure failure within 5–10 min of loading in order to determine the static elastic moduli of the geotechnical units according to ISRM standard (Ulusay and Hudson, 2007); 2) we outfitted another representative plug from each unit with two lateral strain gauges to measure lateral strain and a linear-variable displacement transducer (LVDT) extensometer to measure axial strain. These samples were deformed at a constant strain rate of 1.0×10^{-5} s^{-1}. We chose this strain rate in order to directly compare our results to those of other volcanic suites (e.g. Siratovich et al., 2014; Heap et al., 2015b); and 3) we tested the remaining samples using only an LVDT extensometer at a constant strain rate of 1.0×10^{-5} s^{-1}. Static deformation moduli (see Appendix 3.A.3) were determined by ISRM standard (Ulusay and Hudson, 2007). All measurements were collected at room temperature.

3.3 Results

3.3.1 Field and thin-section observations

We categorize Pinnacle Ridge into seven geotechnical units. Six, consisting of altered and unaltered lavas and intrusions, modifying those defined in del Potro and Hürlimann (2008). We also add a seventh unit comprised of hydrothermal vein material because of the potential importance of hydrothermal veining on the behaviour of the ridge.

The Te Herenga Formation is predominantly composed of altered and unaltered andesitic lava flows and intrusions, appearing dark grey and dark brown to orange-brown in fresh outcrop. The flows slope away from a topographic high (no longer present) centred near the modern resort café (−39.252332, 175.564062; Hackett, 1985). The layered Te Herenga deposits display variable thickness (1–3 m) with varied amounts of vesiculation and discontinuities. A 500 m-wide altered zone in the Te Herenga lavas surrounds a ~130 m wide intrusion exposed as a prominent 100 m-tall cliff face visible from the western exposure of Pinnacle Ridge (Fig. 3.2). Several smaller (metre-scale) intrusions populate the ridge in and outside the altered zone, but no visible alteration surrounding these smaller intrusions was observed. The phenocryst assemblage of the intrusions is similar to the lavas and is described in greater detail below. Within the alteration zone, cross-cutting relationships display at least two generations of intrusions, with the older generation exhibiting evidence of alteration.

Hydrothermal veining, where visible, is often <10 cm wide and observable only from a distance due to hazardous terrain. A single vein, ~1 m across, composed of kaolinite, albite, and smectite, is reasonably accessible and we adopt it as a representative exposure of hydrothermal veining for the purposes of our study. Although hydrothermal veining appears to constitute <0.01% of the volume of Pinnacle Ridge, understanding its physical rock properties may be critical to understanding the mechanical properties of the ridge, as the veining could serve to create planes of structural weakness or barriers to/conduits for fluid flow.

The Te Herenga lavas can be divided into two predominant geotechnical units: 1) dense coherent lava and; 2) brecciated lava margins interlayered with the dense coherent lavas. We further categorize the geotechnical units by the presence or absence of alteration. Therefore, we classify and describe the geotechnical units of Pinnacle Ridge as: unaltered dense coherent lava (UDCL), altered dense coherent lava (ADCL), unaltered brecciated lava margin (UBLM), altered brecciated lava margin (ABLM), unaltered intrusions (UI), altered intrusions (AI), and hydrothermal veining (HV; Fig. 3.2). Each geotechnical unit is detailed below. In the following section, we detail the characteristics of the seven geotechnical units. The discontinuity characteristics of the geotechnical units will be described in a forthcoming study.

3.3.1.1 Unaltered dense coherent lava (UDCL)

UDCL form the grey to dark-grey 1–3 m high cliffs outside of the orange alteration halo surrounding the largest intrusion at Pinnacle Ridge (Fig. 3.2). UDCL are interlayered with UBLM. UDCL appears unaltered with no obviously visible porosity (Fig. 3.3a). Unsurprisingly, the primary mineralogy of UDCL is identical to UBLM and UI. Thin-section analysis shows that the unaltered lavas appear to be primary porphyritic

hosting predominantly plagioclase-, pyroxene-, glass- bearing groundmass (<10 μm) and traces (<1%) of pyrite (<50 μm) with pyroxene glomerocrysts (0.5 cm to >3 cm), characteristically consistent to the composition and texture reported in prior studies of the Te Herenga Formation (Fig. 3.4a; e.g. Hackett, 1985; Conway et al., 2016). UDCL phenocryst sizes (~500 μm) are similar to those of UI. Microfracturing (<5 μm across and >100 μm long) appears limited and isolated. There is no evidence of alteration.

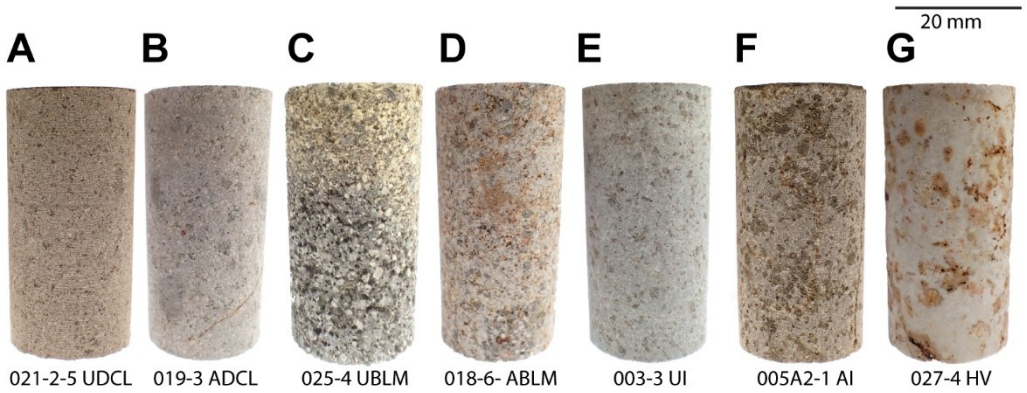

Figure 3.3 Sample cores of the geotechnical units of Pinnacle Ridge. Collection sites are in Fig. 3.2. (A) UDCL samples appear coherent with no visible alteration. (B) This ADLC sample displays a fracture at the bottom of the sample. Alteration is not apparent at the sample scale. (C) UBLM hosts relative high porosity visible at the sample scale. (D) ABLM hosts smectite-group clay alteration products that fill the pore space. (E) UI samples appear coherent with no visible alteration. (F) AI samples appear coherent at sample scale. Alteration is visible in patches along paths of fluid flow. (G) HV samples host isolated pore volumes and fractures (bottom left). See *Section Field and Thin-Section Observations* for full descriptions.

3.3.1.2 Altered dense coherent lava (ADCL)

ADCL are found inside the alteration halo at Pinnacle Ridge and are interlayered with ABLM (Fig. 3.2). The similarities of the ADCL and the UDCL are apparent in thin-section (e.g. similar phenocryst crystal size, frequency, and distribution). The ADCL cores differ from those of UDCL only by slight discoloration of intact rock. Alteration is most apparent in ADCL cores along discontinuity boundaries as a variation in colour (Fig. 3.3b). TerraSpec analysis confirms advanced argillic alteration (i.e. smectite and kaolinite clays). Thin-section analysis reveals that the pervasiveness of the advanced argillic alteration is not extensive nor complete in ADCL. Rather, alteration is light to light-moderate with observable remnants of primary textures and mineralogy (Fig. 3.3b; British Standard, 2007). UDCL and ADCL differ as a result of surficial advanced argillic alteration of the phenocrysts, partial or complete alteration of the groundmass, and surficial alteration along fracture boundaries in ADCL. Although this study does not quantify the microfracture density, ADCL hosts a visibly higher microfracture density in its phenocrysts and groundmass with wider (>10 μm) and longer (>200 μm) microfractures than UDCL (Fig. 3.4b).

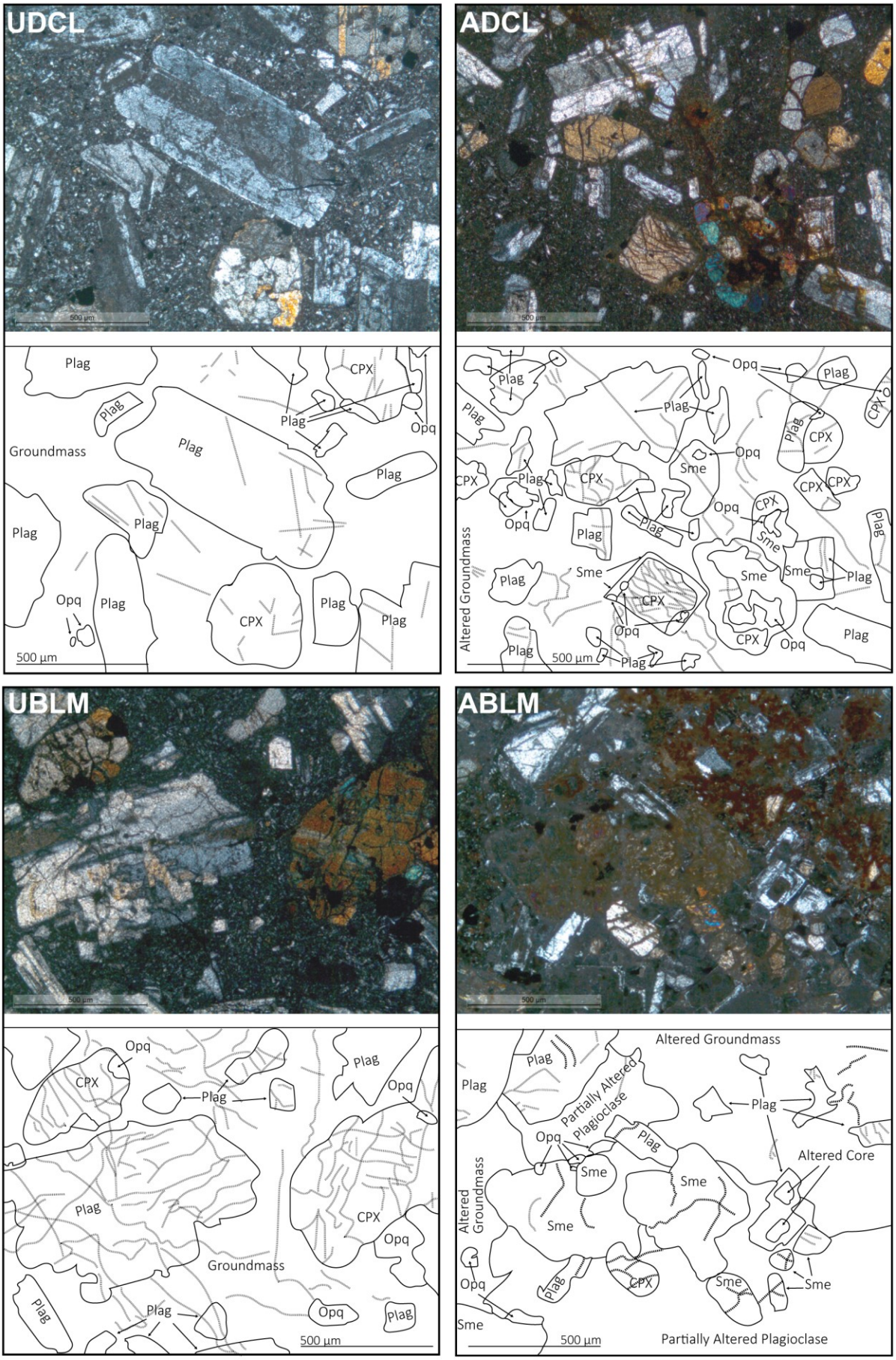
UDCL
ADCL
UBLM
ABLM
Plag
CPX
Opq
Sme
Groundmass
Altered Groundmass
Partially Altered Plagioclase
Altered Core
500 µm
Microfracture
Healed Microfracture

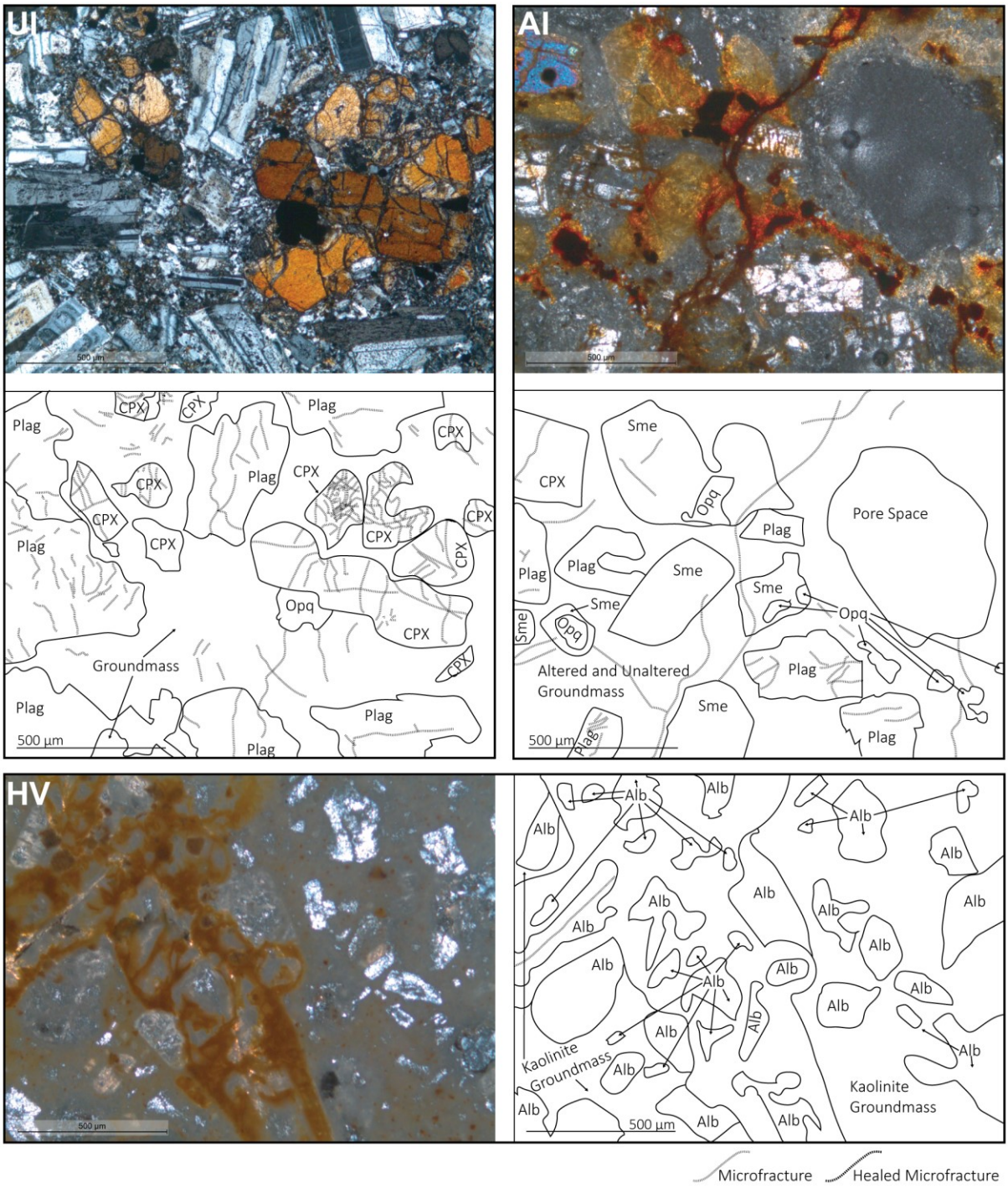

Figure 3.4 Photomicrographs [UDCL (024), ADCL (019), UBLM (025), ABLM (018), UI (003), AI (005c), HV (027)] under cross-polarized light. Crystals (Plag – Plagioclase, Sme – Smectite, Alb – Albite, CPX – Clinopyroxene, Opq – Opaque) and factures are identified. Collection sites are in Fig. 3.2. The sample preparation of UBLM was biased towards a stronger, more coherent piece of rock as UBLM is easily broken with minor hammer strikes by hand in the field. A stronger sample was selected for thin-section analysis so as to survive the sample preparation. Hence, the image of UBLM provided in this study does not likely represent the true porosity of UBLM (i.e. porosity by the triple weight method appear >25%, whereas thin-section observation appears <10%). See *Section Field and Thin-Section Observations* for full descriptions.

3.3.1.3 Unaltered brecciated lava margin (UBLM)

UBLM are interlayered with UDCL outside the alteration halo. Hydrothermal alteration is non-existent to light. UBLM forms grey to dark grey, low-angled 1–3 m high slopes (Fig. 3.2) between the more vertical UDCL units and appears brecciated at the outcrop scale. The breccia is matrix supported with sub-angular to angular clasts varying from <1 cm to 10 s of cm across. At the sample-scale, UBLM porosity appears to be dominated by vesicles (~1 mm in diameter; Fig. 3.3c); however, thin-section analysis also reveals the presence of <5 μm microfractures in the phenocrysts and matrix. UBLM is similar in mineral assemblage to UDCL in thin-section (Fig. 3.4c) with similar phenocryst crystal size, predominant composition, frequency, and distribution.

3.3.1.4 Altered brecciated lava margin (ABLM)

ABLM is interlayered with ADCL in a similar fashion as UBLM is interlayered with UDCL. ABLM is distinct from a distance by its yellow, orange, and red gradual slopes in the otherwise monochromatically grey andesite setting (Fig. 3.2). Like UBLM, the ABLM is matrix supported with sub-angular clasts varying from <1 cm to 10 s of cm across. ABLM cores host noticeably less porosity than UBLM cores (Fig. 3.3d). Alteration products are visible filling several pore spaces creating a discoloured, patchy texture in the sample core. In thin-section, ABLM hosts a moderately- to heavily-altered porphyritic texture (Fig. 3.4d). Like in ADCL, TerraSpec analysis finds alteration products consist predominately of smectite and kaolinite in ABLM. Unlike ADCL, the thin-section observations show that the matrix and clast groundmass as well as the free-surface boundaries (e.g. fractures and pores) are altered in many ABLM samples. Where preserved, the crystals in the matrix appear to be of similar composition and size as UBLM, UDCL, and ADCL. The porosity of ABLM is lower than that of UBLM. Instead, smectite appears to fill pore spaces. Similarly, microfracturing is not visible in the altered ABLM groundmass; however, microfracturing in the remaining phenocrysts has similar frequency of distribution and random orientation as UBLM.

3.3.1.5 Unaltered intrusions (UI)

UI forms the large cliff faces inside the alteration halo and several smaller cliff faces inside and outside the alteration halo (Fig. 3.2). Intrusions appear in two forms in the field area: 1) dikes (2–5 m across; e.g. UI of PR3; see Fig. 3.2); and 2) stocky intrusions (e.g. 10–130 m across; UI of 001; see Fig. 3.2). Dikes are planar structures with high length-width aspect ratios, whereas stocky intrusions are defined dimensionally by low-aspect ratios. Dikes appear ubiquitously distributed inside and outside the alteration halo, while stocky intrusions appear only within the alteration halo. UI appears as grey, nearly vertical outcrops that

form prominent topographical features. The largest UI in the field area cuts across ABLM, ADCL, and AI. Columnar joints with ~50 cm spacing are present in the dikes. Long (>10 m), sub-vertical cooling fractures are present in the larger, stocky intrusions. UI has the lowest porosity of all the geotechnical units, with no visible vesicles/pores from field observation. At the sample-scale, UI cores appear similar to UDCL with no immediately visible alteration or porosity (Fig. 3.3e). The mineral compositions of the groundmass and phenocrysts are similar to the UDCL, but the groundmass crystals appear coarser (>10 μm) than UDCL (Fig. 3.4e). The primary mineralogy and textures remain unaltered. Alteration minerals are nearly non-existent with exception of the margin of the largest UI, where TerraSpec analysis confirmed smectite. While isolated, <5 μm microfractures are prevalent in phenocrysts; these fractures do not continue into the groundmass. With no observed pores, these predominantly isolated microfractures constitute the majority of the void space in UI.

3.3.1.6 Altered intrusions (AI)

AI do not form the same prominent topographic features as UI (Fig. 3.2) and are found only within the alteration halo, primarily adjacent to UI. Instead, AI outcrops form gradually sloping, orange-grey faces and do not display the apparent ~50 cm-spaced joints of UI. Sample cores of AI appear to have more porosity than those of UI. Alteration appears preferentially along fractures (Fig. 3.3f). Thin-section analysis shows that AI hosts the same primary lithology and primary texture as UI, but differing degrees of alteration (Fig. 3.3f). In thin-section, alteration appears to be preferential in clinopyroxene crystals and, to a lesser extent, free surface boundaries (i.e. fracture and pore surfaces). While vesicles are not visible in thin-section, as they are with UI, the microfractures in AI appear wider (>10 μm) than in UI and these larger microfractures cut through the groundmass and link together. TerraSpec observations show that the alteration products consist of kaolinite and smectite (montmorillonite). The porphyritic texture and fabric of the primary magmas remains visible. Thin-section analysis reveals microfractures not observed in UI (Fig. 3.4e,f).

3.3.1.7 Hydrothermal vein (HV)

Hydrothermal veining is not pervasive along Pinnacle Ridge, but minor veining is found within 50 m to the east of the largest UI. Most veining is immediately adjacent (<50 m) to the intrusion and <20 cm wide in the ADCL and ABLM host rock. Unfortunately, these veins are inaccessible to measure or sample due to terrain hazards. HV forms a local topographic low where exposed (Fig. 3.2). It is possible that more hydrothermal veining is present within the alteration halo, but its scale and surface weathering make it

difficult to identify where the ridge is not safely accessible. However, a single vein 1-m thick runs several tens of metres sub-parallel to the ridge ~50 m to the east of the largest UI. Sample cores reveal that fractures <1 mm in width (Fig. 3.3g). The vein material is distinctly white. Thin-section observation shows that it is composed of albite grains (<0.25 mm) in a matrix of aphanitic kaolinite (identified by TerraSpec). The kaolinite constitutes the majority (>90%) of the hydrothermal vein with a minor smectite component (Fig. 3.4g).

3.4 Physical characterization

3.4.1 Porosity and permeability

The connected porosity of the Pinnacle Ridge host rock ranges from <1% to >30%. The unaltered geotechnical units have a narrower connected porosity range than that of the altered geotechnical units (Fig. 3.5; Tables 3.1, 3.S1). UI has the lowest connected porosity (0.71–11.23%). UDCL porosity is marginally higher (1.93–9.41%). The lower connected porosities of ADCL (2.41–24.59%) and AI (1.30–20.01%) overlap with the higher UI and UDCL porosities. UBLM exhibits the highest connected porosity (25.06–30.92%) and is the only unaltered geotechnical unit to have higher connected porosity than its altered counterpart, ABLM (5.49–28.99%). HV porosities overlap (10.94–23.78%) with AI and ABLM (Fig. 3.5).

Connected porosity generally correlates with permeability: low-porosity samples are low-permeability, and high-porosity samples are high-permeability (Fig. 3.6). As with porosity, UI has the lowest permeability (10^{-21}–10^{-16} m^2) while UBLM has the highest permeability (10^{-13}–10^{-12} m^2; Fig. 3.6; Tables 3.1, 3.S1). The most significant deviations from the porosity-permeability relationship are the six AI samples (unfilled pink triangles; Fig. 3.6) and HV samples (unfilled black diamonds; Fig. 3.6), which have a lower permeability (10^{-18}–10^{-16} m^2) than their connected porosity (3.78–14.37%) would suggest (Fig. 3.6).

Samples containing smectite are typically associated with the widest range of porosity (0.71–28.99%) and (10^{-19}–10^{-14} m^2) permeability values (see Table 3.S1). Kaolinite is more common in higher porosity (2.41–28.99%) samples and also covers a wide range of permeability (10^{-18}–10^{-14} m^2). HV, composed almost entirely of kaolinite, has lower permeability when compared to other samples with similar porosities (Fig. 3.6; Table 3.S1).

When comparing connected porosity and permeability to distance from the largest intrusion, there does not appear to be a correlation for most of the geotechnical units; however, ABLM displays a convincing positive correlation between connected porosity and distance (unfilled yellow circles; Fig. 3.7) and permeability and distance (unfilled yellow circles; Fig. 3.8). As distance to contact with the largest

intrusion increases from 20 m, the nearest ABLM sample location, to 237 m, the farthest ABLM sample location, porosity increases from 5.49–8.94% to 25.40–28.99% and permeability increases several orders of magnitude from 10^{-17}–10^{-16} m^2 to 10^{-15}–10^{-14} m^2 (Figs. 3.7, 3.8).

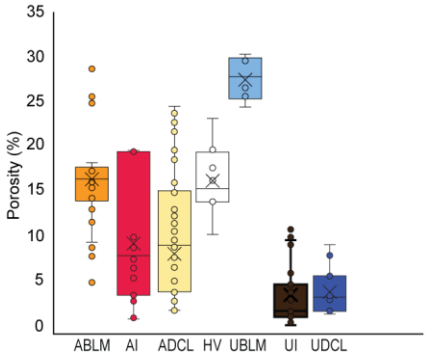

Figure 3.5 Connected porosity (n = 191) grouped according to the seven geotechnical units identified at Pinnacle Ridge (see text for details). Standard Error ≤ 1% of the reported values.

3.4.2. Permeability under varied confining pressure

We performed measurements of permeability on selected samples under effective pressures (p_{eff}) between 2 and 14 MPa (3–15 MPa confining pressure (p_c) at ~1 MPa pore pressure (p_p), assuming a simple effective pressure law where $p_{eff} = p_c - p_p$. The measured permeability of volcanic materials is influenced by the effective pressure under which the measurements are performed (Table 3.2). Permeability decreases with increased confining pressure for all lithologies (Fig. 3.9). This decrease is especially pronounced at low effective pressures (i.e. from $p_{eff} = 2$ to $p_{eff} = 4$MPa). In all but two samples, the initial decrease between 2 and 4 MPa effective pressure is approximately half an order of magnitude, after which samples exhibit relatively little permeability decrease with incrementally higher confining pressures. The stocky UI sample undergoes a more pronounced decrease relative to samples from other lithologies, exhibiting a reduction in permeability nearly two orders of magnitude when effective pressure is increased from 2 to 7 MPa.

Geotechnical Unit	Porosity (%)		Density (kg/m^3)		Permeability (m^2)	
	mean	std	mean	std	mean	std
UDCL	4.39	2.58	2630	106	3.51×10^{-17}	6.49×10^{-17}
	(16)		(16)		(16)	
ADCL	10.79	6.45	2330	255	3.13×10^{-15}	7.44×10^{-15}
	(59)		(59)		(58)	
UBLM	28.24	2.46	1911	63	8.84×10^{-13}	5.69×10^{-13}
	(6)		(6)		(3)	
ABLM	16.86	5.72	2161	189	9.87×10^{-15}	1.16×10^{-14}
	(33)		(34)		(30)	
UI	3.73	3.1	2645	144	3.81×10^{-17}	1.23×10^{-16}
	(41)		(41)		(40)	
AI	9.81	7.02	2523	171	2.44×10^{-16}	9.03×10^{-16}
	(28)		(28)		(27)	
HV	16.64	4	1926	99	2.72×10^{-17}	4.59×10^{-17}
	(8)		(8)		(8)	

Table 3.1 Physical property averages from Pinnacle Ridge. Numbers in parenthesis provide the sample size for the geotechnical unit for the analysis. The permeability values have been corrected for Klinkenberg and Forchheimer effects where appropriate. See Table 3.S1 for complete dataset.

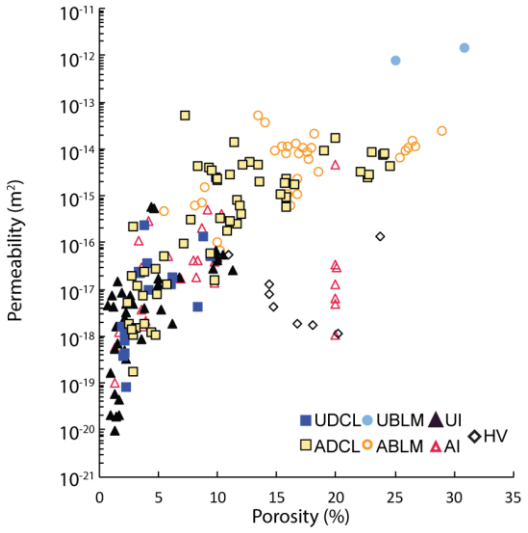

Figure 3.6 Permeability as a function of connected porosity (n = 181), distinguished according to the seven geotechnical units identified at Pinnacle Ridge (see text for details). Standard Error ≤ 1% of the reported values.

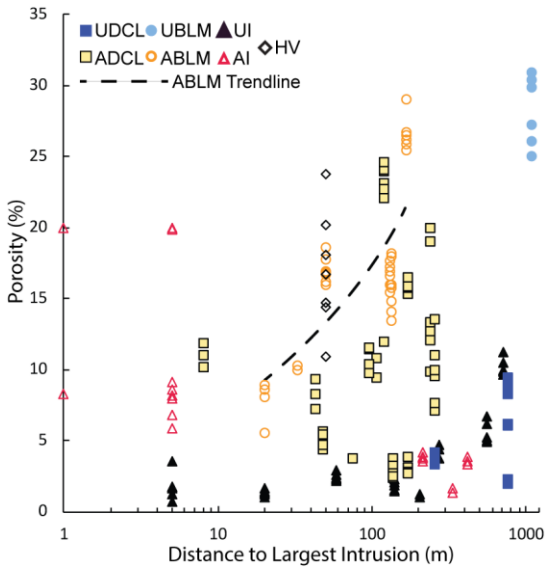

Figure 3.7 Porosity versus distance to the largest intrusion observed at Pinnacle Ridge. The ABLM trendline serves as a visual guide for the relationship between ABLM porosity and distance to the largest intrusion. Standard Error ≤ 1% of the reported values.

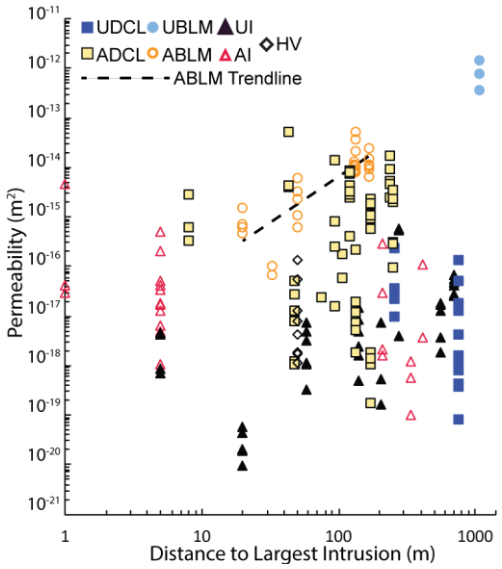

Figure 3.8 Permeability versus distance to the largest intrusion observed at Pinnacle Ridge. The ABLM trendline serves as a visual guide for the relationship between ABLM permeability and distance to the largest intrusion. Standard Error ≤ 1% of the reported values.

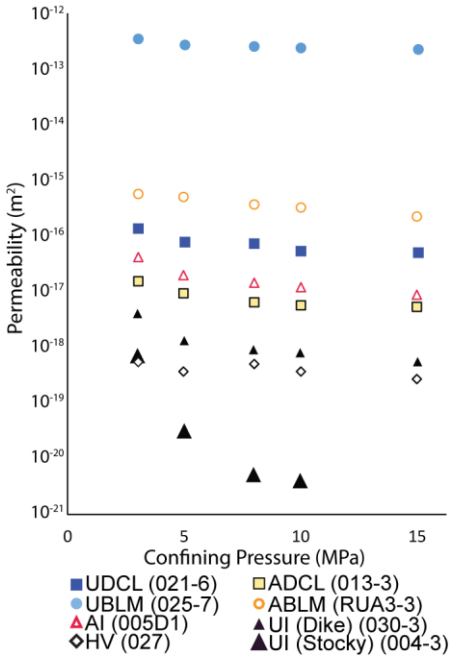

Figure 3.9 Confining pressure (depth) versus permeability with pore pressure (1 MPa) held constant. Numbers in the parentheses indicate sample number. Sample locations are available in Fig. 3.2. Standard Error ≤ 1% of the reported values.

Geotechnical Unit		UDCL	ADCL	ABLM	UI (dike)	UI (stocky)	AI	HV	UBLM
Sample		021-6	013-3	RUA3-3	030-3	004-3	005D1	027-2	025-7
Confining Pressure	3	1.36×10^{-16}	1.57×10^{-17}	5.79×10^{-16}	4.08×10^{-18}	6.95×10^{-19}	4.10×10^{-17}	5.64×10^{-19}	3.67×10^{-13}
	5	8.19×10^{-17}	9.37×10^{-18}	5.07×10^{-16}	1.34×10^{-18}	3.19×10^{-20}	1.93×10^{-17}	3.52×10^{-19}	2.80×10^{-13}
	8	7.62×10^{-17}	6.39×10^{-18}	3.76×10^{-16}	9.11×10^{-19}	4.93×10^{-21}	1.41×10^{-17}	5.02×10^{-19}	2.59×10^{-13}
	10	5.45×10^{-17}	5.63×10^{-18}	3.17×10^{-16}	7.77×10^{-19}	3.90×10^{-21}	1.19×10^{-17}	3.73×10^{-19}	2.43×10^{-13}
	15	5.07×10^{-17}	5.14×10^{-18}	2.26×10^{-16}	5.60×10^{-19}	b.d.l.	8.68×10^{-18}	2.63×10^{-19}	2.36×10^{-13}

Table 3.2 Permeability at different confining pressures. Pore pressure (1 MPa) is held constant while confining pressure varied (i.e. 3, 5, 8, 10, and 15 MPa). b.d.l. – below detectable limits ($<10^{-22}$ m^2). Sample locations are available in Fig. 3.2. Standard Error ≤ 1% of the reported values.

3.4.3 Elastic wave velocity

Elastic P-wave and S-wave velocities are inversely related to porosity (see Appendix 3.B.1). Dense, unaltered materials (i.e. UI and UDCL) have the highest P-wave velocities (~5600 m/s and ~5000 m/s, respectively), whereas the UBLM have the lowest P-wave velocities (~2400 m/s; Fig. 3.B.1; Table 3.3). The samples containing alteration (i.e. ABLM, AI, ADCL, and HV) have P-wave velocities (2406–4157 m/s, 3271–5388 m/s, 2471–4952 m/s, and 2718–4184 m/s, respectively) between the two unaltered end-members and strongly overlap among themselves. The dynamic Young's moduli have a similar relative distribution as the P-wave velocity data with UI having the highest (22.8–61.3 GPa) and UBLM having the lowest (3.6–7.5 GPa; see Appendix 3.B.2).

Geotechnical Unit	P-Wave Velocity (m/s)		S-Wave Velocity (m/s)		Dynamic Poisson Ratio		Dynamic Young's Modulus (GPa)	
	mean	std	mean	std	mean	std	mean	std
UDCL	4472 (16)	410	2339 (16)	267	0.31 (16)	0.04	39 (16)	9
ADCL	3701 (59)	734	1948 (59)	435	0.3 (58)	0.04	26 (59)	12
UBLM	2390 (6)	409	960 (6)	125	0.39 (6)	0.05	5 (6)	1
ABLM	3112 (33)	458	1603 (33)	222	0.32 (33)	0.02	16 (33)	5
UI	4767 (41)	473	2480 (41)	283	0.31 (41)	0.03	44 (41)	10
AI	4118 (28)	576	1991 (28)	362	0.33 (27)	0.05	28 (28)	11
HV	3224 (8)	431	1558 (8)	156	0.33 (8)	0.06	14 (8)	2

Table 3.3 Water-saturated elastic wave velocities and dynamic modulus averages of geotechnical units from Pinnacle Ridge. Numbers in parenthesis provide the sample size for the geotechnical unit for the analysis. See Table 3.S1 for complete dataset.

3.4.4 Uniaxial compressive strength (UCS) data

The distribution of the of UCS by geotechnical unit (Fig. 3.10) is approximately inverse to the distribution of porosity by unit (Fig. 3.5) with dense, unaltered material (i.e. UI and UDCL) serving as an upper UCS limit (73–332 MPa and 60–257 MPa, respectively), UBLM serving as a lower UCS limit (3–7 MPa), and the altered geotechnical units (ABLM, AI, ADCL, and HV) between the two extremes with overlap among

themselves (1–61 MPa, 45–297 MPa, 6–215 MPa, and 20–71 MPA, respectively; Table 3.4). The values of UCS for the ABLM appear to be inversely related to distance to the largest intrusion with a UCS of 8–18 MPa at 237 m from the intrusion and 44–61 MPa 20 m from the intrusion (Fig. 3.11). The static Young's moduli mirror the relative relationships of the dynamic Young's modulus by geotechnical unit classification (see Appendix 3.B.3).

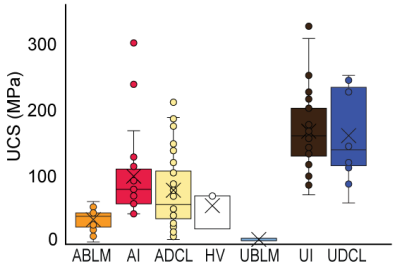

Figure 3.10 Uniaxial compressive strength (n = 159) grouped according to geotechnical unit. Standard Error ≤ 1% of the reported values.

Geotechnical Unit	UCS (MPa)		Static Young's Modulus (GPa)		Static Poisson Ratio	
	mean	std	mean	std	mean	std
UDCL	162 (15)	66	26 (15)	6	0.17 (3)	0.09
ADCL	77 (50)	53	20 (47)	9	0.23 (14)	0.13
UBLM	5 (3)	2	2 (2)	0		
ABLM	35 (29)	15	9 (25)	4	0.25 (5)	0.15
UI	168 (38)	58	29 (36)	10	0.18 (10)	0.06
AI	101 (21)	64	20 (19)	10	0.22 (5)	0.05
HV	54 (3)	29	9 (3)	1	0.17 (2)	0.03

Table 3.4 Uniaxial compressive strength and static elastic modulus averages of geotechnical units from Pinnacle Ridge. Numbers in parenthesis provide the sample size for the geotechnical unit for the analysis. See Table 3.S1 for complete dataset.

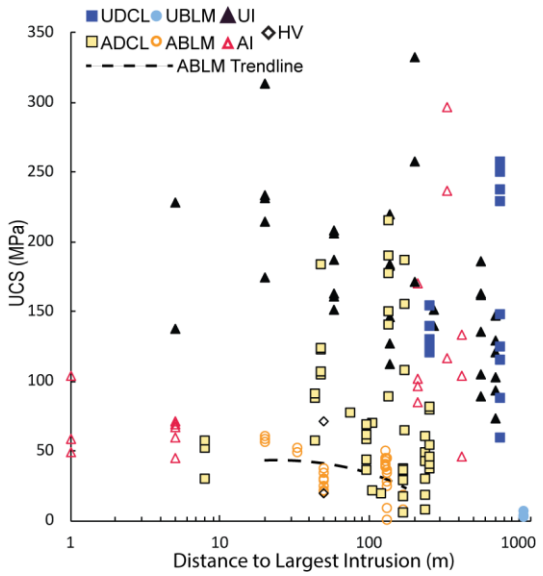

Figure 3.11 UCS versus distance to the largest intrusion observed at Pinnacle Ridge grouped by geotechnical unit. The ABLM trendline serves as a visual guide for the relationship between ABLM UCS and distance to the largest intrusion. Standard Error ≤ 1% of the reported values.

In summary, when altered, the coherent lava and intrusion increase in porosity and permeability, and decrease in elastic wave velocity and strength. In contrast, when altered and with increasing proximity to the intrusion, the lava breccias decrease in porosity and permeability and increase in elastic wave velocity and strength. Finally, the hydrothermal vein (HV) tested has distinct physical and mechanical properties compared to the other volcanic rocks.

3.5 Discussion

3.5.1 Alteration

The largest source of variability in our measurements is sample heterogeneity. All samples are heterogeneous to some degree, as is inherent to sampling volcanic materials (e.g. Apuani et al., 2005; Batzle et al., 2006; del Potro and Hürlimann, 2008). For example, the permeability of cores from the same sample block, drilled centimetres from each other, can vary by several orders of magnitude (e.g. Table 3.S1). Because hydrothermal alteration is produced by the interaction of warm to hot, ion-rich fluids and rock, it can lead to dissolution, deposition, and secondary mineralization (e.g. Frank, 1995; Finizola et al., 2002; Hurwitz et al., 2002; Hase et al., 2005; Pola et al., 2012, Pola et al., 2014), filling pores and cracks; therefore, there is no systematically measurable difference in alteration intensity between samples because it is masked by the heterogeneous modification of the primary porosity. Depending on the temperature of alteration, the physical properties are variably affected by the hydrothermal alteration process (Wyering et al., 2014; and references therein). At Pinnacle Ridge, we observe advanced argillic alteration throughout

the entire alteration halo. The implications of this alteration assemblage on the physical rock properties are discussed below.

3.5.2 Advanced argillic alteration and rock properties

The altered samples from Pinnacle Ridge show evidence of a smectite-group clay and kaolinite alteration assemblage. While we do not observe textural evidence of retrograde alteration, the smectite-kaolinite mineral assemblage we observe is consistent with pervasive advanced argillic alteration, which is typical of high-sulfidation, higher temperature, very acidic fluids in high-terrain composite cone environments (c.f. Henley and Ellis, 1983; Hedenquist and Lowenstern, 1994) and is expected given the temperature of andesitic magmas (e.g. >750 °C; Taylor et al., 1975). Alteration producing smectite-group clays is typically associated with an increase in porosity (e.g. Wyering et al., 2014; and references therein). Indeed, ADCL and AI have a higher porosity than their respective unaltered equivalents, UDCL and UI (Fig. 3.5). Porosity and microstructure act as a first-order control on other rock properties (e.g. permeability, elastic wave velocity, UCS) in altered and unaltered rock (Walsh and Brace, 1966; Heap et al., 2015a). Consequently, the permeability of ADCL and AI is higher than that of UDCL and UI (Figs. 3.6, 3.12b,c; Table 3.1), P-wave velocities of ADCL and AI are lower than those of UDCL and UI (Figs. 3.B.1, 3.B.2; Table 3.3), and the UCS of AI and ADCL are lower than those of UI and UDCL (Fig. 3.10; Table 3.4). The change in these mechanical and physical rock properties is primarily a consequence of increased frequency and widening of groundmass-hosted microfractures in AI and ADCL (Fig. 3.4b,f). This alteration does not increase the porosity of the brecciated lava margins.

The alteration in the more porous breccia appears to be associated with a decrease in porosity (28.99% to 5.49%), and a decrease in permeability (10^{-17} m^2 to 10^{-14} m^2) as distance to the largest intrusion decreases (237 m to 20 m; Figs. 3.7, 3.8, 3.12a, 3.13). In support of this trend the UBLM samples, collected at >1080 m from the largest intrusion, host an even higher porosity (25.06–30.92%) and exhibit higher permeability (10^{-13}–10^{-12} m^2) than ABLM (Table 3.1). The change in porosity relative to the change in permeability we see here is similar to those reported in other studies (e.g. Eichelberger et al., 1986; Klug and Cashman, 1996; Saar and Manga, 1999; Sruoga et al., 2004; Mueller et al., 2005; Gaunt et al., 2014; Heap et al., 2014b; Okumura and Sasaki, 2014).

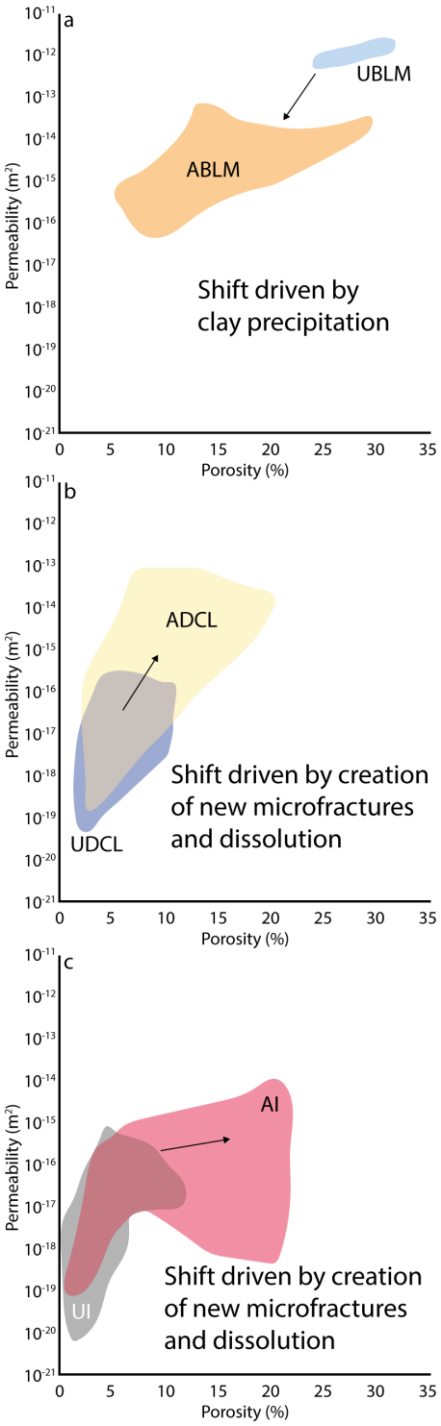

Figure 3.12 Unaltered versus altered geotechnical unit porosity-permeability relationships at Pinnacle Ridge. Shaded regions represent maximum extent of values for marked geotechnical unit. Arrows represent the shift in porosity and permeability the advanced argillic alteration produced in the (a) brecciated lava margins, (b) dense coherent lavas, and (c) intrusions. Unlabelled shaded regions in contact with the shaded regions represent an overlap in properties of the two geotechnical units.

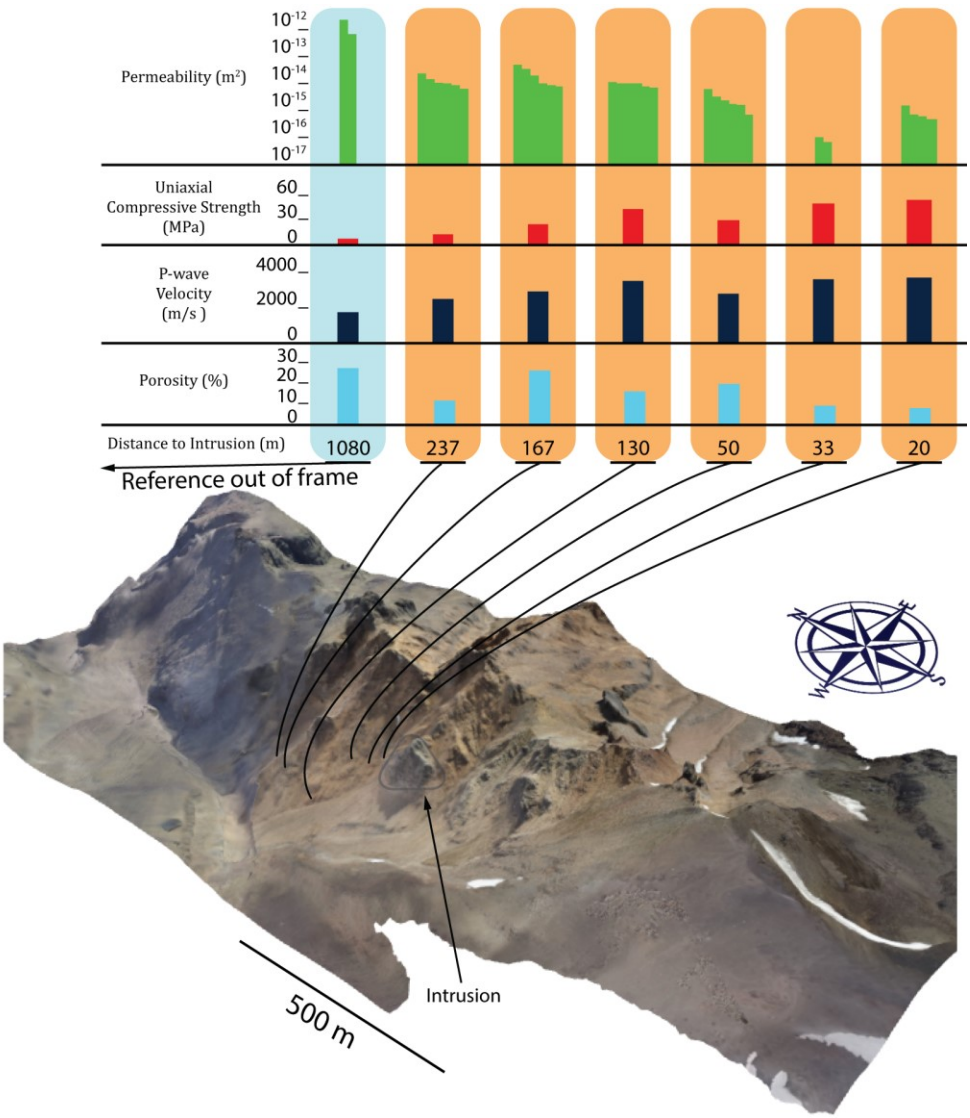

Figure 3.13 Spatial relationships of physical properties in brecciated lava margins at Pinnacle Ridge. Permeability (green), UCS (red), P-wave velocity (black), and porosity (blue) are provided for UBLM (light blue, left-most column) and ABLM (orange) with distances to the large, young intrusion. Scale bar is approximate. UBLM sample location is out of reference frame. Standard Error ≤ 1% of the reported values.

The cause (i.e. advanced argillic alteration) of the decrease in porosity and permeability is clear from thin-section images (Fig. 3.4c,d), with microfractures and vesicles observable in the groundmass of UBLM but not ABLM. In turn, we can infer that this porosity infilled during alteration and subsequently decreased the permeability of the brecciated lavas from 10^{-13}–10^{-12} m² in UBLM to 10^{-17}–10^{-14} m² in ABLM near the intrusion (Figs. 3.8, 3.13). These observations and interpretations are consistent with Heap et al. (2017a), who completed a comprehensive porosity-permeability study on the hydrothermal system at Whakaari/White Island, New Zealand, where pore-filling alteration lowered permeability to 10^{-17} m². Our data show that porosity and permeability express significant variability while sharing a relationship with

distance to a heat source (i.e. the largest Pinnacle Ridge intrusion) in a single alteration assemblage (i.e. advanced argillic) and, because porosity decreases (30.92% to 5.49%) with increasing proximity (>1000 m to 20 m; Fig. 3.13) to the contact with the largest intrusion, permeability decreases (Fig. 3.8) and P-wave velocity and UCS increase (Figs. 3.11; 3.B.3). It is critical to note that this correlation of rock properties and distance remains unique to ABLM.

Previous studies have shown that advanced argillic alteration can have a variable effect on porosity and permeability (e.g. Sruoga et al., 2004; Frolova et al., 2010; Heap et al., 2017a). Frolova et al. (2010) observed that porosity and density either increased or decreased depending on not just temperature and the rock composition, but also the hydrothermal fluid composition, fluid phase, fluid pH, and fluid exposure duration to which the rock was exposed. The complex interaction of these parameters produces variable rates of rock leaching and precipitation of secondary minerals in pores and cracks. The correlation between the ABLM porosity, permeability, and distance to the largest intrusion, along with the lack thereof for the other geotechnical units, suggests that brecciated lava margins preferentially hosted hydrothermal fluid flow in this shallow system due to high bulk permeability (e.g. Steefel and Lasaga, 1994; Morgan et al., 2003; Scott and Driesner, in press). This understanding is consistent with Larson and Taylor (1986), who measured oxygen isotopes in brecciated layers, and suggested that brecciated layers serve as fluid pathways. Therefore, we conclude that the higher-permeability, brecciated units allowed for deposition of secondary minerals (e.g. smectite-group clays). The interpretation derived from our porosity, permeability, and thin-section data is consistent with the findings of Scott et al. (2016), who used numerical modelling to show that alteration-induced compartmentalization of a shallow-intrusion, hydrothermal system is significantly influenced by the primary porosity and permeability of the host rock.

Smectite swells when introduced to water (Yusupova, 1946; Mering, 1947); therefore, porosity and permeability vary between wet and dry conditions (McNeal et al., 1966; Gupta & Verma, 1985). In this study, we measure porosity using methods that involve water-saturation. To account for this, we also completed porosity measurements using dichloromethane, which does not produce swelling in smectitic clay, on a subset of samples and compare these data to porosity values measured using water. The porosity values were consistently similar (within 2 – 3 vol. %) with no clear bias toward either liquid. We suggest the minimal impact of swelling from water is a product of the relatively low smectite contents of the samples. Because we measure permeability using water-free gasses, the permeability we report would likely be higher than that of the hydrothermal system when it was active. However, we argue that the effect on permeability would be low given the minimal swelling effect water produces in the porosity of these

rocks. An alternative source of error could be in the uncertainty of the data collected. If is worth consideration that we did not collect repeated porosity, permeability, and elastic wave velocity values to quantify this uncertainty. If a similar study was conducted again, we recommend recording porosity (i.e. Archimedes Triple Weight measurements), permeability, and elastic wave velocity (e.g. analyzing and picking the wave fronts) measurements a minimum of three times to determine uncertainty. If possible, multiple apparatuses should be used (e.g. the PDP-200 and steady-state permeameters) for the same sample. Doing so would allow more accurate uncertainty estimation.

3.5.3 Hydrothermal vein: a new geotechnical unit

Dense lavas, brecciated lavas, and intrusions constitute the vast majority (>99%) of the material exposed at Pinnacle Ridge. The remainder of this material is hydrothermal deposit. Although several veins within 50 m of the intrusion were observable from a distance, only one was accessible for sampling. The combination of physical properties unique to the kaolinite hydrothermal vein and consequences thereof require special consideration when characterising the materials of the volcanic environment. For example, HV has permeability values similar to UI and UDCL (Fig. 3.14); however, the UCS of HV (20–71 MPa) is substantially less than that of UI or UDCL (73–332 MPa and 60–257, respectively). The UCS of HV appears most like that of ADCL or ABLM (6–215 MPa and 1–61 MPa, respectively; Fig. 3.14). Consequently, intact HV presents the potential to inhibit flow as much as intact UI or UDCL and hinder outgassing processes and, thereby, can serve as a deep-seated destabilizing influence within an edifice. Additionally, HV displays inconsistent relative deformation moduli relationships with the other geotechnical units with dynamic and static Young's moduli similar to ABLM (Figs. 3.B.4, 3.B.6) while the static Poisson ratios are similar to UI and UDCL (Fig. 3.B.7). Existing research has already detailed the relevance and nuances of elastic moduli in intact and damaged volcanic material (e.g. Voight, 1989; Dzurisin, 2006; Heap et al., 2009; Kendrick et al., 2013; and references therein). Given the hazard edifice deformation poses in shallow volcanic environments (e.g. Siebert, 1992; Mcguire, 1996, Mcguire, 1998, Mcguire, 2006, and references therein), the lower Young's modulus of HV underscores the importance of having detailed data specific to each geotechnical unit when modelling processes involved with flank destabilization (e.g. Walter et al., 2005).

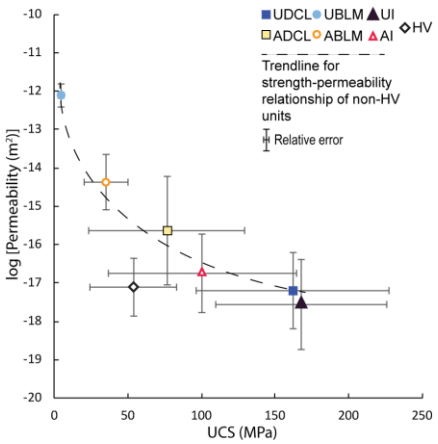

Figure 3.14 Log permeability as a function of uniaxial axial compression strength. The trendline (log Permeability [m^2] = −1.487 × ln [UCS [MPa]] − 9.6054, R^2 = 0.9661) depicts the general strength-permeability relationship of the non-HV geotechnical. HV deviates from this trend with lower strength and permeability inconsistent with the logarithmic function described above. Error bars represent relative error.

The structure of veining also provides sound reason to give HV its own geotechnical unit label. That is, HV does not necessary form parallel with bedding of the already deposited volcanic strata. Instead, HV can crosscut pre-existing strata (e.g. the veining at Pinnacle Ridge). Thus, the potential variance HV introduces to structure compounds a deformation environment already made complex from the interlaying of contrasting mechanical materials (e.g. Gudmundsson, 2002; Manconi, 2007). Therefore, HV presents the potential to cause subsurface compartmentalization (Senger et al., 2017) by acting as a barrier to fluid flow while simultaneously being less able to accommodate the related stresses and therefore be a potential source of edifice failure. This added complexity, coupled with the unique physical properties, requires that, although HV is remarkably low in volume compared to the other materials discussed, HV be considered as its own geotechnical unit.

3.6 Implications

This study's primary objective was to produce a large dataset to inform future modelling of outgassing of magmatic volatiles from the magma-filled conduit (Collombet, 2009; Collinson and Neuberg, 2012), subsurface hydrothermal activity (Hurwitz et al., 2007; Peltier et al., 2009; Christenson et al., 2010; Todesco et al., 2010; Fournier and Chardot, 2012; Scott and Driesner, in press), gas monitoring (Bloomberg et al., 2014; Peiffer et al., 2014), geothermal resources (Scott et al., 2016), and volcano seismicity (Leet, 1988; Nishi et al., 1996; Sherburn et al., 1998; Bean et al., 2014; Chardot et al., 2015). While our observation of hydrothermally induced pore- and crack-filling precipitation is not new knowledge by itself (e.g. Sruoga et al., 2004; Wyering et al., 2014; Heap et al., 2017a), the resulting relationship between the distance to the heat source of the alteration and the porosity of a particular geotechnical unit (Fig. 3.13) is novel and

provides a new perspective for understanding volcanic edifice behaviour. More specifically, the change in porosity has special consideration for edifice strength and permeability.

3.6.1 Strength and toughness

The predominant controls on sample strength appear to be the primary lithology and original porosity for the non-ABLM geotechnical units, and secondary alteration-controlled porosity with distance to the largest heat source for the ABLM (Fig. 3.13). The porosity-UCS relationship (Table 3.S1) exhibits a power law relationship similar to other studies on volcanic rocks (e.g. Al-Harthi et al., 1999; Heap et al., 2014b; Siratovich et al., 2014; Schaefer et al., 2015; Wyering et al., 2015; Zhu et al., 2016). In the context of the Wyering et al. (2015), Alteration Strength Index (ASI)—in which UCS is modelled from alteration zone, mineralogy, and lithological depth—our experimental data highlight that the geotechnical units represent families of different porosity, permeability, extent of alteration and, thereby, strength. As the samples from Pinnacle Ridge were collected from approximately the same depth (tens of metres in vertical difference), they have similar mineralogy, and reside within the same alteration zone, but with differing alteration extent. This underscores the importance of porosity in the ASI.

It is important to consider the extent to which advanced argillic alteration increases the strength of ABLM. Although clay precipitation can increase the strength of the brecciated lava margins greater than an order of magnitude (1 to 61 MPa), the strength of ABLM is still generally weaker than the other units. As such, brecciated lava margins still comprise the material most likely to yield (i.e. the formation of new fractures within the intact material) within the alteration halo; however, our data suggest that this failure is less likely immediately adjacent to and more likely farther from the intrusion (Fig. 3.13). This has important implications for the source of seismicity at active volcanoes and the initiation of slope failure as our data suggests that failure at depth is likely to occur up to several hundred meters from rather than immediately adjacent to an intrusion, where pore pressure is likely greatest (e.g. Elsworth, 1995).

Slope stability assessments for unaltered (e.g. Pacaya Volcano, Guatemala; Schaefer et al., 2015) and highly altered volcanics (e.g. Whakaari/White Island, New Zealand; Moon et al., 2009) have proven useful for considering the risk presented to infrastructure and human lives. The comprehensive dataset we present in this study has potential to substantially aid geoscientists modelling slope stability in geological environments hosting small, shallow intrusions because the change in strength and relative relationships of strength among the differing geotechnical units are critical for engineering assessment of rock mass strength (e.g. Generalized Hoek-Brown failure criterion; Hoek, 1994). Geoscientists must often use pre-determined strength values where mechanical property characterization appropriate for their specific

project is impractical (e.g. Brideau et al., 2011). One prospective example would be the steep, variably altered volcanic walls surrounding the Crater Lake of Mt. Ruapehu that present the potential to collapse and generate a tsunami within the Crater Lake, induce a lahar, and, thereby, pose a hazard to infrastructure (i.e. New Zealand State Highway 1, New Zealand National Electric Grid). The data in this study are directly applicable to slope stability assessment at a site like this, where access is highly restricted by terrain and the variably altered volcanic material would exhibit a range of geomechanical properties.

Similar to, but distinct from, strength is toughness. Toughness serves as a measure of resistance to fracture with more energy needed to fracture tougher materials. As a general rule, interlayered materials with unequal elastic values (Young's moduli) are tougher than homogenous materials (e.g. Gudmundsson, 2009, and references therein). Gudmundsson (2009) concludes that stratovolcanoes (e.g. Mt. Ruapehu) have a higher toughness than basaltic, shield edifices (e.g. Kīlauea Volcano). Our study presents data detailing the need for consideration of not just hydrothermal alteration presented by a small, shallow intrusion for consideration but also hydrothermal veins, as the veins can cut across existing strata (Fig. 3.15) and introduce variability and mismatch of elastic moduli in the structure (Figs. 3.B.4, 3.B.6).

3.6.2 Permeability

The physical properties of the rock around the magma chamber and conduit (i.e. dikes) control volcano outgassing and the development of hydrothermal systems. To understand the behaviour of a volcanic edifice or its hydrothermal systems, one must recognize the factors affecting the outgassing of the magmatic volatiles. Understanding the dynamic behaviour of a volcanic edifice is contingent upon a thorough comprehension of the materials that develop and exist near shallow magma bodies in that edifice. Chief among the material properties is permeability. At Pinnacle Ridge, UI and UDCL host low permeability values (~10^{-21}–10^{-16} m^2 and ~10^{-20}–10^{-16} m^2, respectively) that decrease by orders of magnitude with increasing confining pressure and hence depth (Fig. 3.9). Consequently, outgassing will be localised along UBLM and ABLM given the higher permeability (10^{-13}–10^{-12} m^2 and ~10^{-17}–10^{-14} m^2, respectively) of these units, and their relative permeability insensitivity to depth (Fig. 3.9).

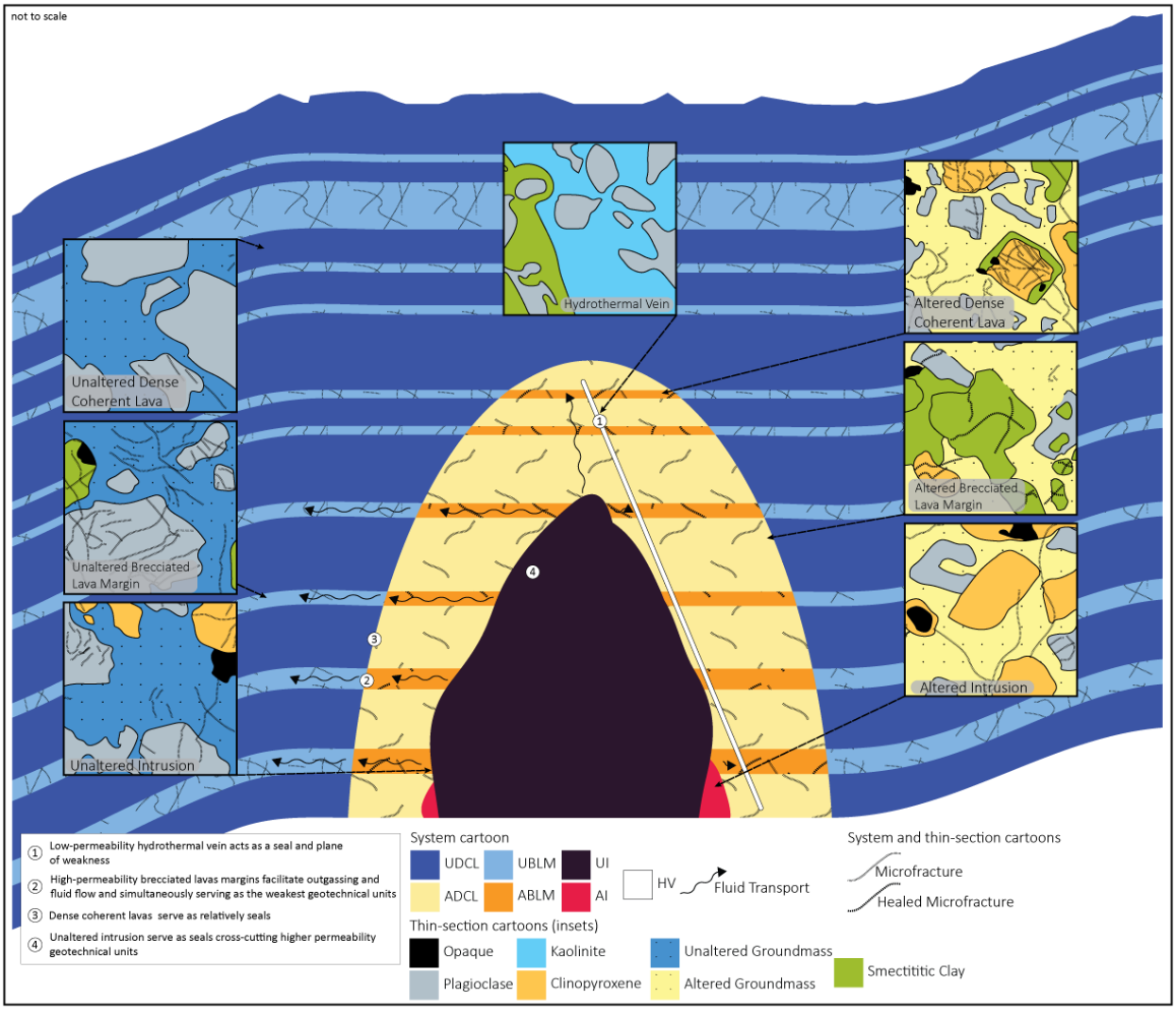

Figure 3.15 Conceptual model of the shallow hydrothermal system from a small intrusion at Pinnacle Ridge. Sketches of each geotechnical unit by thin section according to major mineral assemblage and properly scaled microfractures are linked to their respective geotechnical units (arrows with dashed-lines). The general structural relationships between geotechnical units are depicted in the larger cartoon model. Fluid transport arrows depict preferential flow within brecciated lava margins inside and outside of the alteration halo. Geotechnical units and fractures are not to scale.

3.6.3 Microfracture influence on permeability

In this study, we present the most complete dataset of mechanical and physical rock properties for a hydrothermal system created by the shallow emplacement of a small intrusion. The materials targeted by this study, dense lavas, intrusions, and altered, pore-filled volcanics, generally host lower permeability than those of other studies of more vesiculated or porous materials (Fig. 3.16a,b; Klug and Cashman, 1996; Saar and Manga, 1999; Rust and Cashman, 2004; Stimac et al., 2004; Mueller et al., 2005, Mueller et al., 2008; Bernard et al., 2007; Heap et al., 2014b, Heap et al., 2017a; Farquharson et al., 2015). Previous studies of

porosity-permeability relationships have found a two-slope power law model most accurate for describing their data (e.g. Bourbie and Zinsner, 1985; Heap et al., 2014b, Heap et al., 2015c, Heap et al., 2017a; Farquharson et al., 2015; Heap and Kennedy, 2016; Kushnir et al., 2016; Cant et al., 2018). Using Bayesian Information Criterion analysis described by Main et al. (1999), we find that a single power law describes the porosity-permeability trend for the data of the geotechnical units from Pinnacle Ridge when considered in aggregate (Fig. 3.16b); however, when considered individually, there appears to be a changepoint in ABLM at ~14.8% porosity and UI, UDCL, and ADCL around ~3–7% porosity, suggesting a change in the microstructural influence on permeability.

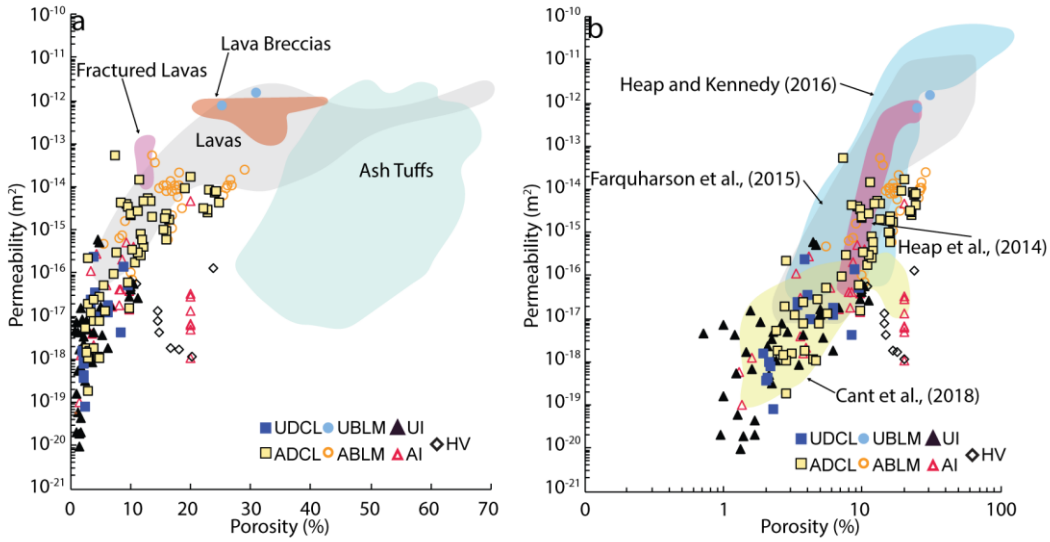

Figure 3.16 Porosity and permeability data from Pinnacle Ridge geotechnical units. (a) Heap et al. (2017a) volcanic facies data (shaded regions) from Whakaari/White Island (New Zealand) compared to Pinnacle Ridge data. The Whakaari lavas display similar porosity and permeability values as the altered dense coherent lavas from Pinnacle Ridge. Whakaari breccias and Pinnacle Ridge UBLM also appear to have similar porosity and permeability values. (b) Pinnacle Ridge materials generally have lower porosity and permeability values than the intersection porosity (0.14–0.20) of other studies represented by the shaded regions (Heap et al., 2014b, Heap et al., 2017a; Farquharson et al., 2015).

The double power law models of the previously published research are defined by two discrete power laws intersecting at a given porosity, at which permeability changes from being microstructurally fracture- to vesicle- dominated (Heap et al., 2014b, Heap et al., 2015c, Heap et al., 2017a; Farquharson et al., 2015; Heap and Kennedy, 2016; Kushnir et al., 2016; Cant et al., 2018). Below the intersection porosity, permeability is governed by the tortuous microfracture structure. Above the intersection porosity, well connected pores and channels present wide flow paths for fluid transport. These authors do not suggest that a rock will travel along the double power law trend as porosity increases or decreases, but rather that there are two distinct populations of volcanic rocks that are best described by their own power law. The

changepoint porosity we identify for ABLM (~14.8%) is consistent with that of the prior discussed research (14–20%). Being noticeably lower, the changepoint porosity of UI, UDCL, and ADCL (~3–7%) suggests that the double-power law relationship is the result of a different microstructural threshold. The low porosity suggests that this changepoint is a product of microfracture density threshold reaching a critical density of interconnectivity and rather than a vesicle-dominated permeable material.

The porosity of UBLM is greater than the common intersection porosities of the double-power law studies and we suspect that had we have focused our analysis on these unaltered, porous volcanics, we would have observed the double-power law common to volcanic permeability studies using the higher-porosity samples. In general, however, the porosities of samples in this study are generally less than or not significantly greater than the given intersection porosity of prior volcanic permeability research (Fig. 3.16b; e.g. Heap et al., 2014b, Heap et al., 2015c, Heap et al., 2017a; Farquharson et al., 2015; Heap and Kennedy, 2016; Kushnir et al., 2016; Cant et al., 2018). We suggest that the single power law relationships or low changepoint porosities indicate that the permeability in our samples from the varying geotechnical units of Pinnacle Ridge is microfracture-dominated except for the brecciated lava margins, which may be partially vesicle-dominated (Fig. 3.4). This interpretation is supported by thin-section (Fig. 3.4) and permeability analysis at higher effective pressures (Fig. 3.9).

3.6.4 Effects of variable confining pressure on permeability

The permeability of rock is influenced substantially by porosity and the tortuosity and connectivity of that porosity (Colombier et al., 2017), and, as demonstrated by prior research, andesites are microstructurally complex and diverse (e.g. Min et al., 1996; Koroknai et al., 2008; Wright et al., 2009; Farquharson et al., 2015). Macrofractures can increase permeability by up to eight orders of magnitude (Heap et al., 2015b; Heap and Kennedy, 2016; Lamur et al., 2017; Pérez-Flores et al., 2017; Eggertsson et al., in press). If there are few pores in a sample, they are unlikely to interact unless they are interconnected by a series of microfractures or pore networks (Kennedy et al., 2016). On the other hand, if there are many pores, linkage by microscopic fractures becomes less crucial (e.g. Farquharson et al., 2015). Thin-section analysis of the Te Herenga andesites from Pinnacle Ridge suggest that low-porosity samples are connected by microcracks while high-porosity samples are connected by pore networks (Heap and Kennedy, 2016).

In addition to the permeability data collected at 3 MPa confining pressure, we collected permeability data at confining pressures of 5, 8, 10, and 15 MPa (while keeping pore pressure constant at 1 MPa). This higher effective pressure data provide permeability values for these rock types approximately analogous from 0 to 500 m depth, which represents the approximate maximum depth this system would

have evolved under (Hackett, 1985). Our results (Fig. 3.9; Table 3.2) are similar to those of Vinciguerra et al. (2005), Nara et al. (2011), Heap et al. (2014a), Lamur et al. (2017), Cant et al. (2018), and Eggertsson et al. (in press) who found that increasing confining pressure from 5 to 50 MPa in micro- and macro-fractured volcanic rocks can decrease permeability by greater than one order of magnitude. Similarly to Vinciguerra et al. (2005), we found the largest decrease in permeability occurred at low effective pressures (<10 MPa) in volcanic rock. Similarly to these studies, we conclude that the fractures in samples (e.g. Fig. 3.4a,b,f) closed as effective pressure increased, thus reducing permeability.

If fluid flow is entirely controlled by fractures, then closing optimally oriented fractures by applying a confining pressure will have a much greater impact on permeability than in a sample with pore-dominated porosity where the fractures are less important. All the geotechnical units experience a decrease in permeability with increase in effective pressure; however, in the low-porosity UI, this permeability decrease is greatest (Fig. 3.9). Using the example of the unaltered and altered intrusions (UI and AI) we show that, in low-porosity rocks, alteration may increase porosity and permeability through dissolution along microcracks, which become more difficult to close with confining pressure (Cant et al., 2018). The ABLM samples, however, show evidence for decreases in porosity and permeability driven by precipitation and mineral deposition and are less susceptible to permeability reduction with the application of confining pressures. Hence, alteration may increase or decrease permeability but tends to create rocks less susceptible to confining pressure-driven changes in permeability. This implies that permeability heterogeneity will increase with depth in volcanological and geothermal systems where unaltered and altered rocks are juxtaposed.

3.6.5 Variable confining pressure and outgassing

It is important to consider the effects the closure of these microfractures have on the outgassing processes in a volcanic system. The permeability of UI was below detectable limits ($<10^{-22}$ m^2) at 15 MPa confining pressure, suggesting that microfractures were effectively closed at this pressure. This implies that unaltered intrusions are effective seals (Figs. 3.9, 3.15), especially in contrast to UBLM (10^{-13} m^2), ABLM (10^{-16} m^2), UDCL ($>10^{-17}$ m^2), AI ($>10^{-18}$ m^2), and ADCL ($>10^{-18}$ m^2) under the same conditions. Moreover, UI stratigraphically crosscuts the interlayered ADCL, ABLM, UDCL, and UBLM and blocks flow along these higher permeability units. The implications for the effects of UI fracture closure under higher effective pressure, conceptually carried to the edifice-scale in a volcanic setting, mean unaltered intrusions can obstruct or divert subsurface fluid flow, an observation consistent with conclusions from Senger et al. (2017). Vertical structures could therefore act as barriers to lateral fluid flow and produce segmented

hydrothermal systems as observed by Chambefort et al. (2014). In the case of sub-horizontal intrusions or intrusions with geometries suitable for fluid traps (e.g. Senger et al., 2017), old, cooled intrusions could restrict outgassing and drive pressurization.

3.6.6 Translating permeability to edifice-scale processes

The impact of the tortuous microstructure inherent to all the materials of a shallow hydrothermal system can affect the behaviour of the entire volcanic edifice. In this study, we demonstrate that distance to the intrusion (from 1080 to 20 m) is associated with decrease in porosity (30.92 to 5.49%) and permeability of brecciated lavas (10^{-12} to 10^{-16} m^2; Figs. 3.12a, 3.13). Higher effective pressures further reduce the permeability of altered brecciated lavas and other geotechnical units of the hydrothermal system (Fig. 3.9). This decrease in permeability has the potential to induce pore pressure augmentation (Christenson et al., 2010; Heap and Wadsworth, 2016) and the resulting increase in pore pressure could compromise the stability of the edifice slopes (Day, 1996; Voight and Elsworth, 1997; Reid et al., 2001; Reid, 2004; Moon et al., 2009), induce seismicity (Gerst and Savage, 2004; Christenson et al., 2010; Jolly et al., 2010), and/or propel the diverse eruptions observed at volcanic edifices (e.g. Kilgour et al., 2010; Siebert et al., 2015, and references therein). For example, unrest at Whakaari/White Island between 2002–2006 and 2007–2009 was thought to be a response to changes in the pore pressure of the hydrothermal system (Fournier and Chardot, 2012).

The presence of HV necessitates further consideration as the nature of its strength, structure, and permeability make HV particularly adept to affect subsurface fluid pathways. Heap et al. (2017a) suggested that the sealing of fractures in lava materials from hydrothermal alteration was at least partially responsible for the dynamic landscape of Whakaari/White Island and its history of ephemeral surficial thermal features. The precipitation of HV from hydrothermal fluid has a strong potential to drastically change fluid pathways and, in the process, expose unaltered materials to warm and acidic hydrothermal fluids while inducing precipitation (Fig. 3.12a) and/or dissolution (Fig. 3.12b,c) in other rock. In much the same way, HV can change or block outgassing and induce edifice behaviour similar to the decrease in porosity of the brecciated lava margins discussed above.

Our study provides the most comprehensive dataset for physical and mechanical rock properties of volcanic host-strata surrounding a shallow intrusion and its hydrothermal system to date. The data display inherent variability characteristic to volcanic materials as well as trends subject to spatial and temporal variation not observed in prior research. These findings will allow for more precise understanding and future modelling of volcanic and hydrothermal processes. For example, the model of

Fournier and Chardot (2012) that associated pore pressure to the Whakaari/White Island unrest assumed an isotropic permeability value (10^{-15} m^2) rather than range of permeability values over several orders of magnitude (10^{-21}–10^{-12} m^2). In another example, the numerical modelling by Scott and Driesner (in press) of time-dependent changes in porosity and permeability in a hydrothermal system produced by a shallow intrusion considered permeability values 10^{-14}, 10^{-15}, and 10^{-16} m^2 as high, moderate, and low, respectively. Although these values proved critical for the fluid flow around the intrusion (Scott et al., 2015), our data clearly caution that a significantly wider range of permeability needs to be considered when modelling processes related to volcanic permeability. Without doing so, one is not precisely constraining volcanic properties. Therefore, we emphasize the need for consideration for a range of mechanical and physical rock properties in future modelling not only to account for the heterogeneity of volcanic material but for the systemic changes in these properties like we observe with ABLM at Pinnacle Ridge.

3.6.7 Scaling strength and permeability

It is important to consider scale. For example, as the length scale of interest increases, rock strength decreases due to the greater number in imperfections in the greater volume of rock mass (Hoek et al., 2002). Therefore, the UCS values we present provide an upper bound for the strength of the geotechnical units at Pinnacle Ridge. Although we do not describe macro-scale discontinuities in this lab-oriented study, we intend to detail our field discontinuity observations in a forthcoming contribution.

Permeability is also dependent on scale. Heap and Kennedy (2016) demonstrated that a single microfracture can increase the permeability of andesite from Mt. Ruapehu by up to eight orders of magnitude in an otherwise-unfractured, low-permeability (<10^{-19} m^2) sample core. It is, thus, common to adopt a dual porosity-permeability perspective in which one considers both matrix and macrofracture permeability have their own distinct characteristics (Jafari and Babadagli, 2011). While we were restricted to <40 mm length cores, which predominantly precluded macrofractures, macroscopic discontinuities (>1 mm aperture) are present in nearly all the studied geotechnical unit outcrops. Although modelling the effects of macrofractures is outside the scope of this laboratory-focused study, it is implicit that at least some of the observed macrofractures predominated fluid flow at Pinnacle Ridge when it was an active geothermal system by channelling flow along these large discontinuities rather than through rock matrix.

3.7 Conclusions

We conducted a detailed lab-based characterization (n = 194) of volcanics from a small hydrothermal thermal system arising from the emplacement of a small, shallow intrusion, using samples from various

geotechnical units at Pinnacle Ridge, Mt. Ruapehu. The large sample size allowed the distinction of systemic change from inherent intact volcanic material heterogeneity, and we make several key findings:

1) Through thin-section and TerraSpec analysis, we identified primary and alteration mineralogies at Pinnacle Ridge. Alteration grade appears consistent across the geotechnical units and confined to smectite-group clays and kaolinite in most samples.
2) Our data show that permeability is governed by porosity, which, in a hydrothermal setting, is determined by a combination of alteration and primary lithology. Alteration can have a varying effect on permeability where alteration increases the permeability of low-porosity geotechnical units (e.g. intrusions and lava flow cores) and decreases the permeability in high-porosity geotechnical units systematically towards the main intrusion (e.g. breccias).
3) Increasing proximity to the intrusion (100 s to 10 s m) correlates with a decrease in the porosity of the brecciated lava margins spanning nearly an order of magnitude, as a result of hydrothermal alteration-induced precipitation of clay minerals in the pore space of the brecciated lava margins. This decrease in porosity corresponds to a decrease of permeability of several orders magnitude. Similar to porosity and permeability, elastic wave velocities and UCS in the breccias appear to be controlled by distance to largest intrusion.
4) Alteration may increase or decrease permeability but tends to create rocks less susceptible to confining pressure driven changes in permeability. This implies that permeability heterogeneity will increase with depth in volcanological and geothermal systems where unaltered and altered rocks are juxtaposed.
5) Effective pressure has the greatest effect on permeability up to 5 MPa. Above 5 MPa, the effect of increasing pressure on permeability is less prominent. However, the extent of the decrease in permeability is controlled by how dominant microfractures are for the porosity of the geotechnical unit. Brecciated lava margins, which are pore dominated, retain much of their unconfined permeability, whereas the unaltered intrusions experienced the largest decrease in permeability with increased effective pressure because permeability of unaltered intrusions is microfracture-dominated. Above an effective pressure of 10 MPa, solid, unaltered intrusions become effectively impermeable at the sample scale, but macrofractures were not considered. Future research is needed to model the effects of these macrofractures on rock-mass permeability.
6) We propose hydrothermal veining as a new geotechnical unit to be considered in a volcanic environment based on intact rock properties of hydrothermal vein material. Although we do not discuss the discontinuity characteristics for complete classification the porosity, permeability,

strength, and deformation moduli properties of hydrothermal veins are unique to hydrothermal veins and therefore require special consideration in edifice stability as, even if the volume of veining is minor, it could act as a significant barrier to fluid or gas flow if located at a critical location within the structure. We intend to complete the classification of the geotechnical units at Pinnacle Ridge in a forthcoming publication that details the discontinuity characteristics of the unaltered and altered volcanics.

3.8 Acknowledgements

The authors would like to thank Harry Keys and Blake McDavitt from the New Zealand Department of Conservation for field support and Graham Leonard, Dougal Townsend, Chris Conway, Rosie Cole, and Leo Purê for their comradery in the field. The first author would like to thank Jim Cole, Mark Simpson, Isabelle Chambefort, Patrick Baud, Alex Nichols, Alex Kushnir, and Luke Griffiths for assistance and discussion. The authors also extend their thanks to two anonymous reviewers, whose constructive comments improved the clarity of this manuscript. The authors of this study acknowledge the support of the UC Doctoral Scholarship, Hubert Curien Partnership (PHC) Dumont D'Urville travel grant (number 31950RK), MBIE catalyst grant "Energy straight from magma", Mercury NZ Limited (formerly Might River Power) grant "Source to Surface", and the UC Mason Trust Fund. The authors also acknowledge support from Labex grant ANR-11-LABX-0050_G-EAU-THERMIE-PROFONDE (this research therefore benefited from state funding managed by the Agence National de la Recherche (ANR) as part of the "Investissements d'avenir" program) and Agence National de la Recherche (ANR) grant CANTARE (ANR-15-CE06-0014-01).

3.A Appendix: Expanded methodology

Our study of the geomechanical parameters of the geotechnical units that compose the hydrothermal system of the small, shallow intrusion at Pinnacle Ridge require several varied methodologies to determine the varied mechanical and physical rock properties. In Appendix 3.A, we provide additional detail to the methods we employ as referenced in the main text. Specifically, we detail the Forchheimer and Klinkenberg corrections (Appendix 3.A.1), the specific conditions for elastic wave velocity collection and calculation of the dynamic deformation moduli (Appendix 3.A.2), and the calculation of the static deformation moduli (Appendix 3.A.3).

3.A.1. Permeability: Forchheimer and Klinkenberg corrections

The Forchheimer and Klinkenberg corrections for permeability are important parameters discussed in the main text and applied when appropriate to permeability measurements. Given their non-trivial qualities, these two correction parameters are discussed further in Appendix 3.A.1.

The Forchheimer correction accounts for non-laminar flow through the sample (Forchheimer, 1901). Forchheimer-corrected permeability, k_{fo}, is a function of gas permeability, k_D, an inertial term obtained through the best fit of experimental data, ι, and the volumetric flow rate, Q_v, and is given in Equation A.1. The Klinkenberg correction accounts for Klinkenberg's 'slip flow' (Klinkenberg, 1941). Klinkenberg-corrected permeability, k_{klink}, is a function of gas permeability, k_D, the Klinkenberg slip factor, b, and the mean pore pressure, P_{mean}, and is given by Equation A.2.

$$\frac{1}{k_{fo}} = \frac{1}{k_D} - \iota \cdot Q_v \tag{A.1}$$

$$k_{klink} = k_D\left(1 + \frac{b}{P_{mean}}\right) \tag{A.2}$$

3.A.2. Acoustic wave velocities and dynamic elastic moduli

Acoustic wave velocity analysis provides a non-destructive characterization parameter with relevance to microfracture density (e.g. Siratovich et al., 2014) and, thereby, deformation moduli (i.e. the dynamic Young's modulus and Poisson ratio). While acoustic wave velocity methods are discussed in the text, we expand on the specifics of the procedure here and detail the calculation of the dynamic Young's modulus and Poisson ratio in Appendix 3.A.2.

During collection, ultrasonic gel and a constant 312 Pa stress was applied via direct weighting to ensure sufficient contact between the sample and platens in order to produce consistent waveforms during testing. Prior work on hydrothermally altered volcanics used acoustic emissions and change in axial strain during loading to suggest that microcrack closure occurs in excess of 10 MPa which was several orders of magnitude greater than 312 Pa used in this analysis (Brace et al., 1966; Martin & Chandler, 1994; Eberhardt et al., 1998; Lion et al., 2005; Nicksiar & Martin, 2012; Siratovich et al., 2014).

The dynamic Poisson's ratio and Young's modulus were calculated from equations A.3 and A.4, respectively, (Gueguen & Palciauskas, 1994; Gudmundsson, 2011):

$$\nu_d = \frac{V_P^2 - V_S^2}{2(V_p^2 - V_s^2)} \tag{A.3}$$

$$E_d = \frac{\rho V_s^2 \left(3V_p^2 - 4V_s^2\right)}{\left(V_p^2 - V_s^2\right)} \quad \text{(A.4)}$$

where ν_d is the Poisson's Ratio, V_P is compressional wave velocity, V_s is shear wave velocity, E_d is the Young's Modulus, and ϱ is bulk density.

3.A.3. Static deformation moduli

Static deformation moduli providing strain behaviour during deformation are discussed and used in the text. The specific formulas for determining these deformation moduli are provided in Appendix 3.A.3. We calculated the static Young's modulus and Poisson's Ratio for each sample using Equations A.5 and A.6, respectively (Ulusay and Hudson, 2007).

$$E_s = \left(\frac{\Delta\sigma_\alpha}{\Delta\varepsilon_\alpha}\right) \quad \text{(A.5)}$$

$$\nu_s = -\left(\frac{\Delta\varepsilon_r}{\Delta\varepsilon_\alpha}\right) \quad \text{(A.6)}$$

where E_s is the static elastic (Young's) modulus, σ_α is axial differential stress, ε_α is the axial strain (in both Equations A. and A.) ν_s is the static Poisson's Ratio, and ε_r is the radial strain. The elastic parameters were determined at 50% of the peak strength (Ulusay & Hudson, 2007).

3.B Appendix: Expanded results

Elastic wave moduli and deformation moduli are essential parameters for the understanding and modelling of deformation in a volcanic edifice. We present a summary of this data in the main text and detail these parameters by geotechnical units here in Appendices 3.B.1 (Elastic Wave Velocities), B.2 (Dynamic Deformation Moduli), and B.3 (Static Deformation Moduli). A complete dataset for each individual sample can be found in Table 3.S1.

3.B.1. Elastic wave velocity

The P-wave and S-wave velocities of the geotechnical units appear to have similar relative relationships to each other and mirror those of porosity (Figs. 3.B.1, 3.B.2; Table 3.3). That is, UI has the highest velocities (~5600 m/s and ~2900 m/s for P-wave and S-wave velocities, respectively) and UBLM has the lowest velocities (~3000 m/s and ~1100 m/s, for P-wave and S-wave velocities, respectively). Similar to

porosity, the P-wave velocities of some of the ABLM appear to be correlated, albeit inversely, with distance to the largest intrusion (Fig. 3.B.3; Table 3.3). The S-waves of ABLM are similarly correlated with distance.

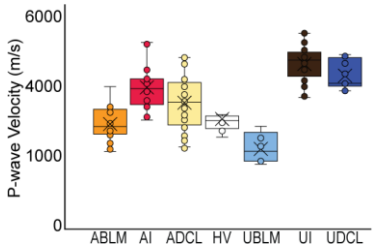

Figure 3.B.1. Water-saturated P-wave velocities (n = 191) grouped according to geotechnical unit. Standard Error ≤ 1% of the reported values.

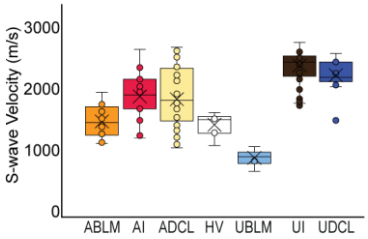

Figure 3.B.2. Water-saturated S-wave velocities (n = 191) grouped according to geotechnical unit. Standard Error ≤ 1% of the reported values.

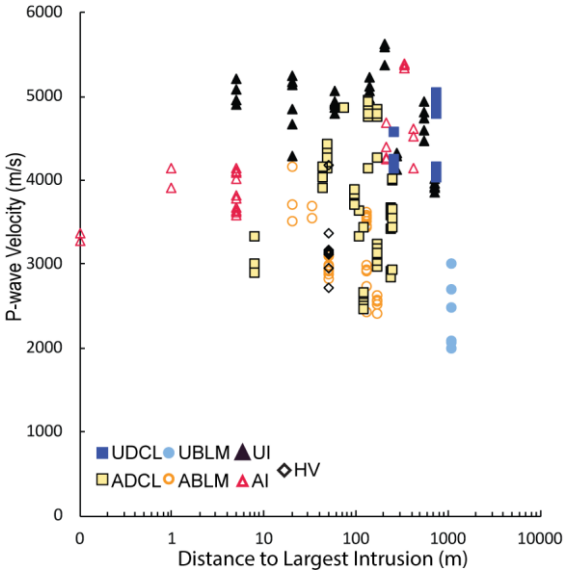

Figure 3.B.3. Water-saturated P-wave velocities versus distance to the largest intrusion observed at Pinnacle Ridge grouped according to geotechnical unit. Standard Error ≤ 1% of the reported values.

3.B.2 Dynamic deformation moduli

The dynamic Young's modulus has a similar relative distribution as the P-wave velocity data with UI and UDCL having the highest values (22.8 – 61.3 GPa and 19.1 – 51.5 GPa, respectively) while UBLM have the lowest dynamic Young's modulus (3.6 – 7.5 GPa). The ABLM, AI, and ADCL values (8.9 – 28.7 GPa, 2.4 – 5.0 GPa, and 8.4 – 51.2 GPa, respectively) are again between the unaltered dense materials (i.e. UI and UDCL) and the unaltered highly porous material (i.e. UBLM) (Fig. 3.B.4; Table 3.3). HV Young's modulus values are 9.2 – 16.0 GPa. Dynamic Poisson's ratio shows no clear geotechnical grouping as opposed to the other physical rock properties, with values between 0.18 -0.47 (Fig. 3.B.5; Table 3.3). Nor do we observe a clear relationship between the dynamic moduli and distance to UI.

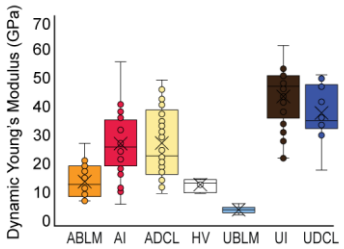

Figure 3.B.4. Water-saturated dynamic elastic moduli (n = 191) grouped according to geotechnical unit. Standard Error ≤ 1% of the reported values.

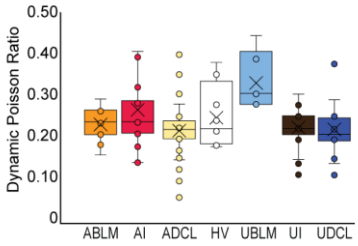

Figure 3.B.5. Water-saturated Poisson ratio (n = 191) grouped according to geotechnical unit. Standard Error ≤ 1% of the reported values.

3.B.3 Static Deformation Moduli

The static Young's modulus mirrors the relative relationships of the dynamic Young's modulus by geotechnical unit classification (Fig. 3.B.6). UI and UDCL have the highest static Young's modulus (0.1 – 4.8 GPa and 15.3 – 32.7 GPa, respectively). UBLM has the lowest static Young's modulus (1.27 – 1.93 GPa). The ABLM, AI, and ADCL values (4.0 – 10.2 GPa, 7.6 – 38.8 GPa, and 0.4 – 31.3 GPa, respectively) were between the unaltered dense materials (i.e. UI and UDCL) and the unaltered highly porous material (i.e. UBLM). HV static Young's modulus is between 8.5 and 9.8 GPa. Static Poisson's ratio shows no clear

geotechnical grouping as with the other physical rock properties, with values between 0.06 -0.49 (Fig. 3.B.7).

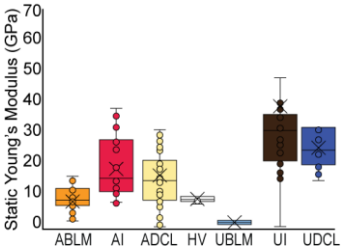

Figure 3.B.6 Static Young's moduli (n = 147) grouped according to geotechnical unit. Standard Error ≤ 1% of the reported values.

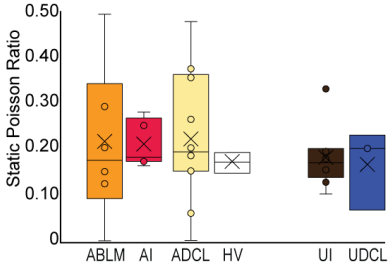

Figure 3.B.7 Static Poisson ratio (n = 39) grouped according to geotechnical unit. Standard Error ≤ 1% of the reported values.

3.9 References

Al-Harthi, A.A., Al-Amri, R.M. and Shehata, W.M., 1999. The porosity and engineering properties of vesicular basalt in Saudi Arabia. Engineering Geology, 54(3-4): 313-320.

Apuani, T., Corazzato, C., Cancelli, A. and Tibaldi, A., 2005. Physical and mechanical properties of rock masses at Stromboli: a dataset for volcano instability evaluation. Bulletin of Engineering Geology and the Environment, 64: 419-431.

Barrington, J. and Kerr, P.F., 1962. Alteration effects at Tuba Dike, Cameron, Arizona. Geological Society Of America Bulletin, 73: 101-112.

Batzle, M., Han, D. and Hofmann, R., 2006. Fluid mobility and frequency-dependent seismic velocity - Direct measurements. Geophysics, 71(1): N1-N9.

Bean, C.J., De Barros, L., Lokmer, I., Métaxian, J.-P., O'Brien, G. and Murphy, S., 2014. Long-period seismicity in the shallow volcanic edifice formed from slow-rupture earthquakes. Nature Geoscience, 7: 71-75.

Bernard, M.-L., Zomara, Y.G. and Boudon, G., 2007. Transport properties of pyroclastic rocks from Montagne Pelée volcano (Martinique, Lesser Antilles). Journal of Geophysical Research, 112(B05205).

Bibby, H.M., Caldwell, T.G., Davey, F.J. and Webb, T.H., 1995. Geophysical evidence on the structure of the Taupo Volcanic Zone and its hydrothermal circulation. Journal of Volcanology and Geothermal Research, 68(1-3): 29-58.

Bloomberg, S., Werner, C., Rissmann, C., Mazot, A., Horton, T., Gravley, D., Kennedy, B. and Oze, C., 2014. Soil CO2 emissions as a proxy for heat and mass flow assessment, Taupo Volcanic Zone, New Zealand. Geochemistry, Geophysics, Geosystems: G3, 15(12): 4885-4904.

Bourbie, T. and Zinsner, B., 1985. Hydraulic and acoustic properties as a function of porosity in Fontainebleau Sandstone. Journal of Geophysical Research, 90(11524-11532).
Brace, W.F., Paulding, B. and Scholz, C., 1966. Dilatancy in the fracture of crystalline rocks. Journal of Geophysical Research, 71: 3939-3953.
Brace, W.F., Walsh, J.B. and Frangos, W.T., 1968. Permeability of granite under high pressure. Journal of Geophysical Research, 73: 2225-2236.
Brideau, M.-A., Pedrazzini, A., Stead, D., Froese, C., Jaboyedoff, M. and van Zeyl, D., 2011. Three-dimensional slope stability analysis of South Peak, Crowsnest Pass, Alberta, Canada. Landslides, 8: 139-158.
British Standard, 2007. Code of Practice for Site Investigations, British Standard 5930-1999, 3rd Edition. Technical Committee.
Byerlee, J., 1967. Friction or rocks. Pure and Applied Geophysics, 116: 615-626.
Cant, J.L., Siratovich, P.A., Cole, J.W., Villeneuve, M.C. and Kennedy, B.M., 2018. Matrix permeability of reservoir rocks, Ngatamariki geothermal field, Taupo Volcanic Zone, New Zealand. Geothermal Energy, 6(2).
Casey, M., Ebinger, C., Keir, D., Gloaguen, R. and Mohamed, F., 2006. Strain accomodation in transitional rifts: extension by magma intrusion and faulting in Ethiopian rift magmatic segments. Geological Society, London, Special Publications, 259: 143-163.
Cathles, L.M., Erendi, H.J. and Barrie, T., 1997. How long can a hydrothermal system be sustained by a single intrusive event. Economic Geology, 92: 766-771.
Chambefort, I., Lewis, B., Wilson, C.J.N., Rae, A.J., Coutts, C., Bignall, G. and Ireland, T.R., 2014. Stratigraphy and structure of the Ngatamariki geothermal system from new zircon U–Pb geochronology: implications for Taupo Volcanic Zone evolution. Journal of Volcanology and Geothermal Research, 274: 51-70.
Chardot, L., Jolly, A.D., Kennedy, B.M., Fournier, N. and Sherburn, S., 2015. Using volcanic tremor for eruption forecasting at White Island volcano (Whakaari), New Zealand. Journal of Volcanology and Geothermal Research, 302: 11-23.
Christenson, B.W., Reyes, A.G., Young, R., Moebis, A., Sherburn, S., Cole-Baker, J. and Britten, K., 2010. Cyclic processes and factors leading to phreatic eruption events: insights from the 25 September 2007 eruption through Ruapehu Crater Lake, New Zealand. Journal of Volcanology and Geothermal Research, 191(1-2): 15-32.
Cole, J., 1990. Structural control and origin of volcanism in the Taupo Volcanic Zone, New Zealand. Bulletin of Volcanology: 445-459.
Collinson, A.S.D. and Neuberg, J., 2012. Gas storage, transport and pressure changes in an evolving permeable volcanic edifice. Journal of Volcanology and Geothermal Research, 243-244(1-13).
Collombet, M., 2009. Two-dimensional gas loss for silicic magma flows: toward more realistic numerical models. Geophysical Journal International, 177: 309-318.
Colombier, M., Wadsworth, F.B., Gurioli, L., Scheu, B., Kueppers, U., Muro, A.D. and Dingwell, D.B., 2017. The evolution of pore connectivity in volcanic rocks. Earth and Planetary Science Letters, 462: 99-109.
Conway, C.E., Leonard, G.J., Townsend, D.B., Calvert, A.T., Wilson, C.J.N., Gamble, J.A. and Eaves, S.B., 2016. A high-resolution $^{40}Ar/^{39}Ar$ lava chronology and edifice construction history for Ruapehu volcano, New Zealand. Journal of Volcanology and Geothermal Research, 327: 152-179.
Cook, S., Kennedy, B. and Villeneuve, M.C., 2018. Engineering geology model of the Crater Lake outlet, Mt. Ruapehu, New Zealand, to inform rim breakout hazard. Journal of Volcanology and Geothermal Research, 350(15): 69-83.
Day, S.J., 1996. Hydrothermal pore fluid pressure and the stability of porous, permeable volcanoes. Geological Society, London, Special Publications, 110(1): 77-93.

del Potro, R. and Hürlimann, M., 2008. Geotechnical classification and characterisation of materials for stability analyses of large volcanic slopes. Engineering Geology, 98(1-2): 1-17.
del Potro, R. and Hürlimann, M., 2009. The decrease in the shear strength of volcanic materials with argillic hydrothermal alteration, insights from the summit region of Teide stratovolcano, Tenerife. Engineering Geology, 104(1-2): 135-143.
Dzurisin, D., 2006. Volcano Deformation. Springer/Praxis, Chichester.
Eberhardt, E., Stead, D., Stimpson, B., & Read, R. S. 1998. Identifying crack initiation and propagation thresholds in brittle rock. Revue canadienne de géotechnique, 35(2): 222-233. doi:10.1139/cgj-35-2-222.
Eggertsson, G.H., Lavallée, Y., Kendrick, J.E. and Markússon, S.H., 2018. Improving fluid flow in geothermal reservoirs by thermal and mechanical stimulation: The case of Krafla volcano, Iceland. Journal of Volcanology and Geothermal Research.
Eichelberger, J.C., Carrigan, C.R., Westrich, H.R. and Price, R.H., 1986. Non-explosive silicic volcanism. Nature, 323(6089): 598-602.
Elsworth, D., 1995. Dike intrusion as a trigger for large earthquakes and the failure of volcano flanks. Journal of Geophysical Research, 100(B4): 6005-6024.
Farquharson, J., Heap, M.J., Baud, P., Reuschlé, T. and Varley, N.R., 2016. Pore pressure embrittlement in a volcanic edifice. Bulletin of Volcanology, 78(1).
Farquharson, J., Heap, M.J., Varley, N.R., Baud, P. and Reuschlé, T., 2015. Permeability and porosity relationships of edifice-forming andesites: A combined field and laboratory study. Journal of Volcanology and Geothermal Research, 297: 52-68.
Finizola, A., Sortino, F., Lénat, J.-F. and Valenza, M., 2002. Fluid circulation at Stromboli volcano (Aeolian Islands, Italy) from self-potential and CO2 surveys. Journal of Volcanology and Geothermal Research, 116(1-2): 1-18.
Forchheimer, P. 1901. Wasserbewegung durch boden. [Water movement through soil.]. Zeitschrift des Vereines Deutscher Ingenieure, 45: 1782-1788.
Fournier, N. and Chardot, L., 2012. Understanding volcano hydrothermal unrest from geodetic observations: insights from numerical modeling and application to White Island volcano, New Zealand. Journal of Geophysical Research, 117(B11).
Frank, D., 1995. Surficial extent and conceptual model of a hydrothermal system at Mount Rainier, Washington. Journal of Volcanology and Geothermal Research, 65(1-2): 51-80.
Frolova, J.V., Ladygin, V.M. and Rychagov, S.N., 2010. Petrophysical alteration of volcanic rocks in hydrothermal systems of the Kuril-Kamchatka Island Arc, World Geothermal Conference, Bali, Indonesia, pp. 25-29.
Galland, O., de Bremond d'Ars, J., Cobbold, P.R. and Hallot, E., 2003. Physical models of magmatic intrusion during thrusting. Terra Nova, 15(6): 405-409.
Galland, O., Planke, S., Neumann, E. and Malthe-Sørenssen, A., 2009. Experimental modelling of shallow magma emplacement: application to saucer-shaped intrusions. Earth and Planetary Science Letters, 277: 373-383.
Gaunt, H.E., Sammonds, P., Meredith, P.G., Smith, R. and Pallister, J.S., 2014. Pathways for degassing during the lava dome eruption of Mount St. Helens 2004-2008. Geology, 42(11): 947-950.
Gerst, A. and Savage, M.K., 2004. Seismic anisotropy beneath Ruapehu volcano: a possible eruption forecasting tool. Science, 306(5701): 1543-1547.
Grant, M.A. and Bixley, P.F., 2011. Geothermal Reservoir Engineering. Elsevier, San Diego, CA.
Gudmundsson, A., 2002. Emplacement and arrest of sheets and dykes in central volcanoes. Journal of Volcanology and Geothermal Research, 116: 279-298.
Gudmundsson, A., 2006. How local stresses control magma-chamber ruptures, dyke injections, and eruptions in composite volcanoes. Earth-Science Reviews, 79(1-2): 1-31.

Gudmundsson, A., 2009. Toughness and failure of volcanic edifices. Tectonophysics, 471: 27-235.
Gudmundsson, A. 2011. Rock Fractures in Geological Processes. United Kingdom: Cambridge University Press (CUP).
Gueguen, Y. and Palciauskas, V., 1994. Introduction to the Physics of Rocks. Princeton University Press, Princeton, New Jersey.
Hackett, W.R., 1985. Geology and Petrology of Ruapehu Volcano and Related Vents, Victoria University of Wellington, Wellington, New Zealand.
Hackett, W.R. and Houghton, B.F., 1985. Pinnacle Ridge Member, Whakapapa Formation; a welded airfall deposit from Ruapehu volcano, Taupo Volcani Zone. Record - New Zealand Geological Survey, 8: 24-29.
Hase, H., Hashimoto, T., Sakanaka, S., Kanda, W. and Tanaka, Y., 2005. Hydrothermal system beneath Aso volcano as inferred from self-potential mapping and resistivity structure. Journal of Volcanology and Geothermal Research, 143(4): 259-277.
Heap, M.J., Baud, P., Meredith, P.G., Vinciguerra, S. and Reuschlé, T., 2014a. The permeability and elastic moduli of tuff from Campi Flegrei, Italy: implications for ground deformation modelling. Solid Earth, 5(1): 25-44.
Heap, M.J., Farquharson, J., Baud, P., Lavallée, Y. and Reuschlé, T., 2015a. Fracture and compaction of andesite in a volcanic edifice. Bulletin of Volcanology, 77(55).
Heap, M.J., Farquharson, J.I., Wadsworth, F.B., Kolzenburg, S. and Russell, J.K., 2015b. Timescales for permeability reduction and strength recovery in densifying magma. Earth and Planetary Science Letters, 429: 223-233.
Heap, M.J. and Kennedy, B., 2016. Exploring the scale-dependent permeability of fractured andesite. Earth and Planetary Science Letters, 447: 139-150.
Heap, M.J., Kennedy, B., Farquharson, J., Ashworth, J., Gilg, H.A., Scheu, B., Lavallée, Y., Siratovich, P.A., Cole, J., Jolly, A. and Dingwell, D.B., 2017a. A multidisciplinary approach to quantify the permeability of a volcanic hydrothermal system (Whakaari/White Island, Taupo Volcanic Zone, New Zealand). Journal of Volcanology and Geothermal Research, 332: 88-108.
Heap, M.J., Kennedy, B.M., Pernin, N., Jacquemard, L., Baud, P., Farquharson, J.I., Scheu, B., Lavallée, Y., Gilg, H.A., Letham-Brake, M., Mayer, K., Jolly, A.D., Reuschlé, T. and Dingwell, D.B., 2015c. Mechanical behaviour and failure modes in the Whakaari (White Island volcano) hydrothermal system, New Zealand. Journal of Volcanology and Geothermal Research, 295: 26-42.
Heap, M.J., Lavallée, Y., Petrakova, L., Baud, P., Reuschlé, T., Varley, N.R. and Dingwell, D.B., 2014b. Microstructural controls on the physical and mechanical properties of edifice-forming andesites at Volcán de Colima, Mexico. Journal of Geophysical Research: Solid Earth, 119(4): 2925-2963.
Heap, M.J., Vinciguerra, S. and Meredith, P.G., 2009. The evolution of elastic moduli with increasing crack damage during cyclic stressing of a basalt from Mt. Etna volcano. Tectonophysics, 471: 153-160.
Heap, M.J., Violay, M., Wadsworth, F.B. and Vasseur, J., 2017b. From rock to magma and back again: the evolution of temperature and deformation mechanism in conduit margin zones. Earth and Planetary Science Letters, 463: 92-100.
Heap, M.J. and Wadsworth, F.B., 2016. Closing an open system: pore pressure changes in permeable edifice rock at high strain rates. Journal of Volcanology and Geothermal Research, 315: 40-50.
Hedenquist, J.W., Arribas, A. and Reynolds, T.J., 1998. Evolution of an intrusion-centered hydrothermal system; far Southeast-Lepanto porphyry and epithermal Cu-Au deposits, Philippines. Economic Geology, 93(4): 373-404.
Hedenquist, J.W. and Lowenstern, J.B., 1994. The role of magmas in the formation of the hydrothermal ore deposit. Nature, 370: 519-527.

Henley, R.W. and Ellis, A.J., 1983. Geothermal systems ancient and modern: a geochemical review. Earth-Science Reviews, 19: 1-50.
Henneberger, R.C. and Browne, P.R.L., 1988. Hydrothermal alteration and evolution of the Ohakuri hydrothermal system, Taupo volcanic zone, New Zealand. Journal of Volcanology and Geothermal Research, 34(3-4): 211-231.
Hoek, E., 1994. Strength of Rock Masses. ISRM News Journal, 2(2): 4-16.
Hoek, E., Carranza-Torres, C. and Corkum, B., 2002. The Hoek-Brown failure criterion, 5th North American Rock Mechanics Symposium and 17th Tunneling Association of Canada Conference. NARMS - TAC, Toronto, Ontario, Canada.
Hoek, E. and Diederichs, M., 2006. Empirical estimation of rock mass modulus. International Journal of Rock Mechanics and Mining Science, 43(2): 203-215.
Hurwitz, S., Christiansen, L.B. and Hsieh, P.A., 2007. Hydrothermal fluid flow and deformation in large calderas: inferences from numerical simulations. Journal of Geophysical Research, 112(B02206).
Hurwitz, S., Ingebritsen, S.E. and Sorey, M.L., 2002. Episodic thermal perturbations associated with groundwater flow: an example from Kilauea Volcano, Hawaii. Journal of Geophysical Research, 107(B11): ECV 13-11-ECV 13-10.
Jafari, A. and Babadagli, T., 2011. Effective fracture network permeability of geothermal reservoirs. Geothermics, 40(1): 25-38.
Jolly, A.D., Sherburn, S., Jousset, P. and Kilgour, P., 2010. Eruption source processes derived from seismic and acoustic observations of the 25 September 2007 Ruapehu eruption–North Island, New Zealand. Journal of Volcanology and Geothermal Research, 191: 33-45.
Keating, G.N., Valentine, G.A., Krier, D.J. and Perry, F.V., 2007. Shallow plumbing systems for small-volume basaltic volcanoes. Bulletin of Volcanology, 70(5): 563-582.
Kendrick, J.E., Smith, R., Sammonds, P., Meredith, P.G., Dainty, M. and Pallister, J.S., 2013. The influence of thermal and cyclic stressing on the strength of rocks from Mount St. Helens, Washington. Bulletin of Volcanology, 75(7)(728).
Kennedy, B., Wadsworth, F.B., Vasseur, J., Schipper, C.I., Jellinek, A.M., Von Aulock, F.W., Hess, K., Russell, J.K., Lavallée, Y. and Nichols, A.R.L., 2016. Surface tension driven processes densify and retain permeability in magma and lava. Earth and Planetary Science Letters, 433: 116-124.
Kerr, A., Rafuse, H., Sparks, G., Hinchey, J. and Sandeman, H., 2011. Visible/Infrared apectroscopy (VIRS) as a research tool in economic geology: background and pilot studies from Newfoundland and Labrador.
Kilgour, G., Manville, V., Pasqua, F.D., Graettinger, A., Hodgson, K.A. and Jolly, G.E., 2010. The 25 September 2007 eruption of Mount Ruapehu, New Zealand: directed ballistics, surtseyan jets, and ice-slurry lahars. Journal of Volcanology and Geothermal Research, 191(1-2): 1-14.
Kissling, W.M. and Weir, G.J., 2005. The spatial distribution of the geothermal fields in the Taupo Volcanic Zone, New Zealand. Journal of Volcanology and Geothermal Research, 145(1-2): 136-150.
Klinkenberg, L. J. 1941. The permeability of porous media to liquids and gases. Drilling and production practice. New York.
Klug, C. and Cashman, K.V., 1996. Permeability development in vesiculating magmas: implications for fragmentation. Bulletin of Volcanology, 58: 87-100.
Koroknai, B., Arkai, P., Horvath, P. and Balogh, K., 2008. Anatomy of a transitional brittle-ductile shear zone developed in a low-T meta-andesite tuff: a microstructural, petrological and geochronological case study from the Bukk Mts. (NE Hungary). Journal of Structural Geology, 30: 159-176.
Kushnir, A.R.L., Martel, C., Bourdier, J.-L., Heap, M.J., Reuschlé, T., Erdmann, S., Komorowski, J.C. and Cholik, N., 2016. Probing permeability and microtexture: unravelling the role of a low-

permeability dome on the explosivity of Merapi (Indonesia). Journal of Volcanology and Geothermal Research, 316: 56-71.
Lamur, A., Kendrick, J.E., Eggertsson, G.H., Wall, R.J., Ashworth, J.D. and Lavallée, Y., 2017. The permeability of fractured rocks in pressurised volcanic and geothermal systems. Scientific Reports, 7(1): 6173.
Larson, P.B. and Taylor, H.P., 1986. An oxygen isotope study of hydrothermal alteration in the Lake City caldera, San Juan Mountains, Colorado. Journal of Volcanology and Geothermal Research, 30: 47-82.
Leet, R.C., 1988. Saturated and subcooled hydrothermal boiling in groundwater flow channels as a source of harmonic tremor. Journal of Geophysical Research, 93: 4835-4849.
Lion, M., Skoczylas, F., & Ledesert, B. 2005. Effects of heating on the hydraulic and poroelastic properties of bourgogue limestone. International Journal of Rock Mechanics and Mining Sciences, 42: 508-520.
Lipman, 2000. Calderas. In: H. Sigurdsson (Editor), Encyclopedia of Volcanoes. Academic Press, San Diego, California, pp. 651-652.
Lundborg, N., 1968. Strength of rock-like minerals. International Journal of Rock Mechanics and Mining Sciences, 5: 427-454.
Main, I.G., Leonard, T., Papasouliotis, O., Hatton, O. and Meredith, P.G., 1999. One slope or two? Detecting statistically significant breaks of slope in geophysical data with application to fracture scaling relationships. Geophysical Research Letters, 26(18): 2801-2804.
Manconi, R., Walter, T.R. and Amelung, F., 2007. Effects of mechanical layering on volcano deformation. Geophysical Journal International, 170: 952-958.
Martin, C.D. and Chandler, N.A., 1994. The progressive fracture of Lac du Bonnet granite. International Journal of Rock Mechanics and Mining Sciences, 31: 643-659.
Mayer, K., Scheu, B., Montanaro, C., Yilmaz, T.I., Isaia, R., Abbichler, D. and Dingwell, D.B., 2016. Hydrothermal alteration of surficial rocks at Solfatara (Campi Flegrei): Petrophysical properties and implications for phreatic eruption processes. Journal of Volcanology and Geothermal Research, 320: 128-143.
McGuire, W.J., 1996. Volcano instability: a review of contemporary themes. Geological Society of London, 110: 1-23.
McGuire, W.J., 1998. Volcanic hazards and their migration. In: J.G. Maund and M. Eddlestron (Editors), Geohazards in Engineering Geology. Engineering Geology Special Publications, Geological Society, London.
McGuire, W.J., 2006. Global risk from extreme geophysical events: threat identification and assessment. Philosophical transactions. Series A, Mathematical, physical, and engineering sciences, 364(1845): 1889-1909.
Min, D., Zhongzi, X., Xianghui, L., Sufen, H. and Mingshu, T., 1996. Microstructures of some alkali-silica reactive aggregates in China. Cement and Concrete Research, 26(5): 663-668.
Moon, V., Bradshaw, J. and de Lange, W., 2009. Geomorphic development of White Island volcano based on slope stability modelling. Engineering Geology, 104: 16-30.
Moon, V., Bradshaw, J., Smith, R. and de Lange, W., 2005. Geotechnical characterization of stratocone crater wall sequences, White Island volcano, New Zealand. Engineering Geology, 81: 146-178.
Morgan, G.C., Shanks III, W.C., Lovalvo, D.A., Johnson, Y.A., Stephenson, W.J., Pierce, K.L., Harlan, S.S., Finn, C.A., Lee, G., Webring, M., Schulze, B., Duhn, J., Sweeney, R. and Balistrieri, L., 2003. Exploration and discovery in Yellowstone Lake: results from high-resolution sonar imaging, seismic reflection profiling, and submersible studies. Journal of Volcanology and Geothermal Research, 122: 221-242.

Mueller, S., Melnik, O., Spieler, O., Scheu, B. and Dingwell, D.B., 2005. Permeability and degassing of dome lavas undergoing rapid decompresion: an experimental determination. Bulletin of Volcanology, 67: 526-538.

Mueller, S., Scheu, B., Spieler, O. and Dingwell, D.B., 2008. Permeability and control on magma fragmentation. Geology, 36(5): 399-402.

Nairn, I.A., Wood, C.P. and Hewson, C.A.Y., 1975. Phreatic eruptions of Ruapehu : April 1975. New Zealand Journal of Geology and Geophysics 22(2): 155-170.

Nara, Y., Meredith, P.G., Yoneda, T. and Kaneko, K., 2011. Influence of macrofractures and microfractures on permeability and elastic wave velocities in basalt at elevated pressure. Tectonophysics, 503(1-2): 52-59.

Nicksiar, M., & Martin, C. D. 2012. Evaluation of Methods for Determining Crack Initiation in Compression Tests on Low-Porosity Rocks. Rock Mech Rock Eng, 45: 607-617.

Nishi, Y., Sherburn, S., Scott, B.J. and Sugihara, M., 1996. High-frequency earthquakes at White Island volcano, New Zealand: insights into the shallow structure of a volcano-hydrothermal system. Journal of Volcanology and Geothermal Research, 72: 183-197.

Okumura, S. and Sasaki, O., 2014. Permeability reduction of fractured rhyolite in volcanic conduits and its control on eruption cyclicity. Geology, 42: 843-846.

Peiffer, L., Bernard-Romero, R., Mazot, A., Taran, Y.A., Guevara, M. and Santoyo, E., 2014. Fluid geochemistry and soil gas fluxes (CO2-CH4-H2S) at a promissory hot dry rock geothermal system: the Acoculco caldera, Mexico. Journal of Volcanology and Geothermal Research, 284: 122-137.

Peltier, A., Scott, B.J. and Hurst, T., 2009. Ground deformation patterns at White Island volcano (New Zealand) between 1967 and 2008 deduced from levelling data. Journal of Volcanology and Geothermal Research, 181: 207-218.

Pérez-Flores, P., Wang, G., Mitchell, T.M., Meredith, P.G., Nara, Y., Sarkar, V. and Cembrano, J., 2017. The effect of offset on fracture permeability of rocks from the Southern Andes Volcanic Zone, Chile. Journal of Structural Geology, 104: 142-158.

Petcovic, H.L. and Dufek, J.D., 2005. Modeling magma flow and cooling in dikes: implications for emplacement of Columbia River flood basalts. Journal of Geophysical Research: Solid Earth, 110(10): 1-15.

Pola, A., Crosta, G., Fusi, N., Barberini, V. and Norini, G., 2012. Influence of alteration on physical properties of volcanic rocks. Tectonophysics, 566-567: 67-86.

Pola, A., Crosta, G.B., Fusi, N. and Castellanza, R., 2014. General characterization of the mechanical behaviour of different volcanic rocks with respect to alteration. Engineering Geology, 169: 1-13.

Price, R.C., Gamble, J.A., Smith, I.E.M., Maas, R., Waight, T., Stewart, R.B. and Woodhead, J.D., 2012. The anatomy of an andesite volcano: a time-stratigraphic study of andesite petrogenesis and crustal evolution at Ruapehu volcano, New Zealand. Journal of Petrology, 42(10): 2139-2189.

Quaderer, A., Mastalerz, M., Schimmelmann, A., Drobniak, A., Bish, D.L. and Wintsch, R.P., 2016. Dike-induced thermal alteration of the Springfield Coal Member (Pennsylvanian) and adjacent clastic rocks, Illinois Basin, USA. International Journal of Coal Geology, 166: 108-117.

Reid, M.E., 2004. Massive collapse of volcano edifices triggered by hydrothermal pressurization. Geology, 32(373-376).

Reid, M.E., Sisson, T.W. and Brien, D.L., 2001. Volcano collapse promoted by hydrothermal alteration and edifice shape, Mount Rainier, Washington. Geology, 29(9): 779.

Rocchi, V., Sammonds, P.R. and Kilburn, C.R.J., 2004. Fracturing of Etnean and Vesuvian rocks at high temperatures and low pressures. Journal of Volcanology and Geothermal Research, 132(2-3): 137-157.

Rosenberg, M.D., Bignall, G. and Rae, A.J., 2009. The geological framework of the Wairakei–Tauhara Geothermal System, New Zealand. Geothermics, 38(1): 72-84.
Rowland, J.V., Bardsley, C., Downs, D., Sepulveda, F., Simmons, S.F. and Scholz, C., 2012. Tectonic controls on hydrothermal fluid flow in a rifting and migrating arc, Taupo Volcanic Zone, New Zealand, New Zealand Geothermal Workshop, Auckland, New Zealand, pp. 19-21.
Rowland, J.V. and Sibson, R.H., 2001. Extensional fault kinematics within the Taupo Volcanic Zone, New Zealand: soft-linked segmentation of a continental rift system. New Zealand Journal of Geology and Geophysics, 44(2): 271-283.
Rowland, J.V. and Sibson, R.H., 2004. Structural controls on hydrothermal flow in a segmented rift system, Taupo Volcanic Zone, New Zealand. Geofluids, 4(4): 259-283.
Rowland, J.V., Wilson, C.J.N. and Gravley, D.M., 2010. Spatial and temporal variations in magma-assisted rifting, Taupo Volcanic Zone, New Zealand. Journal of Volcanology and Geothermal Research, 190(1-2): 89-108.
Rust, A.C. and Cashman, K., 2004. Permeability of vesicular silicic magma: inertial and hysteresis effects. Earth and Planetary Science Letters, 228: 93-107.
Saar, M.O. and Manga, M., 1999. Permeability-porosity relationships in vesicular basalts. Geophysical Research Letters, 26(111-114).
Schaefer, L.N., Kendrick, J.E., Oommen, T., Lavallée, Y. and Chigna, G., 2015. Geomechanical rock properties of a basaltic volcano. Frontiers in Earth Science, 3(29).
Schaefer, L.N., Kennedy, B., Villeneuve, M.C., Cook, S.C.W., Jolly, A., Keys, H. and Leonard, G.J., 2018. Stability assessment of the Crater Lake overflow/Te Wai-ā-moe channel at Mt. Ruapehu (New Zealand), and implications for volcanic lake break-out triggers. Journal of Volcanology and Geothermal Research, 358: 31-44.
Scott, S.W. and Driesner, T., 2018. Permeability changes resulting from quartz precipitation and dissolution around upper crustal intrusions. Geofluids: 19.
Scott, S.W., Driesner, T. and Weis, P., 2015. Geologic controls on supercritical geothermal resources above magmatic intrusions. Nature Communications, 6: 7837-7837.
Scott, S.W., Driesner, T. and Weis, P., 2016. The thermal structure and temporal evolution of high-enthalpy geothermal systems. Geothermics, 62: 33-47.
Seebeck, H., Nicol, A., Giba, M., Pettinga and Walsh, J.B., 2014. Geometry of the subducting Pacific plate since 20 Ma, Hikurangi margin, New Zealand. Journal of the Geological Society, London, 171: 131-143.
Senger, K., Millett, J., Planke, S., Ogata, K., Eide, C.H., Festoy, M., Galland, O. and Jerram, D.A., 2017. Effects of igneous intrusions on the petroleum system: a review. First Break, 35.
Shanks, W.C., 2012. Volcanogenic Massive Sulfide Occurrence Model, US Geological Survey, Reston, Virginia.
Sherburn, S., Scott, B.J., Nishi, Y. and Sugihara, M., 1998. Seismicity at White Island volcano, New Zealand: a revised classification and inferences about source mechanism. Journal of Volcanology and Geothermal Research, 83: 287-312.
Siebert, L., 1992. Threats from debris avalanches. Nature, 356: 658-659.
Siebert, L., Cottrell, E., Venzke, E. and Andrews, B., 2015. Earth's Volcanoes and Their Eruptions: An Overview. In: H. Sigurdsson, B.F. Houghton, S.R. McNutt, H. Rymer and J. Stix (Editors), The Encyclopedia of Volcanoes. Academic Press, London, UK, pp. 245-249.
Sigurdsson, H., Houghton, B.F., McNutt, S.R., Rymer, H., Stix, J. and McBirney, A.R., 2000. Encyclopedia of Volcanoes. Physics Today, 53(10): 84-85.
Simpson, M.P., 2015. Reflectance spectrometry (SWIR) of alteration minerals surrounding the Favona epithermal vein, Waihi vein system, Hauraki Goldfield, AusIMM New Zealand Branch Annual Conference, Dunedin, New Zealand, pp. 490-499.

Simpson, M.P., Mauk, J.L., Bowyer, D. and Worland, R.J., 2006. Alteration mineral studies of an epithermal prospect and a geothermal field using the TerraSpec, 39th Annual Conference of the New Zealand Branch of the AusIMM, pp. 247-256.

Simpson, M.P., Rae, A., Ganefianto, N. and Sepulveda, F., 2009. Short wavelength infrared (SWIR) spectral characterisation of smectite, illite-smectite and illite for geothermal fields of the Taupo Volcanic Zone, New Zealand, New Zealand Geothermal Workshop 2009, Rotorua, New Zealand.

Siratovich, P., Cole, J., Heap, M., Villeneuve, M., Reuschlé, T., Swanson, K., Kennedy, B., Gravley, D. and Lavallée, Y., 2015. Experimental thermal stimulation of the Rotokawa Andesite. Proceedings World Geothermal Congress 2015(April): 1-6.

Siratovich, P.A., Heap, M.J., Villeneuve, M.C., Cole, J.W. and Reuschlé, T., 2014. Physical property relationships of the Rotokawa Andesite, a significant geothermal reservoir rock in the Taupo Volcanic Zone, New Zealand. Geothermal Energy, 2(1): 10-10.

Sruoga, P., Rubinstein, N. and Hinterswimmer, G., 2004. Porosity and permeability in volcanic rocks: a case study on the Serie Tobifera, South Patagonia, Argentina. Journal of Volcanology and Geothermal Research, 132(1): 31-43.

Steefel, C.I. and Lasaga, A.C., 1994. A coupled model for the transport of multiple chemical species and kinetic precipitation/dissolution reactions with application to reactive flow in single phase hydrothermal systems. American Journal of Science, 294: 529-592.

Stimac, J., Powell, T. and Golla, G., 2004. Porosity and permeability of the Tiwi Geothermal Field, Philippines, based on continuous and spot core measurements. Geothermics, 33: 87-107.

Tapponnier, P. and Brace, W.F., 1976. Development of stress-induced microcracks in Westerly granite. International Journal of Rock Mechanics and Mining Science & Geomechanics Abstracts, 13: 103-112.

Thomson, K. and Schofield, N., 2008. Lithological and structural controls on the emplacement and morphology of sills in sedimentary basins. Geological Society, London, Special Publications, 302: 31-44.

Todesco, M., Rinaldi, A.P. and Bonforte, A., 2010. Modeling of unrest signals in heterogeneous hydrothermal systems. Journal of Geophysical Research, 115(B09213).

Tullis, J. and Yund, R.A., 1977. Hydrolytic weakening of experimentally deformed Westerly granite. Journal of Geophysical Research, 82: 5705-5718.

Ulusay, R. and Hudson, J., 2007. The Complete ISRM Suggested Methods for Rock Characterization, Testing and Monitoring: 1974-2006. Elsevier, Antalya, Turkey.

Valentine, G. and Krogh, K., 2006. Emplacement of shallow dikes and sills beneath a small basaltic volcanic center – the role of pre-existing structure (Paiute Ridge, southern Nevada, USA). Earth and Planetary Science Letters, 246(3-4): 217-230.

Vigneresse, J.-L., Tikoff, B. and Améglio, L., 1999. Modification of the regional stress field by magma intrusion and formation of tabular granitic plutons. Tectonophysics, 302(3-4): 203-224.

Vinciguerra, S., Trovato, C., Meredith, P.G. and Benson, P.M., 2005. Relating seismic velocities, thermal cracking and permeability in Mt. Etna and Iceland basalts. International Journal of Rock Mechanics and Mining Sciences, 42(7-8): 900-910.

Voight, B., 1989. A relation to describe rate-dependent material failure. Science, 243: 200-203.

Voight, B., 2000. Structural stability of andesite volcanoes and lava domes. Philosophical Transactions of the Royal Society A: Mathematical, Physical and Engineering Sciences, 358(1770): 1663-1703.

Voight, B. and Elsworth, D., 1997. Failure of volcano slopes. Geotechnique, 47(1): 1-31.

Vutukuri, V.S., Lama, R.D. and Saluja, S.S., 1974. Handbook on mechanical properties of rocks. Testing techniques and results. Volume 1. Textbook. International Journal of Rock Mechanics and Mining Sciences & Geomechanics Abstracts, 11(11): A218.

Walsh, J.B. and Brace, W.F., 1966. Cracks and Pores in Rocks, 1st ISRM Congress, Lisbon, Portugal.

Walter, T.R., Acocella, V., Neri, M. and Amelung, F., 2005. Feedback processes between magmatic events and flank movement at Mount Etna (Italy) during the 2002–2003 eruption. Journal of Geophysical Research, 110(B10205).

Watters, R.J. and Delhaut, W.D., 1995. Effect of argillic alteration on rock mass stability. Geological Society Of America Bulletin, 10: 139-150.

Wilson, C.J.N., Gravley, D., Leonard, G.J. and Rowland, J.V., 2009. Volcanism in the central Taupo Volcanic Zone, New Zealand: tempo, styles and controls. In: T. Thordarson, G. Larsen, S. Self, S. Rowland and A. Hoskuldsson (Editors), Special Publications of IAVCEI 2. Geological Society of London, London, UK, pp. 225-247.

Wilson, C.J.N., Houghton, B.F., McWilliams, M.O., Lanphere, M.A., Weaver, S.D. and Briggs, R.M., 1995. Volcanic and structural evolution of Taupo Volcanic Zone, New Zealand: a review. Journal of Volcanology and Geothermal Research, 68(1-3): 1-28.

Wilson, C.J.N. and Rowland, J.V., 2016. The volcanic, magmatic and tectonic setting of the Taupo Volcanic Zone, New Zealand, reviewed from a geothermal perspective. Geothermics, 59: 168-187.

Wright, H.M.N., Cashman, K.V., Gottesfeld, E.H. and Roberts, J.J., 2009. Pore structure of volcanic clasts: measurements of permeability and electrical conductivity. Earth and Planetary Science Letters, 280(1-4): 93-104.

Wyering, L.D., Villeneuve, M.C., Wallis, I.C., Siratovich, P.A., Kennedy, B.M. and Gravley, D.M., 2015. The development and application of the alteration strength index equation. Engineering Geology, 199: 48-61.

Wyering, L.D., Villeneuve, M.C., Wallis, I.C., Siratovich, P.A., Kennedy, B.M., Gravley, D.M. and Cant, J.L., 2014. Mechanical and physical properties of hydrothermally altered rocks, Taupo Volcanic Zone, New Zealand. Journal of Volcanology and Geothermal Research, 288: 76-93.

Zhu, W., Baud, P., Vinciguerra, S. and Wong, T.F., 2016. Micromechanics of brittle faulting and cataclastic flow in Mount Etna basalt. Journal of Geophysical Research: Solid Earth, 121(6): 4268-4289.

Chapter 4 Preamble

In Chapter 3, I present geomechanical data from intact lab samples from a glacially dissected, fossil hydrothermal system at Pinnacle Ridge, Mt. Ruapehu, New Zealand. Among other findings, I observe: (1) the porosity of the brecciated lava margins increases with proximity to the intrusion; and (2) the geomechanical properties of hydrothermal vein material require it to be considered its own geotechnical unit. In Chapter 4, I focus on the effect alteration has on the physical and mechanical properties of andesitic volcanics using a unique specimen (Fig. 1). Using a sample block hosting two different types of alteration (intermediate argillic and advanced argillic), I observe the effects these two alteration types produce in the geomechanical properties of the rock, and then discuss the consequences of these implications on volcanic monitoring.

Chapter 4 has been submitted, revised, and re-submitted to *Bulletin of Volcanology*. This chapter is presented in its revised format.

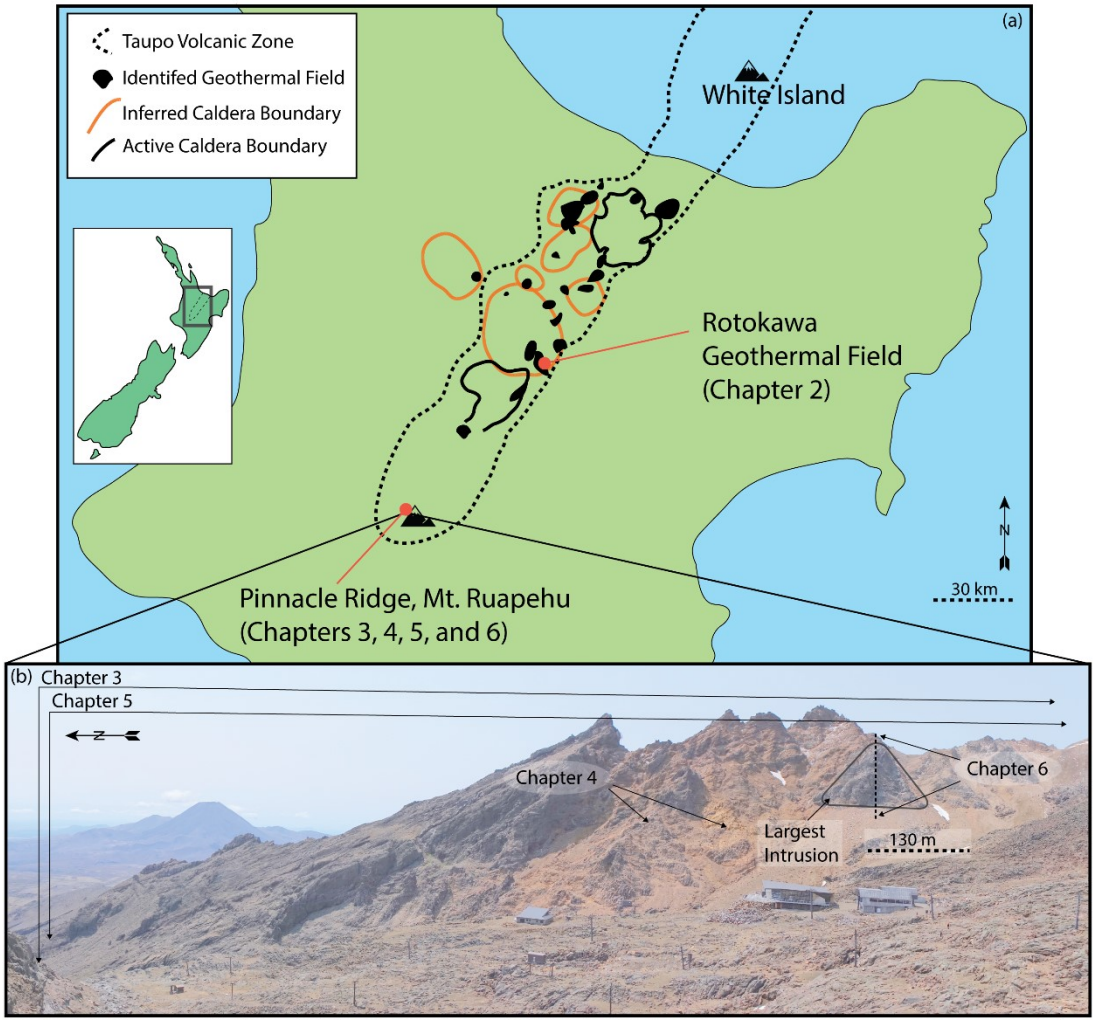

Figure 1. Primary site locations specific to the research presented in this study. (a) Sites of the two hydrothermal systems in New Zealand. (b) Sites specific to Chapters 3 – 6 at Pinnacle Ridge. Solid black polygon marks boundary of the largest young intrusion. Scale is approximate.

Chapter 4

Influence of Alteration on the Mechanical Behavior and Failure Mode of Andesitic Lavas: Implications for Shallow Seismicity and Volcano Monitoring

S. P. Mordensky[1], M. J. Heap[2], B. M. Kennedy[1], H. A. Gilg[3], M. C. Villeneuve[1], J. I. Farquharson[2], D. M. Gravley[1]

[1]Department of Geological Sciences, University of Canterbury, Private Bag 4800, Christchurch 8140, New Zealand

[2]Institut de Physique de Globe de Strasbourg (UMR 7516 CNRS, Université de Strasbourg/EOST), 5 rue René Descartes, 67084 Strasbourg cedex, France

[3]Lehrstuhl für Ingenieurgeologie, Technische Universität München, Arcisstraße 21, 80333 München, Deutschland

Abstract

Volcanoes often host hydrothermal systems that alter the host rock. To understand the influence of alteration on mechanical behavior of edifice-forming rock, we performed a series of triaxial deformation experiments on variably-altered andesite from Mt. Ruapehu (New Zealand) under constant effective pressure. Under the imposed conditions, andesite with intermediate argillic alteration deforms in a brittle manner forming fractures. In contrast, andesite with advanced argillic alteration deforms in a ductile manner, with sample failure driven by distributed cataclastic pore collapse. We consider this the result of an increase in porosity and clay content with increasing alteration. Ancillary experiments highlight that the brittle-ductile transition occurs at a much lower effective pressure—analogous to depth—in andesites with advanced argillic alteration relative to unaltered andesites of comparable porosity. We conclude that advanced argillic alteration can create an anomalous shallow ductile zone, which has important implications for fluid flow and pre-eruptive seismicity.

Plain Language Summary

Observing volcanic seismicity plays an integral role in volcano monitoring. Rising magma creates stresses that often break rock and produce earthquakes indicative of a coming eruption. Unfortunately, not every volcano or eruption at a particular volcano is characterized by these pre-eruptive earthquakes. In our

study, we simulate pressure conditions in a volcano using a specialized loading press to show that alteration from hot circulating fluids can cause rock to flow (no earthquakes) rather than to break and produce earthquakes. We suggest that this change in deformation behavior (flow versus break) is the result of alteration increasing the porosity (void space) and the amount of weak clays within the rock. This may explain why few earthquakes are recorded before some eruptions from volcanoes. The results of our study therefore emphasize the importance of a multi-method monitoring at active volcanoes worldwide.

4.1 Introduction

Volcanic complexes are composed of an assortment of physically and mechanically varied structures (Moon et al., 2005; Schaefer et al., 2015) that contribute to the diverse range of volcanic behaviors, such as outgassing (Farquharson et al., 2015), deformation (Manconi et al., 2007), eruptive activity (Nairn et al., 1975), seismicity (Bryan & Sherburn, 1999), and mass movement (Apuani et al., 2005). Hydrothermal alteration, common to many volcanic edifices (Sigurdsson et al., 2000; and references therein), further increases the mechanical complexity (Pola et al., 2012; Heap et al., 2015b; Wyering et al., 2015; Heap et al., 2017a). Recently, many studies have explored the mechanical behavior and failure modes of unaltered volcanic materials under triaxial conditions (Kennedy et al., 2009; Zhu et al., 2011; Loaiza et al., 2012; Adelinet et al., 2013; Heap et al., 2015a; Zhu et al., 2016; Heap et al., 2017b; Zorn et al., 2018). These studies have shown that brittle and ductile deformation in volcanic rocks manifests as shear fracture formation and cataclastic pore collapse (localized or distributed), respectively. Rock failure mode is considered important in the creation and destruction of permeability (Heap et al., 2015a) and in the interpretation of pre-eruption seismicity (Bryan & Sherburn, 1999; Bean et al., 2014). However, no study investigates the mechanical properties of variably-altered samples prepared from the same block. In this study, using triaxial deformation experiments, we detail the influence of intermediate and advanced argillic hydrothermal alteration on the mechanical behavior and failure mode of andesite sourced from a single block collected from Pinnacle Ridge, Mt. Ruapehu (New Zealand). In doing so, we present novel data that show that mechanical behavior depends on the altered condition of the lava and can be highly variable over short distances. We then discuss the relevance of his behavioral change for volcanic monitoring with respect to fluid flow and volcano-tectonic seismic activity.

4.1.1 Pinnacle Ridge, Mt. Ruapehu

Mt. Ruapehu is an active andesitic stratovolcano on New Zealand's North Island at the southern end of the Taupō Volcanic Zone (Figure 4.1a; Cole, 1990). Pinnacle Ridge, located on the northwestern flank of Mt. Ruapehu, is composed of the oldest (250 *ka*) exposed geologic unit – the Te Herenga Formation (Figure 4.1b). Pinnacle Ridge has been subject to several intrusive events, which provided the heat for a shallow hydrothermal system that altered the volcanic host rock (Hackett, 1985). Younger glaciation (~10 *ka*) exposed a 400 m-wide alteration halo surrounding the shallow intrusive system (Figure 4.1c). The alteration phases of the rocks exposed are predominantly consistent with advanced argillic alteration which occurred at < 500 m depth (Hackett, 1985; Mordensky et al., 2018) and is typical of hot acidic fluids circulating within the shallow parts of andesitic stratovolcanoes (Henley & Ellis, 1983). Pinnacle Ridge therefore emerges as an ideal case study site for investigating the influence of argillic alteration on mechanical behavior and failure mode.

4.2 Materials and methods

4.2.1 Sample description

To study the influence of alteration on mechanical behavior and failure mode, we chose a single block of a single primary lithology that exhibits a variation in alteration intensity. The block (block 031; Figure 4.1d) is altered dense coherent lava, as defined by Mordensky et al. (2018). Six samples (40 mm in length and 20 mm in diameter) were prepared from the block: two with only intermediate argillic alteration and four with later-stage, advanced argillic alteration superimposed upon the earlier intermediate argillic alteration (Figures 4.1d, 4.2). We additionally prepared samples from another block displaying superimposed advanced argillic alteration (block 018) from the altered brecciated lava margin (Figure 4.1e) to study the influence of effective pressure (depth) on the mechanical behavior and failure mode of altered andesitic lava in greater detail. The connected porosity and permeability of these samples (Table 4.S2) were characterized in Mordensky et al. (2018).

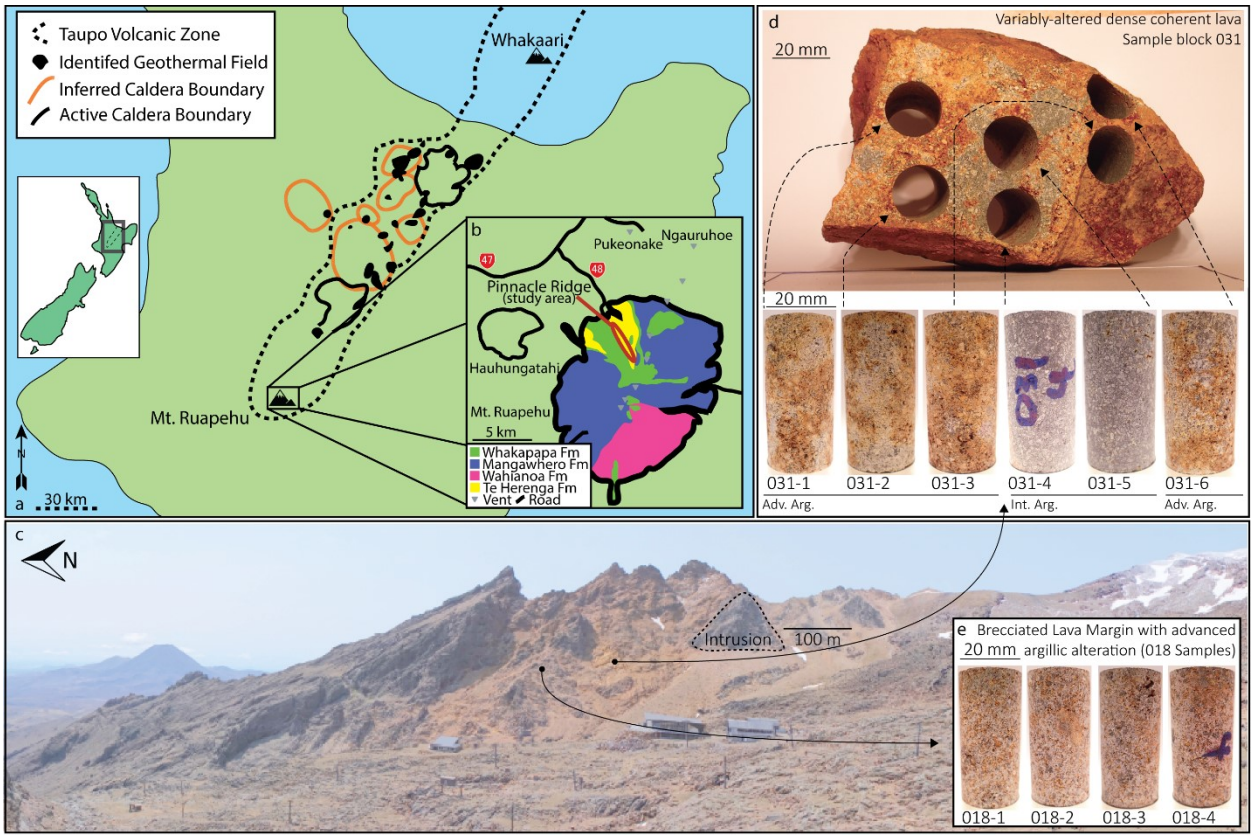

Figure 4.1 Site and sample reference. (a) Location of Pinnacle Ridge on Mt. Ruapehu (New Zealand). The locations of the Taupō Volcanic Zone boundaries are provided along with the locations of geothermal fields, active caldera boundaries, and inferred caldera boundaries. Adapted from Wilson et al. (1995). (b) Geological formations of Mt. Ruapehu and location of Pinnacle Ridge. Adapted from Hackett (1985). (c) Sample locations on Pinnacle Ridge. Exposed intrusion outlined (dashed black) (d) Dense coherent lava sample block (031) from which samples with advanced and intermediate argillic alteration were cored. The samples with advanced argillic alteration are toward the outside of the sample block (031-1, -2, -3 and -6), which was in contact with a joint system. The interior of the sample block has intermediate argillic alteration (031-4 and -5). (e) Brecciated lava margin sample suite with advanced argillic alteration (018 sample series). Adv. Arg. – Advanced argillic. Int. Arg. – Intermediate argillic.

4.2.2 Sample composition and microstructural characterization

Using X-ray powder diffraction analysis, scanning electron microscopy (SEM), and Raman spectroscopy, we find that the samples in this study host one of two alteration types (intermediate argillic and advanced argillic; see Table 4.S1 and Corbett & Leach, 1998). Both types of alteration are commonly found at shallow depths (< 1 km; see Cooke et al., 2014), but can be produced by several processes (Rye et al., 1991). All samples display an early intermediate argillic alteration with smectites and minor illite that is associated with pyrite and cristobalite (Figure 4.2a). Some samples (031-1, -2, -3, -6 and 018-series) show superimposed advanced argillic alteration with pore-filling kaolinite and sulfate phases (Figure 4.2b,c).

The dense coherent lava with only intermediate argillic alteration (from block 031) is composed of a glassy groundmass containing plagioclase microlites and a predominantly plagioclase phenocryst assemblage accompanied by pyroxene phenocrysts mostly altered to smectitic clay (~100 μm-1 mm across; Figure 4.2d). The porosity is predominantly pores ranging from 100 to 200 μm across, with some pores up to 2 mm across; there are few microcracks within the groundmass. The dense coherent lava with advanced argillic alteration (also from block 031) also contains relic phenocryst textures (Figure 4.2e) with more intensely altered plagioclases and completely altered pyroxenes. Several phenocryst relics have void space (< 200 μm across) from dissolution. A smectite- and kaolinite-clay groundmass hosts microcracks (0.5 - > 5 mm in length). The brecciated lava margin with advanced argillic alteration (block 018) contains sub-angular to sub-rounded pores (50-700 μm across) in a very fine clay-rich (smectite and kaolinite) groundmass with mostly plagioclase and pyroxene phenocrysts (~100 μm-1 mm across) partially altered to clay (Figure 4.2e). In general, the samples with advanced argillic alteration host substantially greater clay contents (29 – 45 ± 7 wt.%) than the samples with intermediate argillic alteration (12 ± 2 wt.%; Table 4.S1).

4.2.3 Triaxial deformation experiments

All the prepared samples were deformed under conventional triaxial conditions ($\sigma_1 > \sigma_2 = \sigma_3$) at a constant strain rate of 1.0×10^{-5} s^{-1}. Confining and pore fluid (deionized water) pressures were applied and held constant at the chosen target pressures using servo-controlled pressure intensifiers. During deformation, axial load and displacement were recorded using a load cell and a linear variable differential transducer, respectively. The change in pore volume was monitored using a pore pressure volumometer. These measurements were converted to axial stress, axial strain, and porosity change using the sample dimensions. We assume herein a simple effective pressure law (where effective pressure, P_E, is equal to the confining pressure, P_C, minus the pore fluid pressure, P_P), an assumption shown to be appropriate for porous andesites (Farquharson et al., 2016a).

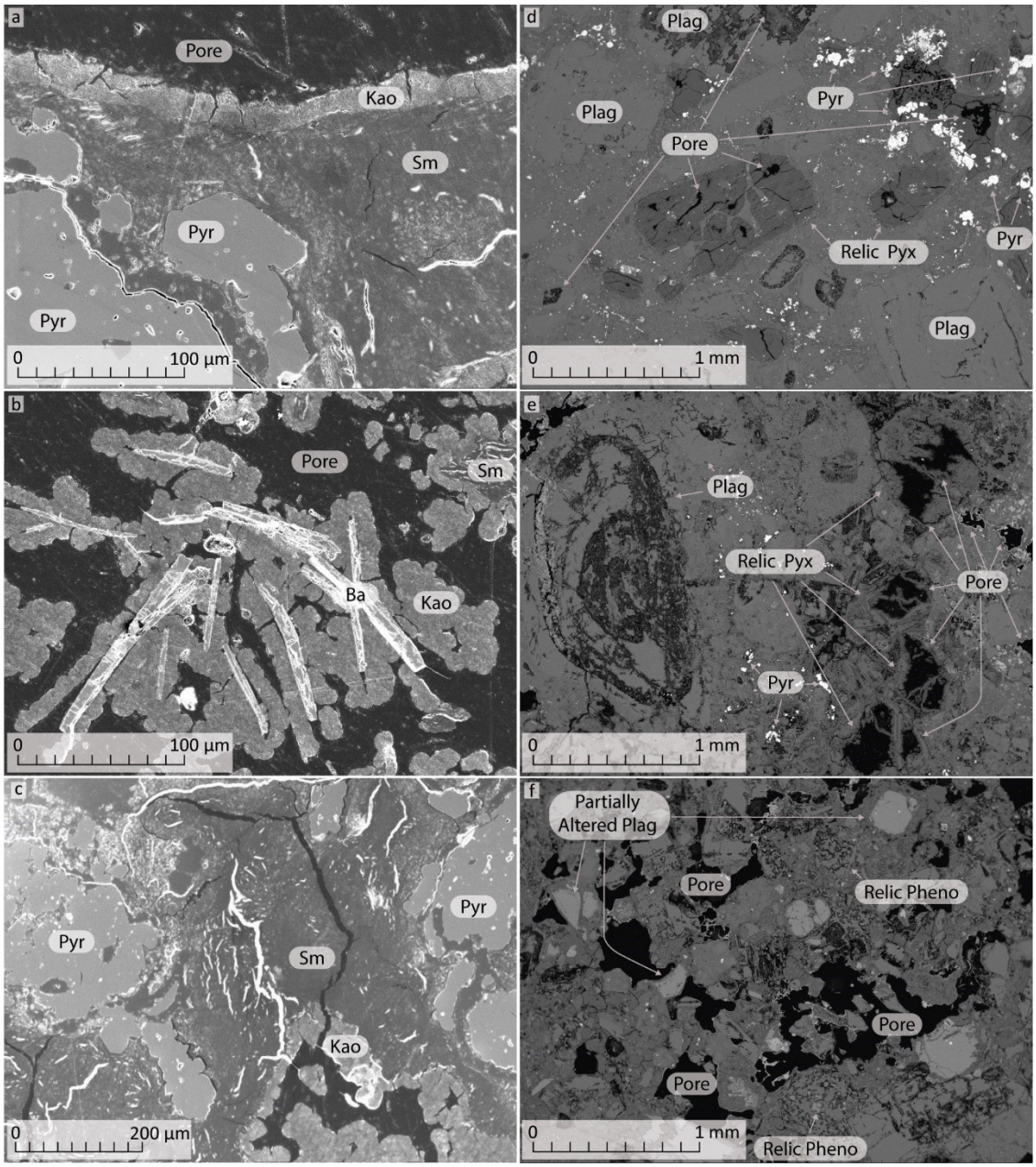

Figure 4.2 Secondary electron (left) and backscattered electron (right) SEM images of undeformed sample microstructure. Porosity is black. (a) Predominantly intermediate argillic alteration with minor kaolinite precipitation along pore boundary. (b) Pore-filling kaolinite and barite precipitates superimposed upon smectite clay. (c) Intermediate argillic alteration (pyrite and smectite clay) superimposed by an advanced argillic phase (pore-filling kaolinite). (d) Dense coherent lava with intermediate argillic alteration (from block 031). (e) Dense coherent lava with advanced argillic alteration (from block 031). (f) Brecciated lava margin with advanced argillic alteration (block 018). Sm-Smectite; Kao-Kaolinite; Pyr-Pyrite; Pyx-Pyroxene; Ba-Barite; Plag-Plagioclase.

4.3 Results

4.3.1 Comparing mechanical behavior between alteration types

The stress-strain curves for the variably altered dense coherent lava (block 031) at an effective pressure of 10 MPa are shown in Figure 4.3a. The corresponding porosity-change curves as a function of axial strain are shown in Figure 4.3b. The samples with intermediate argillic alteration (Figure 4.3a) display classical brittle mechanical behavior (Wong & Baud, 2012): a peak stress is reached (peak differential stresses reported in Table 4.S3), followed by strain softening (a stress decrease). Further evidence is provided by the porosity change data (Figure 4.3b), which show that the less altered samples first show a small amount of compaction (usually interpreted as microcrack closure; Hoek and Bieniawski (1965)) and then dilate significantly (usually interpreted as microcrack initiation; Brace et al. (1966)) as a function of increasing axial strain. The samples with advanced argillic alteration display classically ductile mechanical behavior (Wong & Baud, 2012) characterized by an absence of both strain softening (Figure 4.3a) and dilation (Figure 4.3b).

4.3.2 Mechanical behavior of altered rock under different effective pressures

The stress-strain curves for the brecciated lava margin with advanced argillic alteration (block 018) at effective pressures between 1 and 15 MPa (Table 4.S3) are shown in Figure 4.3c. The corresponding porosity-change curves as a function of axial strain are shown in Figure 4.3d. These data show that the lava is brittle at pressures of 1 and 5 MPa and ductile at pressures of 10 and 15 MPa (Figures 4.3c,d). The sample deformed at a pressure of 15 MPa exhibits strain hardening (Figure 4.3c).

4.3.3 Post-deformation microstructure

Post-deformation microstructures for the brittle and ductile experiments are provided in Figure 4.4. In both sample suites, brittle failure is associated with the formation and coalescence of microcracks to form a through-going shear fracture (Figure 4.4a,c). By contrast, ductile deformation is associated with cataclastic pore collapse and the absence of strain localization (Figure 4.4b,d).

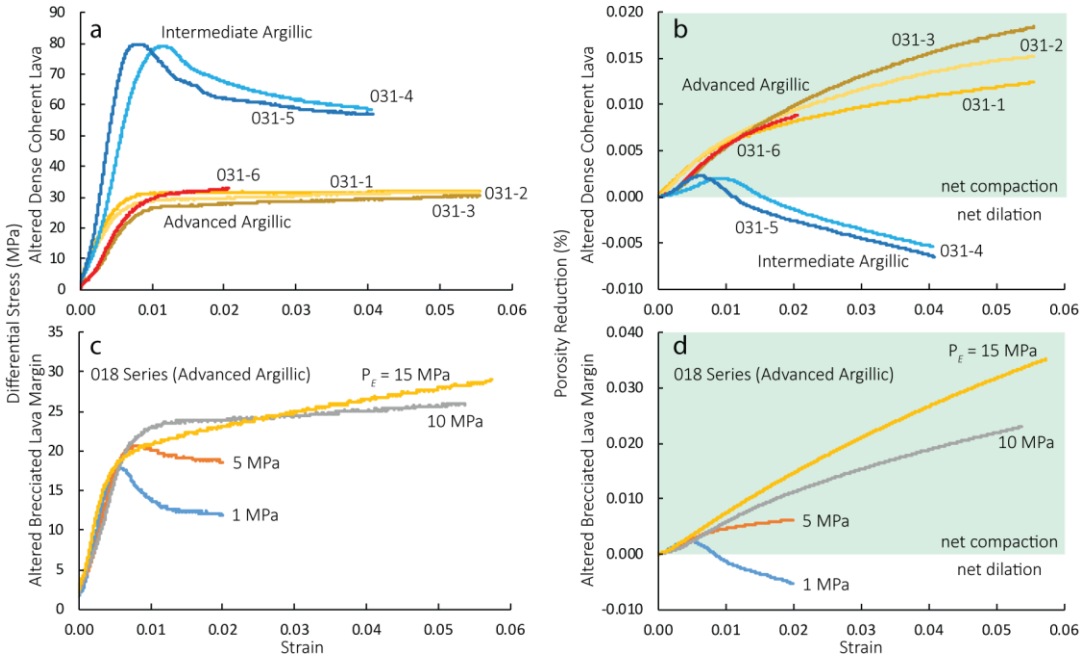

Figure 4.3 Mechanical data for variably altered dense coherent lava hosting varying alteration (a, b) and altered brecciated lava margin under varying deformation conditions (c, d). (a) Stress-strain curves for the 031 sample series deformed at P_E = 10 MPa. (b) Porosity reduction as a function of axial strain for the 031 sample series deformed at P_E = 10 MPa. (c) Stress-strain curves the 018 sample series. (d) Porosity reduction as a function of axial strain for the 018 sample series.

4.4 Discussion

4.4.1 Influence of alteration on mechanical behavior and failure mode

Our mechanical data (Figures 4.3a,b) and post-deformation microstructures (Figures 4.4a,b) show that the presence of advanced argillic alteration leads to a change in sample failure mode: samples without advanced argillic alteration deformed in a brittle manner at P_E = 10 MPa, whereas samples with advanced argillic alteration were ductile under the same conditions. The switch in failure mode is partially a result of the increase in porosity with the advanced argillic alteration: the porosity of the samples with only intermediate argillic alteration (~12 vol.%) is roughly half that of the samples with advanced argillic alteration (~24 vol.%; Table 4.S2). Because of the porosity dependence of the brittle-ductile transition in volcanic rocks (Heap et al., 2015a), high-porosity samples will likely be ductile at lower effective pressures than low-porosity samples. However, we also attribute deformation behavior to the mineralogical composition. Published triaxial data for an unaltered andesite from Volcán de Colima, Mexico, show that ductile behavior in a rock containing 24 vol.% porosity is encountered at an effective pressure of 30 MPa (Heap et al., 2015a), much higher than the effective pressure used for the experiments presented here (10 MPa). We interpret the switch to ductile behavior at low effective pressure compared to similarly porous

unaltered rock (10 versus 30 MPa) as the result of the high clay (smectite and kaolinite) content (45 wt.%; Table 4.S1) in the andesite with advanced argillic alteration. The presence of clays is well-known to reduce rock strength (Hawkins & McConnell, 1992; Baud et al., 2000) and, according to our data, also reduces the effective pressure required for ductile behavior. This interpretation is consistent with existing data of hydrothermally altered andesite from the Rotokawa Geothermal Field, New Zealand, that show moderately and highly altered andesites deform through brittle and ductile behaviour, respectively, despite similar porosity values (14.8 and 14.0 %, respectively) at P_E = 40 MPa (Siratovich et al., 2016).

4.4.2 Influence of effective pressure on mechanical behavior and failure mode

Our mechanical data (Figures 4.3c,d) and post-deformation microstructures (Figures 4.4c,d) show that an increase in effective pressure leads to a change in sample failure mode: samples are brittle at low effective pressures (1-5 MPa) and ductile at high effective pressure (10-15 MPa). The pressure dependence of the brittle-ductile transition in volcanic rocks has been studied by many authors and is accompanied by a switch in the dominant microstructural deformation mechanism from microcracking to cataclastic pore collapse (Kennedy et al., 2009; Zhu et al., 2011; Loaiza et al., 2012; Adelinet et al., 2013; Heap et al., 2015a; Heap et al., 2015b; Siratovich et al., 2016; Zhu et al., 2016). These ancillary data constrain the effective pressure at which andesite with advanced argillic expresses a transition from brittle to ductile behavior. The effective pressures at which andesite with advanced argillic alteration begins (> 5 MPa to < 10 MPa) to express ductile behaviour differs from that of unaltered andesite with similar porosity (see Heap et al., 2015a).

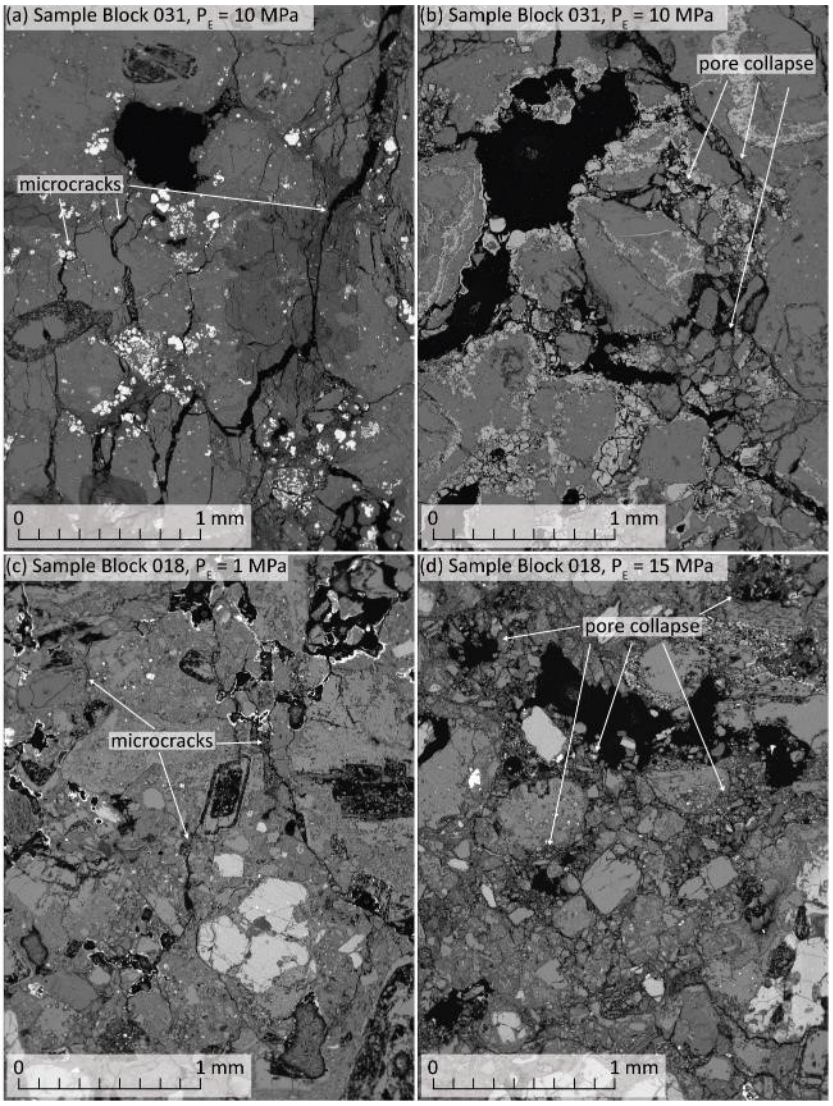

Figure 4.4 Backscattered electron SEM images of deformed sample microstructure. The maximum principal stress is oriented vertically in the images. Porosity is black. (a) Dense coherent lava with intermediate argillic alteration (block 031; P_E = 10 MPa). Microfractures cut axially along the sample. (b) Dense coherent lava with advanced argillic alteration (block 031; P_E = 10 MPa). Pore margins display cataclastic pore collapse. (c) Brecciated lava margin with intermediate argillic alteration (block 018; P_E = 1 MPa). Microfractures cut axially along the sample in a stepwise pattern across crystals and matrix. (d) Brecciated lava margin with advanced argillic alteration (block 018; P_E = 15 MPa). Cataclastic pore collapse predominates deformation.

4.4.3 Implications for fluid flow and seismicity

In volcanic rocks, deformation under triaxial conditions can cause porosity to increase or decrease with a corresponding increase or decrease in permeability (Farquharson et al., 2016b; Farquharson et al., 2017). Mordensky et al. (2018) showed that advanced argillic alteration of andesite can increase the porosity from ~12 to ~24 vol.% and permeability from ~4 × 10^{-16} to ~8 × 10^{-15} m^2 (Table 4.S2). Therefore, although

shallow intrusions have the potential to serve as flow barriers (Senger et al., 2017), they may create intrusion-related halos with high porosity and permeability. However, while brittle deformation is known to increase the permeability of volcanic rocks (Nara et al., 2011; Farquharson et al., 2016b; Pérez-Flores et al., 2017), ductile deformation associated with a decrease in porosity (Figure 4.3b) can, in andesites, reduce permeability by more than an order of magnitude (Farquharson et al., 2017). Our data show that the brittle-ductile transition in andesite with advanced argillic alteration is encountered at low effective pressure (i.e. shallow depths; Figure 4.3). Therefore, advanced argillic alteration presents a means to restrict increases in permeability due to fracturing to the very shallow subsurface (< 100s m) and produce a low permeability zone at shallower depths than expected for unaltered andesite (c.a. 100s m to 1000 m), because inelastic deformation is driven by compactive pore-collapse (Figure 4.5). Below the depths hosting argillic alteration, the deformation processes of other alteration assemblages not addressed in this study (e.g. propylitic) predominate (see Cooke et al., 2014) and substantial porosity loss due to precipitation and/or compaction can promote brittle behavior (Heap et al., 2015a; Siratovich et al., 2016). These changes to permeability within an edifice, as result of a combination of alteration and deformation, have implications for heterogeneous build-up and distribution of pore fluid pressure (Heap & Wadsworth, 2016) as well as outgassing and eruptive character (Woods & Koyaguchi, 1994; Degruyter et al., 2012; Nguyen et al., 2014; Okumura & Sasaki, 2014; Cassidy et al., 2018).

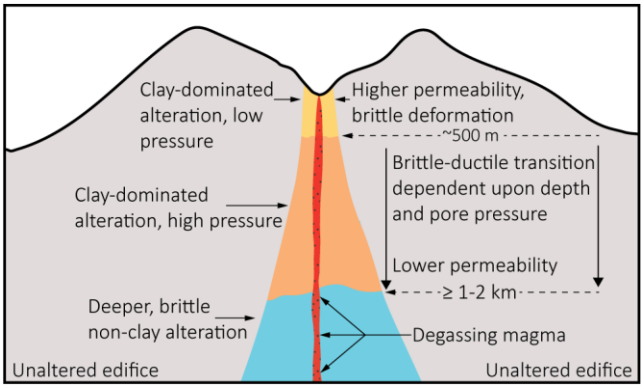

Figure 4.5 Conceptual model showing a shallow high-porosity zone with higher permeability due to the propensity for brittle deformation (yellow), a zone beginning at a few hundred meters depth (~5-10 MPa) with ductile deformation and low-permeability due to pore collapse-driven compaction (orange), and a deeper alteration zone (e.g. propylitic) with potentially brittle behavior (not addressed in this study). Advanced argillic alteration therefore creates an anomalous shallow ductile zone.

Our data may provide an explanation for the absence of volcano-tectonic seismicity prior to some volcanic eruptions. Volcano-tectonic earthquakes are thought to be evidence of brittle host-rock deformation caused by the pressures associated with intruding magma (Latter, 1981). These seismic patterns have proven to be one of the most reliable methods to forecast volcano eruptions (White &

McCausland, 2016). Nonetheless, volcano-tectonic seismicity was notably absent from and, when it rarely did occur, not correlated with, the eruptive activity at Mt. Ruapehu from 1971 to 1996 (Sherburn et al., 1999). Only after several weeks into the 1995-1996 Mt. Ruapehu eruptive sequence, the largest eruptive sequence from Mt. Ruapehu in over 70 years (Sherburn et al., 1999), did volcano-tectonic seismicity return with more regularity to the volcano (Bryan & Sherburn, 1999). Bryan and Sherburn (1999) propose the change in seismicity was a transition from ductile to brittle behavior in the edifice. Our results provide an explanation for this transition, and thereby the absence of volcano-tectonic seismicity prior to an eruption, by showing that a shallow subsurface transition from brittle to ductile behavior is possible in the altered andesites (Figure 4.3). In high-elevation environments, advanced argillic alteration and hence ductility may extend from ~500 m to beyond 2-km depth (Figure 4.5; White & Hedenquist, 1995) explaining the observed absence of earthquakes in this zone. Moreover, absence of volcano-tectonic seismic activity is not limited to Mt. Ruapehu. Similar aseismic phenomena are found worldwide (e.g. Galeras Volcano, Columbia (Munoz et al., 1993), and Pavlof Volcano, USA (Neal, 1996)). Therefore, we suggest that the presence of an anomalous shallow ductile zone in volcanic rocks with advanced argillic alteration has immediate relevance to volcanic monitoring worldwide and could offer an explanation for other seemingly anomalous forms of volcano-related seismic activity (e.g. magma rise dominated by long-period earthquakes; Bean et al., 2014).

The variables involved in the alteration of volcanic rock in a hydrothermal system (e.g. temperature (Jakobsson & Moore, 1986), host-rock composition (Hawkins, 1981), host-rock fracture density (Noh & Boles, 1989), pore structure (Mordensky et al., 2018), and fluid composition (Brendt et al., 1988)) make estimating an alteration rate of volcanics exceedingly difficult and there is no existing model that encapsulates these variables. However, numerical modelling by Petcovic and Dufek (2005) suggest that intrusions 10s to 100s of meters wide (such as those at Pinnacle Ridge) would cool over centuries or even decades. Jakobsson and Moore (1986) observed that hydrothermal activity at Surtsey (Iceland) altered primary volcanic compositions to clays over 12 years. Although the varied conditions may not always foster advanced argillic alteration, warm, acidic fluids (e.g. modern Mt. Ruapehu (Christenson, 2000), Galeras Volcano (Fischer et al., 1996)) will produce similar alteration products (e.g. smectitic and kaolinite clays from palagonitization; Henley & Ellis, 1983; Jakobsson & Moore, 1986) and will likely have similar effects on rock deformation behavior as the clays from advanced argillic alteration. Therefore, we conclude that primary volcanic material can alter to materials that have fundamentally different mechanical properties (i.e. brittle or ductile), in as little as 10 years and, under the right chemical and

physical conditions, these newly altered volcanics could inhibit pre-eruptive indicators (i.e. volcano-tectonic seismicity) that may have otherwise been observed.

4.5 Acknowledgments

The authors would like to thank Harry Keys and Blake McDavitt from the New Zealand Department of Conservation for field support. We thank Thierry Reuschlé, Patrick Baud, Alex Kushnir, and Luke Griffiths for assistance and discussion. The authors also thank two anonymous reviewers, whose comments improved the quality of this publication. The authors of this study acknowledge the support of the UC Doctoral Scholarship, UC Mason Trust Fund, Hubert Curien Partnership (PHC) Dumont D'Urville travel grant (number 31950RK), MBIE catalyst grant "Energy straight from magma", and Mercury NZ Limited (formerly Mighty River Power) "Source to Surface" grant. This research was funded by the "Quantifying exposure to specific and multiple volcanic hazards" program of the New Zealand Natural Hazards Research Platform (NHRP). Data in section 3 are available from https://doi.org/10.6084/m9.figshare.7303967.

4.6 References

Adelinet, M., Fortin, J., Schubnel, A., & Guéguen, Y. (2013). Deformation modes in an Icelandic basalt: From brittle failure to localized deformation bands. *Journal of Volcanology and Geothermal Research, 255*, 15-25. doi:10.1016/j.jvolgeores.2013.01.011.

Apuani, T., Corazzato, C., Cancelli, A., & Tibaldi, A. (2005). Stability of a collapsing volcano (Stromboli, Italy): limit equilibrium analysis and numerical modelling. *Journal of Volcanology and Geothermal Research, 144*(1-4), 191-210.

Baud, P., Zhu, W., & Wong, T. F. (2000). Failure mode and weakening effect of water on sandstone. *Journal of Geophysical Research, 105*(B7), 16371-16389.

Bean, C. J., De Barros, L., Lokmer, I., Métaxian, J.-P., O'Brien, G., & Murphy, S. (2014). Long-period seismicity in the shallow volcanic edifice formed from slow-rupture earthquakes. *Nature Geoscience, 7*, 71-75.

Bergmann, J., Friedel, P., & Kleeberg, R. (1998). BGMN—a new fundamental parameters-based Rietveld program for laboratory X-ray sources, its use in quantitative analysis and structure investigations. *CPD Newsletter, 20*(5).

Brace, W. F., Paulding, B., & Scholz, C. (1966). Dilatancy in the fracture of crystalline rocks. *Journal of Geophysical Research, 71*, 3939-3953.

Brendt, M. E., Seyfried, W., & Warren Beck, J. (1988). Hydrothermal Alteration Processes at Midocean Ridges: Experimental and Theoretical Constraints From Ca and Sr Exchange Reactions and Sr Isotopic Ratios. *Journal of Geophysical Research, 93*(B5), 4573-4583.

Bryan, C. J., & Sherburn, S. (1999). Seismicity associated with the 1995–1996 eruptions of Ruapehu volcano, New Zealand: narrative and insights into physical processes. *Journal of Volcanology and Geothermal Research, 90*, 1-18.

Cassidy, M., Manga, M., Cashman, K., & Bachmann, O. (2018). Controls on explosive-effusive volcanic eruption styles. *Nature communications, 9*, 1-16. doi:10.1038/s41467-018-05293-3.

Christenson, B. W. (2000). Geochemistry of fluids associated with the 1995-1996 eruption of Mt. Ruapehu, New Zealand: Signatures and processes in the magmatic-hydrothermal system. *Journal of Volcanology and Geothermal Research, 97*(1-4), 1-30. doi:10.1016/S0377-0273(99)00167-5.

Cole, J. (1990). Structural control and origin of volcanism in the Taupo Volcanic Zone, New Zealand. *Bulletin of Volcanology*, 445-459. doi:10.1007/BF00268925.

Cooke, D. R., Hollings, P., Wilkinson, J. J., & Tosdal, R. M. (2014). Geochemistry of porphyry deposits. In H. D. Holland & K. K. Turekian (Eds.), *Treatise on Geochemistry* (2nd ed., Vol. 13, pp. 357-381). Oxford: Elsevier.

Corbett, G. J., & Leach, T. M. (1998). Southwest Pacific Rim gold–copper systems: structure, alteration and mineralization. *Society of Economic Geologists Special Publication, 6*, 1-240.

Degruyter, W., Bachmann, O., Burgisser, A., & Manga, M. (2012). The effects of outgassing on the transition between effusive and explosive silicic eruptions. *Earth and Planetary Science Letters, 349-350*, 161-170. doi:10.1016/j.epsl.2012.06.056.

Farquharson, J., Baud, P., & Heap, M. J. (2017). Inelastic compaction and permeability evolution in volcanic rock *Solid Earth, 8*(2), 561-581. doi:10.5194/se-2016-166, 2016.

Farquharson, J., Heap, M. J., Baud, P., Reuschlé, T., & Varley, N. R. (2016a). Pore pressure embrittlement in a volcanic edifice. *Bulletin of Volcanology, 78*(1). doi:10.1007/s00445-015-0997-9.

Farquharson, J., Heap, M. J., Varley, N. R., Baud, P., & Reuschlé, T. (2015). Permeability and porosity relationships of edifice-forming andesites: A combined field and laboratory study. *Journal of Volcanology and Geothermal Research, 297*, 52-68. doi:10.1016/j.jvolgeores.2015.03.016.

Farquharson, J. I., Heap, M. J., & Baud, P. (2016b). Strain-induced permeability increase in volcanic rock. *Geophysical Research Letters, 43*(22).

Fischer, T. P., Arehart, G. B., Sturchio, N. C., & Williams, S. N. (1996). The relationship between fumarole gas composition and eruptive activity at Galeras Volcano, Columbia. *Geology, 24*(6), 531-534.

Hackett, W. R. (1985). *Geology and Petrology of Ruapehu Volcano and Related Vents.* (PhD Thesis), Victoria University of Wellington, Wellington, New Zealand.

Hawkins, A. B., & McConnell, B. J. (1992). Sensitivity of sandstone strength and deformability to changes in moisture content. *Quarterly Journal of Engineering Geology and Hydrogeology, 25*(2), 115-130.

Hawkins, D. B. (1981). Kinetics of glass dissolution and zeolite formation under hydrothermal conditions. *Clays and Clay Minerals, 29*, 331-340.

Heap, M. J., Farquharson, J., Baud, P., Lavallée, Y., & Reuschlé, T. (2015a). Fracture and compaction of andesite in a volcanic edifice. *Bulletin of Volcanology, 77*(55). doi:10.1007/s00445-015-0938-7.

Heap, M. J., Kennedy, B., Farquharson, J., Ashworth, J., Gilg, H. A., Scheu, B., et al. (2017a). A multidisciplinary approach to quantify the permeability of a volcanic hydrothermal system (Whakaari/White Island, Taupo Volcanic Zone, New Zealand). *Journal of Volcanology and Geothermal Research, 332*, 88-108.

Heap, M. J., Kennedy, B. M., Pernin, N., Jacquemard, L., Baud, P., Farquharson, J. I., et al. (2015b). Mechanical behaviour and failure modes in the Whakaari (White Island volcano) hydrothermal system, New Zealand. *Journal of Volcanology and Geothermal Research, 295*, 26-42. doi:10.1016/j.jvolgeores.2015.02.012.

Heap, M. J., Violay, M., Wadsworth, F. B., & Vasseur, J. (2017b). From rock to magma and back again: the evolution of temperature and deformation mechanism in conduit margin zones. *Earth and Planetary Science Letters, 463*, 92-100.

Heap, M. J., & Wadsworth, F. B. (2016). Closing an open system: pore pressure changes in permeable edifice rock at high strain rates. *Journal of Volcanology and Geothermal Research, 315*, 40-50.

Henley, R. W., & Ellis, A. J. (1983). Geothermal systems ancient and modern: a geochemical review. *Earth-Science Reviews, 19*, 1-50.

Hoek, E., & Bieniawski, Z. T. (1965). Brittle fracture propagation in rock under compression. *International Journal of Fracture Mechanics, 1*(3), 137-155.

Jakobsson, S. P., & Moore, J. G. (1986). Hydrothermal minerals and alteration rates at Surtsey volcano, Iceland. *Geological Society Of America Bulletin, 97*, 648-659.

Kennedy, L. A., Russell, J. K., & Nelles, E. (2009). Origins of Mount St. Helens cataclasites: Experimental insights. *American Mineralogist, 94*(7), 995-1004. doi:10.2138/am.2009.3129.

Latter, J. H. (1981). Volcanic earthquakes, and their relationship to eruptions at Ruapehu and Ngauruhoe volcanoes. *Journal of Volcanology and Geothermal Research, 9*(4), 293-309. doi:10.1016/0377-0273(81)90041-X.

Loaiza, S., Fortin, J., Schubnel, A., Gueguen, Y., Vinciguerra, S., & Moreira, M. (2012). Mechanical behavior and localized failure modes in a porous basalt from the Azores. *Geophys. Res. Lett., 39*(19), n/a-n/a. doi:10.1029/2012gl053218.

Manconi, R., Walter, T. R., & Amelung, F. (2007). Effects of mechanical layering on volcano deformation. *Geophysical Journal International, 170*, 952-958.

Moon, V., Bradshaw, J., Smith, R., & de Lange, W. (2005). Geotechnical characterization of stratocone crater wall sequences, White Island volcano, New Zealand. *Engineering Geology, 81*, 146-178.

Mordensky, S. P., Villeneuve, M. C., Kennedy, B. M., Heap, M. J., Gravley, D., Farquharson, J. I., & Reuschlé, T. (2018). Physical and mechanical property relationships of a shallow intrusion and volcanic host rock, Pinnacle Ridge, Mt. Ruapehu, New Zealand. *Journal of Volcanology and Geothermal Research, 359*(15), 1-20. doi:10.1016/j.jvolgeores.2018.05.020.

Munoz, F. A., Calvache, M. L., Cortes, G. P., Gomez, D. M., Narvaez, L., Ordonez, M., et al. (1993). Galeras volcano: international workshop and eruption. *EOS (Transactions - American Geophysical Union), 74*(281), 286-287.

Nairn, I. A., Wood, C. P., & Hewson, C. A. Y. (1975). Phreatic eruptions of Ruapehu : April 1975. *New Zealand Journal of Geology and Geophysics, 22*(2), 155-170. doi:10.1080/00288306.1979.10424215.

Nara, Y., Meredith, P. G., Yoneda, T., & Kaneko, K. (2011). Influence of macrofractures and microfractures on permeability and elastic wave velocities in basalt at elevated pressure. *Tectonophysics, 503*(1-2), 52-59. doi:10.1016/j.tecto.2010.09.027.

Neal, T. (1996). Pavlof volcano darkens the Alaskan sky. *Transactions American Geophysical Union, 77*(51), 519-520.

Nguyen, C. T., Gonnermann, H., & Houghton, B. F. (2014). Explosive to effusive transition during the largest eruption of the 20th century (Novarupta 1912, Alaska). *Geology, 42*(8), 703-706.

Noh, J. H., & Boles, J. R. (1989). Diagenetic alteration of perlite in the Guryongpo, Republic of Korea. *Clays and Clay Minerals, 37*, 47-58.

Okumura, S., & Sasaki, O. (2014). Permeability reduction of fractured rhyolite in volcanic conduits and its control on eruption cyclicity. *Geology, 42*, 843-846.

Pérez-Flores, P., Wang, G., Mitchell, T. M., Meredith, P. G., Nara, Y., Sarkar, V., & Cembrano, J. (2017). The effect of offset on fracture permeability of rocks from the Southern Andes Volcanic Zone, Chile. *Journal of Structural Geology, 104*, 142-158.

Petcovic, H. L., & Dufek, J. D. (2005). Modeling magma flow and cooling in dikes: implications for emplacement of Columbia River flood basalts. *Journal of Geophysical Research: Solid Earth, 110*(10), 1-15. doi:10.1029/2004JB003432.

Pola, A., Crosta, G., Fusi, N., Barberini, V., & Norini, G. (2012). Influence of alteration on physical properties of volcanic rocks. *Tectonophysics, 566-567*, 67-86. doi:10.1016/j.tecto.2012.07.017.

Rye, R. O., Bethke, P. M., & Wasserman, M. D. (1991). The stable isotope geochemistry of acid sulfate alteration. *Economic Geology, 87*, 225-262.

Schaefer, L. N., Kendrick, J. E., Oommen, T., Lavallée, Y., & Chigna, G. (2015). Geomechanical rock properties of a basaltic volcano. *Frontiers in Earth Science, 3*(29). doi:10.3389.

Senger, K., Millett, J., Planke, S., Ogata, K., Eide, C. H., Festoy, M., et al. (2017). Effects of igneous intrusions on the petroleum system: a review. *First Break, 35*.

Sherburn, S., Bryan, C. J., Hurst, a. W., Latter, J. H., & Scott, B. J. (1999). Seismicity of Ruapehu volcano, New Zealand, 1971-1996: A review. *Journal of Volcanology and Geothermal Research, 88*(4), 255-278. doi:10.1016/S0377-0273(99)00014-1.

Sigurdsson, H., Houghton, B. F., McNutt, S. R., Rymer, H., Stix, J., & McBirney, A. R. (2000). Encyclopedia of Volcanoes. *Physics Today, 53*(10), 84-85. doi:10.1063/1.1325206.

Siratovich, P. A., Heap, M. J., Villeneuve, M. C., Cole, J., Kennedy, B., Davidson, J. P., & Reuschlé, T. (2016). Mechanical behaviour of the Rotokawa Andesites (New Zealand): insight into permeability evolution and stress-induced behaviour in an actively utilised geothermal reservoir. *Geothermics, 64*, 163-179. doi:10.1016/j.geothermics.2016.05.005.

Siratovich, P. A., Sass, I., Homuth, S., & Bjornsson, A. (2011). Thermal stimulation of geothermal reservoirs and laboratory investigation of thermally induced fractures. *Transactions - Geothermal Resources Council, 35 2*, 1529-1535.

White, N. C., & Hedenquist, J. W. (1995). Epithermal gold deposits. Styles, characteristics and exploration. *SEG Newsletter*(23), 1, 9-13.

White, R., & McCausland, W. (2016). Volcano-tectonic earthquakes: A new tool for estimating intrusive volumes and forecasting eruptions. *Journal of Volcanology and Geothermal Research, 309*, 139-155.

Wilson, C. J. N., Houghton, B. F., McWilliams, M. O., Lanphere, M. A., Weaver, S. D., & Briggs, R. M. (1995). Volcanic and structural evolution of Taupo Volcanic Zone, New Zealand: a review. *Journal of Volcanology and Geothermal Research, 68*(1-3), 1-28. doi:10.1016/0377-0273(95)00006-g.

Wong, T. F., & Baud, P. (2012). The brittle-ductile transition in porous rocks: a review. *Journal of Structural Geology, 44*, 25-53.

Woods, A. W., & Koyaguchi, T. (1994). Transitions between explosive and effusive eruptions of silicic magmas. *Nature, 370*, 641-644.

Wyering, L. D., Villeneuve, M. C., Wallis, I. C., Siratovich, P. A., Kennedy, B. M., & Gravley, D. M. (2015). The development and application of the alteration strength index equation. *Engineering Geology, 199*, 48-61. doi:10.1016/j.enggeo.2015.10.003.

Zhu, W., Baud, P., Vinciguerra, S., & Wong, T.-f. (2011). Micromechanics of brittle faulting and cataclastic flow in Alban Hills tuff. *J. Geophys. Res., 116*(B6). doi:10.1029/2010jb008046.

Zhu, W., Baud, P., Vinciguerra, S., & Wong, T. F. (2016). Micromechanics of brittle faulting and cataclastic flow in Mount Etna basalt. *Journal of Geophysical Research: Solid Earth, 121*(6), 4268-4289.

Zorn, E. U., Rowe, M. C., Cronin, S. J., Ryan, A. G., Kennedy, L. A., & Russell, J. K. (2018). Influence of porosity and groundmass crystallinity on dome rock strength: a case study from Mt. Taranaki, New Zealand. *Bulletin of Volcanology, 80*(35). doi:10.1007/s00445-018-1210-8.

Chapter 5 Preamble

In Chapter 3, I present mechanical and physical property data data from intact lab samples from a glacially dissected, fossil hydrothermal system at Pinnacle Ridge, Mt. Ruapehu, New Zealand. Then, in Chapter 4, I detail the effect varying types of alteration have on the rock properties of andesite. In Chapter 5, I return to addressing the seven geotechnical units at Pinnacle Ridge and discuss these rock masses at an outcrop-scale using data from field observations (rock mass classification, scanline data of discontinuities, *in situ* permeability data, Schmidt hammer data) (Fig. 1).

Chapter 5 has been published in the *Journal of Volcanology and Geothermal Research*. This chapter is presented in its published format:

> Mordensky, S. P., Villeneuve, M. C., Farquharson, J. I., Kennedy, B. M., Heap, M. J., Gravley, D. (2018) Rock mass properties and edifice strength data from Pinnacle Ridge, Mt. Ruapehu, New Zealand. *Journal of Volcanology and Geothermal Research* 367, 42-62. https://doi.org/10.1016/j.jvolgeores.2018.09.012

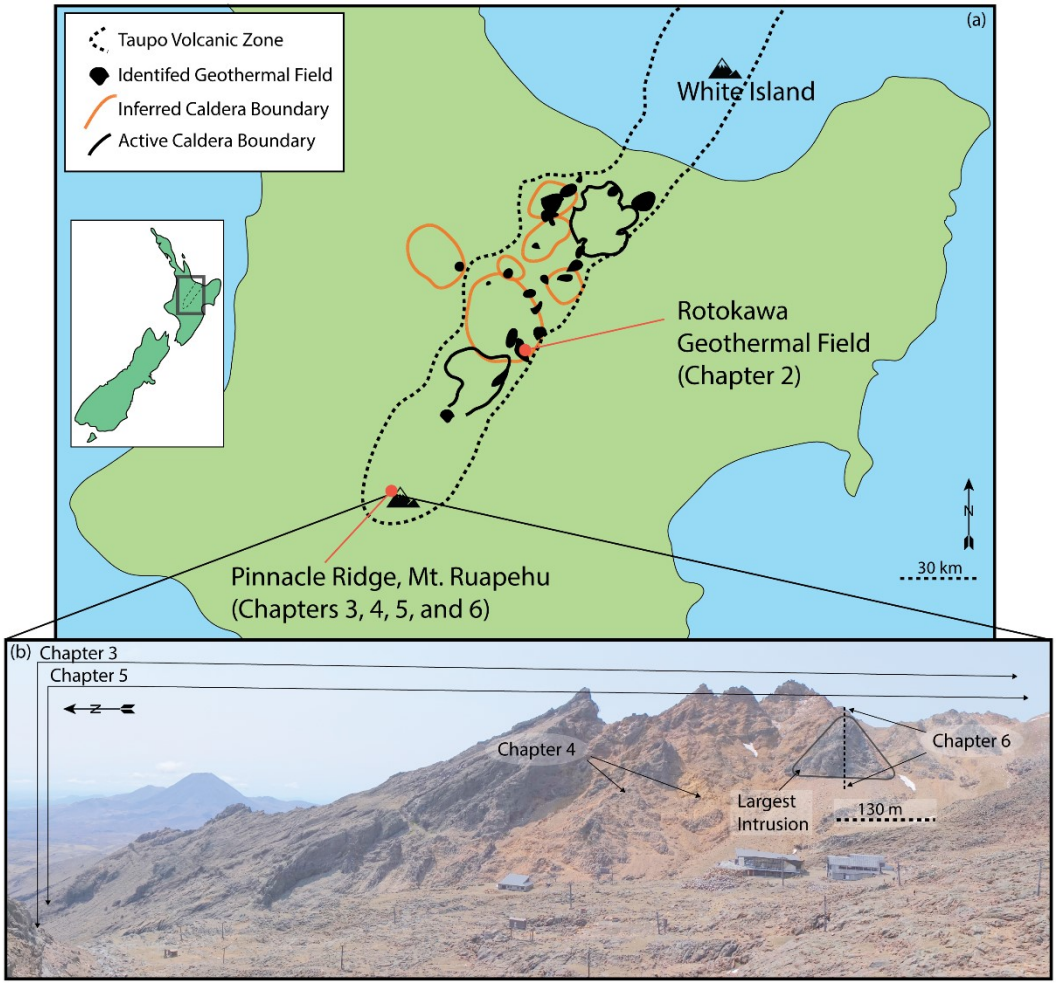

Figure 1. Primary site locations specific to the research presented in this study. (a) Sites of the two hydrothermal systems in New Zealand. (b) Sites specific to Chapters 3 – 6 at Pinnacle Ridge. Solid black polygon marks boundary of the largest young intrusion. Scale is approximate.

Chapter 5

Rock mass properties and edifice strength data from Pinnacle Ridge, Mt. Ruapehu, New Zealand

S. P. Mordensky[1], M. C. Villeneuve[1], J. I. Farquharson[2], B. M. Kennedy[1], M. J. Heap[2], D. M. Gravley[1]

[1]Department of Geological Sciences, University of Canterbury, Private Bag 4800, Christchurch 8140, New Zealand

[2]Institut de Physique de Globe de Strasbourg (UMR 7516 CNRS, Université de Strasbourg/EOST), 5 rue René Descartes, 67084 Strasbourg cedex, France

Abstract

Volcanic edifices exhibit spatially variable physical and mechanical properties. Magmatic intrusions are common at shallow depths within the volcanic edifice and are a poorly-understood contributor to this spatial variability. Intrusion-related alteration has been found to weaken rock mass strength through the development of joints and fractures; however, there is a paucity of research investigating how intrusions affect rock mass strength specific to the geotechnical units that define the rock masses. In this study, we employ a range of field techniques—field permeametry, rock hardness assessment, rock mass classification, and discontinuity mapping—to characterise an exposed fossil geothermal system produced by a shallow intrusion at Pinnacle Ridge, Mt. Ruapehu (New Zealand). We find that intrusions detrimentally affect the rock mass characteristics of altered brecciated lava margins. The resulting change in rock mass strength may be offset by an increase in intact rock strength as a product of alteration mineral precipitation in microfractures. Consequently, the final strength of the rock mass of the altered brecciated lava margins has the potential to be lowest of any of the geotechnical units in the volcanic edifice. We also conclude that these discontinuities increase permeability of the host rock at distances from the intrusion roughly proportional to 1–2 times the thickness of the intrusion itself under near-surface conditions. The data and conclusions presented in this study help to bridge the gap between the lab- and the field-scale and have immediate relevance to engineering geology and geothermal applications worldwide, and to rock mass classification assessments in volcanic environments.

5.1 Introduction

Many studies have raised attention to the hazards presented by volcanoes (e.g. Houghton et al., 1987; McGuire, 1998; Voight, 2000; Lecointre et al., 2004; Thomas et al., 2004a), but understanding these hazards is not straightforward as volcanoes are diverse systems exhibiting heterogeneously composite structures (e.g. McGuire, 1996; Watters et al., 2000; Gudmundsson, 2012, and references therein). In addition to comprising a more-or-less haphazard interlayering of mechanically heterogeneous materials deposited over varying timespans, volcanoes are often also crosscut by intrusive magma bodies. Magmatic intrusion occurs ubiquitously across an array of edifice sizes and shapes (e.g. Mount Kilauea [United States], South Sister [United States], Mt. Ruapehu [New Zealand], Red Crater [New Zealand]). Intrusive events are commonly accepted to be driven by buoyancy disequilibria (Thomson and Schofield, 2008). They occur in both compressional and extensional environments, and the pressure that intrusive magma exerts on its surrounding environment generates compressional and tensile stresses under near-surface conditions (Vigneresse et al., 1999; Galland et al., 2003; Casey et al., 2006; Galland et al., 2009). Magmatic intrusions can exist in several forms: they can be planar (e.g. sills and dikes; Healy et al., 2018), or less geometrically rigid amorphous bodies of magma (Vigneresse et al., 1999; Valentine and Krogh, 2006; Keating et al., 2007).

Given the pervasive nature and occurrence of magmatic intrusions, they exert an influential control on the mechanical and physical characteristics of their volcanic host-rock. There are several parameters that determine edifice behaviour and whether it poses a hazard, including edifice permeability (e.g. Jaupart, 1998; Edmonds et al., 2003; Mueller et al., 2008; Taisne and Juapart, 2008; Gaunt et al., 2014; Okumura and Sasaki, 2014; Farquharson et al., 2015) and discontinuity characteristics (e.g. Schultz, 1995; Watters et al., 2000). Thus, it is necessary to understand how intrusions affect these properties—edifice permeability and discontinuities—in order to model the aggregate hazard presented by an edifice.

Permeability serves as a primary control of outgassing processes in volcanic systems and, therefore, is thought to influence eruptive style (e.g. Jaupart, 1998; Voight and Elsworth, 2000; Edmonds et al., 2003; Taisne and Juapart, 2008; Castro et al., 2014; Farquharson et al., 2017) and explosivity (e.g. Eichelberger et al., 1986; Woods and Koyaguchi, 1994; Edmonds and Herd, 2007; Castro et al., 2014; Okumura and Sasaki, 2014; Chevallier et al., 2017). Consequently, many studies have detailed the permeability of hydrothermally altered material (e.g. Pola et al., 2012; Siratovich et al., 2014; Wyering et al., 2014; Siratovich et al., 2015; Mayer et al., 2016; Heap et al., 2017; Mayer et al., 2017; Mordensky et al., 2018). In general, laboratory-derived permeability data have been obtained on centimetre-scale samples. Accordingly, there are few data that detail the influence of field-scale phenomena on permeability in volcanic environments. Recently,

Mordensky et al. (2018) sought to explore the influence of macro-scale deformation from a shallow igneous intrusion on sample-scale, volcanic rock geomechanical properties (e.g. porosity, permeability, uniaxial compressive strength [UCS]) over edifice-relevant distances (i.e. <10 m to 100 + m). Nevertheless, the issue of upscaling—transferring data from the sample- to the field-scale—still remains: how do the studied volume of rock and the discontinuities contained therein affect permeability? Moreover, how does permeability evolve proximal to an intrusion?

Discontinuities (e.g. joints, fractures, veins, faults, beds) serve as a first-order control in the strength of a rock mass (e.g. Jaeger, 1960; McLamore and Gray, 1967; Schultz, 1995; Watters et al., 2000; Thomas et al., 2004b). Rock blocks move, rotate, and/or crush under stress depending on the number, orientation, and nature of discontinuities (Hoek, 1983). Although Thomas et al. (2004b) observed that volcanic rock mass strength appears independent of magma composition and age, several studies have found hydrothermal alteration weakens rock at the sample-scale (e.g. Watters and Delhaut, 1995; Pola et al., 2012; Frolova et al., 2014; Pola et al., 2014; Wyering et al., 2014; Heap et al., 2015; Wyering et al., 2015; Siratovich et al., 2016). Similarly, hydrothermal alteration of primary volcanic rock is associated with a weaker volcanic edifice (Crowley and Zimbelman, 1997). More specifically, Watters and Delhaut (1995) found that alteration can not only decrease the UCS of rock but also increase the discontinuity density. Similarly, Watters et al. (2000) concluded that discontinuities containing secondary clay or infilling material (i.e. alteration products) contribute to weakening the rock mass of the edifice. Given the prevalence of intrusions in volcanic environments (e.g. Rubin, 1995; Gudmundsson, 2002, Gudmundsson, 2003; Stewart et al., 2003) and the potential for intrusions to alter their host rock (e.g. Henley and Ellis, 1983; Cathles et al., 1997), it is imperative to characterise the discontinuity characteristics surrounding intrusions in order to understand the hazards associated with the intrusions.

To understand how permeability and discontinuity characteristics relate to magmatic intrusions, we spent four field seasons (2015–2018) employing a variety of field methods (e.g. field permeametry, Schmidt hammer analysis, rock mass classification, and discontinuity scanline mapping,) to collect in situ data on a series of outcrops at Pinnacle Ridge (Mount Ruapehu, New Zealand). From the data collected during these field campaigns, we find the following: (1) an intrusion increases permeability in the host rock up to distances 1–2 times the thickness of the intrusion; (2) the rock mass classification values of altered brecciated lava margins are statistically less than that of unaltered brecciated lava margins; (3) although the rock mass classification values for altered intrusions and dense coherent lavas are generally less than that of their counterparts, this difference is not statistically significant; and (4) the lower rock mass

classification values of the altered brecciated lava margin present the potential for the altered brecciated lava margins to be the weakest geotechnical unit in a volcanic edifice.

While doing so, we also complete the geotechnical characterisation of Pinnacle Ridge by describing the macro-discontinuity characteristics of the geotechnical units defined by Mordensky et al. (2018), who characterise lab-scale geomechanical properties. The data collected during this research in conjunction with Mordensky et al. (2018) provide insight for modelling for the effects of shallow intrusion emplacement in a volcanic environment.

5.1.1 Study area

Mt. Ruapehu is an active stratovolcano situated in Tongariro National Park on the North Island of New Zealand (Fig. 5.1a). It is the southernmost expression of the Taupō Volcanic Zone (TVZ). Constructed by four major cone-building episodes (Fig. 5.1b), Mt. Ruapehu is characterise by a range of eruptive styles over the last 240 *ka*, including subplinian, strombolian, phreatomagmatic and vulcanian (Latter, 1986; Houghton et al., 1987; Pardo, 2012; Townsend et al., 2017). It has been postulated that alteration of the cone complex weakened the volcanic edifice and contributed to a substantial flank collapse event ~10 *ka* (Hackett and Houghton, 1989). Slope collapse remains the potentially most destructive force at Mt. Ruapehu given its potential for high velocity and large volume. A modern-day equivalent would be the failure of the summit crater lake wall, which would have catastrophic consequences to the east and southeast, where New Zealand State Highway 1 and high tension electric transmission lines serve as vital infrastructure connecting the northern and southern regions of the island (Hackett and Houghton, 1989). Alteration is prevalent around the crater lake (Hackett, 1985), and the crater lake wall in question is composed of materials of variable strengths and mechanical properties (Cook et al., 2018).

Pinnacle Ridge is located on the north-western flank of Mt. Ruapehu (Fig. 5.1b, c). Although Pinnacle Ridge defines the western boundary of the popularly visited Whakapapa Ski Field, it is several hundred thousand years older than the adjacent lava flows of the Whakapapa formation (Hackett, 1985; Townsend et al., 2017). Consequently, Pinnacle Ridge has also been subject to several intrusive events, which altered the volcanic host rock, before being glacially dissected >10 *ka*, exposing the internal structure of a once shallow subsurface igneous intrusive system (Hackett, 1985). The combination of intrusion-related alteration and glacial carving has created a complex of steep volcanic talus slopes and cliffs with the varying jointing orientations in the host rock and intrusion (Fig. 5.1d, e, f).

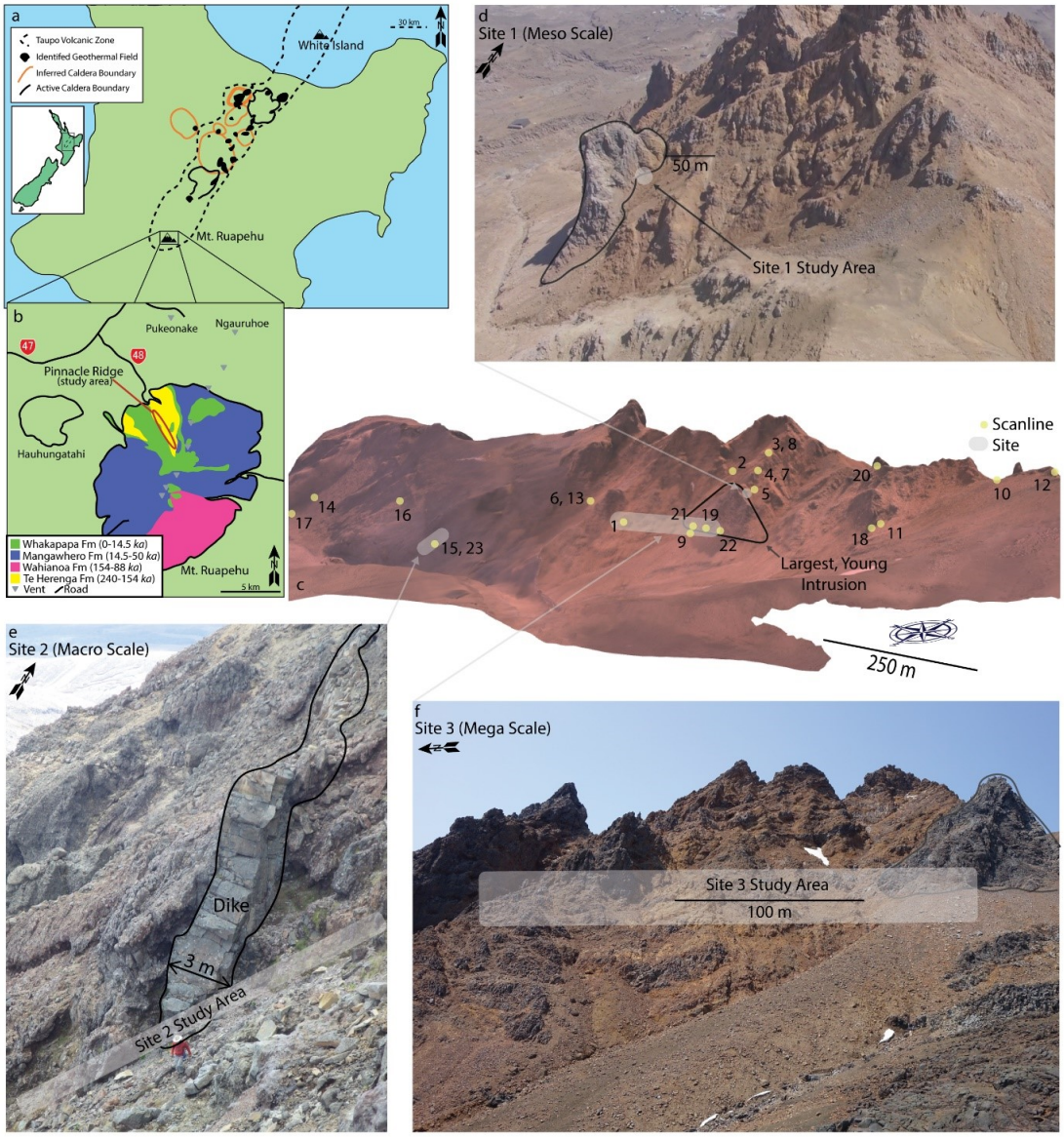

Figure 5.1 Study area on Pinnacle Ridge, Mt. Ruapehu, New Zealand. Scales are approximate. (a) North Island, New Zealand and the active TVZ boundaries (dashed black) with the locations of geothermal fields (black), active caldera boundaries (black outline), and inferred caldera boundaries (red outline). Adapted from Wilson et al. (1995). (b) Simplified depiction of Mt. Ruapehu formations (green, blue, pink, and yellow) as depicted in Hackett (1985). For detailed view of formations, see Townsend et al. (2017). Major roads for reference. Pinnacle Ridge is marked by a hollow, red symbol on the northwestern flank of Mt. Ruapehu. Adapted from Hackett (1985) and Mordensky et al. (2018). Formation ages from Gamble et al. (2003) and Conway et al. (2016). (c) Pinnacle Ridge and locations of TinyPerm and Schmidt hammer analyses (i.e. Site 1, 2, and 3; grey) and scanline transects (yellow) numbered 1–20. The largest, young intrusion is outlined (black) immediately right of centre in frame. (d) Site 1 study area (grey) for meso-scale (<1 m) TinyPerm and Schmidt hammer analyses. The oblique view is to the north-northwest. The largest, young intrusion is outlined (black) left of centre in frame. (e) Site 2 study area (grey) for macro-scale TinyPerm analyses at 1-m intervals. The view is oblique to the north-northwest. (f) Site 3 study area (grey) for mega-scale (10+ m) TinyPerm and Schmidt hammer analyses. The profile view of Pinnacle Ridge is to the east-southeast. The largest, young intrusion is outlined (black) left of centre in frame.

Pinnacle Ridge is composed of the oldest volcanic unit exposed at Mt. Ruapehu, the Te Herenga Formation (240–154 *ka*; Fig. 5.1b; Hackett, 1985; Hackett and Houghton, 1989; Conway et al., 2016). The unaltered Te Herenga lavas (54.9–58.0 wt% SiO_2 and 4.4–5.4 wt% MgO) of Pinnacle Ridge predominantly host clinopyroxene glomerocrysts, orthopyroxene, and plagioclase (Price et al., 2012). Hackett and Houghton (1985) describe Pinnacle Ridge as interlayered lava flows and subplinian welded airfall with original welding textures only observed in weakly welded lenses. The Whakapapa Formation unconformably mantles the Te Herenga Formation to the north, outside the research area of this study (Townsend et al., 2017). Several dikes and stocky intrusions, the largest of which (130 × 64 m) we refer to as the largest, young intrusion (Fig. 5.1c, d, f), are exposed in the dissected region of Pinnacle Ridge. The intrusions at Pinnacle Ridge are chemically similar to the lavas of the Te Herenga formation and are interpreted to be geologically similar in age and origin (Houghton et al., 1987). A 500 m-wide, orange-brown alteration halo surrounding a large intrusion in Pinnacle Ridge is visible from Knoll Ridge Café (New Zealand's highest café at 2020 m). The altered rock contains hydrothermally deposited silica and kaolinite, suggesting shallow alteration depths (Houghton et al., 1987). These observations are reinforced by TerraSpec analysis that revealed advanced argillic alteration consistent with shallow, low-temperature alteration (Mordensky et al., 2018).

5.1.2 Geotechnical units of Pinnacle Ridge

del Potro and Hürlimann (2008) recognised the importance of establishing common nomenclature when discussing the geotechnical and engineering-related aspects of volcanic material, defining geomechanical characterisation that subsequently became standard practice. Mordensky et al. (2018) applied these concepts to Pinnacle Ridge using the geomechanical properties of laboratory samples (20-mm diameter × 40-mm length) and mapped its geotechnical units as: 1) unaltered brecciated lava margin (UBLM); 2) altered brecciated lava margin (ABLM); 3) unaltered dense coherent lava (UDCL); 4) altered dense coherent lava (ADCL); 5) unaltered intrusion (UI); 6) altered intrusion (AI); and 7) hydrothermal vein (HV). In doing so, Mordensky et al. (2018) provided a description of the geotechnical units. Here, we provide a brief summary of the units, but refer the reader to Mordensky et al. (2018) for a more thorough description.

Interlayered UDCL and UBLM constitute the majority rock mass outside the alteration halo. UDCL is observed as grey-dark grey, 1–3 m cliffs and has columnar joints (Conway et al., 2015). In thin-section, UDCL has microfractures that seldom intersect. UBLM forms 1–3 m high, low-angled slopes between the layers of UDCL. UBLM is predominantly matrix supported with sub-angular to angular clasts <1 cm to 10s

of cm across. Vesicles predominate UBLM porosity, but thin-section analysis shows matrix- and phenocryst-hosted microfractures <200 μm in length. Both geotechnical lava units host a porphyritic texture with 100 μm–3 cm plagioclase and clinopyroxene phenocrysts in a plagioclase, pyroxene, glass groundmass.

Inside the alteration halo, ADCL forms 1–3 m cliffs, but have a slight orange-brown discolouration. This discolouration is revealed in thin-section a product of light alteration along discontinuity boundaries from primary igneous minerals (e.g. plagioclase and clinopyroxene) to alteration mineralogy (e.g. kaolinite and smectite). ADCL has matrix-hosted, intersecting microfractures >200 μm in length.

ABLM forms slopes inside the alteration halo and is interbedded with ADCL. The groundmass and phenocryst assemblages of ABLM altered to smectite and kaolinite which give the geotechnical unit its yellow-, orange-, and red-brown colours. These same alteration products precipitated in pore spaces (e.g. microfractures).

UI forms large, grey cliff faces inside and outside the alteration halo at Pinnacle Ridge. UI appear in two varieties: 1) dikes (2–5 m across; Fig. 5.1e) and stocky intrusions (10–130 m across; Fig. 5.1c, d). Both forms bear mineral assemblages similar to UDCL and UBLM and host columnar joints (Hackett, 1985; Conway et al., 2015). In thin-section, UI has isolated, <100-μm microfractures.

AI is found only within the alteration halo with the same primary mineralogy as UI, UDCL, and UBLM. AI appears orange-grey faces as a result of alteration of the primary mineralogy to smectite and kaolinite preferential to free-surface boundaries and clinopyroxene phenocrysts. AI has longer matrix-hosted microfractures (>200+ μm) than UI.

HV appears in 0.5-cm to 1-m vein <50 m around the largest young intrusion at Pinnacle Ridge. Distinctly white from kaolinite precipitation, veins form topographic lows and are often covered by talus. Microfractures have <1-mm apertures and can be >100 s of μm in length.

5.2 Methods

Field permeametry, Schmidt hammer analyses, discontinuity scanline transects, and rock mass classification were predominantly completed along the western exposure of the altered zone of Pinnacle Ridge (Fig. 5.1c) as safety concerns limited access to the east side of the ridge.

5.2.1 Field permeametry

We obtained field permeability measurements using the TinyPerm II and TinyPerm III (by New England Research Inc.) to measure permeability values not captured in the earlier lab-based permeability study (Mordensky et al., 2018). The TinyPerm is a portable air permeameter that is operated by placing its 10-mm nozzle against a rock surface and then creating a vacuum within the nozzle-rock interface. Permeability is calculated as a function of the transient vacuum as described in Brown and Smith (2013). The TinyPerm provided a means of obtaining rapid permeability data in other volcanic studies (e.g. Vignaroli et al., 2014; Farquharson et al., 2015; Schaefer et al., 2015; Heap et al., 2017; Lamur et al., 2017). The TinyPerm III is rated to provide permeabilities as low as 6.92×10^{-16} m^2 and Farquharson et al. (2015) demonstrated that the TinyPerm II can reliably measure volcanic rocks with permeabilities from to 10^{-15} to 10^{-12} m^2. Heap et al. (2017) note that the TinyPerm measuring technique is nominally isotropic even if the rock mass itself is anisotropic, given that the test operates by forcing air through the volume of rock immediately close to the nozzle.

We measured permeability at three scales around Pinnacle Ridge, at varying distances to the main intrusive body to assess the influence of intrusions at the meso- (sub-metre [Site 1]), macro- (1-m [Site 2]), and mega- (10+ m [Site 3]) scales. Sites 1 (Fig. 5.1d) and 3 (Fig. 5.1f) capture permeability values at the meso-scale and mega-scale, respectively, in the altered zone adjacent to the youngest, large intrusion. Site 2 (Fig. 5.1e) captures permeability at macro-scale in unaltered host rock around a dike outside the alteration zone. Given the potential for a falsely high permeability value resulting from a poor seal at the nozzle-rock interface, we collected multiple (n = 5–10) TinyPerm measurements at each site and report the average of the lowest 3 values.

5.2.2 Schmidt hammer analysis

The Schmidt hammer works by releasing a spring-driven piston onto a free surface; the piston rebound is then registered by the hammer and can be read directly by the user. Relatively hard surfaces yield higher rebound values than softer surfaces, and this value has been shown to correlate with the strength of the rock (e.g. Deere and Miller, 1966; del Potro and Hürlimann, 2008; Kilic and Teymen, 2008). A type-L Schmidt hammer was used given its design for weaker (<60 MPa) rocks. During data collection, the Schmidt hammer was held perpendicular to a flat and vertical rock surface so that the Schmidt hammer maintained a horizontal orientation. Following the methods defined by Aydin (2014), we chose areas of outcrop that are representative of the rock mass and free of surface debris for Schmidt hammer rebound measurements.

Single impacts were separated by a minimum of the plunger diameter. We followed the methods of previous geological studies using Schmidt hammers and averaged the highest 10 rebound values from the 50+ rebound values from each test surface (e.g. Torabi et al., 2010).

5.2.3 Discontinuity data collection

We employed two discontinuity collection techniques: rock mass classification and discontinuity scanline mapping of the rock masses of Pinnacle Ridge:

5.2.3.1. Geotechnical characterisation and rock mass classification

Mordensky et al. (2018) parametrized the characteristics of the geotechnical units at Pinnacle Ridge on a sample scale (20-mm diameter × 40-mm length); however, the characterisation for these units stood incomplete as the lab-based study did not detail the discontinuity data required for complete geotechnical classification. We complete the geotechnical characterisation by observing macro-discontinuity characteristics using two rock mass classification methods, the Geological Strength Index (GSI; Marinos and Hoek, 2000; Hoek et al., 2013) and the Rock Mass Rating (RMR; Bieniawski, 1989). We augment our scanline data with rock mass classification data because the terrain hazards of Pinnacle Ridge precluded scanline mapping over the majority of the region. Rock mass classification serves as a first-order method to assess and consider rock mass strength at an outcrop scale. The RMR method considers intact rock strength in conjunction with discontinuity spacing, condition, groundwater, length, aperture, texture, weathering, and infill to assess rock mass strength. The GSI method considers discontinuity structure and surface conditions. These geotechnical techniques have been used in hundreds of excavation, mining, and engineering applications and have also been used in studies of volcanic edifices assessing rock mass strength (e.g. Schultz, 1995; Watters et al., 2000; Okubo, 2004; Apuani et al., 2005; Moon et al., 2005; González de Vallejo and Ferrer, 2006; del Potro and Hürlimann, 2008).

We then conduct a simple two-tailed Student's *t*-test to compare the rock mass classification values of the unaltered and altered geotechnical unit pairs (see Nikulin, 1994). We test the null hypothesis that the mean rock mass classification value of the unaltered rock mass is equal to that of the altered rock mass (Eq. (1)).

$$\bar{x}_a = \bar{x}_u \quad (1)$$

In which $\bar{x}_a$ is the GSI or RMR mean from the outcrops of an altered geotechnical unit, and $\bar{x}_u$ is the GSI or RMR from the outcrops of the respective, unaltered geotechnical unit.

We test the null hypothesis by computing the *t – statistic* (Eq. (2)), which is then compared to the t-value $t_{\frac{\alpha}{2},df}$ at from a Student's t distribution table for which α is the chosen significance level ($\alpha = 0.05$ in this study).

$$t - statistic = \frac{\bar{x}_a - \bar{x}_u}{SE} \tag{2}$$

In which *SE* is the sample standard error and is given by Eq. (3), and *df* is degrees of freedom and is given by Eq. (4).

$$SE_{\bar{x}_a - \bar{x}_u} = \sqrt{\frac{s_a^2}{n_a} + \frac{s_u^2}{n_u}} \tag{3}$$

$$df = \left(\frac{s_a^2}{n_a} + \frac{s_u^2}{n_u}\right)^2 \left(\frac{[s_a^2/n_a]^2}{n_a - 1} + \frac{[s_u^2/n_u]^2}{n_u - 1}\right)^{-1} \tag{4}$$

In which s_a and n_a are the sample standard deviation and sample size, respectively, of the data from the altered geotechnical unit, s_u and n_u are the sample standard deviation and sample size, respectively, of the data from the respective, unaltered geotechnical unit.

If the $|t - statistic| > t_{\frac{\alpha}{2},df}$ at $\alpha = 0.05$ and $t - statistic < 0$, we reject the null hypothesis in favour of the alternative hypothesis (Eq. (5))

$$\bar{x}_a < \bar{x}_u \tag{5}$$

We then provide the 95% confidence interval ($CI_{0.95}$), the interval that has a 95% probability to contain the true mean difference, provided by Eq. (6).

$$CI_{.95} = (\bar{x}_a - \bar{x}_u) \pm t_{\frac{0.05}{2},df} \times SE \tag{6}$$

5.2.3.2. Scanline discontinuity mapping

We conducted limited scanline discontinuity mapping to record detailed discontinuity characteristics, discontinuity type, dip direction, dip, frequency, endpoint visibility, number of visible endpoints, termination type, strike, aperture, rock type, trace length, exposure area, texture, infill, staining, and seepage consistent with other geomechanical studies of igneous systems (e.g. Moon et al., 2005; Garden et

al., 2017) as presented in Manda and Mabee (2010) to assess discontinuity characteristics along accessible regions of the ridge. We did not record discontinuities <10 cm long.

Areas along Pinnacle Ridge were chosen for scanline mapping as a function of level of representation of geotechnical units and accessibility to the site. The 23 scanlines (Fig. 5.1c) were completed in pairs (i.e. 46 scanlines total) perpendicular to each other in order to capture discontinuity characteristics representative of the rock mass and to minimise directionality bias. The RocScience Dips software was used to plot the data for stereonet presentation (Figs. 5.S1–5.S5).

5.3 Results

5.3.1 TinyPerm & Schmidt hammer analysis

The TinyPerm analyses were conducted at three sites around the largest young intrusion to capture data at three scales (*meso* [Fig. 5.2], macro [Fig. 5.3], and mega [Fig. 5.4]). On the meso- (i.e. within 1 m of the contact at 50-cm intervals between the largest intrusion and the host rock) and mega-scale (i.e. across the western face of Pinnacle Ridge at intervals spanning 10s of metres up to 237 m from the intrusion), Schmidt hammer rebound values were collected in conjunction with the TinyPerm measurements. At macro-scale (i.e. several hundred metres away from the largest young intrusion) TinyPerm measurements were collected at 1-m intervals around a 3 m-wide dike.

5.3.2 Meso-scale (Site 1)

Site 1 is located along the eastern contact between the intrusion and the host rock, ABLM (Fig. 5.1c, d), where we made measurements at 1, 0.5, and < 0.05 m from the intrusion-host rock contact (Fig. 5.2). The ABLM permeability data (3.53×10^{-14}, 2.10×10^{-13}, 1.27×10^{-13} m^2 at 1, 0.5, and <0.05 m, respectively, from the intrusion-host rock contact) show an increase toward the intrusion while Schmidt hammer rebound values (22, 18, and 11, respectively) show a decrease (Fig. 5.2). The intrusion permeability data (6.78×10^{-16}, 8.63×10^{-16}, and 4.93×10^{-16} m^2, respectively) and Schmidt hammer rebound values (37, 32, and 41, respectively) show variability as the contact is approached.

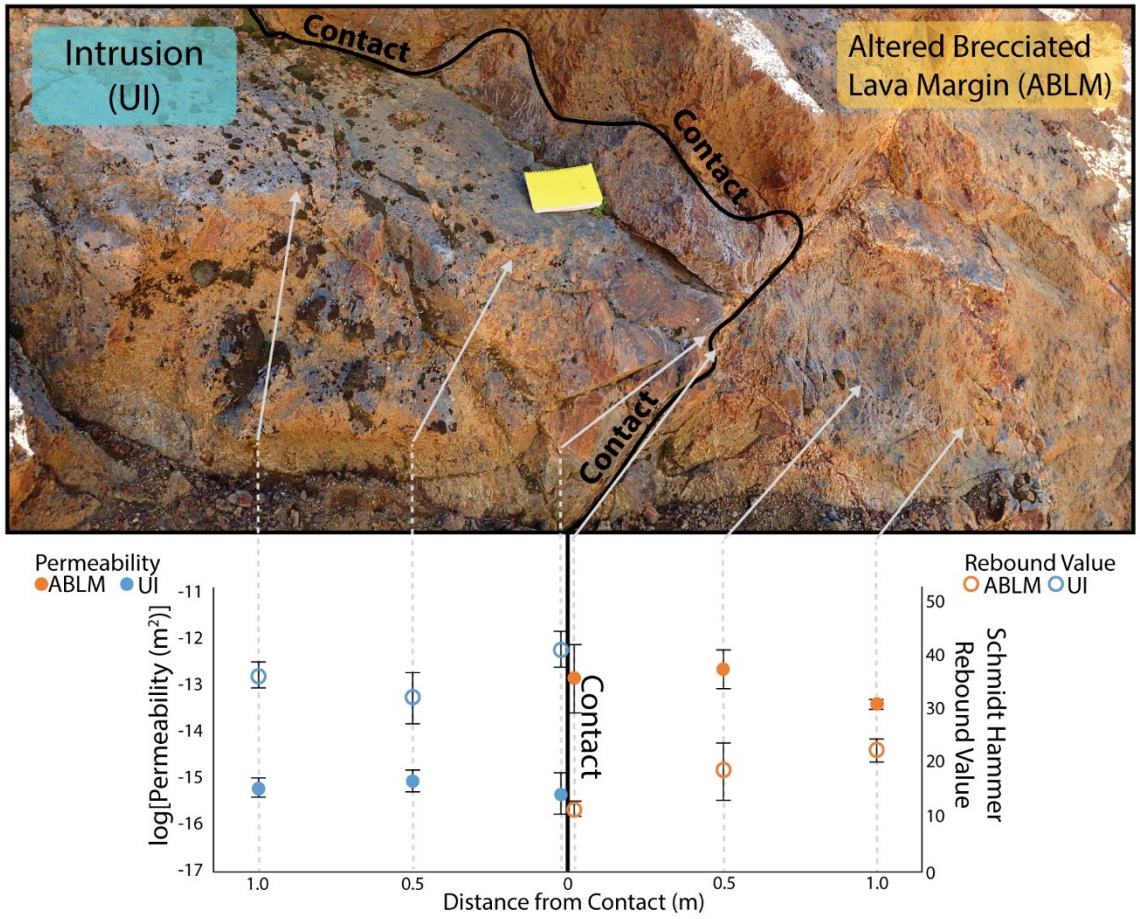

Figure 5.2 Site 1 TinyPerm (circle) and Schmidt hammer (square) measurements of ABLM (right, red) and UI (left, blue) at 1.0, 0.5, and <0.05 m from the host rock-intrusion contact (black line) east of the largest, young intrusion. TinyPerm values are averaged from lowest 3 values of several collected. Schmidt hammer values are averaged from the highest 10 values of 50+ values collected. Error bars on Schmidt hammer represent one standard deviation. Error bars on permeability data represent relative error. Measurements were taken on similarly weathered surfaces. Rite-In-The-Rain notebook (17 × 15 cm) for scale. The solid black line depicts the contact between the ABLM host rock (right) and the intrusion (left).

5.3.3 Macro-scale (Site 2)

The second site of permeability measurements centre around a 3 m-wide dike located 555 m from the largest young intrusion (Figs. 5.1c, e and 5.3). We chose this site to make measurements at 1-m intervals because of its continuous, accessible exposure of the same lithology for 10 m on either side of the dike. Permeability of the host rock vary by several orders of magnitude (10^{-16}–10^{-12} m²) while the permeability of the dike span a smaller range (10^{-15}–10^{-12} m²; Fig. 5.3). The highest host-rock permeability (1.98×10^{-12} m²) is found near (<3 m) the dike. The lowest host-rock permeability (6.67×10^{-16} m²) is found farthest from the dike (13 m).

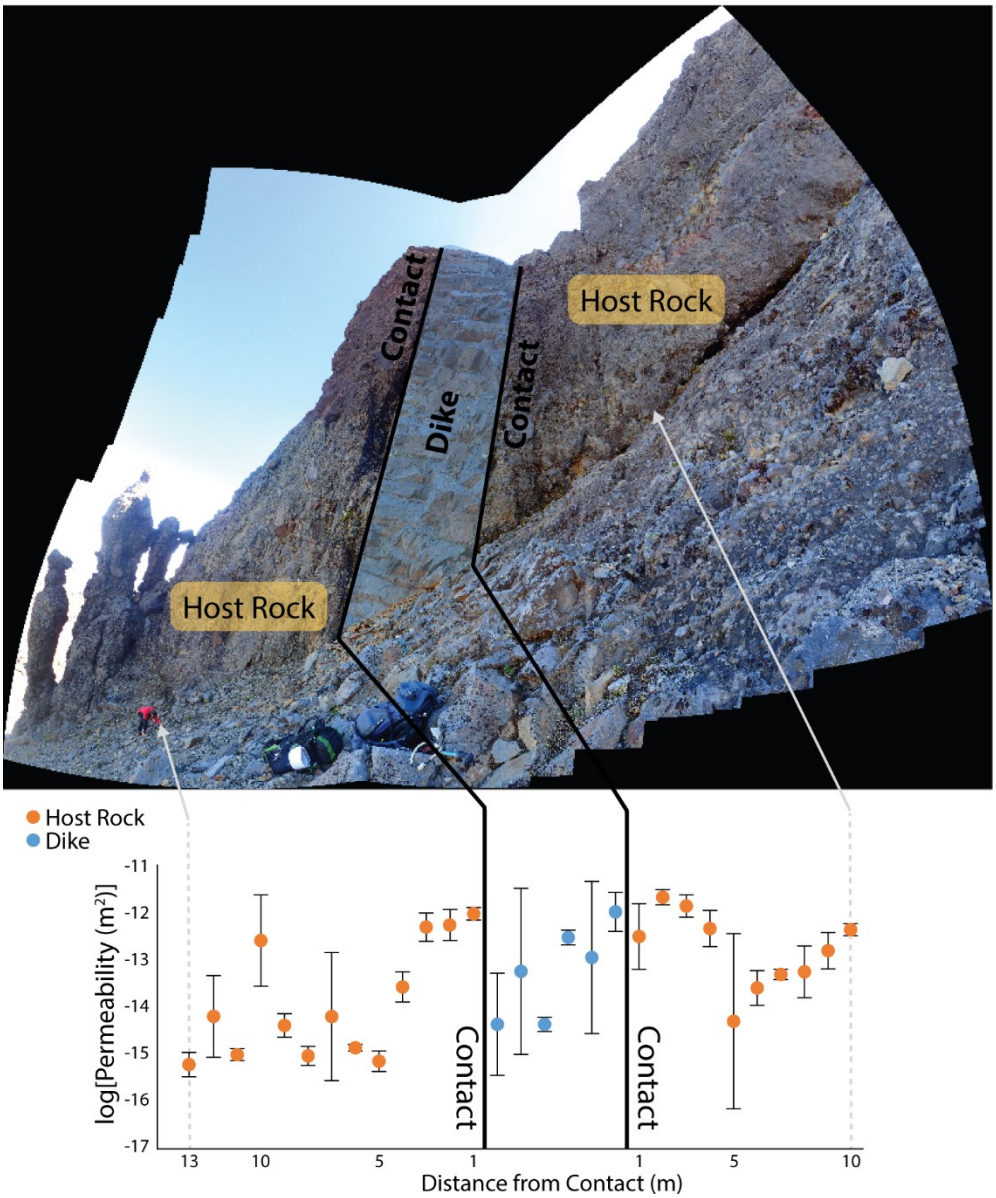

Figure 5.3 Site 2 TinyPerm measurements along dike exposure outside the alteration halo of Pinnacle Ridge, Mt. Ruapehu on host rock (red) and dike (blue) lithologies at 1-m intervals from dike-host rock contact. Although the dike is 3 m-across, there are 5 m of dike data because the effect of the dip of the dike coupled with slope. TinyPerm values are averaged from lowest 3 values of several collected. Error bars represent relative error. Measurements were taken on similarly weathered surfaces. The solid black lines depict the contact between the dike and host rock. Jamie Farquharson (bottom-left) for scale.

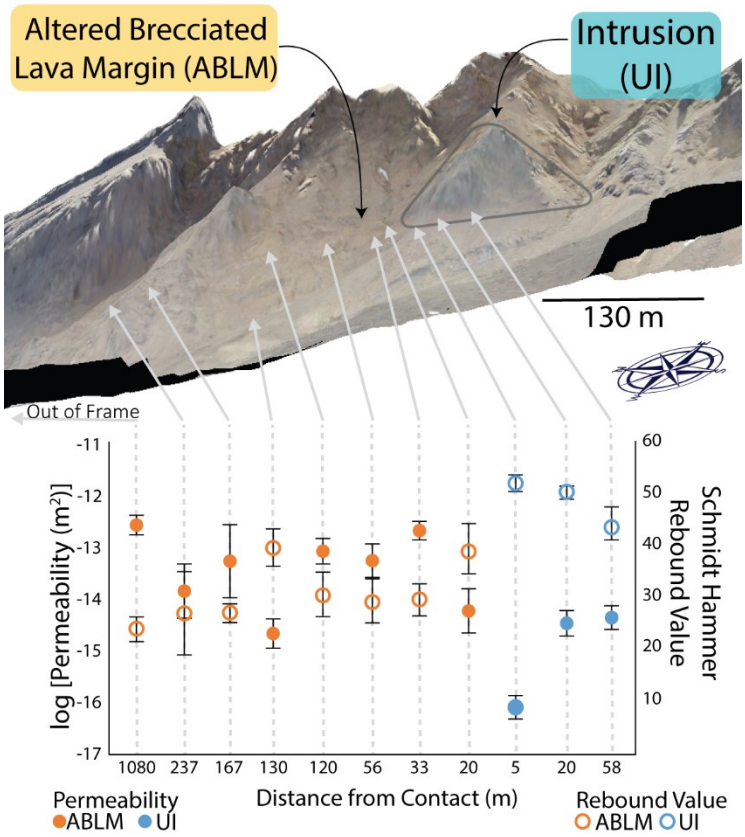

Figure 5.4 Site 3 TinyPerm (circle) and Schmidt hammer sample (square) measurements along West Face of Pinnacle Ridge, Mt. Ruapehu in the brecciated lava margins (left, red) and unaltered intrusion (right, blue) at 1080, 237, 167, 130, 120, 56, 33, 20, 5, 20, and 58 m from host rock-intrusion contact (left to right, respectively). TinyPerm values are averaged from lowest 3 values of several collected. Schmidt hammer values are averaged from the highest 10 values of 50+ values collected. Error bars for Schmidt hammer rebound values provide one standard deviation. Error bars for permeability represent relative error. Measurements were taken on similarly weathered surfaces. Triangular polygon represents approximate location of the unaltered intrusion from the western perspective.

5.3.4 Mega-scale (Site 3)

At Site 3, we collected permeability data from the host rock (ABLM) and the largest intrusion (UI; Figs. 5.1c, f, 5.4). We chose this site for the ability to measure permeability at sites of similar lithology 10s of metres apart at varying distances from the largest young intrusion. We collected permeability data in the host rock from 1080 m to 20 m from the host rock-intrusion contact. ABLM permeability (2.34×10^{-15}–2.99×10^{-13} m^2) does not vary systematically with distance to the intrusion. As permeability increases or decreases from one location to the next, Schmidt hammer rebound values (23.7–39.6) inversely decrease or increase. Within the intrusion, we measured the permeability of the largest intrusion at 5, 20, and 50 m from the contact. In the intrusion, permeability is lower (9.03×10^{-17} m^2) closer (5 m) to the intrusion-host rock

contact and higher toward the centre of the intrusion (3.77×10^{-15} m^2 at 20 m) while Schmidt hammer rebound values decrease from 53.0 to 45.2 toward the centre of the intrusion (Fig. 5.3).

5.3.5 Rock mass classification

In engineering geology, it is common practice to assess rock mass characteristics by GSI and RMR classification. GSI and RMR data are collected by assessing rock mass characteristics (e.g. discontinuity length, discontinuity surface conditions; see Methods) and assigning values specific to these attributes using standardised tables (see Tables 5.S3 and 5.S4, respectively, for the GSI and RMR tables used in this study). These values are then summed to provide a final rock mass classification value representative of the rock (see Bieniawski, 1989; Hoek et al., 2013). Higher values are indicative of stronger rock masses, while lower values are indicative of weaker rock masses.

We classify the rock mass according to GSI and RMR over varying geotechnical units from 42 locations around Pinnacle Ridge. Table 5.1 summarises the rock mass classification data by geotechnical unit. Fig. 5.5 shows that the geotechnical units maintain their relative relationships from RMR to GSI (Table 5.2).

Geotechnical Unit	*n*	GSI Average	GSI Standard Deviation	GSI Min	GSI Max	RMR Average	RMR Standard Deviation	RMR Min	RMR Max
UBLM	3	78	2	76	80	75	1	74	76
ABLM	10	53	12	35	70	53	8	41	66
UDCL	3	75	13	65	90	78	11	66	86
ADCL	12	56	16	30	75	59	14	41	81
UI	7	49	19	20	70	67	18	40	87
AI	6	48	10	37	60	62	9	50	72
HV	1	46		46	46	47		47	47

Table 5.1 GSI and RMR values averaged by each geotechnical unit collected from locations on Pinnacle Ridge. *n* is sample count. The GSI and the RMR values were collected from 42 locations of altered and unaltered rock masses and are presented in Fig. 5.5.

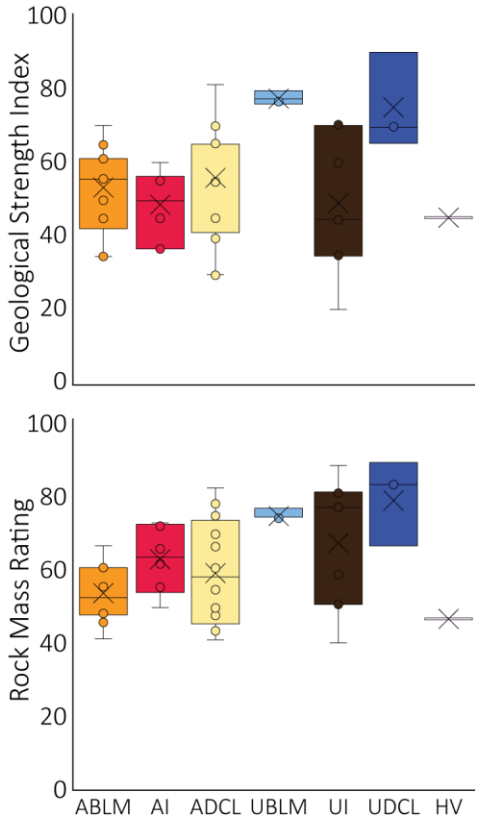

Figure 5.5 GSI and RMR values with geotechnical unit classification collected from locations on Pinnacle Ridge. The GSI and RMR values were collected from 42 locations of altered and unaltered rock mass. The GSI of the unaltered brecciated lava margin is disproportionally higher than its corresponding RMR rating when compared to the other units because of its low discontinuity density in the unaltered brecciated lava margin, contributing to a high GSI, and low UCS, contributing to a low RMR.

UDCL and UBLM have the highest GSI values (65–90 and 76–80, respectively), and the GSI values of their altered components (ADCL and ABLM) are lower (30–75 and 35–70, respectively). AI and HV have an intermediary GSI range (37–60 and 46, respectively), and UI has the lowest GSI with the greatest variation (20–70). The RMR values follow trends similar those of the GSI values between the altered and unaltered lithologies (Fig. 5.5). RMR values for UDCL and UBLM (66–86 and 74–76, respectively) are higher than those for ADCL, ABLM, and HV (41–81 and 41–66, and 47 respectively); however, the RMR values for UI (40–87) are generally higher than those for AI (50–72).

RMC ID	Structure	Surface Quality	GSI	RMR Total	Geotechnical Unit	Distance to Intrusion Contact (m)
39	Very Blocky	Fair	45	49	ABLM	20
32	Blocky/Very Blocky	Good/Fair	60	60	ABLM	25
38	Blocky	Rough	65	60	ABLM	33
10	Very Blocky	Highly Weathered	35	48	ABLM	52
31	Blocky	Fair	55	48	ABLM	74
1	Blocky	Good	70	66	ABLM	120
37	Very Blocky	Good/Fair	50	46	ABLM	130
3	Very Blocky	Good/Fair	55	60	ABLM	132
27	Very Blocky	Poor	35	41	ABLM	167
36	Blocky/Very Blocky	Good/Fair	55	54	ABLM	237
9	Blocky	Poor	45	49	ADCL	8
33	Blocky/Very Blocky	Good	70	77	ADCL	25
11	Blocky	Good	65	74	ADCL	48
19	Blocky/Seamy	Poor	30	41	ADCL	66
22	Blocky	Rough	65	43	ADCL	70
30	Blocky	Good	75	81	ADCL	74
2	Blocky	Good	65	60	ADCL	110
26	Blocky	Fair	55	54	ADCL	170
4	Blocky	Good	65	69	ADCL	172
23	Blocky	Rough	65	65	ADCL	237
20	Blocky/Very Blocky	Poor	40	47	ADCL	250
24	Blocky/Seamy	Poor	30	44	ADCL	252
5	Blocky	Poor	45	61	AI	5
17	Blocky/Seamy	Fair	37	54	AI	49
15	Blocky	Fair	55	65	AI	202
14	Blocky/Seamy	Fair	37	71	AI	322
13	Very Blocky to Seamy	Good	55	50	AI	359
12	Blocky/Very Blocky	Good	60	72	AI	427
40	Blocky/Very Blocky	Fair/Poor	46	47	HV	50
35	Intact	Good/Fair	80	74	UBLM	555
41	Intact	Good/Very Good	76	76	UBLM	841
28	Massive/Blocky	Very Good/Good	77	74	UBLM	1080
25	Blocky	Rough	65	66	UDCL	254
29	Massive	Very Good	90	83	UDCL	755
42	Very Blocky	Good	70	86	UDCL	1080

6	Very Blocky	Fair	45	80	UI	5
7	Very Blocky	Good	60	76	UI	20
8	Blocky	Good	45	77	UI	58
18	Disintegrated	Poor	20	40	UI	63
16	Blocky/Seamy	Fair	35	50	UI	212
21	Blocky	Good	70	58	UI	262
34	Blocky	Good	70	87	UI	555

Table 5.2 GSI and RMR values for geotechnical unit at Pinnacle Ridge. Structure records field observations for the vertical axis from Table 5: Characterisation of blocky rock masses on the basis of interlocking joint conditions from Hoek et al. (2013). Surface quality records field observation for the horizontal axis from Table 5: Characterisation of blocky rock masses on the basis of interlocking joint conditions from Hoek et al. (2013). Because GSI assessment provides a range rather than a point value (Marinos and Hoek, 2000; Hoek et al., 2013), GSI values given provide the centre value for a ± 5 range. RMR Total records the sum of the complete RMR parameterisation by site with individual parameter values provided in Table 5.S2. GSI table from Hoek et al. (2013) provided in Table 5.S3. RMR table from Bieniawski (1989) provided in Table 5.S4. Data collected for 42 sites on Pinnacle Ridge.

We conducted a statistical analysis (two-tailed Student's *t*-test for independent populations) on each unaltered-altered geotechnical unit pair using the null hypotheses $\bar{x}_{UBLM} = \bar{x}_{ABLM}$, $\bar{x}_{UDCL} = \bar{x}_{ADCL}$, and $\bar{x}_{UI} = \bar{x}_{AI}$, in which $\bar{x}$ is the mean GSI or RMR value for the geotechnical unit (Table 5.3). We find:

1) Among the outcrops of brecciated lava margins recorded for GSI ($n = 13$), there was a statistically significant difference between the unaltered and altered brecciated lava margins, UBLM ($\bar{x} = 77.67$, SD = 2.08) and ABLM ($\bar{x} = 52.5$, SD = 11.61), $|t(10)| > 4.587$, $t(10) < 0$, $CI_{0.95}$–33.77 to −16.56. Therefore, we reject the null hypothesis that there is no significant difference in GSI values between UBLM and ABLM in favour of the alternative hypothesis that $\bar{x}_{ABLM}^{GSI} < \bar{x}_{UBLM}^{GSI}$.
2) Among of the brecciated lava margins recorded for RMR ($n = 13$), there was a statistically significant difference between the unaltered and altered brecciated lava margins, UBLM ($\bar{x} = 74.67$, SD = 1.15) and ABLM ($\bar{x} = 53.20$, SD = 8.00), $|t(10)| > 4.587$, $t(10) < 0$, $CI_{0.95}$–27.29 to −15.64. Therefore, we reject the null hypothesis that there is no significant difference in RMR values between UBLM and ABLM in favour of the alternative hypothesis that $\bar{x}_{ABLM}^{RMR} < \bar{x}_{UBLM}^{RMR}$.
3) At $\alpha = 0.05$, we fail to reject the null hypotheses ($\bar{x}_{ADCL}^{GSI} = \bar{x}_{UDCL}^{GSI}$, $\bar{x}_{ADCL}^{RMR} = \bar{x}_{UDCL}^{RMR}$) for the dense coherent lavas.
4) At $\alpha = 0.05$, we fail to reject the null hypotheses ($\bar{x}_{AI}^{GSI} = \bar{x}_{UI}^{GSI}$, $\bar{x}_{AI}^{RMR} = \bar{x}_{UI}^{RMR}$) for the intrusions.

GSI	*df*	*SE*	$\bar{x}_a - \bar{x}_u$	t-statistic	$t_{\alpha/2, df}$	$CI_{.95}$
Brecciated Lava Margins	10.49	3.86	-25.17	-6.516	2.228	-33.77 – -16.56
Dense Coherent Lavas	3.56	8.87	-19.17	-2.160	3.182	-47.40 – 9.07
Intrusions	9.41	8.11	-1.12	-0.138	2.262	-19.46 – 17.22

RMR	*df*	*SE*	$\bar{x}_a - \bar{x}_u$	t-statistic	$t_{\alpha/2, df}$	$CI_{.95}$
Brecciated Lava Margins	10.08	2.62	-21.47	-8.208	2.228	-27.29 – -15.64
Dense Coherent Lavas	4.00	7.47	-19.67	-2.634	2.776	-40.40 – 1.06
Intrusions	9.17	7.57	-4.69	-0.620	2.262	-21.82 – 12.43

Table 5.3 Statistical summary of unaltered-altered geotechnical unit pairs for two-tailed Student *t*-test. *df* is degrees of freedom. *s* is sample standard error. ¯ is the difference in sample means. $CI_{0.95}$ is the 95% confidence interval.

We highlight that the Student's *t*-test rests upon a number of assumptions, including normal distribution of data, an adequately large sample size, and homogeneity of variance. We acknowledge that for some of the geotechnical units the sample size (upon which the other assumptions rely) is smaller than ideal. While the fact that these analyses yield results that are significant according to the imposed confidence interval suggests that the difference is real and not merely an artefact of our sampling, larger sample sizes would be desirable in future research.

5.3.6 Scanline mapping

We group scanline transects by their geotechnical units:

1) ABLM (transects 1, 2, 3, 4);

2) UBLM (transect 15, 16, 17);

3) ADCL (transects 5, 6, 7, 8);

4) UDCL (transect 13, 14);

5) AI (transects 9, 10, 11, 12); and

6) UI (transects 18, 19, 20, 21, 22, 23).

Scanline lengths vary from <2 m to >40 m depending on ground conditions and discontinuity density totalling over 190 m of scanline transect with 927 discontinuities characterise (Table 5.4). Joints constitute the majority (>99%) of the discontinuities at Pinnacle Ridge. Given the compounded complexity from local and regional stresses at Mt. Ruapehu, we focus on describing discontinuity densities and dimensions in this section of the text and Table 5.2 and reserve orientation details for the supplementary material (Figs. 5.S1–5.S5).

Scanline ID	Geotechnical Unit	Average Discontinuity Density (#/m)	Scanline Length (m)	Discontinuity Count	Average Spacing Between Discontinuities (m)	Average Aperture (mm)	Average Discontinuity Length (m)	Average Fracture Area (m^2)	Interest Area (m^2)	Distance to Intrusion Contact (m)
4	ABLM	10.42	1.92	20	0.0960	1.04	0.78	0.00081	0.92	25
2	ABLM	8.82	1.70	15	0.1133	1.35	0.24	0.00033	0.38	52
3	ABLM	12.97	5.01	65	0.0771	0.82	0.27	0.00022	5.08	73
1	ABLM	7.08	5.37	38	0.1413	1.25	1.82	0.00227	5.40	120
5	ADCL	17.97	3.06	55	0.0556	1.11	1.29	0.00143	9.07	8
7	ADCL	6.30	2.70	17	0.1588	1.30	0.56	0.00073	1.80	25
8	ADCL	7.87	5.21	41	0.1271	1.77	1.12	0.00198	6.61	73
6	ADCL	4.35	8.73	38	0.2297	4.34	1.67	0.00724	76.21	252
9	AI	4.67	10.50	49	0.2143	1.55	0.74	0.00115	27.34	20
11	AI	13.23	2.57	34	0.0756	1.66	0.77	0.00127	1.46	212
10	AI	10.56	5.02	53	0.0947	1.18	1.21	0.00143	6.25	359
12	AI	28.77	2.12	61	0.0348	0.90	1.32	0.00119	0.47	427
15	UBLM	0.91	24.26	22	1.1027	3.98	4.59	0.01827	588.55	555
16	UBLM	1.86	15.56	29	0.5366	2.48	2.97	0.00737	74.51	841
17	UBLM	0.43	44.2	19	2.3263	1.00	8.48	0.00848	555.00	1080
13	UDCL	5.59	8.77	49	0.1790	3.34	1.38	0.00459	16.04	254
14	UDCL	6.23	8.83	55	0.1605	1.00	1.74	0.00174	18.83	1080
21	UI	12.50	6.08	76	0.0800	1.07	1.51	0.00162	6.62	5
19	UI	10.21	3.33	34	0.0979	0.88	0.69	0.00060	2.42	20
22	UI	16.34	3.06	50	0.0612	0.32	6.70	0.00214	2.07	58
18	UI	7.74	4.39	34	0.1291	0.65	0.62	0.00040	4.71	202
20	UI	5.86	3.07	18	0.1706	1.22	0.47	0.00057	2.36	273
23	UI	4.30	7.67	33	0.2324	1.08	2.17	0.00234	14.54	555

Table 5.4 Scanline transect data for 23 scanline sets collected from 6 geotechnical units on Pinnacle Ridge.

5.3.6.1 Dense coherent lavas

Dense coherent lava constitutes a major component (>45% volumetrically) of the geotechnical units at Pinnacle Ridge. Discontinuity densities of UDCL (5.59–6.23 discontinuities/m; Table 5.4) are similar to those of ADCL (2.70–10.50 discontinuities/m). The average discontinuity apertures of the UDCL (1.00–3.34 mm) are slightly lower than those of ADCL (1.11–4.34 mm). The average discontinuity lengths of UDCL (1.38–1.74 m) are slightly more than those of the ADCL (0.56–1.67 m). The discontinuity surfaces of UDCL are predominantly very rough, while those of ADCL are rough to very rough. The discontinuities are free of soils; however, debris infill composed of erosional volcanic material (<2 cm in length) is present in some of the discontinuities of UDCL and is common in the ADCL. The predominant joint orientation (~090°–115°) and high dip angle (>75°) are consistent between UDCL and ADCL (Figs. 5.S1, 5.S2), although the UDCL contains less variation in orientation than ADCL.

5.3.6.2 Brecciated lava margins

Brecciated lava margins are the other major geotechnical unit (>45% volumetrically) found along Pinnacle Ridge. The discontinuity densities of UBLM (0.43–1.86 discontinuities/m; Table 5.4) are lower than those of ABLM (7.08–12.97 discontinuities/m). The average discontinuity lengths of UBLM (2.48–8.48 m) are greater than those of ABLM (0.24–1.82 m). Unlike with the other geotechnical units, the unaltered component of the brecciated lava margins appears to average wider discontinuity apertures (1.00–3.98 mm) than the corresponding altered rock mass (0.82–1.35 mm). The discontinuity surfaces of ABLM appear smoother than UBLM. That is, UBLM exhibits surface conditions varying from slightly rough to rough, while those of ABLM range from smooth to slightly rough. Although no soil development is observed, some joints are filled with eroded lava fragments (<2 cm length). Altered and unaltered breccias express the near-vertical jointing striking ~340°–345°, similar to UDCL and ADCL to north of the intrusion (Figs. 5.S1, 5.S2, 5.S3).

5.3.6.3 Intrusions

Intrusions host the smallest average discontinuity apertures of the geotechnical units studied. UI hosts discontinuity densities (4.30–16.34 discontinuities/m; Table 5.4), less than the densities of AI (4.67–28.77 discontinuities/m). Average discontinuity length in UI (0.47–6.70 m) bounds that of AI (0.74–1.32 m). The average apertures of the discontinuities in UI averaged (0.32–1.22 mm) are lower than those of AI (0.90–1.66 mm). Average aperture in the largest intrusion appears to correlate with distance to the centre of the intrusion. Scanlines 19 (inner), 18 (intermediate), and 16 (margin) show increasing average apertures (0.32 mm, 0.88 mm, and 1.07 mm, respectively; Table 5.4) toward the contact of the intrusion with the host

rock. The discontinuity orientations of UI vary to a greater extent than those of the lavas (Fig. 5.S4). The discontinuity conditions of UI and AI are similar, ranging from slightly rough to rough. Although no intrusion discontinuities host soil infilling, volcanic debris (<2 cm in length) is commonly found in the discontinuities of AI.

5.4 Discussion

5.4.1 TinyPerm vs Schmidt hammer

Linking TinyPerm and Schmidt hammer rebound field analyses was not a primary objective in this study; however, the correlation between the two data sets is evident. In the absence of more TinyPerm sample points, the Schmidt hammer data reinforce the geospatial trends observed in Fig. 5.2, Fig. 5.4 as the TinyPerm and Schmidt hammer data display a general negative correlation (Fig. 5.6) where rock hardness increases with decreasing permeability. Fig. 5.6 depicts that Site 3 data have a moderate correlation ($r^2 = 0.75$). The correlation holds when Site 1 and Site 3 are considered together ($r^2 = 0.68$). The correlation is a product of the first-order control that porosity (pores and microcracks) exerts on both strength (e.g. Schaefer et al., 2015) and permeability (e.g. Farquharson et al., 2015). A decrease in rebound values with the increase in permeability also suggests that the higher permeability is in part a product of more intense microfracturing (e.g. Moomivand, 2011) as more, larger microfractures would increase the probability of interconnection between the fractures, which would in turn increase permeability (Wei et al., 1995). From this correlation, Schmidt hammer rebound values in the host rock and in the intrusion are easily distinguishable and appear to have the potential to provide estimates of permeability within two orders of magnitude (Fig. 5.6). We suggest future study could provide a detailed investigation regarding the full potential of using Schmidt hammer rebound analysis as an index of permeability in volcanic rock.

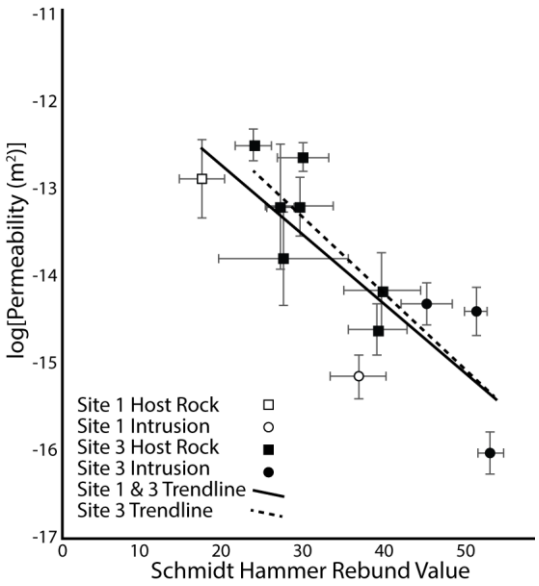

Figure 5.6 Comparison of TinyPerm and Schmidt hammer measurements display moderate negative relationship (see trendlines for visual guide). Host rock generally displays lower rebound values with higher permeability compared to the unaltered intrusions. Error bars represent one standard deviation for Schmidt hammer rebound values and relative error for the permeability data.

5.4.2 Meso-scale (Site 1)

Mordensky et al. (2018) observed a decrease in matrix permeability in ABLM toward the intrusion at 10+ m sampling intervals due to clay precipitation in the host-rock microstructure. This trend is not observed at the sub-metre scale (Fig. 5.2). Instead, we note that permeability of ABLM increases toward the intrusion at the sub-metre scale, consistent with other studies, which have shown that host-rock permeability tends to be highest along intrusion contacts (e.g. Le Ravelec and Gueguen, 1994; Chevallier et al., 2001; Matter et al., 2006). This phenomenon has been interpreted as being due to hydraulic fracturing induced by pressurisation from the emplacement of the intrusion (e.g. Chevallier et al., 2001; Matter et al., 2006; Healy et al., 2018).

5.4.3 Macro-scale (Site 2)

Unfortunately, difficult terrain did not allow permeability analysis away from Site 1 at a reasonable macro-scale interval. Instead, Site 2 was investigated (Fig. 5.3), where a 3 m-wide andesitic dike crosscuts an UBLM deposit several hundreds of metres outside the alteration halo (Fig. 5.1c, e). Permeability of the host rock from the host rock-dike contact decreases over the first 3 m away from the contact (10^{-14} to 10^{-12} m^2 and 10^{-16} to 10^{-13} m^2; Fig. 5.3). The higher permeability can be attributed hydraulic microcracking induced by higher pore pressure from the emplacement of the dike (e.g. Chevallier et al., 2001; Matter et al., 2006). The dike itself does not display consistent permeability (10^{-15}–10^{-12} m^2) across its width. This range in permeability

also suggests heterogeneous microstructure inherent to volcanic material as detailed by existing studies (e.g. Fortin et al., 2011; Heap et al., 2014; Farquharson et al., 2016; Colombier et al., 2017).

5.4.4 Mega-scale (Site 3)

It appears that the diverse and localised microstructure of volcanic material in the alteration halo dominates the mega scale (>100+ m). We found permeability in ABLM does not show a clear trend with distance to the centre of the largest intrusion (Figs. 5.1f, 5.4, 5.7), suggesting that the influence of the intrusion is less than that of the heterogeneity that typifies volcanic material. We observe clay-infilling of macro-fractures in localised areas (e.g. 20 and 130 m from the host rock-intrusion contact) of ABLM (Fig. 5.8a, b), where TinyPerm measurements show lower permeability (Figs. 5.4, 5.7); however, neither the distribution of macro-scale infilling nor the lower TinyPerm values appear to show a geospatial trend with other properties of the fossil hydrothermal system (Fig. 5.1). This is in contrast with the conclusions of Mordensky et al. (2018), who found the lab-based matrix permeability of ABLM decreases as the intrusion was approached due to precipitation of clay minerals from advanced argillic alteration in the pore spaces (Fig. 5.1).

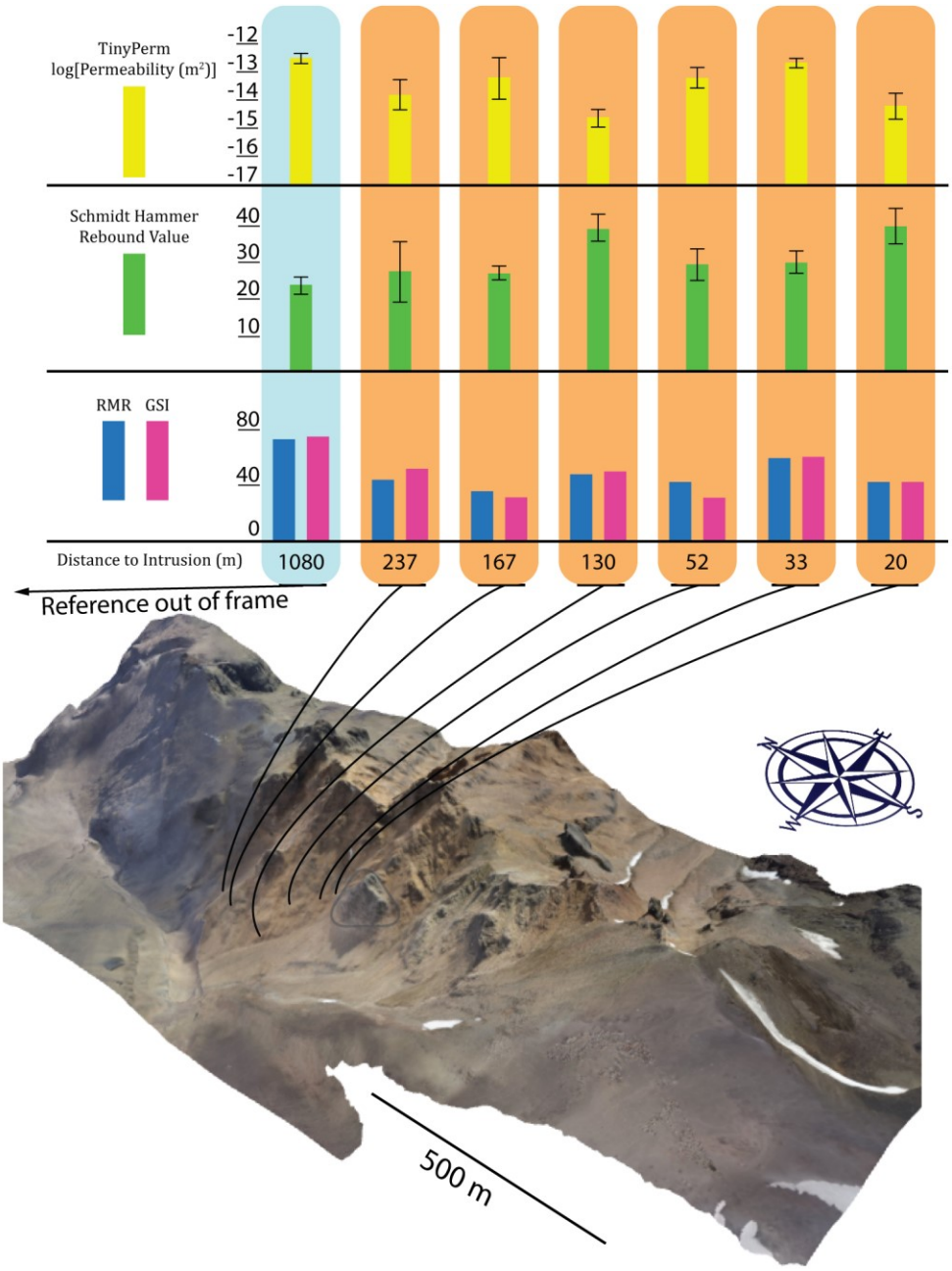

Figure 5.7 Field-based data in brecciated lava margin sorted by distance to the youngest large intrusion. The data presented are from UBLM (blue column) and ABLM (orange column). The sample location for UBLM is outside of the reference frame 1080 m from the host rock-intrusion contact. Field-based permeametry (yellow, top), Schmidt hammer rebound value (green, middle), RMR (blue, bottom left), and GSI (maroon, bottom right) do not correlate with distance to the intrusion. Distance is given in metres from intrusion-host rock contact. Error bars for Schmidt hammer rebound values provide one standard deviation. Error bars for permeability represent relative error.

Figure 5.8 Infilled jointing found in ABLM, 20 m from the host-rock intrusion contact (a, b) and along intrusion margin found at Site 3 (c, d). Infilling appears reddish-brown (a, c) and similar in colour to advanced argillic alteration found in adjacent host rock (Mordensky et al., 2018). Not all the fractures are infilled, suggesting two generations of fracture formation. Fractures with infilling are outlined (b, d). The presence of immediately local, clay-infilled macro-discontinuities corresponds with lower TinyPerm values than other areas of the same geotechnical unit (i.e. ABLM and UI). Brunton compass for scale.

While permeability in ABLM does not display consistent change with distance to the intrusion-host rock contact, the permeability of the intrusion increases toward its interior (Fig. 5.4). Coincident with this decrease of permeability in the intrusion, we again observe clay-infilled macrofractures (Fig. 5.8c, d) similar to those observed in ABLM (Fig. 5.8a, b) that were also associated with lower TinyPerm values. We suggest

that infilling of macro and microfractures by clay decreases the permeability at the intrusion margins and in certain ABLM localities (e.g. Mordensky et al., 2018). This interpretation is consistent with numerical modelling from Scott and Driesner (2018), who found mineral precipitation along intrusion margins decreased local permeability over time, while the interior of the intrusion maintained permeability. This means that the influence of the cooling on the intrusion is scale-dependent (e.g. meso- vs mega-) as it does not appear that there is a strong relationship between distance to the contact and permeability in the intrusion at the meso-scale (1-m; Fig. 5.2). We interpret this to mean that infilling has affected permeability in the intrusion at least as far as 1 m from the intrusion/host-rock contact and our meso-scale analyses were completely within the clay-infilled, lower permeability margin of the intrusion. Moreover, the TinyPerm data in the intrusion suggest that permeability, and thus microfracturing and mineral precipitation, are not ubiquitous across a young intrusion. Instead, matrix permeability appears to change from the exterior toward the interior of the intrusion (Fig. 5.4).

5.4.5 Permeability: field vs laboratory data

In general, the field permeametry from the TinyPerm produced higher values than the lab-based permeametry. These results differ with those of Farquharson et al. (2015), who found laboratory-derived permeability values of sandstones and limestones to be within error of TinyPerm analyses using large, homogenous blocks. However, Heap et al. (2017) reported the TinyPerm produced values different than those from laboratory analysis using hand samples from Whakaari/White Island (New Zealand). Heap et al. (2017) interpreted the deviation as a result of sample size and internal sample structure. Given that we measured permeability of in situ material, we suggest the discrepancy we observe between the two methods is a result of differing internal pore structure. More specifically, the rocks measured in the field are sometimes heavily microfractured and those typically selected for laboratory studies are required to be of a certain coherence in order to prepare intact cylindrical cores. Similarly, the permeability value provided by the TinyPerm field permeameter will be influenced by meso-scale fractures (cm to several 10s of cm) that are not considered in laboratory measurements on 20 mm-diameter core samples (as in Mordensky et al., 2018). Therefore, we conclude that the differing permeability values between TinyPerm analyses and laboratory analyses reflect the importance of scale when measuring rock properties. In the case of permeability, our data suggest that the two methods observe the effects of differently scaled discontinuities (e.g. Fig. 5.4 vs Mordensky et al., 2018).

5.4.6 Volcanic discontinuities and rock strength

Our discontinuity observations (e.g. Fig. 5.5; Tables 5.1, 5.2, 5.4) appear consistent with existing research of unaltered volcanic materials (Watters and Delhaut, 1995; Watters et al., 2000; Concha-Dimas, 2004; Apuani et al., 2005; Moon et al., 2005; del Potro and Hürlimann, 2008). Although it is important to consider the potential impact of freeze-thaw processes in this alpine environment, our discontinuity density and aperture data were consistent with that of other intrusion-hosting volcanic settings, being numerous and <1 mm-wide (e.g. Senger et al., 2015; Garden et al., 2017) and a many discontinuities lacked infill (Table 5.4), suggesting impact of freeze-thaw processes was minimal. Senger et al. (2015) found intrusive rock masses host higher discontinuity densities (5–20 discontinuities/m) than the host rock masses (3–12 discontinuities/m) in and around the Svalbard intrusion, Norway. At Pinnacle Ridge, UI also generally has higher discontinuity densities (4.30–16.34 discontinuities/m) than the host rock (0.43–13.23 discontinuities/m excluding two outliers at 17.97 [Scanline 5] and 28.77 [Scanline 12] discontinuities/m). Also like Senger et al. (2015), we found no robust relationship with distance from the intrusion affecting discontinuity qualities in any geotechnical unit. Instead, it appears that the heterogeneity of volcanic material masks whatever potential influence the intrusion may have on the discontinuity characteristics of the host rock within the alteration halo.

Jointing is pervasive across all the identified geotechnical units, but the altered geotechnical units appear to have higher discontinuity densities than their unaltered equivalents (Fig. 5.5, Tables 5.1, 5.2, 5.4). This is consistent with other studies (e.g. Watters and Delhaut, 1995; Watters et al., 2000; Thomas et al., 2004b). Thomas et al. (2004b) suggested that rock mass strength (a combination of intact laboratory strength and rock mass quality) decreases as the intensity of alteration increases. Given an exponential relationship between RMR and rock mass strength identified by Thomas et al. (2004b), seemingly minor decreases in rock mass classification between unaltered and altered rock can reduce rock mass strength by up to 96% to <1 MPa. Using a two-tailed Student's *t*-test, we find that ABLM has GSI and RMR values that are significantly less than of the respective, unaltered counterpart (i.e. UBLM) at $\alpha = 0.05$ (Table 5.3). Therefore, although Mordensky et al. (2018) identified UBLM as the weakest geotechnical unit when measuring the UCS of intact rock, our rock mass data suggest that ABLM rock masses could be weaker than UBLM rock masses. We explore this consideration using the Generalised Hoek-Brown Criterion, initially proposed in Hoek (1983) and provided in Eq. (7) (Eberhardt, 2012):

$$\sigma_1' = \sigma_3' + C_o\left(m_b \frac{\sigma_3'}{C_o} + s\right)^a \tag{7}$$

In which σ_1' is the major principal stress, σ_3' is the minor principal stress, C_o is the UCS for intact rock, and s, a, and m_b are material constants calculated using Eqs. (8), (9), (10) respectively:

$$s = exp\left(\frac{GSI - 100}{9}\right) \tag{8}$$

$$a = \frac{1}{2} + \frac{1}{6}\left(e^{-GSI/15} - e^{-20/3}\right) \tag{9}$$

$$m_b = m_i \exp\left(\frac{GSI - 100}{28}\right) \tag{5}$$

In which m_i is a material constant from the Hoek-Brown criterion from triaxial testing for intact rock (Eq. (11)) as described in Hoek (1968) and (Eberhardt, 2012):

$$\sigma_1' = \sigma_3' + C_o(m_i \frac{\sigma_3'}{C_o} + 1)^{0.5} \tag{11}$$

For which UCS values come from Mordensky et al. (2018). Given the absence of triaxial strength data for the advanced argillic altered andesites like those found at Pinnacle Ridge, we must assume an m_i from pre-existing literature. Hoek and Brown (1997) provide a range of m_i values for breccia (19 ± 5).

Determining the relative rock mass strengths of the brecciated lava margins is not straightforward. Mordensky et al. (2018) reports the UCS of intact UBLM (3–7 MPa) to be less than that of ABLM (1–61 MPa), while this study finds UBLM to have higher GSI values than ABLM (Fig. 5.5; Tables 5.1, 5.2, 5.3). Further compounding the complexity, Mordensky et al. (2018) found that the UCS of intact ABLM increases with proximity to the intrusion. In order to observe the relative rock mass strength relations between the unaltered altered brecciated lava margins, we consider and compare the rock mass strength of three brecciated lava margin rock masses: 1) UBLM (RMC ID 28, Mordensky et al. (2018) Sample ID 025); 2) ABLM near the intrusion (RMC ID 36, Mordensky et al. (2018) Sample 006); and ABLM near the unaltered-altered halo boundary (RMC ID 27, Mordensky et al. (2018) Sample ID 018).

In Fig. 5.9, we use Eq. (7) to plot the Generalised Hoek-Brown failure envelopes using for these rock masses in terms of minor and major principal stress. Without triaxial testing, a value for the material constant m_i must be assumed. The material constant m_i can vary and is generally greater with stronger rock and lower for weaker rock (Hoek, 1968). Therefore, we use the recommended value for breccias (19 ± 5) from pre-existing sample tests (see Hoek and Brown, 1997). To observe the full range of potential affects,

we vary m_i in three different scenarios: 1) UBLM m_i = ABLM m_i at its a mid-range value (19; Fig. 5.9a); 2) UBLM m_i is set to its maximum recommended value (24) while ABLM m_i is set to its minimum (14; Fig. 5.9b); and 3) UBLM m_i is set to its minimum given value (14) while ABLM m_i is set to its maximum (24; Fig. 5.9c).

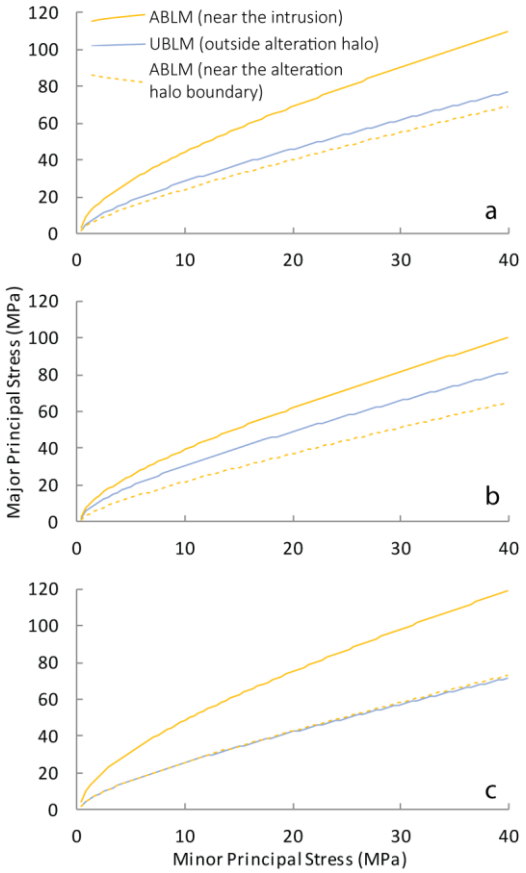

Figure 5.9 Diagram representing effective stress state at failure of brecciated lava margins (i.e. UBLM [1080 m], ABLM [167 m], ABLM [20 m] using UCS and GSI values specific to each location). At stresses outside (above) the failure envelope, the rock masses will have undergone mechanical (inelastic) failure. Stresses below the failure envelope indicate conditions for which deformation is elastic and recoverable. (a) m_i assumed to 19 for UBLM and ABLM as recommended in Hoek and Brown (1997). (b) m_i assumed to 24 for UBLM and 14 for ABLM. (c) m_i assumed to 14 for UBLM and 24 for ABLM. For UCS values see Mordensky et al. (2018).

Fig. 5.9 demonstrates that ABLM has the potential to be weaker than UBLM and, therefore, the weakest rock masses found on the volcanic edifice. However, we emphasise that rock mass properties are highly variable inside the alteration halo due to the heterogeneous nature of the discontinuities (e.g. variable discontinuity densities [Figs. 5.5, 5.4] and fracture-infilling [Figs. 5.7, 5.8]). Therefore, we also highlight that, although the UCS of ABLM generally increases toward the intrusion due to the precipitation of alteration minerals (Mordensky et al., 2018) and presents the possibility for ABLM rock mass near the

intrusion to be a stronger than UBLM, the influence of the higher UCS is easily exceeded by the highly variable discontinuity characteristics.

When considering UBLM m_i = ABLM m_i (19; Fig. 5.9a), the relative rock mass strength of the two ABLM sites bands that of ABLM. That is, the ABLM near (20 m) the intrusion has higher rock mass strength than UBLM farther afield (1080 m from the intrusion; Fig. 5.9a), while, the lower UCS of ABLM farther from the intrusion (167 m) contributes to lower rock mass strength than that of UBLM. These relative relationships are similar when UBLM m_i (14) < ABLM m_i (24; Fig. 5.9b). In both these scenarios, the weakest rock mass is not found where intact rock strength (UCS) is lowest, but where the combination of intact rock strength (e.g. UCS) and field parameters (e.g. GSI) contribute to the weakest rock mass by means of Eq. (7). Although the intrusion does not appreciably change the rock mass strength of the brecciated lava margin when UBLM m_i is greatest (24) and ABLM m_i is lowest (14; Fig. 5.9c), these simple models demonstrate that a small intrusive body has the potential to further reduce the rock mass strength of the already weakest geotechnical units in the host rock (e.g. Fig. 5.9a, b; Tables 5.1, 5.2, 5.3; Mordensky et al., 2018).

These results can be extrapolated beyond surface expression to models from geophysical studies (e.g. Planke et al., 2015), in which intrusive bodies are indirectly observed within an edifice but cannot be sampled or measured directly. In doing so, the weakening effect of the magmatic intrusions can be anticipated and properly mitigated. We note that variation of GSI has substantially greater impact on rock mass strength than similar relative variation of m_i (see Villeneuve et al., 2018). We, therefore, stress that individual rock masses should be assessed for their unique qualities when hazard mapping or modelling because the heterogeneous characteristics of the altered rock surrounding intrusions present the potential to change permeability and, thereby outgassing, while simultaneously reducing the strength of the volcanic edifice, rendering it unable to accommodate additional stress elastically.

5.4.7 Potential implications of discontinuities on rock mass permeability

Outgassing of a volcanic system is dependent on the permeability of the edifice. In volcanic rocks, matrix permeability can range from very tight (e.g. $<10^{-21}$ m^2; Sruoga et al., 2004; Mordensky et al., 2018) to highly permeable ($>10^{-11}$ m^2; Heap and Kennedy, 2016); however, discontinuities provide permeability through this otherwise low-permeability rock (e.g. Sagar and Runchal, 1982; Evans et al., 1997; Cartwright et al., 2007; Senger et al., 2012; Senger et al., 2015). Given the dichotomy between matrix permeability and discontinuity permeability, modelling endeavours take a dual approach to properties that independently consider the two scales (Jafari and Babadagli, 2011). Although simple models exist to quantify the effects of discontinuities and matrix properties on general rock mass permeability (e.g. Snow, 1968, Snow, 1969;

Louis, 1974) and, more specifically, volcanic rock mass permeability (e.g. Heap and Kennedy, 2016; Lamur et al., 2017), doing so precisely and accurately is exceedingly complex and time-intensive. Therefore, quantifying the permeability of volcanic systems remains a largely unapproached endeavour. We do not attempt precise and accurate rock mass permeability modelling, we make some general deductions regarding fluid flow involving a hydrothermal system in a shallow-intrusion environment.

Prior research has found that an open, through-cutting fracture can increase permeability by orders of magnitude (e.g. Lomize, 1961; Snow, 1965; Louis, 1969, Louis, 1974; Krantz et al., 1979; Heap and Kennedy, 2016; Lamur et al., 2017), and brecciated lava margins within the alteration halo host higher discontinuity densities than those outside of the alteration zone (e.g. 0.91 discontinuities/m [transect 15] vs. 12.97 discontinuities/m [transect 3]; Fig. 5.5; Tables 5.1, 5.3, 5.4). These discontinuities would contribute to the rock mass permeability. Simultaneously, the matrix permeability of ABLM (i.e. the altered geotechnical units with the highest matrix permeability) decreases as the intrusion is approached (Mordensky et al., 2018), placing a greater emphasis on permeability through discontinuities in the alteration halo. Hence, fluid flow within the alteration halo and nearer to the intrusion is more discontinuity-controlled than farther from the intrusion and/or outside the alteration halo. Given the magnitude(s) by which through-cutting fractures affect permeability (e.g. Heap and Kennedy, 2016; Lamur et al., 2017), we conclude that host-rock permeability within the alteration halo is greater than that of the unaltered host rock at near-surface conditions. However, as depth and, thereby, effective pressures increase, our interpretation of the effects from the discontinuities on permeability changes because macrofractures and micro fractures close with applied effective pressure (e.g. Gudmundsson, 2011; Nara et al., 2011). Rock masses with low matrix permeability (e.g. $<10^{-18}$ m^2; e.g. intrusions; Mordensky et al., 2018) are more likely to serve as barriers to subsurface flow at depth because their permeability depends on flow through discontinuities (see Senger et al., 2017).

We suggest that the effect of the intrusion on rock mass permeability is depth dependent. At shallow depths, the intrusion may result in higher permeability in the host rock as a product of hydraulic fracturing. We observe these effects from in situ permeametry (Figs. 5.2, 5.3) and discontinuity assessment (Fig. 5.5; Tables 5.1, 5.2, 5.3). At greater depths, where discontinuities are closed to fluid flow, the intrusion and its alteration of the originally vesicle-dominated permeability host rock reduce permeability of the system. This would be consistent with the model of (Farquharson et al., 2017) from which it was observed that shallow discontinuities contribute more greatly to Darcian flow outgassing than deeper discontinuities.

5.4.8 Effect of shallow intrusion on edifice stability

As discussed above, we associate the increase in shallow permeability to the macrofractures induced during the intrusion of the magma body (Figs. 5.2, 5.3). We also propose that the effect of shallow magmatic intrusions on rock mass permeability is depth-dependent. That is, we suggest intrusions at depth (>2–3 km) may reduce the permeability of volcanic edifices and, thereby, reduce the outgassing processes of the system into which they intrude (see Senger et al., 2017). The influence of the resulting pore pressure augmentation (e.g. Christenson et al., 2010; Heap and Wadsworth, 2016) would compromise the already weakened rock masses within the altered zone around the intrusion (e.g. GSI, RMR [Figs. 5.5, 5.9a, b; Tables 5.1, 5.2, 5.3], UCS [Mordensky et al., 2018]). The results of these processes (i.e. weakening and/or permeability reduction of altered rock masses) are evidenced by the common presence of altered debris in mass wasting event deposits (e.g. Mt. Ruapehu, New Zealand [Hackett and Houghton, 1989], Mt. Shasta, USA [Crandell, 1989], Citlaltépetl, Mexico [Carrasco-Núñez and Gomez-Tuena, 1993] Mt. Rainer, USA [Reid et al., 2001]).

5.5 Conclusions

The flanks of many volcanic edifices are composed of a range of spatially variable geotechnical units similar to those described in this study. Intrusions disrupt the layered stratigraphy of the classic stratovolcano, causing local variation in mechanical properties. In this study, data are presented for in situ permeametry, rock mass properties, and discontinuity characteristics from rock masses surrounding a small, shallow magmatic intrusion exposed by glaciation at Pinnacle Ridge (New Zealand). Then, the influence of these properties on rock mass strength and permeability are discussed. The data presented within this study may support future models for the reduction in edifice strength (e.g. Donnadieu et al., 2001) and change in outgassing (e.g. Collinson and Neuberg, 2012) related to intrusions in volcanic environments. These field observations also serve as a companion study to upscale the laboratory-scale data of the same geotechnical units from Mordensky et al. (2018) and complete the geotechnical unit characterisation of these rock masses. In doing so, we find:

- Altered brecciated lava margins have discontinuity characteristics (e.g. density, aperture) that, when considered together, contribute to a lower rock mass strength than that of their unaltered geotechnical unit equivalent (i.e. unaltered brecciated lava margins). Therefore, altered brecciated lava margins can be the weakest rock mass in a volcanic edifice.

- The decrease in strength in the brecciated lava margins around a stocky (130 × 64 m) intrusion is observable up to a distance from the intrusion that is roughly twice the average dimensions of the width of the intrusion.
- At the surface, permeability in the host rock increases proximally to the host rock adjacent to an intrusion, as seen in TinyPerm measurements at sub-metre and several-metre spacing. These margins can be >1 m across.
- TinyPerm measurements are inversely correlated to Schmidt hammer rebound values. While a Schmidt hammer analysis cannot be used to provide absolute permeability values, they can provide a cost-efficient, time-saving means to measure relative permeability between sites of similar lithology. The strong correlation between these two analysis techniques presents the potential for rapid field assessment by Schmidt hammer analysis that can be used to estimate permeability within two orders of magnitude. This strong correlation is a result of porosity serving as a first-order control for both the TinyPerm and Schmidt hammer analyses.

Finally, we conclude intrusions drive hazards associated with mechanical stability of the volcano. Because the effects of the intrusion on these processes will change with scale and effective pressure (depth), it is crucial to use appropriately heterogeneous rock properties with appropriate scale and depth relationships when modelling the processes responsible for these hazards.

5.6 Acknowledgements

This work has also benefitted from discussion with Jim Cole. We would like to thank Graham Leonard, Dougal Townsend, James White, Colin Wilson, Rosie Cole, Leo Purê, and Chris Conway for their guidance, discussion, and comradery in the field. The authors also thank the contribution of two anonymous journal reviewers. The authors of this study acknowledge the support of the UC Doctoral Scholarship and the UC Mason Trust Fund. M.J. Heap acknowledges a Visiting Erskine Fellowship from the University of Canterbury (New Zealand). The authors of this study acknowledge a Dumont d'Urville Hubert Curien Partnership (PHC) grant (number 31950RK) funded and implemented by the New Zealand Ministry of Business, Innovation and Employment (MBIE), the Royal Society of New Zealand, and the Ministry of Foreign Affairs (MAEDI) and the Ministry of Higher Education and Research (MENESR) in France. We also acknowledge Catalyst Fund project "Energy straight from magma", funded and implemented by the Royal Society of New Zealand and the New Zealand Ministry of Business, Innovation and Employment (MBIE).

5.7 Supplemental figures

Figure 5.S1 – 5.S5: Numbers in upper left of stereonet provide scanline identification. Discontinuity orientations are displayed as poles to the planes of the recorded discontinuities and plotted on a lower hemisphere stereonet. Triangular polygon represents approximate location of the altered intrusion from the western perspective. Cooler colours (blue) in stereonet contours represent a lower pole density for discontinuities while warmer colours (red) represent a pole density for discontinuities. Data summarized in Table 5.4. Figure modified from (Mordensky et al., 2018).

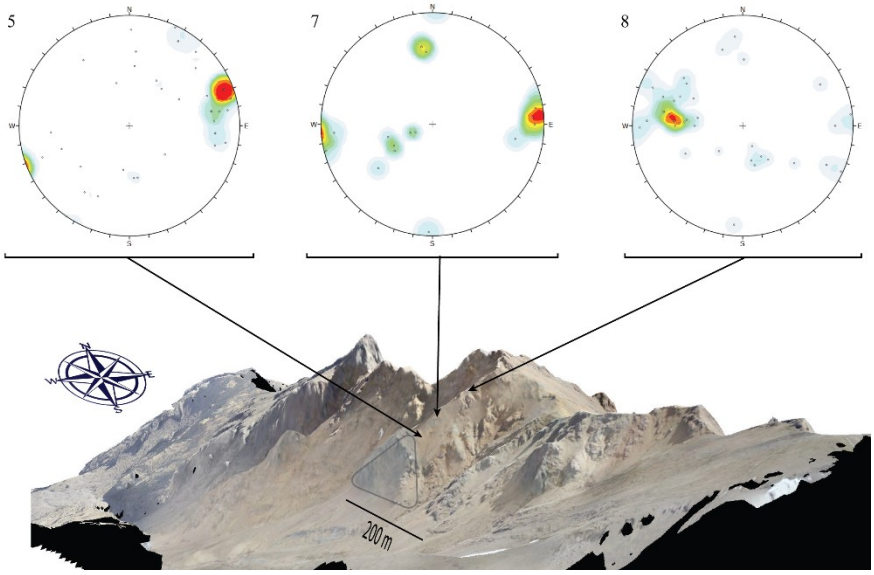

Figure 5.S1 Discontinuity orientations in altered dense coherent lavas

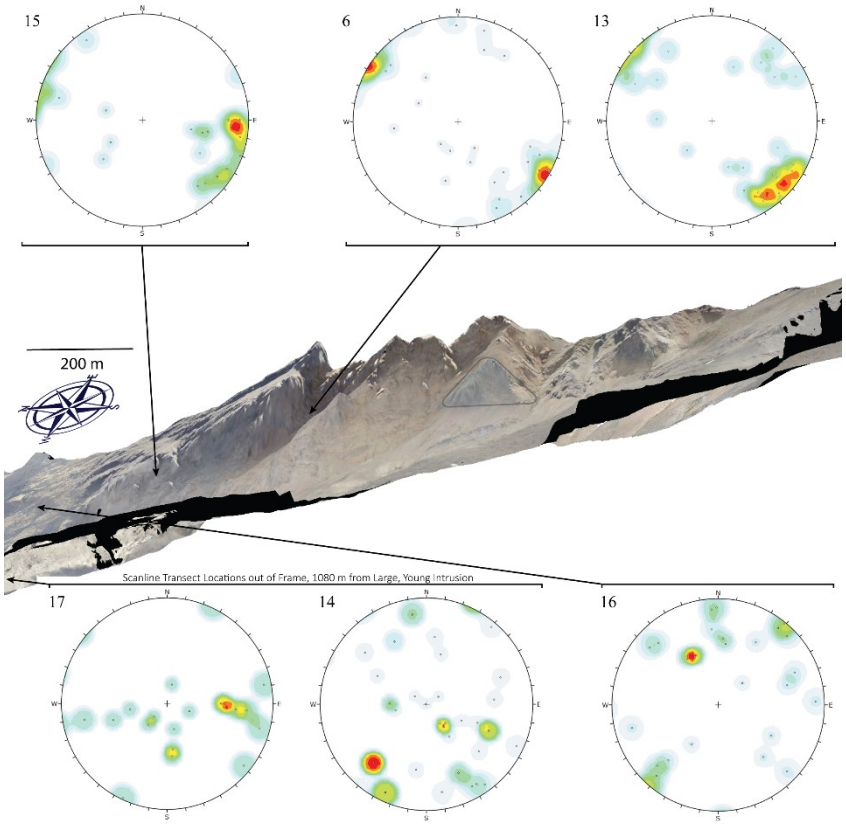

Figure 5.S2 Discontinuity orientation in the scanline transect 15 (UBLM, top left), 6 (UDCL, top middle), 13 (ADCL, top right), 17 (UBLM, bottom left), 14 (UDCL, bottom middle), and 16 (UBLM, bottom right). Additional scanline data for ADCL can be found in Fig. 5.S1. Scanline 13 (ADCL) is displayed alongside Scanline 6 (UDCL) because of the proximity of these two scanlines.

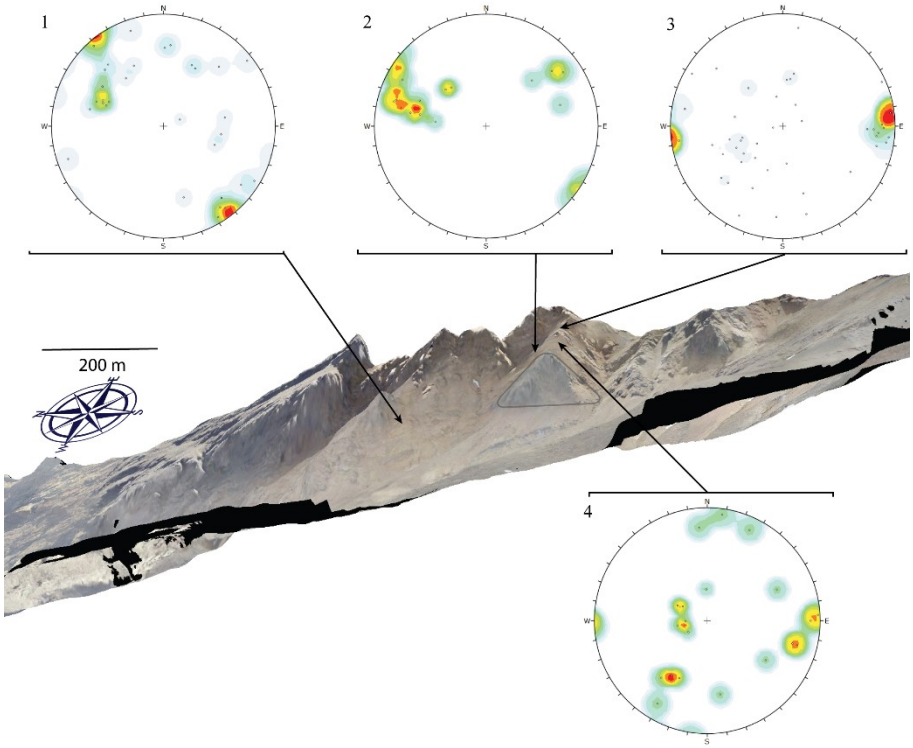

Figure 5.S3 Discontinuity orientation in the altered brecciated lava margins

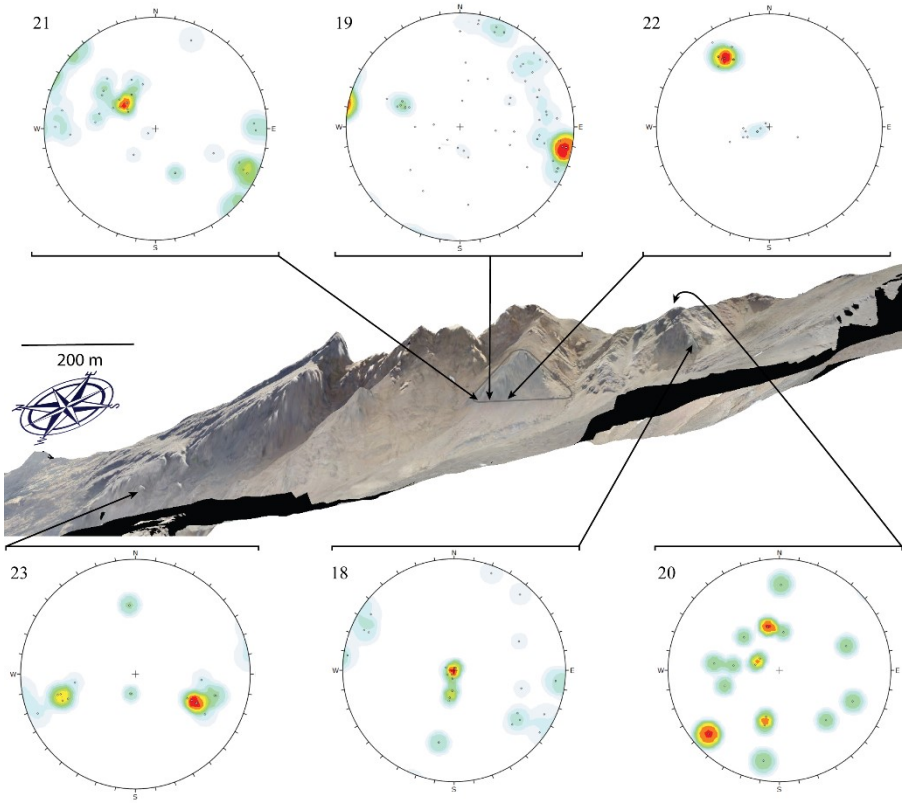

Figure 5.S4 Discontinuity orientation in the unaltered intrusions

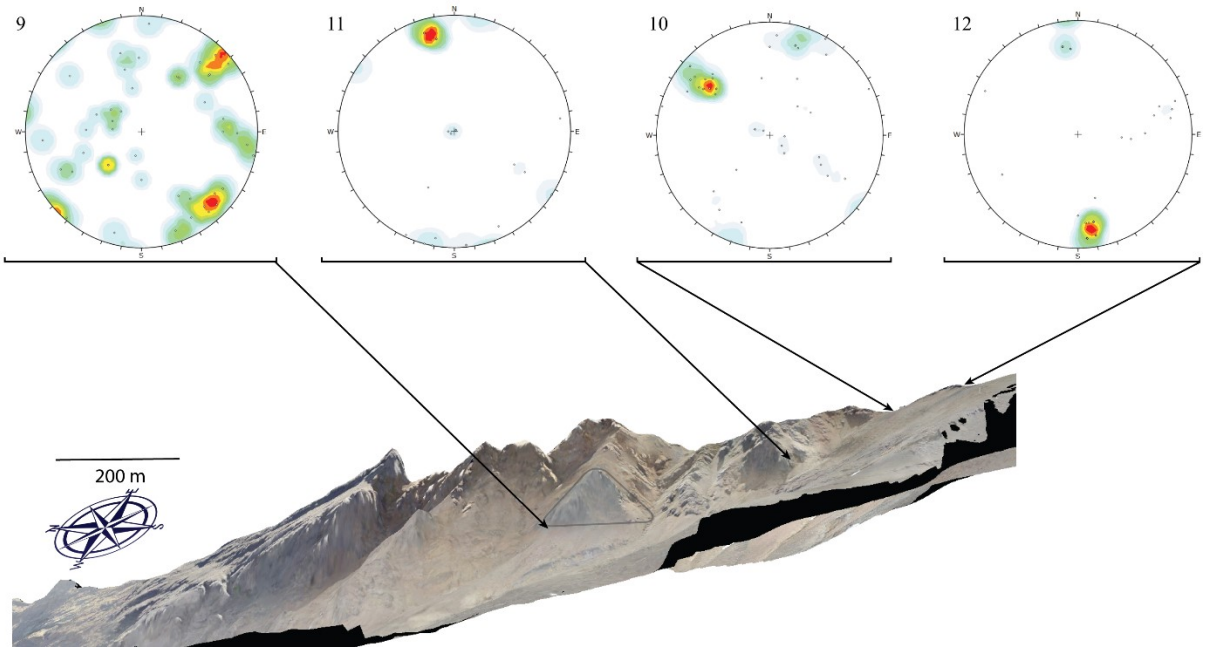

Figure 5.S5 Discontinuity orientation in the altered intrusions

5.8 References

Apuani, T., Corazzato, C., Cancelli, A., and Tibaldi, A., 2005, Physical and mechanical properties of rock masses at Stromboli: a dataset for volcano instability evaluation: Bulletin of Engineering Geology and the Environment, v. 64, p. 419-431.

Aydin, A., 2014, ISRM suggested method for determination of the Schmidt hammer rebound hardness: revised version, *in* Ulusay, R., ed., The ISRM Suggested Methods for Rock Characterization, Testing and Monitoring 2007-2014, Elsevier, Ltd., p. 25-33.

Bieniawski, Z. T., 1989, Engineering rock mass classifications: a complete manual for engineers and geologists in mining, civil, and petroleum engineering, New York, John Wiley & Sons, Inc.

Brown, S., and Smith, M., 2013, A transient-flow syringe air permeameter: Geophysics, v. 78, no. 5, p. D307-D313.

Carrasco-Núñez, G., and Gomez-Tuena, A., 1993, A voluminous avalanche-induced lahar from Citlaltepetl Volcano, Mexico: implications for hazard assessment: Journal of Volcanology and Geothermal Research, v. 59, p. 35-46.

Cartwright, J., Huuse, M., and Aplin, A., 2007, Seal bypass systems: AAPG Bulletin, v. 91, no. 8, p. 1141-1166.

Casey, M., Ebinger, C., Keir, D., Gloaguen, R., and Mohamed, F., 2006, Strain accomodation in transitional rifts: extension by magma intrusion and faulting in Ethiopian rift magmatic segments: Geological Society, London, Special Publications, v. 259, p. 143-163.

Castro, J. M., Bindeman, I., Tuffen, H., and Schipper, C. I., 2014, Explosive origin of silicic lava: textural and δD–H2O evidence for pyroclastic degassing during rhyolite effusion: Earth and Planetary Science Letters, v. 405, p. 52-61.

Cathles, L. M., Erendi, H. J., and Barrie, T., 1997, How long can a hydrothermal system be sustained by a single intrusive event: Economic Geology, v. 92, p. 766-771.

Chevallier, L., Collombet, M., and Pinel, V., 2017, Temporal evolution of magma flow and degassing conditions during dome growth, insights from 2D numerical modelling: Journal of Volcanology and Geothermal Research, v. 333, p. 116-133.

Chevallier, L., Goedhart, M., and Woodford, A., 2001, The influences of dolerite sill and ring complexes on the occurrence of groundwater in Karoo fractured aquifers: a morpho-tectonic approach: Water Resource Commission.

Christenson, B. W., Reyes, A. G., Young, R., Moebis, A., Sherburn, S., Cole-Baker, J., and Britten, K., 2010, Cyclic processes and factors leading to phreatic eruption events: insights from the 25 September 2007 eruption through Ruapehu Crater Lake, New Zealand: Journal of Volcanology and Geothermal Research, v. 191, no. 1-2, p. 15-32.

Collinson, A. S. D., and Neuberg, J., 2012, Gas storage, transport and pressure changes in an evolving permeable volcanic edifice: Journal of Volcanology and Geothermal Research, v. 243-244, no. 1-13.

Colombier, M., Wadsworth, F. B., Gurioli, L., Scheu, B., Kueppers, U., Muro, A. D., and Dingwell, D. B., 2017, The evolution of pore connectivity in volcanic rocks: Earth and Planetary Science Letters, v. 462, p. 99-109.

Concha-Dimas, A., 2004, Numerical modeling in understanding catastrophic collapse at Pico de Orizaba, Mexico [PhD Thesis.

Conway, C. E., Leonard, G. J., Townsend, D. B., Calvert, A. T., Wilson, C. J. N., Gamble, J. A., and Eaves, S. B., 2016, A high-resolution $^{40}Ar/^{39}Ar$ lava chronology and edifice construction history for Ruapehu volcano, New Zealand: Journal of Volcanology and Geothermal Research, v. 327, p. 152-179.

Conway, C. E., Townsend, D. B., Leonard, G. S., Wilson, C. J. N., Calvert, A. T., and Gamble, J. A., 2015, Lava-ice interaction on a large composite volcano: a case study from Ruapehu, New Zealand: Bulletin of Volcanology, v. 77, no. 3, p. 21-21.

Cook, S., Kennedy, B., and Villeneuve, M. C., 2018, Engineering geology model of the Crater Lake outlet, Mt. Ruapehu, New Zealand, to inform rim breakout hazard: Journal of Volcanology and Geothermal Research, v. 350, no. 15, p. 69-83.

Crandell, D. R., 1989, Gigantic debris avalanche of Pleistocene age from ancestral Mount Shasta volcano, California, and debris-avalanche hazard zonation: US Geological Survey Bulletin, v. 1861.

Crowley, J. K., and Zimbelman, D. R., 1997, Mapping hydrothermally altered rocks on Mount Rainer, Washington, with airborne visible/infrared imaging spectrometer (AVIRS) data: Geology, v. 25, no. 6, p. 559-562.

Deere, D. U., and Miller, R. P., 1966, Engineering classification index properties for intact rock: Air Force Weapons Laboratory.

del Potro, R., and Hürlimann, M., 2008, Geotechnical classification and characterisation of materials for stability analyses of large volcanic slopes: Engineering Geology, v. 98, no. 1-2, p. 1-17.

Donnadieu, F., Merle, O., and Besson, J., 2001, Volcanic edifice stability during cryptodome intrusion: Bulletin of Volcanology, v. 63, p. 61-72.

Eberhardt, E., 2012, The Hoek-Brown failure criterion: Rock Mech Rock Eng, v. 45, p. 981-988.

Edmonds, M., and Herd, R. A., 2007, A volcanic degassing event at the explosive-effusive transition: Geophys. Res. Lett., v. 34, no. 21.

Edmonds, M., Oppenheimer, C., Pyle, D. M., Herd, R. A., and Thompson, G., 2003, SO_2 emissions from Soufrière Hills Volcano and their relationship to conduit permeability hydrothermal interaction and outgassing regime: Journal of Volcanology and Geothermal Research, v. 124, p. 23-43.

Eichelberger, J. C., Carrigan, C. R., Westrich, H. R., and Price, R. H., 1986, Non-explosive silicic volcanism: Nature, v. 323, no. 6089, p. 598-602.

Evans, J. P., Forster, C. B., and Goddard, J. V., 1997, Permeability of fault-related rocks, and implications for hydraulic structure of fault zones: Journal of Structural Geology, v. 19, p. 1393-1404.

Farquharson, J., Heap, M. J., Lavallée, Y., Varley, N. R., and Baud, P., 2016, Evidence for the development of permeability anisotropy in lava domes and volcanic conduits: Journal of Volcanology and Geothermal Research, v. 323, p. 163-185.

Farquharson, J., Heap, M. J., Varley, N. R., Baud, P., and Reuschlé, T., 2015, Permeability and porosity relationships of edifice-forming andesites: A combined field and laboratory study: Journal of Volcanology and Geothermal Research, v. 297, p. 52-68.

Farquharson, J., Wadsworth, F. B., Heap, M. J., and Baud, P., 2017, Time-dependent permeability evolution in compacting volcanic fracture systems and implications for gas overpressure: Journal of Volcanology and Geothermal Research, v. 339, p. 81-97.

Fortin, J., Stanchits, S., Vinciguerra, S., and Gueguen, Y., 2011, Influence of thermal and mechanical cracks on permeability and elastic wave velocities in a basalt from Mt. Etna volcano subjected to elevated pressure: Tectonophysics, v. 503, p. 60-74.

Frolova, J. V., Ladygin, V. M., Rychagov, S. N., and Zukhubaya, D., 2014, Effects of hydrothermal alterations on physical and properties of rocks in the Kuril-Kamchatka island arc: Engineering Geology, v. 183, p. 80-95.

Galland, O., de Bremond d'Ars, J., Cobbold, P. R., and Hallot, E., 2003, Physical models of magmatic intrusion during thrusting: Terra Nova, v. 15, no. 6, p. 405-409.

Galland, O., Planke, S., Neumann, E., and Malthe-Sørenssen, A., 2009, Experimental modelling of shallow magma emplacement: application to saucer-shaped intrusions: Earth and Planetary Science Letters, v. 277, p. 373-383.

Gamble, J. A., Price, R. C., Smith, I. E. M., McIntosh, W. C., and Dunbar, N. W., 2003, $^{40}Ar/^{39}Ar$ geochronology of magmatic activity, magma flux and hazards at Ruapehu volcano, Taupo Volcanic Zone, New Zealand: Journal of Volcanology and Geothermal Research, v. 120, no. 3-4, p. 271-287.

Garden, T., Gravley, D. M., Kennedy, B., Deering, C. D., and Chambefort, I., 2017, Controls on hydrothermal fluid flow in caldera-hosted settings: New insights from Lake City caldera, USA: Geosphere, v. 13, no. 6.

Gaunt, H. E., Sammonds, P., Meredith, P. G., Smith, R., and Pallister, J. S., 2014, Pathways for degassing during the lava dome eruption of Mount St. Helens 2004-2008: Geology, v. 42, no. 11, p. 947-950.

González de Vallejo, L. I., and Ferrer, M., 2006, Caracterización geomecánica de los materiales volcánicos de Tenerife, Madrid, Instituto Geológico y Minero de España, 148 p.:

Gudmundsson, A., 2002, Emplacement and arrest of sheets and dykes in central volcanoes: Journal of Volcanology and Geothermal Research, v. 116, p. 279-298.

Gudmundsson, A., 2003, Surface stresses associated with arrested dykes in rift zones: Bulletin of Volcanology, v. 65, no. 606-619.

Gudmundsson, A., 2011, Rock Fractures in Geological Processes, United Kingdom, Cambridge University Press (CUP).

Gudmundsson, A., 2012, Strengths and strain energies of volcanic edifices: implications for eruptions, collapse calderas, and landslides: Natural Hazards Earth Systems, v. 12, p. 2241-2258.

Hackett, W. R., 1985, Geology and Petrology of Ruapehu Volcano and Related Vents [PhD Thesis: Victoria University of Wellington.

Hackett, W. R., and Houghton, B. F., 1985, Pinnacle Ridge Member, Whakapapa Formation; a welded airfall deposit from Ruapehu volcano, Taupo Volcani Zone: Record - New Zealand Geological Survey, v. 8, p. 24-29.

Hackett, W. R., and Houghton, B. F., 1989, A facies model for a Quaternary andesitic composite volcano: Ruapehu, New Zealand: Bulletin of Volcanology, v. 51, no. 1, p. 51-68.

Healy, D., Rizzo, R. E., Duffy, M., Farrell, N. J. C., Hole, M. J., and Muirhead, D., 2018, Field evidence for the lateral emplacement of igneous dykes: implications for 3D mechanical models and the plumbing beneath fissure eruptions: Volcanica, v. 1, p. 85-105.

Heap, M. J., and Kennedy, B., 2016, Exploring the scale-dependent permeability of fractured andesite: Earth and Planetary Science Letters, v. 447, p. 139-150.

Heap, M. J., Kennedy, B., Farquharson, J., Ashworth, J., Gilg, H. A., Scheu, B., Lavallée, Y., Siratovich, P. A., Cole, J., Jolly, A., and Dingwell, D. B., 2017, A multidisciplinary approach to quantify the permeability of a volcanic hydrothermal system (Whakaari/White Island, Taupo Volcanic Zone, New Zealand): Journal of Volcanology and Geothermal Research, v. 332, p. 88-108.

Heap, M. J., Kennedy, B. M., Pernin, N., Jacquemard, L., Baud, P., Farquharson, J. I., Scheu, B., Lavallée, Y., Gilg, H. A., Letham-Brake, M., Mayer, K., Jolly, A. D., Reuschlé, T., and Dingwell, D. B., 2015, Mechanical behaviour and failure modes in the Whakaari (White Island volcano) hydrothermal system, New Zealand: Journal of Volcanology and Geothermal Research, v. 295, p. 26-42.

Heap, M. J., Lavallée, Y., Petrakova, L., Baud, P., Reuschlé, T., Varley, N. R., and Dingwell, D. B., 2014, Microstructural controls on the physical and mechanical properties of edifice-forming andesites at Volcán de Colima, Mexico: Journal of Geophysical Research: Solid Earth, v. 119, no. 4, p. 2925-2963.

Heap, M. J., and Wadsworth, F. B., 2016, Closing an open system: pore pressure changes in permeable edifice rock at high strain rates: Journal of Volcanology and Geothermal Research, v. 315, p. 40-50.

Henley, R. W., and Ellis, A. J., 1983, Geothermal systems ancient and modern: a geochemical review: Earth-Science Reviews, v. 19, p. 1-50.

Hoek, E., 1968, Brittle Failure of Rock, London, Wiley and Sons, Rock Mechanics in Engineering Practice.

Hoek, E., 1983, Strength of jointed rock masses: Geotechnique, v. 33, no. 3, p. 187-223.

Hoek, E., and Brown, E. T., 1997, Practical estimates of rock mass strength: International Journal of Rock Mechanics and Mining Sciences, v. 34, no. 8, p. 1165-1186.

Hoek, E., Carter, T. G., and Diederichs, M., 2013, Quantification of the Geological Strength Index, 47th US Rock Mechanics / Geomechanics Symposium: San Francisco, CA, RocNews.

Houghton, B. F., Latter, J. H., and Hackett, W. R., 1987, Volcanic hazard assessment for Ruapehu composite volcano, Taupo Volcanic Zone, New Zealand: Bulletin of Volcanology, v. 49, no. 6, p. 737-751.

Jaeger, C., 1960, Shear fracture of anisotropic rocks: Geological Magazine, v. 97, no. 1, p. 65-72.

Jafari, A., and Babadagli, T., 2011, Effective fracture network permeability of geothermal reservoirs: Geothermics, v. 40, no. 1, p. 25-38.

Jaupart, C., 1998, Gas loss from magmas through conduit walls during eruption: Journal of Geological Sciences, v. 143, p. 73-90.

Keating, G. N., Valentine, G. A., Krier, D. J., and Perry, F. V., 2007, Shallow plumbing systems for small-volume basaltic volcanoes: Bulletin of Volcanology, v. 70, no. 5, p. 563-582.

Kilic, A., and Teymen, A., 2008, Determination of mechanical properties of rocks using simple methods: Bull Eng Geol Environ, v. 67, no. 237-244.

Krantz, R. E., Frankel, A. D., Engelder, T., and Scholz, C. H., 1979, The permeability of whole and jointed Barre granite: International Journal of Rock Mechanics and Mining Science, v. 16, p. 225-234.

Lamur, A., Kendrick, J. E., Eggertsson, G. H., Wall, R. J., Ashworth, J. D., and Lavallée, Y., 2017, The permeability of fractured rocks in pressurised volcanic and geothermal systems: Scientific Reports, v. 7, no. 1, p. 6173.

Latter, J. H., 1986, Volcanic risk and surveillance in New Zealand: New Zealand Geological Survey Record, v. 10, p. 5-22.

Le Ravelec, M., and Gueguen, Y., 1994, Permeability models for heated igneous rocks: Journal of Geophysical Research, v. 99(B12), no. 24, p. 251-261.
Lecointre, J., Hodgson, K., Neall, V., and Cronin, S., 2004, Lahar-triggering mechanisms and hazard at Ruapehu volcano, New Zealand: Natural Hazards, v. 31, no. 1, p. 85-109.
Lomize, G. M., 1961, Filtrarsiia v Treshchinovatykh Porod [Water flow in jointed rock]: Gosenergoizdat.
Louis, C. A., 1969, A study of groundwater flow in jointed rock and its influence of the stability of rock masses: Imperial College.
Louis, C. A., 1974, Rock hydraulics, *in* Muller, L., ed., Rock Mechanics: Vienna, Springer, p. 299-382.
Manda, A. K., and Mabee, S. B., 2010, Comparison of three fracture sampling methods for layered rocks: International Journal of Rock Mechanics and Mining Sciences, v. 47, no. 2, p. 218-226.
Marinos, P., and Hoek, E., GSI: A geologically friendly tool for rock mass strength estimation, *in* Proceedings GeoEng2000 Conference, Melbourne, Australia, 2000.
Matter, J., Goldberg, D., Morin, R., and Stute, M., 2006, Contact zone permeability at intrusion boundaries: new results from hydraulic testing and geophysical logging in the Newark Rift Basin, New York, USA: Hydrogeology Journal, v. 14, no. 5, p. 689-699.
Mayer, K., Scheu, B., Montanaro, C., Yilmaz, T. I., Isaia, R., Abbichler, D., and Dingwell, D. B., 2016, Hydrothermal alteration of surficial rocks at Solfatara (Campi Flegrei): Petrophysical properties and implications for phreatic eruption processes: Journal of Volcanology and Geothermal Research, v. 320, p. 128-143.
Mayer, K., Scheu, B., Rott, S., Montanaro, C., Yilmaz, T. I., Gilg, H. A., Joseph, E. P., and Dingwell, D. B., 2017, Phreatic activity and hydrothermal alteration in the Valley of Desolation, Dominica: Bulletin of Volcanology, v. 79, no. 12.
McGuire, W. J., 1996, Volcano instability: a review of contemporary themes: Geological Society of London, v. 110, p. 1-23.
McGuire, W. J., 1998, Volcanic hazards and their migration, *in* Maund, J. G., and Eddlestron, M., eds., Geohazards in Engineering Geology: London, Engineering Geology Special Publications, Geological Society.
McLamore, R., and Gray, K. A., 1967, The mechanical behavior of anisotropic sedimentary rocks: Journal of Engineering for Industry, Transactions of the American Society of Mechanical Engineers, v. B89, no. 1, p. 62-73.
Moomivand, H., 2011, Development of a new method for estimating the indirect uniaxial compressive strength of rock using Schmidt hammer: Berg- und Hüttenmännische Monatshefte, v. 156, no. 4, p. 142-146.
Moon, V., Bradshaw, J., Smith, R., and de Lange, W., 2005, Geotechnical characterization of stratocone crater wall sequences, White Island volcano, New Zealand: Engineering Geology, v. 81, p. 146-178.
Mordensky, S. P., Villeneuve, M. C., Kennedy, B. M., Heap, M. J., Gravley, D., Farquharson, J. I., and Reuschlé, T., 2018, Physical and mechanical property relationships of a shallow intrusion and volcanic host rock, Pinnacle Ridge, Mt. Ruapehu, New Zealand: Journal of Volcanology and Geothermal Research, v. 359, no. 15, p. 1-20.
Mueller, S., Scheu, B., Spieler, O., and Dingwell, D. B., 2008, Permeability and control on magma fragmentation: Geology, v. 36, no. 5, p. 399-402.
Nara, Y., Meredith, P. G., Yoneda, T., and Kaneko, K., 2011, Influence of macrofractures and microfractures on permeability and elastic wave velocities in basalt at elevated pressure: Tectonophysics, v. 503, no. 1-2, p. 52-59.
Nikulin, M. S., 1994, Student t-test, *in* Hazewinkel, M., ed., Encyclopedia of Mathematics: Netherlands, Springer Science, Business Media B.V., and Kluwer Academic Publishers.

Okubo, C. H., 2004, Rock mass strength and slope stability of the Hilina slump, Kilauea volcano, Hawai'i: Journal of Volcanology and Geothermal Research, v. 138, no. 1-2, p. 43-76.
Okumura, S., and Sasaki, O., 2014, Permeability reduction of fractured rhyolite in volcanic conduits and its control on eruption cyclicity: Geology, v. 42, p. 843-846.
Pardo, N., 2012, Andesitic plinian eruptions at Mt. Ruapehu (New Zealand): from lithofacies to eruption dynamics [PhD Thesis: Massey University.
Planke, S., Svensen, H., Myklebust, R., Bannister, S., Manton, B., and Lorenz, L., 2015, Geophysics and remote sensing: Advances in Volcanology, p. 1-16.
Pola, A., Crosta, G., Fusi, N., Barberini, V., and Norini, G., 2012, Influence of alteration on physical properties of volcanic rocks: Tectonophysics, v. 566-567, p. 67-86.
Pola, A., Crosta, G. B., Fusi, N., and Castellanza, R., 2014, General characterization of the mechanical behaviour of different volcanic rocks with respect to alteration: Engineering Geology, v. 169, p. 1-13.
Price, R. C., Gamble, J. A., Smith, I. E. M., Maas, R., Waight, T., Stewart, R. B., and Woodhead, J. D., 2012, The anatomy of an andesite volcano: a time-stratigraphic study of andesite petrogenesis and crustal evolution at Ruapehu volcano, New Zealand: Journal of Petrology, v. 42, no. 10, p. 2139-2189.
Reid, M. E., Sisson, T. W., and Brien, D. L., 2001, Volcano collapse promoted by hydrothermal alteration and edifice shape, Mount Rainier, Washington: Geology, v. 29, no. 9, p. 779.
Rubin, A. M., 1995, Propagation of magma-filled cracks: Annual Review of Earth and Planetary Sciences, v. 23, p. 287-336.
Sagar, B., and Runchal, A., 1982, Permeability of fractured rock: Effect of fracture size and data uncertainties: Water Resources Research, v. 18, p. 266-274.
Schaefer, L. N., Kendrick, J. E., Oommen, T., Lavallée, Y., and Chigna, G., 2015, Geomechanical rock properties of a basaltic volcano: Frontiers in Earth Science, v. 3, no. 29.
Schultz, R. A., 1995, Limits on strength and deformation properties of jointed basaltic rock masses: Rock Mech Rock Eng, v. 28, no. 1, p. 1-15.
Scott, S. W., and Driesner, T., 2018, Permeability changes resulting from quartz precipitation and dissolution around upper crustal intrusions: Geofluids, p. 19.
Senger, K., Buckley, S. J., Chevallier, L., Fagereng, A., Galland, O., Kurz, T., Ogata, K., Planke, S., and Tveranger, J., 2015, Fracturing of doleritic intrusions and associated contact zones: Implications for fluid flow in volcanic basins: Journal of African Earth Sciences, v. 102, p. 70-85.
Senger, K., Millett, J., Planke, S., Ogata, K., Eide, C. H., Festoy, M., Galland, O., and Jerram, D. A., 2017, Effects of igneous intrusions on the petroleum system: a review: First Break, v. 35.
Senger, K., Tveranger, J., Planke, S., Ogata, K., Alvar, B., Wheeler, W., Chevallier, L., and Fagereng, A., Flow flow around igneous intrusions: from outcrop to simulator, *in* Proceedings LASI 5 Conference, Port Elizabeth, South Africa, 2012.
Siratovich, P., Cole, J., Heap, M., Villeneuve, M., Reuschlé, T., Swanson, K., Kennedy, B., Gravley, D., and Lavallée, Y., 2015, Experimental thermal stimulation of the Rotokawa Andesite: Proceedings World Geothermal Congress 2015, no. April, p. 1-6.
Siratovich, P. A., Heap, M. J., Villeneuve, M. C., Cole, J., Kennedy, B., Davidson, J. P., and Reuschlé, T., 2016, Mechanical behaviour of the Rotokawa Andesites (New Zealand): insight into permeability evolution and stress-induced behaviour in an actively utilised geothermal reservoir: Geothermics, v. 64, p. 163-179.
Siratovich, P. A., Heap, M. J., Villeneuve, M. C., Cole, J. W., and Reuschlé, T., 2014, Physical property relationships of the Rotokawa Andesite, a significant geothermal reservoir rock in the Taupo Volcanic Zone, New Zealand: Geothermal Energy, v. 2, no. 1, p. 10-10.

Snow, D. T., 1965, A parallel plate model of fractured permeable media [PhD: University of California: Berkeley, USA.
Snow, D. T., 1968, Rock fracture spacings, openings, and porosities: Proceedings ASCE, v. 96, p. 73-91.
Snow, D. T., 1969, Anisotropic permeability of fractured media: Water Resources Research, v. 5, no. 6.
Sruoga, P., Rubinstein, N., and Hinterswimmer, G., 2004, Porosity and permeability in volcanic rocks: a case study on the Serie Tobifera, South Patagonia, Argentina: Journal of Volcanology and Geothermal Research, v. 132, no. 1, p. 31-43.
Stewart, M. A., Klein, E. M., Karson, J. A., and Brophy, J. G., 2003, Geochemical relationships between dikes and lavas at the Hess Deep Rift: implications for magma eruptibility: Journal of Geophysical Research, v. 108.
Taisne, B., and Juapart, C., 2008, Magma degassing and intermittent lava dome growth: Geophys. Res. Lett., v. 35, no. 20.
Thomas, M. E., Petford, N., and Bromhead, E. N., 2004a, The effect of internal gas pressurization on volcanic edifice stability: evolution towards a critical state: Terra Nova, v. 16, p. 312-317.
Thomas, M. E., Petrford, N., and Bromhead, E. N., 2004b, Volcanic rock mass properties from Snowdonia and Tenerife: implications for volcano edifice strength: Journal of the Geological Society, v. 161, p. 939-946.
Thomson, K., and Schofield, N., 2008, Lithological and structural controls on the emplacement and morphology of sills in sedimentary basins: Geological Society, London, Special Publications, v. 302, p. 31-44.
Torabi, S. R., Ataei, M., and Javanshir, M., 2010, Application of Schmidt rebound number for estimating rock strength under specific geological conditions: Journal of Mining & Environment, v. 1, no. 2, p. 1-8.
Townsend, D. B., Leonard, G. S., Conway, C. E., Eaves, S. B., and Wilson, C. J. N., 2017, Geology of the Tongariro National Park area: GNS Science, 1 Sheet + 109, scale 1:60000.
Valentine, G., and Krogh, K., 2006, Emplacement of shallow dikes and sills beneath a small basaltic volcanic center – the role of pre-existing structure (Paiute Ridge, southern Nevada, USA): Earth and Planetary Science Letters, v. 246, no. 3-4, p. 217-230.
Vignaroli, G., Aldega, L., Balsamo, F., Billi, A., De Benedetti, A. A., De Filippis, L., and Rossetti, F., 2014, A way to hydrothermal paroxysm, Colli Albani volcano, Italy: Geological Society Of America Bulletin, no. B31139-1.
Vigneresse, J.-L., Tikoff, B., and Améglio, L., 1999, Modification of the regional stress field by magma intrusion and formation of tabular granitic plutons: Tectonophysics, v. 302, no. 3-4, p. 203-224.
Villeneuve, M. C., Heap, M. J., Kushnir, A. R. L., Qin, T., Baud, P., Zhou, G., & Xu, T., 2018, Estimating in situ rock mass strength and elastic modulus of granite from the Soultz-sous-Forêts geothermal reservoir (France): Geothermal Energy, v. 6, no. 11. doi:10.1186/s40517-018-0096-1.
Voight, B., 2000, Structural stability of andesite volcanoes and lava domes: Philosophical Transactions of the Royal Society A: Mathematical, Physical and Engineering Sciences, v. 358, no. 1770, p. 1663-1703.
Voight, B., and Elsworth, D., 2000, Instability and collapse of hazardous gas-pressurized lava domes: Geophys. Res. Lett., v. 27, no. 1, p. 1-4.
Watters, R. J., and Delhaut, W. D., 1995, Effect of argillic alteration on rock mass stability: Geological Society Of America Bulletin, v. 10, p. 139-150.
Watters, R. J., Zimbelman, D. R., S.D., B., and Crowley, J. K., 2000, Rock mass strength assessment and significance to edifice stability, Mount Rainier and Mount Hood, Cascade Range volcanoes: Pure and Applied Geophysics, v. 157, no. 6-8, p. 957-976.

Wei, Z. Q., Egger, P., and Descoeudres, F., 1995, Permeability predictions for joint rock masses: International Journal of Rock Mechanics and Mining Science & Geomechanics Abstracts, v. 32, no. 3, p. 251-261.

Wilson, C. J. N., Houghton, B. F., McWilliams, M. O., Lanphere, M. A., Weaver, S. D., and Briggs, R. M., 1995, Volcanic and structural evolution of Taupo Volcanic Zone, New Zealand: a review: Journal of Volcanology and Geothermal Research, v. 68, no. 1-3, p. 1-28.

Woods, A. W., and Koyaguchi, T., 1994, Transitions between explosive and effusive eruptions of silicic magmas: Nature, v. 370, p. 641-644.

Wyering, L. D., Villeneuve, M. C., Wallis, I. C., Siratovich, P. A., Kennedy, B. M., and Gravley, D. M., 2015, The development and application of the alteration strength index equation: Engineering Geology, v. 199, p. 48-61.

Wyering, L. D., Villeneuve, M. C., Wallis, I. C., Siratovich, P. A., Kennedy, B. M., Gravley, D. M., and Cant, J. L., 2014, Mechanical and physical properties of hydrothermally altered rocks, Taupo Volcanic Zone, New Zealand: Journal of Volcanology and Geothermal Research, v. 288, p. 76-93.

Chapter 6 Preamble

In Chapter 5, I find that altered rock masses generally host higher discontinuity densities, wider discontinuity apertures, and longer discontinuity lengths than unaltered volcanics. These qualities thereby lower the rock mass strength of the altered volcanics; however, several assumptions on modelling parameters were made (e.g. m_i) to complete this assessment. In Chapter 6, I complete the assessment of the geotechnical units at Pinnacle Ridge (Fig. 1) that I present in Chapter 3 by conducting triaxial deformation testing. In doing so, I establish Hoek-Brown failure criteria parameters for the geotechnical units. I am then able to numerically model the influence varying pore pressure has on the stability of the rock masses of the fossil hydrothermal system.

Chapter 6 has been written for submission to and publication in *Engineering Geology*.

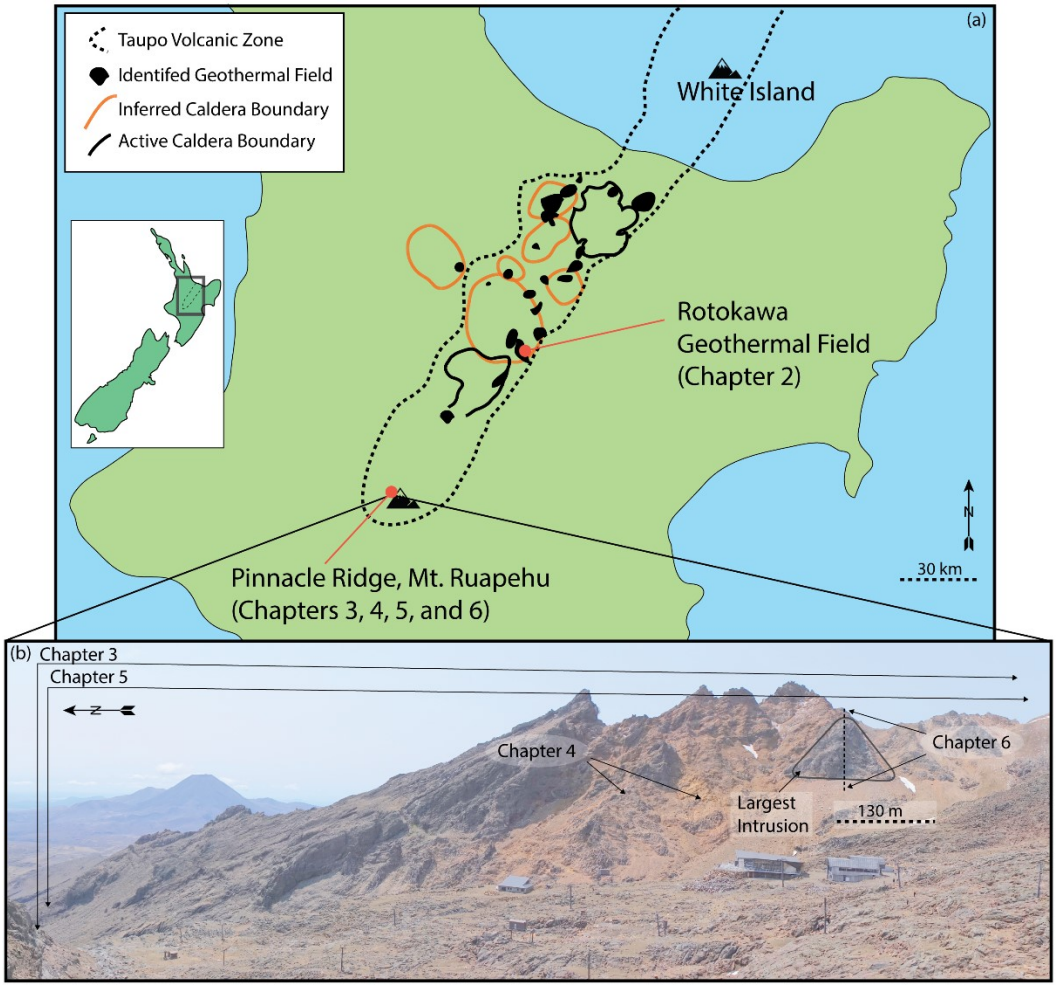

Figure 1. Primary site locations specific to the research presented in this study. (a) Sites of the two hydrothermal systems in New Zealand. (b) Sites specific to Chapters 3 – 6 at Pinnacle Ridge. Solid black polygon marks boundary of the largest young intrusion. Scale is approximate.

Chapter 6

Mechanical rock mass behaviour surrounding a shallow intrusion in andesitic lavas at Pinnacle Ridge, Mt. Ruapehu (New Zealand): pore-pressure induced edifice destabilisation

S. P. Mordensky[1], M. C. Villeneuve[1], B. M. Kennedy[1], J. Struthers[1], D. M. Gravley[1]

[1]Department of Geological Sciences, University of Canterbury, Private Bag 4800, Christchurch 8140, New Zealand

Abstract

Volcanic edifices are commonly composed of an assortment of varied mechanical materials. However, the range of mechanical behaviour associated with an intrusion within a volcanic edifice represents a key unknown critical to volcanic stability assessments. In this study, we explore the triaxial and tensile strength of the seven geotechnical units associated with a small shallow intrusion at Pinnacle Ridge, Mt. Ruapehu, New Zealand. We provide a complete characterisation of the rock masses and model the stability under varying pore pressures. We present laboratory data from tensile and triaxial compression tests to characterise failure conditions. We find that advanced argillic hydrothermal alteration can change the transition pressure for deformation behaviour (i.e. brittle and ductile) of some geotechnical units (i.e. brecciated lava margins) at low effective confining stresses (< 5 MPa). We combine this data with field rock mass characterisation in a stability model. Although the triaxial compression testing reveals nothing anomalous regarding hydrothermal vein material, finite element modelling shows that when the rock mass properties of the hydrothermal vein material are considered in conjunction with the laboratory-based deformation behaviour, a relatively minor increase in pore pressure (e.g. < 5 MPa above hydrostatic conditions) in a shallow hydrothermal system similar to the one found at Pinnacle Ridge is sufficient to induce failure in the hydrothermal vein material. Under these conditions, the other geotechnical units remain intact. Therefore, when oriented unfavourably, this small volume hydrothermal vein can fail and

form a failure plane, destabilising a large portion of the system, representing a landslide hazard. The current exposure of the vein at Pinnacle ridge is significantly far from the active hydrothermal system to be frequently exposed to elevated pore pressures. However, we propose similar veins may be present in proximity to active parts of Mt. Ruapehu's hydrothermal system and are an important consideration for future stability models.

6.1 Introduction

Slope instability is implicit to volcanic edifices given the inherent nature for constant change of these systems (e.g. pressurisation (e.g. Newhall et al., 2001), eruption (e.g. Kilgour et al., 2010), and seismic activity (e.g. Sherburn et al., 1999). Consequently, rockfall, landslide, and sector collapse events and deposits have been observed worldwide (e.g. Pacaya, Guatemala (Vallance et al., 2005), Mt. Ruapehu, New Zealand (Houghton et al., 1987), Stromboli Volcano, Italy (Tibaldi, 2001), Mt. Shasta, USA (Crandell, 1989), Citlaltépetl, Mexico (Carrasco-Núñez & Gomez-Tuena, 1993) Mt. Rainer, USA (Reid et al., 2001) and Mt. St. Helens (Voight et al., 1983)). Given the prevalence for these events, it is important to comprehend the characteristics controlling the probability and nature of slope failure on volcanic edifices.

Volcanic complexes are varied structures that can host a broad range of physical and mechanical characteristics (e.g. Apuani et al., 2005a; Moon et al., 2005; del Potro & Hürlimann, 2008; Schaefer et al., 2015; Cook et al., 2018; Schaefer et al., 2018). Material is often classified and mapped by the character of its physical and mechanical properties into specific geotechnical units for geotechnical consideration (e.g. Apuani et al., 2005a; del Potro & Hürlimann, 2008; Mordensky et al., 2018b). Small shallow intrusions are a common aspect and cause of mechanical variability in any volcanic domain (e.g. Sigurdsson et al., 2000; and references therein). Intrusions create mineralogical (e.g. Pola et al., 2012), physical (e.g. Wyering et al., 2015), and mechanical (e.g. Siratovich et al., 2016) changes through alteration. At the same time, the thermal and dynamic stresses induced by an intrusion can cause fractures that influence rock-mass and intact-rock properties (e.g. Mordensky et al., 2018a), and magmatic intrusion can modify the pore pressure of the hydrothermal system and host rock (Day, 1996).

Compressive deformation testing (e.g. uniaxial, triaxial) provides a means to observe mechanical behaviour under varied stress conditions (e.g. Hoek & Brown, 1980). Triaxial studies of the mechanical properties of volcanic materials have been completed across a range of compositions (e.g. Shimada, 1986; Kennedy et al., 2009; Smith et al., 2011; Loaiza et al., 2012; Violay et al., 2012; Adelinet et al., 2013; Heap et al., 2015a; Violay et al., 2015; Heap & Wadsworth, 2016); however, studies on the mechanical rock properties of altered volcanic material (e.g. Heap et al., 2015b; Siratovich et al., 2016) are rarer and there has

never been a comprehensive study detailing the triaxial mechanical properties of the differing altered volcanic geotechnical units related to the emplacement of a small shallow intrusion into a volcanic edifice nor the application of these data to volcanic stability modelling.

Slope stability modelling of a volcanic edifice requires understanding the geomechanical properties of the rocks composing an edifice (Schaefer et al., 2015; Cook et al., 2018; Schaefer et al., 2018) and distinguishing rock masses into geotechnical units by those geomechanical properties (Apuani et al., 2005a; Moon et al., 2005; del Potro & Hürlimann, 2008; Mordensky et al., 2018a; Mordensky et al., 2018b). When assessing volcanic edifice stability, it is important to understand the role of pore pressure. Prior research has found elevated pore pressure to be a major cause of volcanic instability (e.g. Elsworth, 1995; Day, 1996; Apuani et al., 2005b). Permeability reduction serves a means to inhibit subsurface fluid transport and, thereby, augment pore pressure. Mordensky et al. (2018b) found that alteration reduced permeability in altered brecciated lava margins and that hydrothermal veining had a lower permeability than the rock it replaced. Hence, by combining laboratory-based rock properties, rock mass assessments and stability modelling we assess whether pore pressures associated with hydrothermal alteration presents a viable means to lower the permeability, increase the pore pressure, and decrease the stability of a volcanic edifice.

Specifically, this paper describes the effect of varying effective confining stress on the strength and deformation of unaltered and hydrothermally altered volcanic material related to the emplacement of a small shallow intrusion exposed on the western flanks of Pinnacle Ridge, Mt. Ruapehu (New Zealand). Triaxial and tensile datasets are combined with uniaxial compression strength (UCS) data from Mordensky et al. (2018b) and Geological Strength Index observations (GSI) from Mordensky et al. (2018a). By doing so, we present the first comprehensive suite of geotechnical parameters to describe the geotechnical units surrounding and related to the emplacement of a small shallow intrusion and its subsequent alteration in a volcanic environment. We then use finite element modelling with the Generalised Hoek-Brown failure criterion to model and discuss the stability of Pinnacle Ridge with its current topography. We also consider a similar volume intrusion at depth (~500 m) considering the implications of varying pore pressure for the present day active Ruapehu system. We emphasise that these models serve primarily as a proof of concept to demonstrate the susceptibility of the weakest geotechnical unit (i.e. hydrothermal vein material) to pore pressure variation and that the pore pressure distribution used in the modelling (i.e. decreasing toward the surface) may not accurately represent the pore pressure distribution in a shallow volcanic environment.

6.1.1 Pinnacle Ridge, Mt. Ruapehu, New Zealand

Mt. Ruapehu is an active andesitic stratovolcano on the North Island of New Zealand. Located at the southern end of the Taupō Volcanic Zone (TVZ), Mt. Ruapehu is the southernmost volcanic center on the 1375-km Tonga-Kermadec volcanic arc, which is a product of oblique subduction of the Pacific plate beneath the Indian-Australian plate (Cole, 1990). Pinnacle Ridge is found on the northwestern flank of Mt. Ruapehu and defines the western boundary of the popularly visited Whakapapa Ski Field. Constituting part of the Te Herenga Formation, the oldest (250 *ka*) geological unit exposed on Mt. Ruapehu, Pinnacle Ridge has also been subject to several intrusive events and associated hydrothermal systems, which altered the volcanic host rock, before being glacially dissected ~10 *ka*, exposing the once internal structure of a shallow subsurface igneous intrusive system. The intrusion is surrounded by a ~400 m-diameter alteration halo containing sulphides, suggesting shallow alteration depths (< 500 m; Houghton et al., 1987), and light to heavy, advanced argillic alteration consistent with epithermal conditions (Mordensky et al., 2018b).

The combination of intrusion-related alteration and glacial carving has created a complex of steep volcanic talus slopes and cliffs with varying jointing orientations in the host rock and intrusion. Mordensky et al. (2018b) defined, mapped, and characterised the intact rock properties (e.g. porosity, permeability, P-wave velocity, S-wave velocity, UCS) for the seven geotechnical units of Pinnacle Ridge: 1) unaltered brecciated lava margin (UBLM); 2) altered brecciated lava margin (ABLM); 3) unaltered dense coherent lava (UDCL); 4) altered dense coherent lava (ADCL); 5) unaltered intrusion (UI); 6) altered intrusion (AI); and 7) hydrothermal vein (HV). Mordensky et al. (2018a) completed rock mass descriptions of these geotechnical units by detailing the *in situ* macro discontinuity characteristics by three methods: 1) the Geological Strength Index (as described in Marinos & Hoek, 2000; Hoek et al., 2013); 2) Rock Mass Rating (as described in Bieniawski, 1989); and 3) scanline transect methods (as described in Manda & Mabee, 2010) for the geotechnical units. Although Mordensky et al. (2018a) modelled the rock mass strength of UBLM and ABLM, several assumptions (i.e. parameters within the Generalised Hoek-Brown Failure Criterion) were made because of the lack of published laboratory data for the geotechnical units. This manuscript summarises data from Mordensky et al. (2018b) and Mordensky et al. (2018a) along with the additional triaxial and tensile strength data presented herein to supply a complete analytical parameter suite to model the geomechanical effects of a small shallow intrusion into a volcanic rock mass.

6.2 Methods

6.2.1 Sample locations

Cylindrical intact-rock samples (40 mm in length × 20 mm in diameter) for UI, AI, UBLM, and HV from Pinnacle Ridge (Fig. 6.1) were collected and their physical properties (e.g. porosity, density, permeability, P-wave velocity, and S-wave velocity; for property values and uncertainty see Table S1) were characterised in Mordensky et al. (2018b). In order to provide volcanic material for all the geotechnical units of Pinnacle Ridge, we collected and characterised additional samples for UDCL, ADCL, UBLM, and ABLM (Fig. 6.1) using methods consistent with Mordensky et al. (2018b).

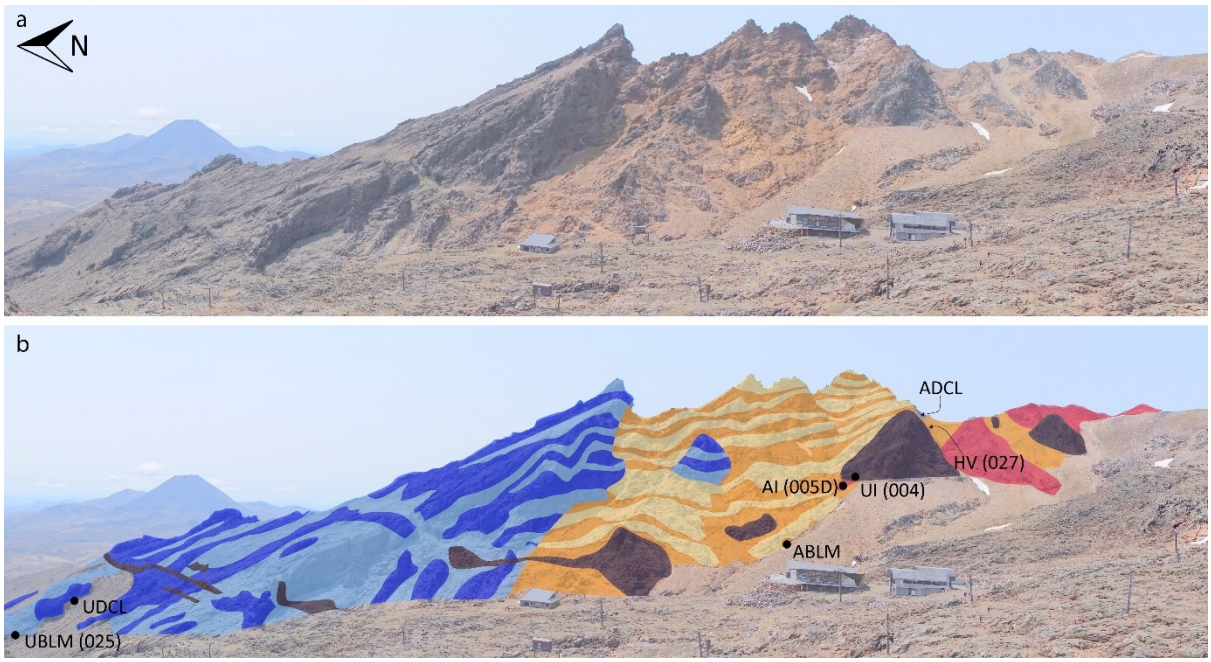

Figure 6.1 Pinnacle Ridge (a) Photo of Pinnacle Ridge taken from ~600 m east (bearing 270°) of the largest intrusion of Pinnacle Ridge. North is frame-left. (b) Geotechnical unit overlay from Mordensky et al. (2018b) with sample locations for UDCL, UBLM, ADCL, ABLM, UI, AI, HV. Sample locations ADCL and HV are located behind the largest, young intrusion as indicated by arrows.

6.2.2. Triaxial deformation and strength

Varying the effective confining stress imposed upon a rock during compression strength testing provides the means of understanding mechanical rock properties over a range of stress conditions (Mogi, 1966; Hoek, 1968). The Pinnacle Ridge samples were tested under conventional triaxial conditions ($\sigma_1' > \sigma_2' = \sigma_3'$; in which σ_1' is the major effective principal stress, σ_2' is the intermediate effective stress, and σ_3' is the minor effective principal stress) at a constant strain rate (1.0×10^{-5} s^{-1}). The sample sets were confined using a Hoek cell and deformed with a Technotest loading frame at the University of Canterbury. Axial stress and strain

were recorded using a load cell and a linear variable differential transducer (LVDT), respectively. Note that we use the convention that compressive stresses are positive and tensile stress are negative, as is common practice in geological applications.

The Hoek cell used at the University of Canterbury is one of the most commonly used types of pressure vessels in rock mechanics testing (e.g. Smart, 1995). The Hoek cell applies σ_2 and σ_3 by fluid pressure contained in a sleeve around the cylindrical sample (Hoek & Franklin, 1968; Franklin & Hoek, 1970). The maximum principal stress, σ_1 is applied by the loading frame on the steel platens located at either end of the Hoek cell with the sample deformed between the platens. It is important to note that the Hoek cell does not vary pore pressure, which is negligible at atmospheric conditions (~0.1 MPa).

To simulate varying depths (0 to < 500 m), σ_3' was varied (1 – 20 MPa) by changing the confining stress (i.e. the minor effective stress [σ_3]) in accordance with a simple effective pressure law (Equation 1):

$$\sigma_3' = \sigma_3 - \alpha\sigma_P \quad (1)$$

In which Farquharson et al. (2016a) found α, the effective stress coefficient, is unity for porous andesites. The rocks in the study also include altered andesite and hydrothermal vein material (e.g. albite, kaolinite, and smectite). Although α for altered andesite and hydrothermal vein material has not been specifically studied, existing research (e.g. Baud et al., 2015) has found that α = 1 for other rock types as well; therefore we assume α = 1 for all samples.

6.2.3 Indirect tensile strength testing

Brazilian strength testing, a simple indirect tensile strength test, was used to acquire the tensile strength for each of the geotechnical units. In the Brazilian strength test, a circular disk, 40 mm in diameter and optimally ground 20 to 24 mm in length, is diametrically loaded (Ulusay & Hudson, 2007). The compression produces tensile stress normal to the loading axis until tensile forces corresponding to Equation 2 induce failure (Akazawa, 1943; Carneiro, 1943):

$$\sigma_t = \frac{2P}{\pi D t} \quad (2)$$

In which σ_t is the calculated tensile strength, P is the load at failure, D is the diameter of the specimen, and t is thickness of the test specimen (Perras & Diederichs, 2014).

6.2.4 Geotechnical parameters

Geotechnical parameters were derived from the Generalised Hoek-Brown Failure Criterion (Equation 3) as detailed in Hoek and Brown (1980) with subsequent updates described in Eberhardt (2012) and Hoek et al. (2013):

$$\sigma_1' = \sigma_3' + C_o\left(m_b\frac{\sigma_3'}{C_o} + s\right)^a \tag{3}$$

C_o is the mean uniaxial compressive strength for intact rock, and D is the damage index associated with excavation. Note that for natural slopes D is 0. s, a, and m_b are material constants calculated using Equations 4, 5, and, 6 respectively:

$$s = exp\left(\frac{GSI - 100}{9 - 3D}\right) \tag{4}$$

$$a = \frac{1}{2} + \frac{1}{6}\left(e^{-GSI/15} - e^{-20/3}\right) \tag{5}$$

$$m_b = m_i \exp\left(\frac{GSI - 100}{28 - 14D}\right) \tag{6}$$

In which GSI is a rock mass classification index (Hoek et al., 2013) for which the data were obtained from Mordensky et al. (2018a) and m_i is a material constant derived from the Hoek-Brown criterion for intact rock (Equation 7) as described in Hoek (1968) using the triaxial data collected in this study.

$$\sigma_1' = \sigma_3' + C_o\left(m_i\frac{\sigma_3'}{C_o} + 1\right)^{0.5} \tag{7}$$

A curve was fit to the intact rock deformation data using a Modified Cuckoo fit algorithm with residuals calculated by the vertical distance between the curve and intact rock test data using the RocScience software RocData©. It is worth noting that the Hoek-Brown failure criterion applies only to brittle rock failure and precludes ductile behaviour.

The Generalised Hoek and Diederichs equation (Equation 888) was used to derive the rock mass deformation modulus (Hoek & Diederichs, 2006).

$$E_{rm} = E_i\left(0.002 + \frac{1 - D/2}{1 + e^{((60+15D-GSI)/11)}}\right) \tag{8}$$

Where E_{rm} is the elastic modulus of the rock mass and E_i is the elastic modulus of the intact rock.

6.2.5 Modelling

Photogrammetric modelling was used to create a three-dimensional topographic profile across Pinnacle Ridge. Photo imagery was collected using a Phantom 3 unmanned aerial vehicle with a 12.1-megapixel camera. The images were run in Agisoft Photoscan Professional © software to produce a digital elevation model (DEM). Twelve ground control points in combination with GPS tagging of all collected imagery calibrated dimensions and locations within the model. The DEM was exported to Seequent LeapFrog © to produce a topographic profile, which was then used to export to Rocscience RS^2 © for stability analysis.

Numerical finite element modelling was undertaken in RocScience RS^2 © with a plain strain analysis employing uncoupled solid-fluid interaction and a Gaussian Elimination solver type to test two scenarios: 1) the strength of the geotechnical units as they currently exposed at Pinnacle Ridge; and 2) the strength of the geotechnical units at ~500-m depth. The rock mass input parameters were derived from the Generalised Hoek-Brown failure criterion (Equation 3) and Hoek-Diederichs equation (Equation 8) for each geotechnical unit. Boundary conditions were set so that x- and y-boundaries were fixed. In the modelling of Pinnacle Ridge in its presently exposed topographic configuration, we assume a simple pore pressure gradient of 0 MPa at the surface interpolating to the targeted maximum pore pressure at the maximum depth of the model so as to prevent inelastic deformation in the rock masses at shallow subsurface conditions but allow elevated pore pressures at greater depths. In the second, hypothetical model, we test three scenarios: 1) a simple pore pressure gradient under hydrostatic conditions; 2) a scenario in which there is a pore pressure gradient under hydrostatic conditions until 400-m depth, where a hypothetical seal in the model increases pore pressure to 10 MPa below this depth; and 3) a pore pressure gradient in which pore pressures increase at a rate twice that of the hydrostatic with respect to depth. When we refer to elevated pore pressure, we are referring to pore pressures greater than the hydrostat. Pore pressures are imposed using a water pressure grid. Gravity provided the initial load conditions with all rock masses given a 0.027 MN/m^3 unit weight and an *in situ* stress ratio of 1. A graded mesh was discretised using 3-noded triangles with a default of 200 nodes on the external boundary. Dimensions of the geotechnical unit were determined by a combination of the DEM and field observation from Pinnacle Ridge.

The stability of each geotechnical unit is given by a strength factor. A strength factor > 1 indicates a rock mass strength greater than the induced stresses applied to it. Reciprocally, a strength factor < 1 indicates that the stresses acting on the rock exceed the rock mass strength, indicating the potential for inelastic deformation and failure of the rock mass.

6.3 Results and discussion

6.3.1 Physical rock properties

Before triaxial testing, physical rock properties (i.e. porosity, permeability, and elastic wave velocities) of the samples were characterised (Table 6.S1). UI and UDCL have the lowest porosities (0.71 – 3.52 % and 2.51 – 4.88 %, respectively) with correspondingly low permeability values (10^{-19} – 10^{-18} m^2) and high dry P-wave velocities (4625 – 4380 m/s and 4074 – 3521 m/s, respectively). UBLM has the highest porosity (25.40 – 30.38 %) and slowest dry P-wave velocity (1603 – 1937 m/s). ABLM, ADCL, AI, and HV have physical rock property values intermediate between the end-members defined by the unaltered geotechnical units.

6.3.2 Indirect tensile strength

We conducted 29 Brazilian (indirect tensile) strength tests to estimate tensile strength of the geotechnical units (Table 6.S2 with averages given in Table 6.1). These data are averaged by their geotechnical classification to provide the tensile cut-off strengths for the Hoek-Brown Failure Criterion. The unaltered geotechnical units (i.e. UDCL, UI, and UBLM) consistently have greater magnitude tensile strength (-10.18, -8.67, and -2.23 MPa, respectively) than their altered equivalents (ADCL, AI, ABLM; -1.91, -7.03, and -1.93 MPa, respectively). HV has a tensile strength (-4.74 MPa) intermediate between the altered and unaltered volcanic materials.

	Effective Confining Stress (MPa)									
Geotechnical Unit	0.5	1	2	3	5	6	10	15	20	Tensile Strength (MPa)
UI					189			319	329	-8.67
AI					82			124	169	-7.03
ABLM			35	50	*36*	*45*	*71*		*95*	-1.93
UBLM	6	12	*11*		*17*			*22*	*23*	-2.23
UDCL					176		326	357	469	-10.18
ADCL					135		195	221	194	-1.91
HV					59			109	112	-4.74

Table 6.1 Triaxial compression test results (peak stress for brittle, initiation of inelastic strain for ductile) for Pinnacle Ridge samples according to geotechnical unit. Italicised data represent ductile deformation behaviour and are not used in the criterion. Tensile strength data are averaged from indirect Brazilian strength test data (see Table 6.S2). Standard Error ≤ 1% of the reported values.

6.3.3 Triaxial deformation

Twenty-six samples were tested under triaxial compression such that 3 – 6 triaxial tests were completed for each geotechnical unit (Table 6.S3). In this study, we use the term yield strength to refer to the peak differential stress ($\sigma_1' - \sigma_3'$) in experiments in which inelastic deformation initiated with strain softening

(i.e. a decrease in differential stress following peak differential stress; that is, brittle behaviour) or the differential stress at which elastic behaviour transitioned to inelastic strain hardening (i.e. a departure from the initial, linear section of the stress-strain curve associated with elastic deformation; that is, ductile behaviour) following practices in engineering geology nomenclature (e.g. Gonzalez de Vallejo & Ferrer, 2011). In general, higher effective confining stress produced higher yield strength for each geotechnical unit (Fig. 6.2; Table 6.1).

Five of the seven geotechnical units exhibit no change in deformation mode under the triaxial conditions of this study. Relatively low-porosity samples (i.e. UI, AI, UDCL, and ADCL) yielded by brittle deformation characterised by strain softening at all observed confining stresses. HV expressed moderate strain softening before transitioning into strain hardening at higher strain at the lowest effective confining stress.

Unlike the other geotechnical units, the failure modes of UBLM and ABLM, which have relatively high porosity (26 – 31 % and 17 – 26 %, respectively) are dependent on changes that occur under low effective confining stress conditions (σ_3' = 0 – 5 MPa). We observe strain softening in UBLM between σ_3' = 0.5 – 1 MPa and strain hardening at $\sigma_3' \geq 2$ MPa. We observe strain softening in ABLM between σ_3' = 2 – 3 MPa and near perfectly plastic behaviour at $\sigma_3' \geq 5$ MPa. Therefore, a < 2 MPa change in σ_3' is sufficient to change the failure mode of UBLM and a < 5 MPa change in σ_3' is sufficient to change the failure mode of ABLM.

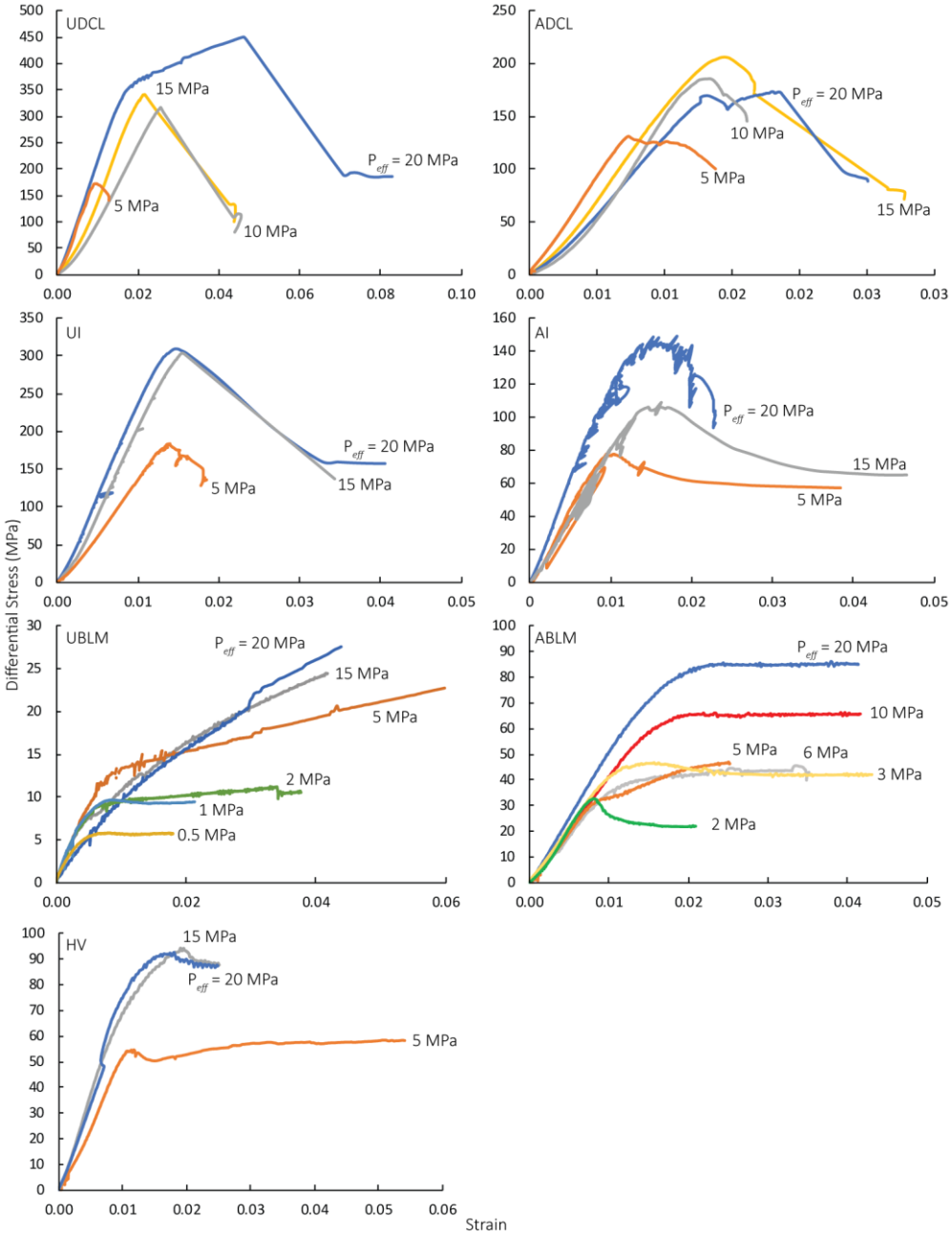

Figure 6.2 Differential stress versus strain at varying effective confining stresses.

6.3.4 Geotechnical parameters

The triaxial data and UCS data from Mordensky et al. (2018b) for each geotechnical unit are plotted with their Hoek-Brown failure criterion fits in Fig. 6.3a. The intact rock geotechnical parameters, C_o and m_i derived from the Hoek-Brown failure criterion Equation 7, as well as E_i from Mordensky et al. (2018b), are summarised in Table 6.2. We then used the corresponding GSI data from Mordensky et al. (2018a) to determine the rock mass strength (Fig. 6.3b) and stiffness parameters using the Generalised Hoek-Brown failure criterion Equations 3-6 and the Hoek-Diederichs (Equation 8), respectively (Table 6.2). We derived

the equivalent Mohr-Coulomb parameters for each geotechnical rock mass (Table 6.2), cohesion (c) and friction angle (ϕ) by fitting to the Generalised Hoek-Brown failure criterion according to Equations 9 and 10 (see Hoek & Brown, 1997).

$$c = \frac{\sigma_c}{2\sqrt{k}} \tag{9}$$

$$sin\ \phi = \frac{k-1}{k+1} \tag{10}$$

Where k is the slope of the line relating σ_1' and σ_3' and σ_c is the uniaxial compressive strength of the rock mass (Equation 11).

$$\sigma_c = \mathrm{C}_O + s^a \tag{11}$$

We also report the equivalent rock mass tensile strength (σ_T) and global rock mass compressive strength (σ_{cm}), according to Equations 12 and 13 (see Hoek et al., 2002; and references therein).

$$\sigma_T = \frac{C_O}{2}\left(m_b - \sqrt{m_b^2 + 4s}\right) \tag{12}$$

$$\sigma_{cm} = \frac{2c \times \cos\phi}{1 \times \mathrm{sen}\,\phi} \tag{13}$$

The C_O values of UI and UDCL are greater than their altered equivalents, AI and ADCL (Table 6.2), whereas the C_O value of UBLM is less than its altered equivalent, ABLM. In general, m_i values are at least one order of magnitude greater than m_b values (Table 6.2). Similarly, C_O values are one to several orders of magnitude greater than that of σ_c. Although σ_c maintains similar relationships between corresponding unaltered and altered geotechnical units as the intact rock C_O, the m_b relationships are not the same as for m_i (Table 6.2). This is because GSI affects different components of the Generalised Hoek-Brown failure criterion differently.

6.3.5 Ductile deformation and the Hoek-Brown failure criterion

The difference between brittle and ductile deformation of a material is commonly considered as a first-order distinction when describing rock deformation from an engineering perspective (e.g. Gonzalez de Vallejo & Ferrer, 2011). Byerlee (1968) distinguishes between brittle behaviour as a decrease in compressive strength following the onset of inelastic deformation and ductile as no loss in compressive strength following the onset of inelastic deformation. However, in other contexts (e.g. rock physics) the defining specifics of brittle and ductile vary (e.g. Rutter, 1986; Wong & Baud, 2012). In our study providing

geomechanical parameters for engineering geology concepts, we ascribe to the distinction provided by Byerlee (1968) and Gonzalez de Vallejo and Ferrer (2011).

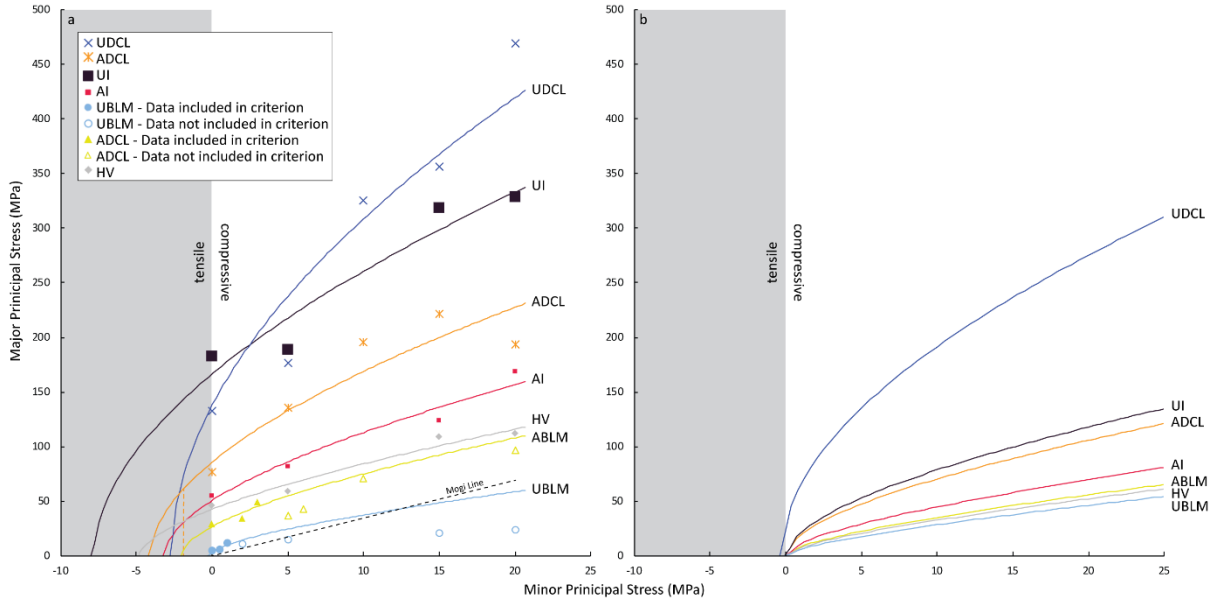

Figure 6.3 (a) Intact Hoek-Brown failure criteria. Orange vertical dashed line is ADCL tensile strength cut-off. Filled data points indicate (brittle) data used to derive the criterion. Hollow points (e.g. UBLM and ABLM) indicate (ductile) data not used to derive the criterion. Mogi Line provides brittle-ductile transition from Mogi (1966). (b) Generalised (rock mass) Hoek-Brown failure criteria for all geotechnical units.

Ductile deformation is not applicable for the Hoek-Brown failure criterion (Hoek & Brown, 1997; Bewick & Kaiser, 2013). Therefore, m_i was calculated from tests that exhibited brittle (i.e. strain softening) behaviour (Figs. 6.2, 6.4). We also compared our results with the Mogi line (Fig. 6.3a). The Mogi line (Mogi, 1966) is a 3.4:1 ratio between major and minor principal stresses and serves as a measure of the brittle-ductile transition in rock (e.g. Bewick & Kaiser, 2013). Test results plotting below this line are expected to be ductile, and test results plotting above are expected to be brittle. It is worth noting, we find that both UBLM and ABLM produced ductile test results that plot above the Mogi line. Hence, the Mogi line may not serve as an accurate model for determining brittle-ductile behaviour in primary or altered volcanics. We saw no evidence of brittle behaviour in any of the results that plot below the Mogi line.

Geotechnical Unit	Intact Rock Hoek-Brown Failure Criterion				Generalised Hoek-Brown Criterion Failure Criterion				Derived Mohr-Coulomb for x m high slope		Rock Mass Mechanical Parameters			
	σ_{ci} (MPa)	m_i	Ei (GPa)	Residuals (MPa)	GSI	m_b	a	s	ϕ (°)	c (MPa)	σ_c (MPa)	σ_{cm} (MPa)	σ_t (MPa)	E_{rm} (GPa)
ABLM	28	13	8.4	49	35 - 70 (53)	2.4	0.505	0.0054	33	1.5	2	5.8	-0.06	3.1
ADCL	87	20	21.5	2386	30 - 75 (56)	4.3	0.504	0.0075	39	5.9	7	24.3	-0.15	9.2
AI	52	16	9.4	329	37 - 60 (48)	2.4	0.507	0.0031	34	2.9	3	10.7	-0.07	2.5
HV	43	9	9.1	132	41 - 51 (46)	1.2	0.508	0.0025	28	1.9	2	6.4	-0.09	2.2
UBLM	4	17	1.6	6	77 - 80 (79)	8.0	0.501	0.0970	44	0.4	1	1.9	-0.05	1.4
UDCL	141	50	24.1	6762	65 - 90 (78)	22.8	0.501	0.0868	52	16.1	41	94.2	-0.54	20.7
UI	168	21	38.0	1517	20 - 70 (45)	2.9	0.508	0.0022	35	9.7	8	37.7	-0.13	8.5

Table 6.2 Summary of geotechnical parameters. σ_{ci} — modelled UCS from intact Hoek-Brown failure criterion; m_i — material constant derived from Equation 7; E_i – Elastic modulus of intact rock; GSI—Geological Strength Index; m_b — material constant derived from Equation 6; a —material constant derived from Equation 5; s — material constant derived from Equation 4; φ — friction angle; c — cohesion; σ_c — uniaxial strength of rock mass; σ_{cm} — global strength (see Hoek et al. (2002)); σ_T — tensile strength of rock mass; E_{rm} — elastic modulus of rock mass; Residual — Residual error between the failure envelope and the lab data.

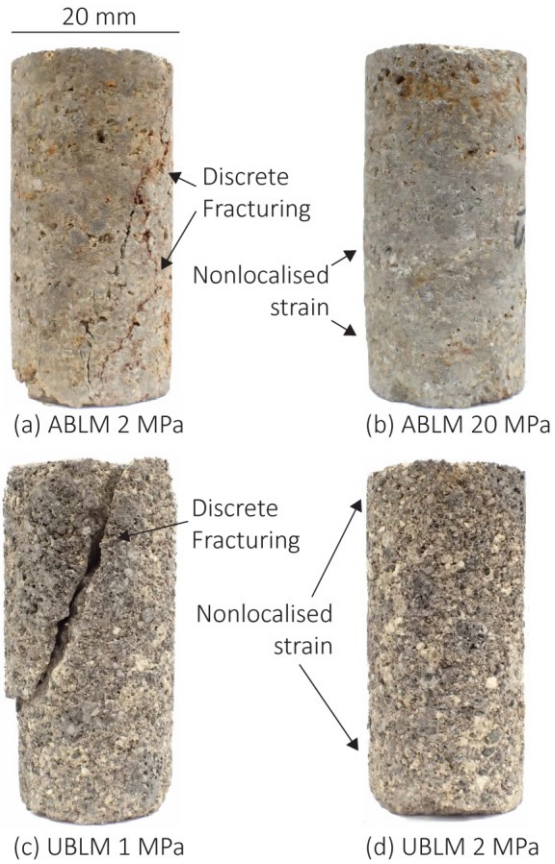

Figure 6.4 Post-deformation core images. (a) ABLM deformed brittlely at P_{eff} = 2 MPa. Strain accommodated by discrete fractures. (b) ABLM deformed ductilely at P_{eff} = 20 MPa. Strain remains nonlocalised across length of sample. (c) UBLM deformed brittlely at P_{eff} = 1 MPa. Strain accommodated by discrete fractures. (d) UBLM deformed ductilely at P_{eff} = 2 MPa. Strain remains nonlocalised across length of sample.

6.4 Edifice stability modelling

6.4.1 Numerical modelling the effect of pore pressure variation with current topography

We first consider the effect of pore pressure in present-day Pinnacle Ridge. We use a cross-section of Pinnacle Ridge intersecting the largest young intrusion at Pinnacle Ridge (Fig. 6.5a,f,k). We model the effect of different pore pressures with (Fig. 6.5a,b,c,d,e) and without (Fig. 6.5f,g,h,i,j) the HV geotechnical unit as described in Mordensky et al. (2018b).

In the scenario without HV, the brecciated lava margins (e.g. UBLM and ABLM) have a noticeable drop in strength factor as σ_P is increased from 0 MPa to 0.5 MPa, while UI, AI, UDCL, and ADCL are not greatly affected (Fig. 6.5b,c). Although strength factors decrease as σ_P is increased to 1 MPa, strength factors remain > 1 (Fig. 6.5d); however, when σ_P = 2 MPa, all geotechnical units have a strength factor < 1 (Fig. 6.5e) in the shallow portions of the ridge.

In the scenario with the prominent hydrothermal vein, all geotechnical units except HV express similar behaviour as the scenario without the hydrothermal vein; however, HV consistently exhibits a lower strength factor at greater depths than the other geotechnical units. When σ_p = 0 MPa, the section of HV with a strength factor < 1 is 10s of m deep. When σ_p = 2 MPa, HV has a strength factor less than 1 from the surface to 100+ m into the ridge. This scenario presents the potential for a seemingly small change in pore pressure to destabilise the ridge and mobilise several hundred cubic metres of rock.

6.4.2 Numerical modelling pore pressure variation at depth at an active portion of Ruapehu

Before comparing the results of our study to that of others' research and the consequential implications, we consider one more scenario of elevated pore pressure conditions on hydrothermally altered material at an active magmatic system at depth. In this scenario, we model the effect elevated pore pressure would have had on the hydrothermal system shortly after forming. We assume a depth of ~500 m as suggested by Hackett (1985). We use ABLM, ADCL, UI, AI, and HV as our rock mass materials.

In Fig. 6.6 we present a finite element model depicting a geological environment similar to that mapped by Mordensky et al. (2018b) and presented in Fig. 6.1. That is, there is an intrusion (UI) at a depth surrounded by interlayered ADCL and ABLM and adjacent to a minor volume of AI (Fig. 6.6a). An HV vein runs ~50 m on one side of UI. However, the model assumes the top extent of UI to be at ~500 m depth rather than daylighting at the surface (e.g. Fig. 6.5). At 500-m depth, pore pressure resulting from the hydrostat is near 5 MPa. We consider a maximum pore pressure up to 10 MPa at these depths as a reasonably conservative estimate of potential pore pressures in a volcanic system, because confined volcanic systems can host pore pressures exceeding several tens of megapascals (see Chugh, 1981; Day, 1996; Newhall et al., 2001). Therefore, we consider three conditions: 1) the system under simple hydrostatic conditions (σ_p = 0 MPa at the surface and interpolates to σ_p = 6 MPa at 600-m depth; Fig. 6.6c); 2) the system with a seal at 400-m depth that inhibits outgassing below these depths (σ_p = 0 MPa at the surface and interpolates to σ_p = 4 MPa at 400-m depth, but then is 10 MPa below 400-m depth; Fig. 6.6d); and 3) a scenario similar to 6.6c, but with outgassing inhibited at the surface so that pore pressure increases at twice the rate of the hydrostat (σ_p = 0 MPa at the surface and increases linearly to σ_p = 12 MPa at 600-m depth (Fig. 6.6e). Under all pore-pressure conditions, the UI, AI, ADCL, and ABLM have a strength factor > 5, while HV has a lower strength factor with greater variability between the imposed pore pressures (Fig. 6.6c,d,e). In the scenario with hydrostatic conditions at all depths (Fig. 6.6c), HV has a strength factor > 1. In the scenarios with elevated pore pressures (pressure greater than the hydrostat), HV has a strength of < 1 as pore pressures exceed the hydrostat.

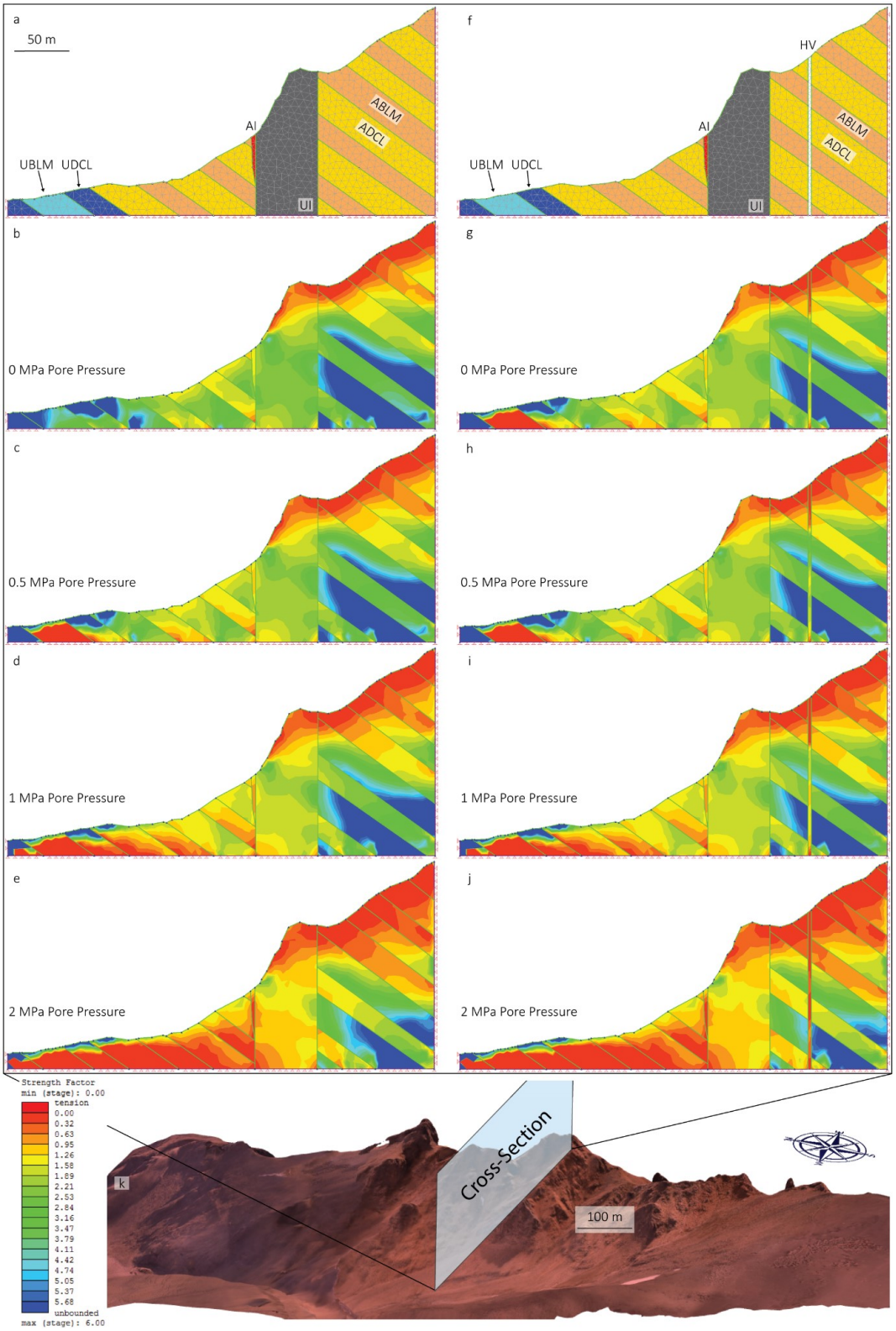

Figure 6.5 Pinnacle Ridge depicted by geotechnical units with (a) and without (f) a hydrothermal vein and the strength factors for its geotechnical units at σ_p = 0 MPa (b,g), σ_p = 0.5 MPa (c,h), σ_p = 1 MPa (d,i), and σ_p = 2 MPa. The cross-section of the ridge runs from the crest of Pinnacle Ridge through the western face of the large, young intrusion (k).

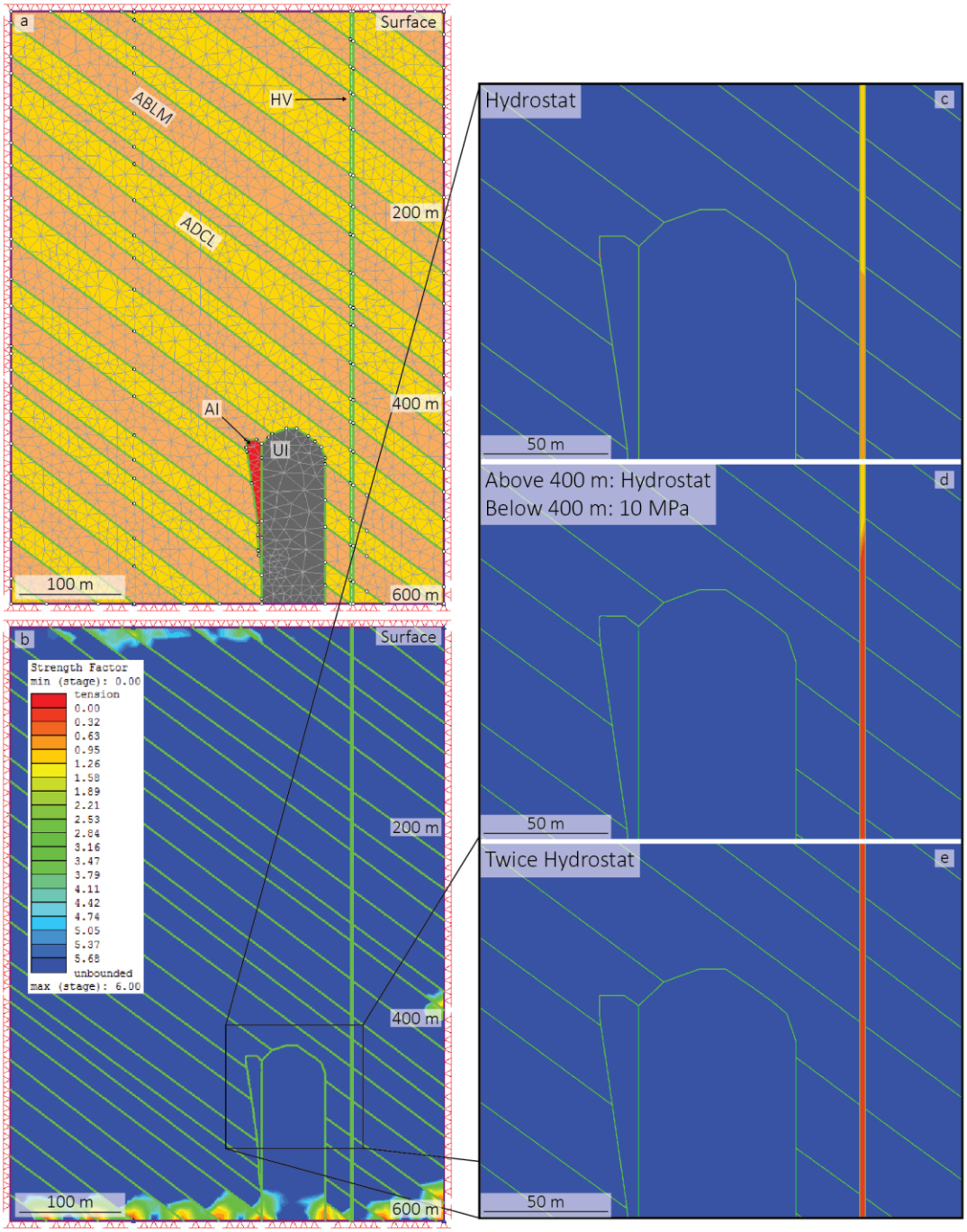

Figure 6.6 (a) Small intrusion at depth (~500 m) depicted by the geotechnical units of Pinnacle Ridge. (b) Strength factor modelled by RocScience RS² © of same rock mass as frame (a) under hydrostatic conditions. UI, AI, UBLM, and ABLM appear to have a strength factor > 5. Lower strength factors at edges of model frame are boundary effects. Note that the strength factor of HV is unobservable due to the scale. (c) Inset of region encompassing HV, UI, and AI from frame (b). σ_p is set to hydrostatic conditions. (d) Inset of the same rock mass as frame (c) but with σ_p set to hydrostatic conditions from the surface to 400-m depth and then 10 MPa below 400-m depth. HV has a strength factor of less than 1 at > 400-m depth, indicating that HV would fail below this depth. (e) Inset of the same rock mass as frame (c) and (d) but with σ_p at twice that imposed under hydrostatic conditions. HV has a strength factor less than 1, indicating that this geotechnical unit will have failed. The strength factor of the other geotechnical units remains > 5.

6.5 Implications

The numerical models presented in Figs. 6.5 and 6.6 do not serve as true slope-stability analyses of Pinnacle Ridge, but they depict the destabilising influence of a hydrothermal vein on a rock mass and that a minor increase in pore pressure (0.5 – 10 MPa) can lead to rock mass failure.

Mordensky et al. (2018b) reported that for its strength, HV had relatively low permeability when compared to the other geotechnical units. In other words, HV serves not only as a plane of weakness within an altered zone but also as a means to inhibit outgassing and augment pore pressure. Previous research has demonstrated that hydrothermally altered material weakens an edifice (e.g. Watters et al., 2000). We expand from this using the numerical models (Figs. 6.5, 6.6) presented in this study to demonstrate that suitably weak hydrothermal veins can produce a greater effect on stability than the loss of strength of altered volcanics.

The effect of elevated pore pressure presented in our numerical models (Figs. 6.5, 6.6) is consistent with results of Day (1996) and Apuani et al. (2005b) in that elevated pore pressure reduces the stability of a volcanic edifice. Change in pore pressure could be brought about by a variable gas flux from a magma body (e.g. Rye, 1993; Wallace, 2005) or a decrease in permeability of the host rock (e.g. Farquharson et al., 2017b; Schaefer et al., 2018).

Another means of discussing deformation behaviour is using the terms dilatant and compactant. Dilatant and compactant behaviour refers to the increase or decrease, respectively, in the porosity of the rock in response to stress (e.g. Read et al., 1995; Wong & Baud, 2012; Heap et al., 2015a). Under low effective confining stress conditions, rocks dilatantly fail (e.g. axial splitting, shear failure) regardless of intact-rock porosity (e.g. Faulkner, 2006). Under high effective confining stress, low-porosity rocks still fail dilatantly, but high-porosity rocks experience compaction through cataclastic pore collapse and grain crushing (e.g. Kennedy et al., 2009; Zhu et al., 2011; Loaiza et al., 2012; Wong & Baud, 2012; Adelinet et al., 2013; Heap et al., 2014; Heap et al., 2015b). Deformation behaviour can play a role in determining permeability (Farquharson et al., 2016b; Farquharson et al., 2017a). Generally, an increase in porosity is associated with an increase in permeability in volcanic material (e.g. Klug & Cashman, 1996; Rust & Cashman, 2004; Mueller et al., 2005; Mueller et al., 2008; Wright et al., 2009; Rust & Cashman, 2011; Farquharson et al., 2015; Kushnir et al., 2016; Heap et al., 2017; Mordensky et al., 2018b). Consequently, deformation behaviour is critical to understanding the outgassing behaviour and, thereby, eruptive behaviour of a volcanic system (i.e. explosive versus effusive behaviour; e.g. Upton & Wadsworth, 1970; Woods & Koyaguchi, 1994; Sparks, 1997; Kennedy et al., 2016).

Heap et al. (2015a) associated dilatant behaviour with strain softening and compactant behaviour with an absence of significant strain softening in andesitic lavas. We observe that alteration changes the deformation mode of the brecciated lava margins at low σ_3' (< 5 MPa). Specifically, we observe a transition from substantial drops in peak differential stress during the UCS testing from Mordensky et al. (2018b) to strain hardening in UBLM at lower effective confining stress (1 – 2 MPa) than in ABLM (3 – 5 MPa; Fig. 6.2). We, therefore, interpret the strain hardening of UBLM at > 1 MPa and ABLM at > 3 MPa as strong evidence of compactant behaviour. When considered in conjunction with porosity-change deformation studies (e.g. Heap et al., 2015a; Farquharson et al., 2017a), our stress-strain data (Fig. 6.2) suggest that some geotechnical units (e.g. UBLM and ABLM) may further compromise the strength of HV by decreasing permeability during inelastic deformation and thereby augment pore pressure. The reduction in permeability reduces outgassing potential (e.g. Richard et al., 2013) and presents not just a higher likelihood of explosive eruptions (e.g. Sparks, 1997) but of increased compartmentalisation within the edifice leading to higher pore pressure (e.g. Day, 1996).

Given sufficiently high pore pressure, volcanic material at depth can change its deformation mode from compactant to dilatant as a function of decreasing σ_3' (e.g. Farquharson et al., 2016a). The fractures resulting from the dilatant behaviour present a high likelihood of increasing rock mass permeability (e.g. Raven & Gale, 1985; Heap & Kennedy, 2016; Lamur et al., 2017), decreasing pore pressure and, thus, increasing effective confining stress. In other words, sufficient pore pressure presents the potential to induce a negative feedback loop within the system (e.g. Heap & Wadsworth, 2016). However, it is worth noting the strength factor of HV decreased to < 1 (Fig. 6.6e) while that of the other geotechnical unit remained > 5 (Fig. 6.6b,e). Hence, an increase in pore pressure sufficient to cause failure within HV may not be sufficient initially to induce failure in the other rock masses. At Pinnacle Ridge, the hydrothermal vein in Mordensky et al. (2018a), Mordensky et al. (2018b), and this study is not presently oriented sufficiently to induce failure of the slope. However, depending on the dimensions and orientation of the other geotechnical units, the geomorphology of a volcano, and the kinematics at play, the failure of HV may cascade into a large edifice collapse or lahar generation (e.g. Cook et al., 2018; Schaefer et al., 2018). In an effort to understand these comparisons, we emphasise the need for additional research on this subject.

It is worth consideration that the thin and continuous nature of hydrothermal veins may mean that motion may not be sustained if failure initiated solely in hydrothermal veins; however, we highlight that the residual strengths of indurated and non-indurated rocks are generally lower than their peak strengths (see Elsworth & Voight, 1995). Furthermore, the low permeability (as low as 10^{-18} m^2) of hydrothermal vein

material (Mordensky et al., 2018b) may foster an undrained environment in which excess pore pressure may build despite the degree of inelastic deformation. Frictional heat during initial failure may provide yet another means to augment pore pressure and decrease strength that could lead to larger, edifice-scale ramifications (Voight & Faust, 1982). Should initial failure occur in the hydrothermal vein material, there is means for this failure to cascade to the edifice scale. Finally, seismicity, ubiquitously common to volcanic environments (see Zobin, 2012), increases the likelihood for hydrothermal vein material to serve as means to destabilise other rock masses (see Hoek et al., 2013).

We note the importance of careful observation when completing rock mass characterisation. In the modelling we conduct, GSI represents the most likely means by which rock mass strength may be inaccurately determined. In addition to variation in GSI having a relatively stronger impact on modelled rock mass strength than variations in the other parameters (see Villeneuve et al., 2018), the other parameters involved in the Generalised Hoek-Brown failure criterion (i.e. C_o, s, a, and m_i) can be compared and checked to subsequent uniaxial and triaxial deformation tests. GSI, however, relies upon qualitative assessment by experienced geotechnical personnel. Inaccurately characterising a rock mass will substantially influence the modelled rock mass strength as rock mass strength changes exponentially with changes in GSI values (e.g. Thomas et al., 2004).

We conclude that a shallow intrusion can make host rock more vulnerable to rock mass failure by a combination of alteration of the primary volcanics and deposition of hydrothermal veins. Both processes present the potential to decrease the overall permeability of the edifice (e.g. Table 6.S1; Mordensky et al., 2018b). The hydrothermal veining in particular represents the weakest rock mass within the alteration halo (Figs. 6.2, 6.3) and can serve as a plane of weakness in the edifice that could lead to the displacement of a large volume of rock. The hazard imposed by hydrothermal veining is further exacerbated by elevated pore pressures that could result from strain on the surrounding rock masses.

6.6 Conclusions

This study presents and discusses triaxial deformation strength data of the seven geotechnical units of Pinnacle Ridge, Mt. Ruapehu, New Zealand in which a small shallow intrusion variably altered primary andesitic material to advanced argillic smectitic and kaolinite clays in a small epithermal system. Using these data in combination with lab and field data from other Pinnacle Ridge studies, we use numerical modelling to demonstrate that hydrothermal vein material is the weakest rock mass of the hydrothermally altered rocks and presents a risk of failure at elevated pore pressures. Ductile deformation and the likely resulting compactant deformation in the brecciated lava margins at low effective confining pressure

exacerbates this risk. Although hydrothermal veins are a seemingly trivial volume of rock, its failure could destabilise larger rock volumes. Therefore, advanced argillic alteration serves as a critical element when modelling the stability of andesitic volcanoes. Additionally, the presented physical, mechanical, and geotechnical properties will facilitate modelling of other systems for which data may not be so readily accessible (e.g. active subsurface systems).

6.7 Acknowledgements

Thank you to Hollei Gabrielsen, Harry Keys, and Blake McDavitt from the New Zealand Department of Conservation, and we would like to acknowledge the people of Ngāti Tūwharetoa and Ngāti Rangi for their support of our work at Mt. Ruapehu. This work has also benefitted from discussions with Jim Cole. The authors of this study acknowledge the support of the UC Doctoral Scholarship and the UC Mason Trust Fund. This research was supported by the "Quantifying exposure to specific and multiple volcanic hazards" program of the New Zealand Natural Hazards Research Platform (NHRP).

6.8 References

Adelinet, M., Fortin, J., Schubnel, A., & Guéguen, Y. (2013). Deformation modes in an Icelandic basalt: From brittle failure to localized deformation bands. *Journal of Volcanology and Geothermal Research, 255*, 15-25. doi:10.1016/j.jvolgeores.2013.01.011.

Akazawa, T. (1943). New test method for evaluating internal stress due to compression of concrete: the splitting tension test. *Journal of Japan Society of Civil Engineers, 29*, 777-787.

Apuani, T., Corazzato, C., Cancelli, A., & Tibaldi, A. (2005a). Physical and mechanical properties of rock masses at Stromboli: a dataset for volcano instability evaluation. *Bulletin of Engineering Geology and the Environment, 64*, 419-431.

Apuani, T., Corazzato, C., Cancelli, A., & Tibaldi, A. (2005b). Stability of a collapsing volcano (Stromboli, Italy): limit equilibrium analysis and numerical modelling. *Journal of Volcanology and Geothermal Research, 144*(1-4), 191-210.

Baud, P., Reuschlé, T., Ji, Y., Cheung, C. S., & Wong, T. F. (2015). Mechanical compaction and strain localization in Bleurswiller sandstone. *Journal of Geophysical Research: Solid Earth*.

Bewick, R., & Kaiser, P. (2013). Discussion on "An empirical failure criterion for intact rocks" by Peng et al. (2013). *Rock Mech Rock Eng, 47*(2), 817-823.

Bieniawski, Z. T. (1989). *Engineering rock mass classifications: a complete manual for engineers and geologists in mining, civil, and petroleum engineering*. New York: John Wiley & Sons, Inc.

Byerlee, J. (1968). Brittle-Ductile Transition in Rocks. *Journal of Geophysical Research, 73*(14).

Carneiro, F. L. L. B. (1943). *A new method to determine the tensile strength of concrete. In: Paper presented at the Proceedings of the 5th meeting of the Brazilian Association for Technical Rules*. Paper presented at the Associac¸a˜o Brasileire de Normas Te´cnicas—ABNT.

Carrasco-Núñez, G., & Gomez-Tuena, A. (1993). A voluminous avalanche-induced lahar from Citlaltepetl Volcano, Mexico: implications for hazard assessment. *Journal of Volcanology and Geothermal Research, 59*, 35-46.

Chugh, A. K. (1981). Pore water pressures in natural slopoes. *International Journal for Numerical and Analytical Methods in Geomechanics, 5*, 449 - 454.

Cole, J. (1990). Structural control and origin of volcanism in the Taupo Volcanic Zone, New Zealand. *Bulletin of Volcanology*, 445-459. doi:10.1007/BF00268925.

Cook, S., Kennedy, B., & Villeneuve, M. C. (2018). Engineering geology model of the Crater Lake outlet, Mt. Ruapehu, New Zealand, to inform rim breakout hazard. *Journal of Volcanology and Geothermal Research, 350*(15), 69-83.

Crandell, D. R. (1989). Gigantic debris avalanche of Pleistocene age from ancestral Mount Shasta volcano, California, and debris-avalanche hazard zonation. *US Geological Survey Bulletin, 1861*.

Day, S. J. (1996). Hydrothermal pore fluid pressure and the stability of porous, permeable volcanoes. *Geological Society, London, Special Publications, 110*(1), 77-93. doi:10.1144/gsl.sp.1996.110.01.06.

del Potro, R., & Hürlimann, M. (2008). Geotechnical classification and characterisation of materials for stability analyses of large volcanic slopes. *Engineering Geology, 98*(1-2), 1-17. doi:10.1016/j.enggeo.2007.11.007.

Eberhardt, E. (2012). The Hoek-Brown failure criterion. *Rock Mech Rock Eng, 45*, 981-988.

Elsworth, D. (1995). Dike intrusion as a trigger for large earthquakes and the failure of volcano flanks. *Journal of Geophysical Research, 100*(B4), 6005-6024.

Elsworth, D., & Voight, B. (1995). Dike intrusion as a trigger for large earthquakes and the failure of volcano flanks. *Journal of Geophysical Research, 100*(B4), 6005-6024.

Farquharson, J., Baud, P., & Heap, M. J. (2017a). Inelastic compaction and permeability evolution in volcanic rock *Solid Earth, 8*(2), 561-581. doi:10.5194/se-2016-166, 2016.

Farquharson, J., Heap, M. J., Baud, P., Reuschlé, T., & Varley, N. R. (2016a). Pore pressure embrittlement in a volcanic edifice. *Bulletin of Volcanology, 78*(1). doi:10.1007/s00445-015-0997-9.

Farquharson, J., Heap, M. J., Varley, N. R., Baud, P., & Reuschlé, T. (2015). Permeability and porosity relationships of edifice-forming andesites: A combined field and laboratory study. *Journal of Volcanology and Geothermal Research, 297*, 52-68. doi:10.1016/j.jvolgeores.2015.03.016.

Farquharson, J., Wadsworth, F. B., Heap, M. J., & Baud, P. (2017b). Time-dependent permeability evolution in compacting volcanic fracture systems and implications for gas overpressure. *Journal of Volcanology and Geothermal Research, 339*, 81-97.

Farquharson, J. I., Heap, M. J., & Baud, P. (2016b). Strain-induced permeability increase in volcanic rock. *Geophysical Research Letters, 43*(22).

Faulkner, D. R. (2006). PATERSON, M. S. & WONG T.-F. 2005. Experimental Rock Deformation – The Brittle Field, 2nd ed. x + 348 pp. Berlin, Heidelberg, New York: Springer-Verlag. Price Euros 89.95 (+ VAT at local rate), SFr 152.50, £69, US $119 (hard covers). ISBN 3 540 24023 3. *Geological Magazine, 143*(06), 934. doi:10.1017/s0016756806242973.

Franklin, J. A., & Hoek, E. (1970). Developments in triaxial testing equipment. *Rock Mechanics, 2*(223-228).

Gonzalez de Vallejo, L. I., & Ferrer, M. (2011). *Geological Engineering*. Boca Raton, FL: Taylor & Francis Group, LLC.

Hackett, W. R. (1985). *Geology and Petrology of Ruapehu Volcano and Related Vents.* (PhD Thesis), Victoria University of Wellington, Wellington, New Zealand.

Heap, M. J., Baud, P., Meredith, P. G., Vinciguerra, S., & Reuschlé, T. (2014). The permeability and elastic moduli of tuff from Campi Flegrei, Italy: implications for ground deformation modelling. *Solid Earth, 5*(1), 25-44. doi:10.5194/se-5-25-2014.

Heap, M. J., Farquharson, J., Baud, P., Lavallée, Y., & Reuschlé, T. (2015a). Fracture and compaction of andesite in a volcanic edifice. *Bulletin of Volcanology, 77*(55). doi:10.1007/s00445-015-0938-7.

Heap, M. J., & Kennedy, B. (2016). Exploring the scale-dependent permeability of fractured andesite. *Earth and Planetary Science Letters, 447*, 139-150.

Heap, M. J., Kennedy, B., Farquharson, J., Ashworth, J., Gilg, H. A., Scheu, B., et al. (2017). A multidisciplinary approach to quantify the permeability of a volcanic hydrothermal system

(Whakaari/White Island, Taupo Volcanic Zone, New Zealand). *Journal of Volcanology and Geothermal Research, 332*, 88-108.

Heap, M. J., Kennedy, B. M., Pernin, N., Jacquemard, L., Baud, P., Farquharson, J. I., et al. (2015b). Mechanical behaviour and failure modes in the Whakaari (White Island volcano) hydrothermal system, New Zealand. *Journal of Volcanology and Geothermal Research, 295*, 26-42. doi:10.1016/j.jvolgeores.2015.02.012.

Heap, M. J., & Wadsworth, F. B. (2016). Closing an open system: pore pressure changes in permeable edifice rock at high strain rates. *Journal of Volcanology and Geothermal Research, 315*, 40-50.

Hoek, E. (1968). *Brittle Failure of Rock*. London: Wiley and Sons.

Hoek, E., & Brown, E. T. (1980). Empirical strength criterion for rock masses. *Journal of Geotechnical and Geoenvironmental Engineering, 106*, 1013-1035.

Hoek, E., & Brown, E. T. (1997). Practical estimates of rock mass strength. *International Journal of Rock Mechanics and Mining Sciences, 34*(8), 1165-1186.

Hoek, E., Carranza-Torres, C., & Corkum, B. (2002, 7-10 July). *The Hoek-Brown failure criterion.* Paper presented at the 5th North American Rock Mechanics Symposium and 17th Tunneling Association of Canada Conference, Toronto, Ontario, Canada.

Hoek, E., Carter, T. G., & Diederichs, M. (2013). *Quantification of the Geological Strength Index*. Paper presented at the 47th US Rock Mechanics / Geomechanics Symposium, San Francisco, CA.

Hoek, E., & Diederichs, M. (2006). Empirical estimation of rock mass modulus. *International Journal of Rock Mechanics and Mining Science, 43*(2), 203-215.

Hoek, E., & Franklin, J. (1968). A simple triaxial cell for field and laboratory testing of rock. *Trans. Inst. Min. Metall., 77(A)*(22-26).

Houghton, B. F., Latter, J. H., & Hackett, W. R. (1987). Volcanic hazard assessment for Ruapehu composite volcano, Taupo Volcanic Zone, New Zealand. *Bulletin of Volcanology, 49*(6), 737-751.

Kennedy, B., Wadsworth, F. B., Vasseur, J., Schipper, C. I., Jellinek, A. M., Von Aulock, F. W., et al. (2016). Surface tension driven processes densify and retain permeability in magma and lava. *Earth and Planetary Science Letters, 433*, 116-124.

Kennedy, L. A., Russell, J. K., & Nelles, E. (2009). Origins of Mount St. Helens cataclasites: Experimental insights. *American Mineralogist, 94*(7), 995-1004. doi:10.2138/am.2009.3129.

Kilgour, G., Manville, V., Pasqua, F. D., Graettinger, A., Hodgson, K. A., & Jolly, G. E. (2010). The 25 September 2007 eruption of Mount Ruapehu, New Zealand: directed ballistics, surtseyan jets, and ice-slurry lahars. *Journal of Volcanology and Geothermal Research, 191*(1-2), 1-14. doi:10.1016/j.jvolgeores.2009.10.015.

Klug, C., & Cashman, K. V. (1996). Permeability development in vesiculating magmas: implications for fragmentation. *Bulletin of Volcanology, 58*, 87-100.

Kushnir, A. R. L., Martel, C., Bourdier, J.-L., Heap, M. J., Reuschlé, T., Erdmann, S., et al. (2016). Probing permeability and microtexture: unravelling the role of a low-permeability dome on the explosivity of Merapi (Indonesia). *Journal of Volcanology and Geothermal Research, 316*, 56-71.

Lamur, A., Kendrick, J. E., Eggertsson, G. H., Wall, R. J., Ashworth, J. D., & Lavallée, Y. (2017). The permeability of fractured rocks in pressurised volcanic and geothermal systems. *Scientific Reports, 7*(1), 6173. doi:10.1038/s41598-017-05460-4.

Loaiza, S., Fortin, J., Schubnel, A., Gueguen, Y., Vinciguerra, S., & Moreira, M. (2012). Mechanical behavior and localized failure modes in a porous basalt from the Azores. *Geophys. Res. Lett., 39*(19), n/a-n/a. doi:10.1029/2012gl053218.

Manda, A. K., & Mabee, S. B. (2010). Comparison of three fracture sampling methods for layered rocks. *International Journal of Rock Mechanics and Mining Sciences, 47*(2), 218-226. doi:10.1016/j.ijrmms.2009.12.004.

Marinos, P., & Hoek, E. (2000). *GSI: A geologically friendly tool for rock mass strength estimation.* Paper presented at the GeoEng2000 Conference, Melbourne, Australia.

Mogi, K. (1966). Pressure Dependence of Rock Strength and Transition from Brittle Fracture to Ductile Flow. *Earthquake Research Institute, 4*, 215-232.

Moon, V., Bradshaw, J., Smith, R., & de Lange, W. (2005). Geotechnical characterization of stratocone crater wall sequences, White Island volcano, New Zealand. *Engineering Geology, 81*, 146-178.

Mordensky, S. P., Villeneuve, M. C., Farquharson, J., Kennedy, B., Heap, M. J., & Gravley, D. (2018a). Rock mass properties and edifice strength data from Pinnacle Ridge, Mt. Ruapehu, New Zealand. *Journal of Volcanology and Geothermal Research, 367*, 47-62.

Mordensky, S. P., Villeneuve, M. C., Kennedy, B. M., Heap, M. J., Gravley, D., Farquharson, J. I., & Reuschlé, T. (2018b). Physical and mechanical property relationships of a shallow intrusion and volcanic host rock, Pinnacle Ridge, Mt. Ruapehu, New Zealand. *Journal of Volcanology and Geothermal Research, 359*(15), 1-20. doi:10.1016/j.jvolgeores.2018.05.020.

Mueller, S., Melnik, O., Spieler, O., Scheu, B., & Dingwell, D. B. (2005). Permeability and degassing of dome lavas undergoing rapid decompresion: an experimental determination. *Bulletin of Volcanology, 67*, 526-538.

Mueller, S., Scheu, B., Spieler, O., & Dingwell, D. B. (2008). Permeability and control on magma fragmentation. *Geology, 36*(5), 399-402.

Newhall, C. G., Albano, S. E., Matsumoto, N., & Sandoval, T. (2001). Roles of groundwater in volcanic unrest. *Geological Society of the Philippines, 56*, 69-84.

Perras, M., & Diederichs, M. (2014). A Review of the Tensile Strength of Rock: Concepts and Testing. *Geotechnical and Engineering Geology, 32*, 525-546. doi:10.1007/s10706-014-9732-0.

Pola, A., Crosta, G., Fusi, N., Barberini, V., & Norini, G. (2012). Influence of alteration on physical properties of volcanic rocks. *Tectonophysics, 566-567*, 67-86. doi:10.1016/j.tecto.2012.07.017.

Raven, K. G., & Gale, J. E. (1985). Water flow in a natural rock fracture as a function of stress and sample size. *International Journal of Rock Mechanics and Mining Science, 22*(4), 251-261. doi:10.1016/0148-9062(85)92952-3.

Read, M. D., Ayling, M. R., Meredith, P. G., & Murrell, S. A. F. (1995). Microcracking during triaxial deformation of porous rocks monitored by changes in rock physical properties, II. Pore volumometry and acoustic emission measurements on water-saturated rocks. *Tectonophysics, 245*(3-4), 223-235. doi:10.1016/0040-1951(94)00236-3.

Reid, M. E., Sisson, T. W., & Brien, D. L. (2001). Volcano collapse promoted by hydrothermal alteration and edifice shape, Mount Rainier, Washington. *Geology, 29*(9), 779. doi:10.1130/0091-7613(2001)029<0779:vcpbha>2.0.co;2.

Richard, D., Scheu, B., Mueller, S., Spieler, O., & Dingwell, D. B. (2013). Outgassing: Influence on speed of magma fragmentation. *Journal of Geophysical Research: Solid Earth, 118*, 862-877.

Rust, A. C., & Cashman, K. (2004). Permeability of vesicular silicic magma: inertial and hysteresis effects. *Earth and Planetary Science Letters, 228*, 93-107.

Rust, A. C., & Cashman, K. (2011). Permeability controls on expansion and size distributions of pyroclasts. *Journal of Geophysical Research, 116*(B11202,). doi:10.1029/2011JB008494.

Rutter, E. (1986). On the nomenclature of mode of failure transitions in rocks. *Tectonophysics, 122*, 381-387.

Rye, R. O. (1993). The evolution of magmatic fluids in the epithermal environment: the stable isotope perspective. *Economic Geology, 88*(3), 733-753.

Schaefer, L. N., Kendrick, J. E., Oommen, T., Lavallée, Y., & Chigna, G. (2015). Geomechanical rock properties of a basaltic volcano. *Frontiers in Earth Science, 3*(29). doi:10.3389.

Schaefer, L. N., Kennedy, B., Villeneuve, M. C., Cook, S. C. W., Jolly, A., Keys, H., & Leonard, G. J. (2018). Stability assessment of the Crater Lake overflow/Te Wai-ā-moe channel at Mt. Ruapehu (New

Zealand), and implications for volcanic lake break-out triggers. *Journal of Volcanology and Geothermal Research, 358*, 31-44. doi:10.1016/j.jvolgeores.2018.06.011.

Sherburn, S., Bryan, C. J., Hurst, a. W., Latter, J. H., & Scott, B. J. (1999). Seismicity of Ruapehu volcano, New Zealand, 1971-1996: A review. *Journal of Volcanology and Geothermal Research, 88*(4), 255-278. doi:10.1016/S0377-0273(99)00014-1.

Shimada, M. (1986). Mechanism of deformation in a dry porous basalt at high pressures. *Tectonophysics, 121*, 153-173.

Sigurdsson, H., Houghton, B. F., McNutt, S. R., Rymer, H., Stix, J., & McBirney, A. R. (2000). Encyclopedia of Volcanoes. *Physics Today, 53*(10), 84-85. doi:10.1063/1.1325206.

Siratovich, P. A., Heap, M. J., Villeneuve, M. C., Cole, J., Kennedy, B., Davidson, J. P., & Reuschlé, T. (2016). Mechanical behaviour of the Rotokawa Andesites (New Zealand): insight into permeability evolution and stress-induced behaviour in an actively utilised geothermal reservoir. *Geothermics, 64*, 163-179. doi:10.1016/j.geothermics.2016.05.005.

Smart, B. G. D. (1995). A true triaxial cell for testing cylindrical rock specimens. *International Journal of Rock Mechanics and Mining Science & Geomechanics Abstracts, 32*(3), 269-275.

Smith, R., Sammonds, P., Tuffen, H., & Meredith, P. G. (2011). Evolution of the mechanics of the 2004–2008 Mt St. Helens lava dome with time and temperature. *Earth and Planetary Science Letters, 307*, 191-200.

Sparks, R. S. J. (1997). Causes and consequences of pressurisation in lava dome eruptions. *Earth and Planetary Science Letters, 18*, 1139-1149.

Thomas, M. E., Petrford, N., & Bromhead, E. N. (2004). Volcanic rock mass properties from Snowdonia and Tenerife: implications for volcano edifice strength. *Journal of the Geological Society, 161*, 939-946.

Tibaldi, A. (2001). Multiple sector collapses at Stromboli volcano, Italy: How they work. *Bulletin of Volcanology, 63*(2), 112-125. doi:10.1007/s004450100129.

Ulusay, R., & Hudson, J. (2007). *The Complete ISRM Suggested Methods for Rock Characterization, Testing and Monitoring: 1974-2006*. Antalya, Turkey: Elsevier.

Upton, B. G. J., & Wadsworth, W. J. (1970). Early volcanic rocks of Reunion and their tectonic significance. *Bulletin Volcanologique, 33*, 1246-1268.

Vallance, S., Trovato, C., Meredith, P. G., & Benson, P. M. (2005). Relating seismic velocities, thermal cracking and permeability in Mt. Etna and Iceland basalts. *International Journal of Rock Mechanics and Mining Science, 42*, 900-910. doi:10.1016/j.ijrmms.2005.05.022.

Villeneuve, M. C., Heap, M. J., Kushnir, A. R. L., Qin, T., Baud, P., Zhou, G., & Xu, T. (2018). Estimating in situ rock mass strength and elastic modulus of granite from the Soultz-sous-Forêts geothermal reservoir (France). *Geothermal Energy, 6*(11). doi:10.1186/s40517-018-0096-1.

Violay, M., Gibert, B., Mainprice, D., & Burg, J.-P. (2015). Brittle versus ductile deformation as the main control of the deep fluid circulation in oceanic crust. *Geophys. Res. Lett.*

Violay, M., Gibert, B., Mainprice, D., Evans, B., Dautria, J. M., Azais, P., & Perzard, P. (2012). An experimental study of the brittle-ductile transition of basalt at oceanic crust pressure and temperature conditions. *Journal of Geophysical Research, 117*(B03213).

Voight, B., & Faust, C. (1982). Frictional heat and strength loss in some rapid landslides. *Geotechnique, 33*, 43-54.

Voight, B., Janda, R. J., & Douglas, P. M. (1983). Nature and mechanism of the Mount St. Helens rockslide avalanche of 18 May 1980. *Geotechnique, 33*, 224-273.

Wallace, P. J. (2005). Volatiles in subduction zone magmas: concentrations and fluxes based on melt inclusion and volcanic gas data. *Journal of Volcanology and Geothermal Research, 140*(1-3), 217-240. doi:10.1016/j.jvolgeores.2004.07.023.

Watters, R. J., Zimbelman, D. R., S.D., B., & Crowley, J. K. (2000). Rock mass strength assessment and significance to edifice stability, Mount Rainier and Mount Hood, Cascade Range volcanoes. *Pure and Applied Geophysics, 157*(6-8), 957-976. doi:10.1007/s000240050012.

Wong, T. F., & Baud, P. (2012). The brittle-ductile transition in porous rocks: a review. *Journal of Structural Geology, 44*, 25-53.

Woods, A. W., & Koyaguchi, T. (1994). Transitions between explosive and effusive eruptions of silicic magmas. *Nature, 370*, 641-644.

Wright, H. M. N., Cashman, K. V., Gottesfeld, E. H., & Roberts, J. J. (2009). Pore structure of volcanic clasts: measurements of permeability and electrical conductivity. *Earth and Planetary Science Letters, 280*(1-4), 93-104.

Wyering, L. D., Villeneuve, M. C., Wallis, I. C., Siratovich, P. A., Kennedy, B. M., & Gravley, D. M. (2015). The development and application of the alteration strength index equation. *Engineering Geology, 199*, 48-61. doi:10.1016/j.enggeo.2015.10.003.

Zhu, W., Baud, P., Vinciguerra, S., & Wong, T.-f. (2011). Micromechanics of brittle faulting and cataclastic flow in Alban Hills tuff. *J. Geophys. Res., 116*(B6). doi:10.1029/2010jb008046.

Zobin, V. M. (2012). *Introduction to Volcanic Seismology* (2nd ed.). London, UK: Elsevier.

Chapter 7
Conclusions

7.1 Key findings of the thesis

In this thesis, I investigate the effects a small shallow intrusion produces in volcanic host rock through a series of laboratory studies (Chapters 2, 3, 4, 6) and fieldwork (Chapter 5). In doing so, I observe the influence of intrusions at micro-, meso-, macro-, and mega-scales. I conclude that alteration ultimately weakens the rock mass inside the alteration halo (Chapters 3, 5, 6) and makes these rocks more susceptible to ductile behaviour (Chapter 4) at shallow depths. Moreover, I emphasize that hydrothermal vein material is a presently overlooked geotechnical unit that can act as a zone of weakness and provide means of weakening entire rock slopes and augmenting pore pressure (Chapter 6). However, these effects are dependent on the maximum temperature (Chapter 2) and cooling rate of the intrusion (Chapter 2 versus Chapter 3). The key findings of this combined research are depicted in Figure 7.1 and listed in Table 7.1.

I initiated my research by thermally stressing hydrothermally altered Rotokawa Andesite samples using the high-temperature, high-pressure Magma Brewery autoclave at the University of Canterbury (Chapter 2). During this period, I was simultaneously planning and conducting the preliminary assessment for the site investigation at Pinnacle Ridge, Mt. Ruapehu. I used the results of the thermal stimulation – o*ver short-durations (circa 30 min), as maximum treatment temperature (350 – 739 °C) increases, the porosity and permeability of altered andesite increases* – to inform my sampling plan and field observations at Pinnacle Ridge, Mt. Ruapehu.

I approached Pinnacle Ridge with the intent to measure the geomechanical properties of the host rock and observe their relationship with distance to the largest intrusion at Pinnacle Ridge (Chapter 3) and found that *the brecciated lava margins decrease in porosity and permeability and increase in strength at the sample-scale as distance to the intrusion decreases*. The changes in these geomechanical properties are a product of smectitic clay precipitation that fills pore cavities from advanced argillic alteration. *The advanced argillic alteration increases the porosity and permeability and decreases the strength of the other geotechnical units (i.e. intrusions and dense coherent lavas) at the sample scale. Increased confining pressure decreases permeability for all the geotechnical units; however, dissolution appears to decrease the effect of effective (confining) pressure on permeability*. Therefore, permeability heterogeneity between the geotechnical units increases with depth.

Finally, I argue that *hydrothermal vein material needs to be considered as its own geotechnical unit because of its unique geomechanical properties*.

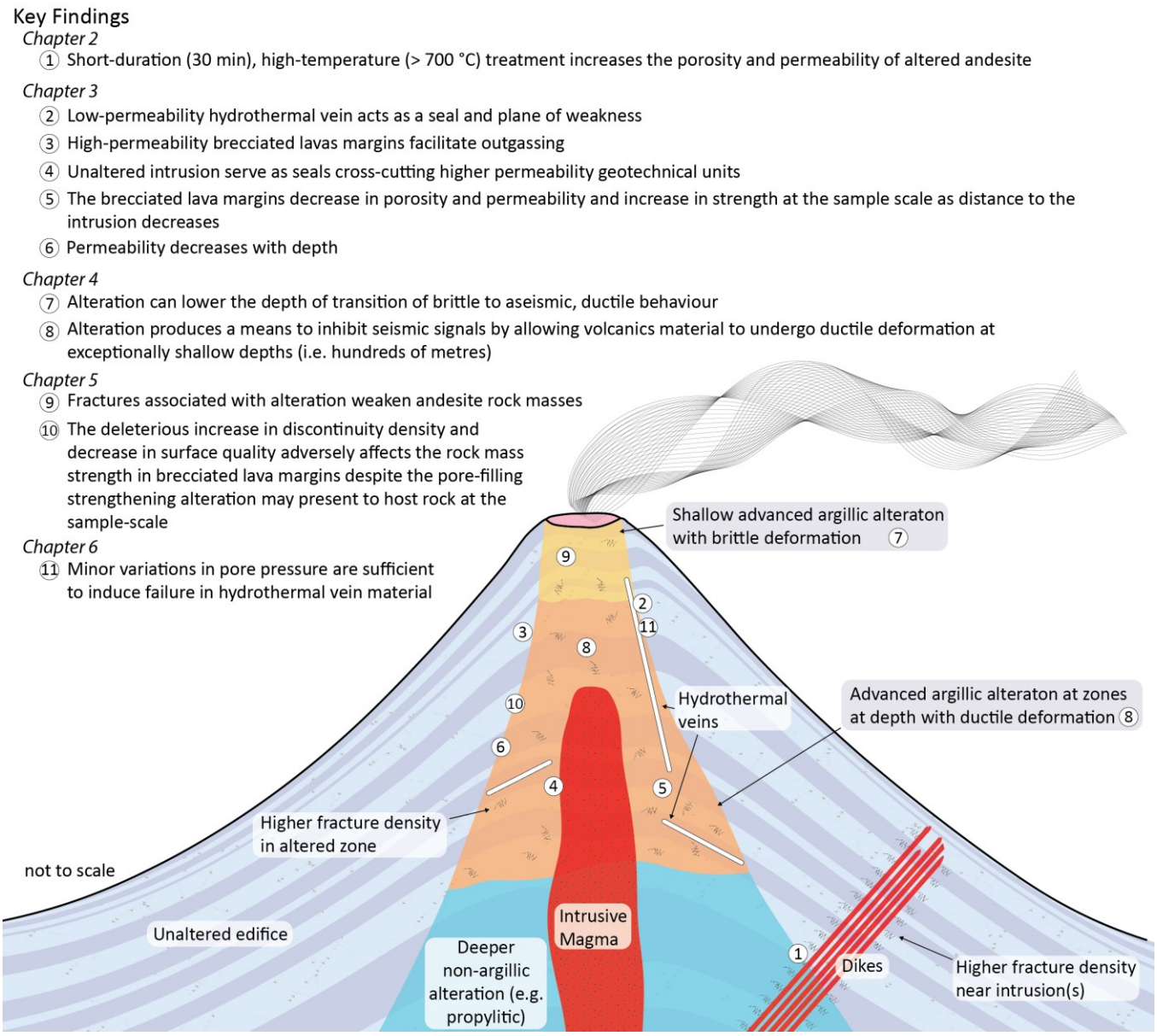

Figure 7.1 Key findings in dissertation. Major conclusions are provided by their respective chapters of the dissertation. For additional detail, see each respective chapter.

I follow my geomechanical characterization of Pinnacle Ridge with another study investigating the difference in deformation behaviour between andesite with intermediate argillic alteration and andesite with advanced argillic alteration (Chapter 4). Using a unique sample of dense coherent lava material hosting both forms of alteration, I observe that *advanced argillic alteration lowers the effective (confining) pressure at which the sample transitions from brittle to ductile behaviour through increased porosity and replacement*

of primary mineralogy with smectitic clays. I reflect that *alteration produces a means to inhibit seismicity by allowing volcanic material to undergo ductile deformation at exceptionally shallow depths (i.e. hundreds of metres)*.

Chapter	Specific Aim(s)	Outcome(s)
Chapter 2	Detail the petrophysical effects that varying peak temperatures (350 – 739 °C) at 20 MPa produces in hydrothermally altered Rotokawa andesite	*Over short-durations (circa 30 min), as maximum treatment temperature (350- 739 °C) increases, the porosity and permeability of altered andesite increases.*
Chapter 3	Characterise the mechanical and physical rock properties of the geotechnical units related to the emplacement of a small, shallow intrusion in a volcanic domain	*The brecciated lava margins decrease in porosity and permeability and increase in strength as distance to the intrusion decreases.* *The advanced argillic alteration increases the porosity and permeability and decreases the strength of the other geotechnical units.* *Increased confining pressure decreases permeability for all the geotechnical units; however, dissolution appears to decrease the effect of effective confining pressure on permeability.* *Hydrothermal vein material needs to be considered as its own geotechnical unit because of its unique geomechanical properties.*
Chapter 4	Identify the relevant pressure conditions for a change in brittle to ductile failure mode in argillic and advanced argillic altered andesites with a range of porosity	*Advanced argillic alteration lowers the effective confining pressure at which the sample transitions from brittle to ductile behaviour through increased porosity and replacement of primary mineralogy with smectitic clays.* *Alteration produces a means to inhibit seismicity by allowing volcanic material to undergo ductile deformation at exceptionally shallow depths (i.e. hundreds of metres).*
Chapter 5	Characterise the discontinuity properties of the shallow hydrothermal system at Pinnacle Ridge Assign the rock mass properties of the intrusions at Pinnacle Ridge and the host rocks of the shallow hydrothermal system	*Scale is an important consideration when considering the effect of alteration on rock mass properties.* *Alteration increases the discontinuity density and decreases the discontinuity surface quality. These changes adversely affect the rock mass strength in brecciated lava margins despite the pore-filling strengthening that alteration may cause to host rock at the sample-scale.* *The higher discontinuity density of the altered rock masses promotes higher rock mass permeability than the unaltered rock masses.*
Chapter 6	Define the Generalised Hoek-Brown failure criterion parameters for the geotechnical units of Pinnacle Ridge associated with the shallow hydrothermal system Asses the pore pressure influence on the rock mass strength of the geotechnical units associated with a hydrothermal system	*Minor variations in pore pressure are sufficient to induce failure in hydrothermal vein material before the strength the other geotechnical units become compromised.* *Altered and unaltered brecciated lava margins can transition from brittle to ductile behaviour at < 10 MPa. The other geotechnical units remain brittle to > 20 MPa.*

Table 7.1 Key research topics and conclusions (outcomes) developed from this thesis.

It is necessary to recognize that scale plays a role in rock property characterization. Through examining the influence of advanced argillic alteration on andesitic volcanics at the field-scale, I find that, in general, *alteration weakens andesite rock masses* (Chapter 5). *The increase in discontinuity density and decrease*

in surface quality adversely affects the rock mass strength in brecciated lava margins despite the pore-filling strengthening that alteration may cause to host rock at the sample-scale (e.g. in the brecciated lava margins). These discontinuity qualities are reflected by an increase in *in situ* permeability immediately surrounding intrusions at the metre-scale. This investigation highlights the importance and need for accurate rock mass parameters when assessing rock mass strength.

A subsequent investigation using triaxial deformation allowed me to constrain the rock mass parameters (Chapter 6) for application at sector-scale. I then use these data with the data presented in Chapters 3 and 5 using the Generalised Hoek-Brown failure criterion to numerically model rock mass strength under varying stress conditions. I find that *minor variations in pore pressure are sufficient to induce failure in hydrothermal vein material before the strength of the other geotechnical units become compromised*.

7.2 Implications

The research I present has implications ranging from the geothermal power production industry to volcanic monitoring and slope stability assessment.

The changes in permeability presented by a magmatic intrusion have direct consequence in the geothermal industry. I demonstrate that consideration should be given to rock from geothermal systems that may have recently been exposed to short-lived, high-temperature conditions. This scenario has already occurred at the Ngatamariki Geothermal Field, New Zealand, where drilling intersected an intrusion at 2.2 km depth (see Chambefort et al., 2014). Under these conditions, permeability can increase by over an order of magnitude in response to the thermal effects (e.g. Chapter 2). A one order of magnitude change in permeability can affect the economic viability of geothermal power facilities (e.g. Krafla, Iceland), where a narrow range (< 1 order of magnitude) of permeability may be required to maintain economically viable power production (Scott et al., 2015). The research presented in this thesis also highlight the importance of scale when attempting to assess permeability (e.g. Chapter 3 [sample-scale] versus Chapter 5 [field-scale]). That is, macro-scale discontinuities are not reflected in sample-scale permeability testing, and reservoir permeability cannot be measured by sample-scale properties alone (e.g. Heap & Kennedy, 2016). Rock mass properties and macro structures are important considerations when assessing geothermal fluid pathways (e.g. Rissmann et al., 2011).

Volcanic monitoring presents a varied range of challenges with pre-eruptive processes varying between volcanoes (e.g. Mt. Ruapehu versus Mt. St. Helens; e.g. Endo et al., 1981; Bryan & Sherburn, 1999) or simply over time at the same volcano (e.g. Mt. Ruapehu; Sherburn et al., 1999). Chapter 4 shows that

alteration (i.e. intermediate argillic alteration versus advanced argillic alteration) influences the deformation behavior (i.e. brittle versus ductile) of andesite. Advanced argillic alteration can create zones of anomalously shallow (< 500 m) ductile behaviour. Advanced argillic alteration is common at many stratavolcanoes (e.g. Mt. Rainer, USA (Crowley & Zimbelman, 1997), Teide, Tenerife, Spain (del Potro & Hürlimann, 2009; Villasante-Marcos et al., 2014)) and caldera volcanoes with active hydrothermal systems (e.g. Whakamaru caldera, New Zealand (Krupp & Seward, 1987), Long Valley caldera, USA (Flexser, 1991)). Consequently, volcano-tectonic seismicity, which is requisite upon the brittle breaking of rock, is less likely from these zones dominated by shallow ductile deformation (e.g. Chapter 4). Hence, the results of this research could allow deformation associated with magma rise without significant volcano-tectonic seismicity where ductile deformation was dominant. Additionally, this work illustrates the heterogeneity of volcanic rocks over short distances allowing varied deformation modes under similar pressure conditions as seen at other volcanoes (Heap et al., 2015a; Heap et al., 2015b). The deformation modes also have implications for permeability, where brittle deformation may increase permeability (Nara et al., 2011; Farquharson et al., 2016; Pérez-Flores et al., 2017) and ductile deformation may reduce permeability (Farquharson et al., 2017); this affects the volcanoes ability to outgas and may control explosive effusive transitions (e.g. Cassidy et al., 2018). Overall, our variable deformation underscores the necessity of a multiple monitoring methods (e.g. seismic, deformation, gas; Bamler & Hartl, 1998; Dehn et al., 2000; Baldi et al., 2002; Bechor & Zebker, 2006; Mori & Burton, 2006; Thomas et al., 2009) at volcanic edifices rather than relying upon a single pre-eruptive indicator.

The empirical rock mass strength parameters established in Chapter 6 can be used for volcanoes worldwide to asses volcano stability (Hoek, 1968; Hoek & Brown, 1980; Hoek, 1983, 1994; Hoek et al., 2002; Eberhardt, 2012; Hoek et al., 2013). The values presented in this thesis provide the first, complete parameterisation of rock masses associated with the intrusion of a magma into a volcanic edifice (Chapters 3, 5, 6). Chapter 6 also shows how minor variation in pore pressure can induce failure in hydrothermal vein rock mass material before the other geotechnical units. Pore pressure has been implicated in past and future volcano collapse scenarios (e.g. Schaefer et al., 2018). Hydrothermal vein material presents a failure surface which requires careful attention when completing stability assessments in altered parts of an edifice and may be easily overlooked in less detailed assessment and analysis. The edifice compromising characteristics hydrothermal vein material require clear distinction from other hydrothermal alteration products (e.g. quartz precipiation in the Ohakuri hydrothermal system, New Zealand; Henneberger & Browne, 1988) that can increase the strength of altered rock (see Wyering et al., 2014; Wyering et al., 2015). Also, the methodology to develop high-resolution topographic cross-sections using UAV-collected

imagery and photogrammetric processing in Chapter 6 may prove useful for slope stability modelling as this workflow creates centimetre-scale DEMs and serves to augment studies were only metre-scale LiDAR datasets are available. Similar approaches have proved useful in volcanic slope stability assessments (e.g. Roberti et al., 2018; Török et al., 2018).

Individually, the independent studies in this thesis answer specific questions related to the effects that shallow intrusions have on their volcanic host rock at a variety of scales and confining stresses and have a wide range of applications. Taken together, the combined research presented provides a comprehensive understanding of the effect intrusions have on volcanoes.

7.3 Future Work

While this research addressed many topics regarding the physical and mechanical rock properties related to a shallow intrusion, I did not have time to address several questions that arose in my three years at the University of Canterbury. I provide several of these questions below.

- How would the effect of thermal stressing (like that completed in Chapter 2) affect unaltered andesite? How do different pressures varying the effect of thermal stressing on the geomechanical properties of unaltered and altered volcanic material? How does thermal stressing affect the triaxial deformation of volcanic material? How does peak-temperature duration affect the change geomechanical properties of the volcanic rock?
- What specific attributes (e.g. higher permeability) of brecciated lava margins make them more susceptible to mineral precipitation in a hydrothermal system? Conversely, what specific attributes of the other geotechnical units make them more susceptible to dissolution in a hydrothermal system?
- What is the nature of porosity and alteration at depth within Mt. Ruapehu, can we use geochemical models to predict pore precipitation, compaction, and strengthening to better inform our deeper rock mass properties? How do other forms of alteration (e.g. propylitic) affect deformation of volcanic material?
- How can we use scanline and rock mass data to model rock mass permeability? What are the critical variables needed to accurately model permeability and can rock mass assessments be used to estimate the permeability of volcanic rock?

- What are the constraints on the composition and extent of hydrothermal veining within a volcanic edifice? What is the average extent and geometry of hydrothermal vein in a rock mass? How do these attributes between different types of rock masses? At what orientation relative to a free surface and/or load is a hydrothermal veining weakest? Does the composition, depth, and temperature of the hydrothermal system produce any systematic variation in vein type that could inform future modelling? What are the dimensional constraints at which hydrothermal vein failure presents a substantial risk of a large mass movement event?
- Could sub-surface hydrothermal veins be mapped by ground penetrating radar, electro-resistivity surveys, aeromagnetic surveys, or another remote sensing means?
- How quickly can pore pressure change and over what scale in a volcanic edifice? How does pore-pressure cycling and its consequential fatigue affect the slope stability of a volcanic edifice? How can one account for fatigue using the generalised Hoek-Brown failure criterion? Given the active hydrothermal system present beneath Mt. Ruapehu's crater lake and the data collected from this thesis, is Mt. Ruapehu at risk of a catastrophic collapse event today? What combinations of alteration intensity, pore pressure, macro structures (e.g. stratigraphy, discontinuity characteristics) would be required to induce failure today?
- Could evidence be seen in past collapse events for similar pore-pressure, hydrothermal-vein induced destabilisation of the volcanic edifice as hypothesised in this thesis?
- In carbonate-bearing hydrothermal systems, does climate change present the potential to weaken rock masses and, if so, at what elevations and latitudes and at what rate(s) would these changes occur?

7.4 Appendices

Contents of Electronic Appendices

- Appendix A: Stress-strain data in Chapter 2
- Appendix B: Ultrasound data in Chapter 2
- Appendix C: Rock property data in Chapter 3 (Supplemental data for publication)
- Appendix D: Stress-strain data in Chapter 3
- Appendix E: Ultrasound data in Chapter 3
- Appendix F: Thin-section photos of sample in Chapter 3
- Appendix G: Supporting information from Chapter 4 submission
- Appendix H: Stress-strain data in Chapter 4
- Appendix I: Supplemental tables from Chapter 5 publication
- Appendix J: Scanline data in Chapter 5
- Appendix K: Supplemental tables from Chapter 6 submission
- Appendix L: Stress-strain data in Chapter 6
- Appendix M: Ultrasound data in Chapter 6

7.5 References

Baldi, P., Bonvalot, S., Briole, P., Coltelli, M., Gwinner, K., Marsella, M., et al. (2002). Validation and comparison of diVerent techniques for the derivation of digital elevation models and volcanic monitoring (Vulcano Island, Italy). *International Journal of Remote Sensing, 23*(22), 4783-4800.

Bamler, R., & Hartl, P. (1998). Synthetic aperture radar interferometry. *Inverse Problems, 14*, R1-R54.

Bechor, N. B. D., & Zebker, H. A. (2006). Measuring two-dimensional movements using a single InSAR pair. *Geophysical Research Letters, 33*(L16311). doi:10.1029/2006GL026883.

Bryan, C. J., & Sherburn, S. (1999). Seismicity associated with the 1995–1996 eruptions of Ruapehu volcano, New Zealand: narrative and insights into physical processes. *Journal of Volcanology and Geothermal Research, 90*, 1-18.

Cassidy, M., Manga, M., Cashman, K., & Bachmann, O. (2018). Controls on explosive-effusive volcanic eruption styles. *Nature communications, 9*, 1-16. doi:10.1038/s41467-018-05293-3.

Chambefort, I., Lewis, B., Wilson, C. J. N., Rae, A. J., Coutts, C., Bignall, G., & Ireland, T. R. (2014). Stratigraphy and structure of the Ngatamariki geothermal system from new zircon U–Pb geochronology: implications for Taupo Volcanic Zone evolution. *Journal of Volcanology and Geothermal Research, 274*, 51-70. doi:10.1016/j.jvolgeores.2014.01.015.

Crowley, J. K., & Zimbelman, D. R. (1997). Mapping hydrothermally altered rocks on Mount Rainer, Washington, with airborne visible/infrared imaging spectrometer (AVIRS) data. *Geology, 25*(6), 559-562.

Dehn, J., Dean, K., & Engle, K. (2000). Thermal monitoring of North Pacific volcanoes from space. *Geology, 28*(8), 755-758.

del Potro, R., & Hürlimann, M. (2009). The decrease in the shear strength of volcanic materials with argillic hydrothermal alteration, insights from the summit region of Teide stratovolcano, Tenerife. *Engineering Geology, 104*(1-2), 135-143. doi:10.1016/j.enggeo.2008.09.005.

Eberhardt, E. (2012). The Hoek-Brown failure criterion. *Rock Mech Rock Eng, 45*, 981-988.

Endo, E. T., Malone, S. D., Nosen, L. L., & Weaver, C. S. (1981). *Locations, mangitudes, and statistics of the March 20-May 18 earthquake sequence*. Retrieved from

Farquharson, J., Baud, P., & Heap, M. J. (2017). Inelastic compaction and permeability evolution in volcanic rock *Solid Earth, 8*(2), 561-581. doi:10.5194/se-2016-166, 2016.

Farquharson, J. I., Heap, M. J., & Baud, P. (2016). Strain-induced permeability increase in volcanic rock. *Geophysical Research Letters, 43*(22).

Flexser, S. (1991). Hydrothermal alteration and past and present thermal regimes in the western moat of Long Valley caldera. *Journal of Volcanology and Geothermal Research, 48*, 303-318.

Heap, M. J., Farquharson, J., Baud, P., Lavallée, Y., & Reuschlé, T. (2015a). Fracture and compaction of andesite in a volcanic edifice. *Bulletin of Volcanology, 77*(55). doi:10.1007/s00445-015-0938-7.

Heap, M. J., & Kennedy, B. (2016). Exploring the scale-dependent permeability of fractured andesite. *Earth and Planetary Science Letters, 447*, 139-150.

Heap, M. J., Kennedy, B. M., Pernin, N., Jacquemard, L., Baud, P., Farquharson, J. I., et al. (2015b). Mechanical behaviour and failure modes in the Whakaari (White Island volcano) hydrothermal system, New Zealand. *Journal of Volcanology and Geothermal Research, 295*, 26-42. doi:10.1016/j.jvolgeores.2015.02.012.

Henneberger, R. C., & Browne, P. R. L. (1988). Hydrothermal alteration and evolution of the Ohakuri hydrothermal system, Taupo volcanic zone, New Zealand. *Journal of Volcanology and Geothermal Research, 34*(3-4), 211-231. doi:10.1016/0377-0273(88)90034-0.

Hoek, E. (1968). *Brittle Failure of Rock*. London: Wiley and Sons.

Hoek, E. (1983). Strength of jointed rock masses. *Geotechnique, 33*(3), 187-223.

Hoek, E. (1994). Strength of Rock Masses. *ISRM News Journal, 2*(2), 4-16.

Hoek, E., & Brown, E. T. (1980). Empirical strength criterion for rock masses. *Journal of Geotechnical and Geoenvironmental Engineering, 106*, 1013-1035.

Hoek, E., Carranza-Torres, C., & Corkum, B. (2002, 7-10 July). *The Hoek-Brown failure criterion.* Paper presented at the 5th North American Rock Mechanics Symposium and 17th Tunneling Association of Canada Conference, Toronto, Ontario, Canada.

Hoek, E., Carter, T. G., & Diederichs, M. (2013). *Quantification of the Geological Strength Index*. Paper presented at the 47th US Rock Mechanics / Geomechanics Symposium, San Francisco, CA.

Krupp, R. E., & Seward, T. M. (1987). The Rotokawa geothermal system, New Zealand; an active epithermal gold-depositing environment. *Economic Geology, 82*, 1109-1129.

Mori, T., & Burton, M. (2006). The SO2 camera: A simple, fast and cheap method for ground-based imaging of SO2 in volcanic plumes. *Geophysical Journal International, 33*(L24804). doi:10.1029/2006GL027916.

Nara, Y., Meredith, P. G., Yoneda, T., & Kaneko, K. (2011). Influence of macrofractures and microfractures on permeability and elastic wave velocities in basalt at elevated pressure. *Tectonophysics, 503*(1-2), 52-59. doi:10.1016/j.tecto.2010.09.027.

Pérez-Flores, P., Wang, G., Mitchell, T. M., Meredith, P. G., Nara, Y., Sarkar, V., & Cembrano, J. (2017). The effect of offset on fracture permeability of rocks from the Southern Andes Volcanic Zone, Chile. *Journal of Structural Geology, 104*, 142-158.

Rissmann, C., Nicol, A., Cole, J., Kennedy, B., Fairley, J., Christenson, B., et al. (2011). Fluid flow associated with silicic lava domes and faults, Ohaaki hydrothermal field, New Zealand. *Journal of Volcanology and Geothermal Research, 204*(1-4), 12-26. doi:10.1016/j.jvolgeores.2011.05.002.

Roberti, G., Ward, B., Van Wyk de Vries, B., Friele, P., Pierre, F., Clague, J. J., & Giardino, M. (2018). Precursory slope distress prior to the 2010 Mount Meager landslide, British Columbia. *Landslides, 15*, 637-647. doi:10.1007/s10346-017-0901-0.

Schaefer, L. N., Kennedy, B., Villeneuve, M. C., Cook, S. C. W., Jolly, A., Keys, H., & Leonard, G. J. (2018). Stability assessment of the Crater Lake overflow/Te Wai-ā-moe channel at Mt. Ruapehu (New Zealand), and implications for volcanic lake break-out triggers. *Journal of Volcanology and Geothermal Research, 358*, 31-44. doi:10.1016/j.jvolgeores.2018.06.011.

Scott, S. W., Driesner, T., & Weis, P. (2015). Geologic controls on supercritical geothermal resources above magmatic intrusions. *Nature communications, 6*, 7837-7837. doi:10.1038/ncomms8837.

Sherburn, S., Bryan, C. J., Hurst, a. W., Latter, J. H., & Scott, B. J. (1999). Seismicity of Ruapehu volcano, New Zealand, 1971-1996: A review. *Journal of Volcanology and Geothermal Research, 88*(4), 255-278. doi:10.1016/S0377-0273(99)00014-1.

Thomas, H. E., Watson, I. M., Kearney, C., Carn, S. A., & Murray, S. J. (2009). A multi-sensor comparison of sulphur dioxide emissions from the 2005 eruption of Sierra Negra volcano, Galápagos Islands. *Remote Sensing of Environment, 113*, 1331-1342.

Török, Á., Barsi, Á., Bögöly, G., Lovas, T., Somogyi, Á., & Görög, P. (2018). Slope stability and rockfall assessment of volcanic tuffs using RPASwith 2-D FEM slope modelling. *Natural Hazards and Earth System Sciences, 18*, 583-597. doi:10.5194/nhess-18-583-2018.

Villasante-Marcos, V., Finizola, A., Abella, R., Barde-Cabusson, S., J., B. M., Brenes, B., et al. (2014). Hydrothermal system of Central Tenerife Volcanic Complex, Canary Islands (Spain), inferred from self-potential measurement. *Journal of Volcanology and Geothermal Research, 272*, 59-77. doi:10.1016/j.jvolgeores.2013.12.007.

Wyering, L. D., Villeneuve, M. C., Wallis, I. C., Siratovich, P. A., Kennedy, B. M., & Gravley, D. M. (2015). The development and application of the alteration strength index equation. *Engineering Geology, 199*, 48-61. doi:10.1016/j.enggeo.2015.10.003.

Wyering, L. D., Villeneuve, M. C., Wallis, I. C., Siratovich, P. A., Kennedy, B. M., Gravley, D. M., & Cant, J. L. (2014). Mechanical and physical properties of hydrothermally altered rocks, Taupo Volcanic Zone, New Zealand. *Journal of Volcanology and Geothermal Research, 288*, 76-93. doi:10.1016/j.jvolgeores.2014.10.008.